



ASPHALTENE AGGREGATION VIA DISSIPATIVE PARTICLE DYNAMICS

Fellipe Carvalho de Oliveira

Tese de Doutorado apresentada ao Programa de Pós-graduação em Engenharia Química, COPPE, da Universidade Federal do Rio de Janeiro, como parte dos requisitos necessários à obtenção do título de Doutor em Engenharia Química.

Orientadores: Frederico Wanderley Tavares
João Manuel Luís Lopes Maia

Rio de Janeiro
Março 2021

ASPHALTENE AGGREGATION VIA DISSIPATIVE PARTICLE DYNAMICS

Fellipe Carvalho de Oliveira

TESE SUBMETIDA AO CORPO DOCENTE DO INSTITUTO ALBERTO LUIZ COIMBRA DE PÓS-GRADUAÇÃO E PESQUISA DE ENGENHARIA DA UNIVERSIDADE FEDERAL DO RIO DE JANEIRO COMO PARTE DOS REQUISITOS NECESSÁRIOS PARA A OBTENÇÃO DO GRAU DE DOUTOR EM CIÊNCIAS EM ENGENHARIA QUÍMICA.

Orientadores: Frederico Wanderley Tavares

João Manuel Luís Lopes Maia

Aprovada por: Paulo Roberto de Souza Mendes

Júlio Cesar Guedes Correia

Sônia Maria Cabral de Menezes

Márcio Nele de Souza

RIO DE JANEIRO, RJ – BRASIL

MARÇO 2021

Oliveira, Fellipe Carvalho de
Asphaltene Aggregation via Dissipative Particle
Dynamics/Fellipe Carvalho de Oliveira. – Rio de Janeiro:
UFRJ/COPPE, 2021.

XXV, 157 p.: il.; 29, 7cm.

Orientadores: Frederico Wanderley Tavares

João Manuel Luís Lopes Maia

Tese (doutorado) – UFRJ/COPPE/Programa de
Engenharia Química, 2021.

Referências Bibliográficas: p. 124 – 144.

1. Molecular Simulation. 2. DPD. 3. Asphaltenes.
4. Rheology. I. Tavares Frederico Wanderley *et al.*
II. Universidade Federal do Rio de Janeiro, COPPE,
Programa de Engenharia Química. III. Título.

Agradecimentos

Aqui deixarei meus agradecimentos a estes sem os quais não teria sido possível a realização desta tese.

Primeiramente a meu orientador Frederico Tavares pelo apoio intelectual, emocional, por todo seu compromisso para com este trabalho, deixo aqui minha gratidão e admiração pela pessoa do seu ser. Expresso igualmente minha gratidão a meu coorientador João Maia por sua valorosa contribuição neste trabalho. Agradeço, também, a Chloe pelas discussões e ensinamentos. Manifesto imenso agradecimento também a Nathália Sales pela ajuda com os clusters lobo carneiro e santos dumont que foram essenciais para execução das simulações moleculares.

Agradeço à minha família Régia, Camila, Rafael, Arthur, Athena, Anthony e Pedro, que em todos os momentos de saudades me escutaram e trouxeram-me o conforto da alma. À minha mãe Régia, com quem aprendi o real sentido de amor incondicional e a lutar pelos meus sonhos. Ao meu amor Pedro Rafael, pelo seu amor e dedicação para comigo e para com nossa relação. À minha irmã Camila, que sempre esteve ao meu lado apoiando-me. Ao meu cunhado Rafael, que nos ensina a sorrir nos momentos de adversidade. Ao Arthur, pelos sorrisos que já me ofereceu, lembro-me deles com imenso carinho. À Athena, por sua simpatia e alegria contagiante. Ao Anthony, por me mostrar que meus percalços são menores que o que eu pensava serem. A Beatriz e Carolina, minhas afilhadas, que me dão muito orgulho na vida. Às minhas irmãs e irmãos de coração Jeanne, Pâmela, Poliane, Bruno, Tayná e ao meu mais novo afilhado, Pedro Caetano, e a tantos outros primos, primas e tios e tias que estiveram a meu lado durante toda a vida, sem os quais não estaria aqui hoje.

A Débora, Carol, Tahyná, Neto, Felipe Gomide (Prenhos), Marlon, Idia, Afrânio, Rafael Pereira que me acompanham desde o mestrado. São grandes amigos que o Rio de Janeiro me deu.

A Érika, Felipe Lelis, Ítalo, Isabela, Hanna, Michael, Robert, Henrique, Sophie, Donovan, Isack, Cristian e tantos outros amigos que fiz durante minha estadia em

Cleveland.

Ao meu mais que amigo Marcus Vinícius que há muito tempo me acompanha.
Sinto muito sua falta

A todos os meus amigos de Fortaleza, do laboratório ATOMS, do Programa de Engenharia Química (PEQ) da COPPE.

Agradeço à Capes, ao PEQ e à Escola de Química pelo apoio financeiro e de infra-estrutura.

Sim, todo amor é sagrado. E o fruto do trabalho é mais que sagrado, meu amor.

Beto Guedes e Ronaldo Bastos

Resumo da Tese apresentada à COPPE/UFRJ como parte dos requisitos necessários para a obtenção do grau de Doutor em Ciências (D.Sc.)

AGREGAÇÃO DE ASFALTENOS VIA DINÂMICA DE PARTÍCULAS DISSIPATIVAS

Fellipe Carvalho de Oliveira

Março/2021

Orientadores: Frederico Wanderley Tavares
João Manuel Luís Lopes Maia

Programa: Engenharia Química

Asfaltenos são as frações mais pesadas do petróleo que podem formar agregados moleculares. Durante a extração e processamento, estas frações podem precipitar, entupir as tubulações, o que pode danificá-las ou mesmo inviabilizar o processo de produção. As condições cinéticas da precipitação dos asfaltenos dependem da estrutura e do tamanho dos nanoagregados formados. Neste trabalho, a simulação molecular foi usada para estudar as características da agregação de asfaltenos tanto em solução quanto em interfaces água-óleo. O processo de agregação dos asfaltenos acontece em uma escala de tempo grande, quando comparada a outros fenômenos atomísticos. Soluções diluídas de asfaltenos em tolueno foram analisadas e os resultados de função de distribuição radial e coeficiente de difusão representaram bem os dados experimentais. Nos sistemas água-asfalteno-óleo, o ciclohexano foi escolhido como fase óleo. Foi calculada a curva de decaimento da tensão interfacial em função da concentração de asfalteno na solução, e a concentração micelar crítica estimada está em consistência com dados experimentais da literatura. O perfil de densidade linear das moléculas de asfalteno na interface foi medido assim como a distribuição de ângulos de contato entre moléculas de asfalteno e a interface água/óleo. Conclui-se, desta maneira, que o método DPD pode ser apropriadamente utilizado para calcular tanto as características estruturais e dinâmicas de asfaltenos em solução quanto as suas propriedades na interface água/óleo.

Abstract of Thesis presented to COPPE/UFRJ as a partial fulfillment of the requirements for the degree of Doctor of Science (D.Sc.)

ASPHALTENE AGGREGATION VIA DISSIPATIVE PARTICLE DYNAMICS

Fellipe Carvalho de Oliveira

March/2021

Advisors: Frederico Wanderley Tavares
João Manuel Luís Lopes Maia

Department: Chemical Engineering

Asphaltenes compose the heaviest fraction of crude oil that can form nanoaggregates. These fractions can precipitate, clog pipes during extraction and processing, which can make the production process unfeasible. The kinetic conditions of asphaltene precipitation depend on the structure and size of the nanoaggregates formed. In this work, the molecular simulation was used to study the characteristics of asphaltene aggregation both in solution and on water-oil interfaces. The asphaltene aggregation process takes place over a large time scale, when compared to other atomistic phenomena. Diluted solutions of asphaltenes in toluene were analyzed, and the results of the radial distribution function and diffusion coefficient represented the experimental data well. In water-asphaltene-oil systems, cyclohexane was chosen as the oil phase. The decay curve of the interfacial tension as a function of the asphaltene concentration and the estimated critical micelle concentration is consistent with experimental data from the literature. The linear density profile of the asphaltene molecules at the interface was measured, as well as the distribution of contact angles between asphaltene molecules and the water/oil interface. In conclusion, the DPD method can be appropriately used to simulate both the structural and dynamic characteristics of asphaltenes in solution, moreover, it also describes well the asphaltene properties at the water/oil interface.

Contents

Agradecimientos	iv
List of Figures	xii
List of Tables	xx
List of Symbols	xxii
List of Abbreviations	xxv
1 Introduction	1
1.1 Motivation	1
1.2 General and Specific Objectives	3
1.3 Thesis Structure	4
2 Literature Review	6
2.1 Asphaltene Aggregation and Modeling Strategies	6
2.1.1 Development of Equations of State	6
2.1.2 Atomistic Molecular Simulation	8
2.1.3 Molecular Mechanics and <i>Coarse-Graining</i>	12
2.1.4 DPD (<i>Dissipative Particle Dynamics</i>)	13
2.1.5 General Comments	17
3 Method	19

3.1	Molecular Dynamics	19
3.2	Integration Schemes	22
3.3	Microscopic States and <i>Ensembles</i>	23
3.3.1	<i>Microcanonical Ensemble</i> (NVE)	24
3.3.2	<i>Canonical Ensemble</i> (NVT)	24
3.3.3	<i>Isothermal–Isobaric Ensemble</i> (NPT)	25
3.4	The DPD method	26
3.5	Simulator <i>LAMMPS</i>	29
4	Clustering Algorithm	31
4.1	Algorithm Implementation	33
4.2	Application 1 - Aggregation of Lennard-Jones Particles	37
4.3	Application 2 - Asphaltene Aggregation in Heptane	45
5	Bulk Simulation of Asphaltene Aggregation	52
5.1	Coarse-Graining and Simulation Details	52
5.2	Microstructure	57
5.2.1	Radial Distribution Function - $g(r)$	60
5.2.2	Angle Between Molecules	63
5.3	Kinetics of Aggregation	66
5.4	Dynamics of Aggregation	71
5.5	Rheological Properties	74
5.5.1	Thermostat	74
5.5.2	Viscosity	75
5.5.3	Oscillatory Shear and Linear Viscoelastic Regime (LVR)	80
6	Asphaltenes at the Water/Oil Interface	93
6.1	Coarse-Graining and Simulation Details	97
6.2	Hydrocarbon-Water Systems	100

6.3	Asphaltene Solutions in Toluene	107
6.4	Asphaltenes at the Water-Oil Interface	110
7	Conclusions and Future Perspectives	121
	Bibliography	124
	Appendices	145
A	3D Linear Regression	146
B	Clustering Algorithm in Fortran 90	151

List of Figures

1.1	Aggregation hierarchy according to the Yen-Mullins model. Asphaltene molecules aggregate first into nanostructures. These nanoaggregates form clusters. (MULLINS, 2010)	2
3.1	Graph of the classical Lennard-Jones potential for $\epsilon = 1$ e $\sigma = 1$	20
3.2	<i>Periodic boundary conditions</i> and the <i>minimum-image convention</i> . Figure extracted from (ALLEN and TILDESLEY, 1991).	21
3.3	Example of coarse-grained representation of a collection of particles.	29
4.1	Example: system of molecules whose contacts have been verified in SUBROUTINE <code>neighboring</code>	34
4.2	Vector <code>nodeL</code> labels after the first clustering step for the stated example. It contains the cluster label for each molecule.	35
4.3	Vector <code>nodeL</code> labels after the correction label step for the stated example. <code>nodeL</code> contains the cluster label for each molecule.	36
4.4	Final result for the stated example using the proposed algorithm. The Figure also indicates the scan direction in <code>nodeL</code> to verify if <code>condition2</code> and <code>condition3</code> are being satisfied.	37
4.5	Initial and final configurations for Brownian dynamics of Lennard-Jones particles at different temperatures and volume fractions. At the initial configurations particles are randomly dispersed in the medium, they aggregate over time. a) $T^* = 0.3$ and $\phi = 0.05$ at $t^* = 0$. b) $T^* = 0.3$ and $\phi = 0.05$ at $t^* = 74$. c) $T^* = 0.5$ and $\phi = 0.05$ at $t^* = 0$. d) $T^* = 0.5$ and $\phi = 0.05$ at $t^* = 74$. e) $T^* = 0.3$ and $\phi = 0.16$ at $t^* = 0$. f) $T^* = 0.3$ and $\phi = 0.16$ at $t^* = 74$. g) $T^* = 0.5$ and $\phi = 0.16$ at $t^* = 0$. h) $T^* = 0.5$ and $\phi = 0.16$ at $t^* = 74$	38

4.6	Mean Square Displacement (<i>MSD</i>) for Lennard-Jones particles under Brownian dynamics at different temperatures and volume fractions. t^* represents time in Lennard-Jones units.	39
4.7	Diffusion Coefficient for Lennard-Jones particles under Brownian dynamics at different temperatures and volume fractions. t^* represents time in Lennard-Jones units.	40
4.8	Number of cluster evolution for Lennard-Jones particles under Brownian dynamics at different temperatures and volume fractions. t^* represents time in Lennard-Jones units.	41
4.9	Number of links (proportional to the mean size) evolution for Lennard-Jones particles under Brownian Dynamics at different temperatures and volume fractions. t^* represents time in Lennard-Jones units.	42
4.10	Number of clusters and numbers of links obtained by using Al-Futaisi and Patzek algorithm and the MATLAB version of the proposed clustering routine. Both algorithms produce the same results. . . .	43
4.11	Average spent time comparison for both algorithms (using the MATLAB version of the proposed clustering routine) for 100 timesteps. The proposed routine is less time consuming. Triplicate has been performed for average and standard deviation calculations. In some cases standard deviations are too small, seeming not visible.	44
4.12	Initial configuration. Molecules are randomly dispersed in the medium. Only asphaltene (solute) molecules are shown for better viewing.	46
4.13	Final configuration. Asphaltene molecules are forming a aggregated structure. Only asphaltene (solute) molecules are shown for better viewing.	47
4.14	Time evolution of the number of clusters (NC) and links (NL) of asphaltene molecules for Al-Futaisi and Patzek algorithm and the proposed clustering routine. The number of clusters is diminishing as initially each molecule represents one isolated cluster which is aggregating in time. Curves tend to constant values as equilibrium is being attained. Both algorithms give the same results.	48

4.15	Time performance comparison between Al-Futaisi and Patzek algorithm and the proposed clustering routine for 100 timesteps. The proposed routine is faster. Triplicate has been performed for average and standard deviation calculations. In some cases standard deviations are too small, seeming not visible.	49
4.16	Evolution of number of links comparing different asphaltene concentrations.	50
4.17	Evolution of number of clusters comparing different asphaltene concentrations. The inset represents the curves normalized by the initial number of clusters (number of molecules). As the concentration increases, the plateau to which those curves tend decreases, as a consequence of high number of links (See Figure 4.16.)	51
5.1	Molecules representation: B bead (blue) represents a moiety of aromatic rings which is the benzene in this approach, H bead (green) represents a butane molecule which forms the alkyl side chains, T bead (red) represents a thiourea molecule which is the heteroatom group. (a) Asphaltene molecule structure. (b) Heptane molecule structure formed by two butane molecules. (c) Toluene molecule structure formed by butane and benzene. each bead corresponds to the volume of three water molecules.	54
5.2	Structural formula of the hypothetical asphaltene molecule model used in this work. The heteroatoms were described in detail.	55
5.3	Sequential scheme of equilibration, aggregation and shearing simulations.	57
5.4	Temperature equilibration profile for asphaltene simulation in heptane and toluene. Different colors represent different mass fractions.	58
5.5	Pressure equilibration profile for asphaltene simulation in heptane (top) and toluene (bottom). Different colors represent different mass fractions.	59
5.6	(Left) Parallel, T-shaped and offset conformations have been found, as obtained by previous works (XU <i>et al.</i> , 2011; ZHANG <i>et al.</i> , 2010). Only asphaltene particles are shown to better visualization. (Right) Schematically representation of stacking types.	60
5.7	Scheme for counting particles and calculating $g(r)$	61

5.8	Radial Distribution Function extracted from TUCKERMAN (2010) for a Lennard-Jones fluid with $\sigma = 3.405 \text{ \AA}$ and $\epsilon/k_B = 119.8 \text{ K}$ (Argon).	62
5.9	Radial distribution function $g(r)$ for center of mass distances between asphaltene molecules in heptane (top) and toluene (bottom) at 90 ns. The insets show $g(r)$ at long distances. Different colors represent different mass fractions.	63
5.10	Angle between asphaltene planes. Each asphaltene is represented by the straight lines AB and BC.	64
5.11	Angle distributions histograms for asphaltene solution in heptane for different mass fractions at 90 ns. It is shown that the most part of molecules are stacked parallel to each other.	65
5.12	Angle distributions histograms for asphaltene solution in toluene for different mass fractions at 90 ns. It is shown that the most part of molecules are stacked parallel to each other.	66
5.13	Number of aggregates evolution as a function of time for suspensions in heptane (top) and toluene (bottom). The number of aggregates N is normalized by the initial number of aggregates N_0 . The cutoff distance separation is $1.1 r_c$, in other words if two particles belonging to different molecules are separated by a distance smaller then $1.1 r_c$ these molecules are aggregated.	67
5.14	Average aggregate size S in function of time for asphaltene in heptane (top) and toluene (bottom). S is calculated using Equation 5.14 which takes into account the number of aggregates n_s of s molecules.	69
5.15	Average aggregate size S comparison between solvents for different mass fractions in function of time. Solutions in heptane have larger aggregates, therefore asphaltenes are more diluted in toluene.	70
5.16	Random movements and their MSD . From the left to the right: Isotropic random movement, confined and partially confined. Image obtained from SCHWEIZER (2007).	72
5.17	MSD curves for asphaltene in (top) heptane and (bottom) toluene for different mass fractions. The molecule centroids were used in the MSD calculation (Equation 5.15). The MSD measures the molecule mobility, as it can seen their moviment is being arrested in time.	73

5.18	<i>MSD</i> curves for pure solvent (top) heptane and (bottom) toluene using DPD and Nose Hoover Thermostat.	75
5.19	Application of a linear velocity profile on the simulation box.	76
5.20	Viscosity as a function shear rate for different solvents and mass fractions. Viscosity is calculated dividing the stress by a constant shear rate applied at the box edge in one direction. Shear-thinning behavior has been verified over all shear rates. Lower mass fractions present higher Newtonian behavior.	77
5.21	Snapshot of asphaltene structure with and without shear rate for mass fraction of 0.20 in toluene. (a) Structure acquired after 90 ns of aggregation. (b) Structural breaking with shear simulation, shear started right after aggregation and lasted 90 ns more.	78
5.22	Number of aggregates N against time during simple shear for asphaltenes in heptane at different mass fractions. The number of aggregates is growing which means molecules are being separated. . . .	79
5.23	Number of aggregates N against time during simple shear for asphaltenes in toluene at different mass fractions. The number of aggregates is growing which means molecules are being separated. . . .	80
5.24	Stress and strain curves for oscillatory test. The phase angle δ is related to the observation time, given by $\delta = \omega(t_2 - t_1)$	83
5.25	Strain, Stress (generated by the simulator) and Stress Fitted (calculated using equation $\sigma(t) = \sigma_0 \sin(\omega t + \delta)$ after estimating σ_0 and δ by <i>swarm</i> optimization procedure) curves for small amplitude oscillatory shear applied to asphaltene solution in heptane at 298 K, $X = 0.4$, amplitude deformation = 0.8 \AA , frequency = $6.28 \cdot 10^{11} \text{ rad/s}$. The strain values were multiplied by the edge length of the simulation box, so it has angstrom units.	85
5.26	Linear viscoelastic region for asphaltene in heptane and toluene at different mass fractions and 298 K. Storage modulus G' against strain amplitude at frequency = $6.28 \cdot 10^{11} \text{ rad/s}$. G' is calculated by $G' = \frac{\sigma_0 \cos(\delta)}{\gamma_0}$ after estimating σ_0 and δ by <i>swarm</i> optimization procedure. The strain values were multiplied by the edge length of the simulation box, so it has angstrom units, as a consequence G' , and G'' will have units of stress/length.	86

5.27	Storage (G') and loss moduli (G'') evolution over frequency for asphaltene suspensions at different mass fractions and strain amplitude = 0.5 Å. The strain values were multiplied by the edge length of the simulation box, so it has angstrom units, as a consequence G' , and G'' will have units of stress/length.	87
5.28	Storage (G') and loss moduli (G'') evolution over frequency for asphaltene suspensions at different mass fractions and strain amplitude = 0.5 Å. The strain values were multiplied by the edge length of the simulation box, so it has angstrom units, as a consequence G' , and G'' will have units of stress/length.	88
5.29	Storage (G') and loss moduli (G'') evolution over frequency for asphaltene suspensions at different mass fractions and strain amplitude = 0.5 Å. The strain values were multiplied by the edge length of the simulation box, so it has angstrom units, as a consequence G' , and G'' will have units of stress/length.	89
5.30	Storage (G') and loss moduli (G'') evolution over frequency for asphaltene suspensions at different mass fractions and strain amplitude = 0.5 Å. The strain values were multiplied by the edge length of the simulation box, so it has angstrom units, as a consequence G' , and G'' will have units of stress/length.	90
5.31	Storage (G') and loss moduli (G'') evolution over frequency for asphaltene suspensions at different mass fractions and strain amplitude = 0.5 Å. The strain values were multiplied by the edge length of the simulation box, so it has angstrom units, as a consequence G' , and G'' will have units of stress/length.	91
6.1	Asphaltene molecular structure representation: B bead (blue) represents a moiety of aromatic rings which is the benzene in this approach, H bead (green) represents a butane molecule which forms the alkyl side chains, T bead (red) represents the thioglycolic acid molecule which is the heteroatom group. Each bead corresponds to the volume of 4 water molecules.	98
6.2	Water-octane molecular simulation at the initial step and at the final equilibration step. Water is represented by blue beads, whereas octane by pink beads. Two interfaces naturally form, which leads to a 1/2 multiplication prefactor in Equation 6.3.	101

6.3	Water/hexane IFT calculation for different temperatures using DPD. The black curve is the DPD simulation, and the red curve is the experimental data ZEPPIERI <i>et al.</i> (2001). Standard deviations are shown as error bars.	103
6.4	Water/octane IFT calculation for different temperatures using DPD. The black curve is the DPD simulation, and the red curve is the experimental data ZEPPIERI <i>et al.</i> (2001). Standard deviations are shown as error bars.	104
6.5	Water/dodecane IFT calculation for different temperatures using DPD. The black curve is the DPD simulation, and the red curve is the experimental data ZEPPIERI <i>et al.</i> (2001). Standard deviations are shown as error bars.	105
6.6	Water/decane IFT calculation for different temperatures using DPD. The black curve is the DPD simulation, and the red curve is the experimental data ZEPPIERI <i>et al.</i> (2001). Standard deviations are shown as error bars.	106
6.7	Water/benzene and water/cyclohexane IFT calculation for different temperatures using DPD. The black curves are the DPD simulation, and the red curves are the experimental data MAYORAL and GOICOCHEA (2013). Filled points represent water/benzene data; empty points represent water/cyclohexane data. Standard deviations are shown as error bars.	107
6.8	Radial Distribution Function $g(r)$ for asphaltene in toluene solutions. The interlayer distance between molecular centers d is represented by the first peak distance, which represents the first shell of aggregation. It is seen that for all concentrations, the interlayer distance d is $\sim 5 \text{ \AA}$, which agrees with several molecular dynamics studies (DE OLIVEIRA <i>et al.</i> , 2020a; DUAN <i>et al.</i> , 2017).	109
6.9	MSD curves for asphaltene solutions in toluene at different mass fractions $X = 0.02, 0.05, 0.10,$ and 0.15 . At higher concentrations, the MSD decreases because of lower particle mobility.	110
6.10	Interfacial tension of asphaltenes at the water/cyclohexane interface at 298 K. Results from molecular simulation using DPD/COSMO-SAC. Standard deviations represented by error bars. Red lines to guide the eyes. The CMC is about 48 g/L.	112

6.11	Initial micelle formation of asphaltenes in water/cyclohexane interfaces. That figure shows the water in oil micelle formation with asphaltene concentration = 40 g/L. Oil (cyclohexane) beads have been omitted for better visualization.	113
6.12	Interface formed in the water/cyclohexane system with asphaltene concentration = 125.0 g/L, 298 K. The interface is supersaturated. (left) Asphaltene beads. (right) water beads. Cyclohexane (oil) beads have been omitted for better visualization.	114
6.13	Interface formed in the water/cyclohexane system with asphaltene concentration = 150.0 g/L, 298 K. The surface acquires a complex geometry that resembles droplets of a microemulsion. (left) Asphaltene beads. (right) water beads. Cyclohexane (oil) beads have been omitted for better visualization.	115
6.14	Domain division into slabs for linear density calculations. Density is being calculated along with z axis with Δz accuracy. Each slab has a volume $LxLy\Delta z$, for linear density $Lx = Ly = 1$. Bin b holds all molecules within $b \leq z/\Delta z \leq b + 1$. Figure obtained from GIORGINO (2014).	116
6.15	Linear Density Profile (LDP) for asphaltenes at the water/cyclohexane interface. The asphaltene concentrations is 7.5 g/L. The homogeneity of the two peaks means that the system is well equilibrated with the same number of molecules at each interface.	117
6.16	Linear Density Profile (LDP) for asphaltenes at the water/cyclohexane interface. Concentrations ranging between 7.5-125 g/L. Higher concentrations produce higher peaks at the interfaces and broader distributions (higher standard deviations), as a consequence of the great number of molecules settling at the interfaces.	118
6.17	Schematic representation of the separation angle θ between asphaltene molecular plane α and the interface. The molecular plane vector is defined by \vec{v} (position vector between the first (1 st) and the last particle (16 th) of the polyaromatic nuclei), the vector normal to the interface is \vec{n}	119
6.18	$\langle \theta \rangle$ against asphaltene concentration at the water/cyclohexane interface. $\langle \theta \rangle$ is the ensemble-averaged angle between asphaltene molecular planes and the interfaces.	120

List of Tables

2.1	Solubility parameters via molecular simulation of asphaltenes (ROGEL, 1995). As the aggregate size increases, the solubility parameter decreases.	8
2.2	Cohesion energies $E_{cohesive}$ for asphaltene aggregates according to the Groenzin model as well as the calculated Hildebrand solubility parameters (δ) (Through Molecular Dynamics) and experimental values (δ_{exp}). Obtained from VICENTE <i>et al.</i> (2006).	9
4.1	Final number of clusters for aggregation of Lennard-Jones particles at different volume fractions and temperatures.	41
4.2	Comparison between LAMMPS cluster analysis and the algorithm proposed in this work. 1000 particles were simulated with 1000 timesteps. (1) LAMMPS time duration for simulation running the cluster analysis. (2) LAMMPS time duration for simulation without cluster analysis. Tests were run in serial to avoid parallelism bias. Triplicate has been performed for average and standard deviation calculations. Time in seconds.	45
4.3	Influence of <code>neighboring</code> routine parallelization on its running time for different number of molecules (100 run timesteps). Time in seconds and % of improvement compared to 1 processor. Triplicate has been performed for average and standard deviation calculations. . . .	49
5.1	Hansen solubility parameters (δ^{Hansen}) and molar volume (v) of particles B, H e T at 298 K.	56
5.2	Interaction parameters a_{ij} between particles B,H e T in DPD units. . .	56
5.3	Relaxation modulus $G(t)$ for simple linear viscoelastic models. δ is the Dirac delta function.	81

6.1	Bead sizes of molecules studied in this section, data taken from MULLINS <i>et al.</i> (2006).	99
6.2	Linear relationship between water and alkane bead interaction parameters a_{ij} and the temperature. χ_{ij}^{∞} were calculated before scaling, Equation 6.2. $\chi_{ij}^{\infty}(N_m)$ calculated after scaling, Equation 6.4. a_{ij} calculated using $\chi_{ij}^{\infty}(N_m)$ values in Equation 6.1.	102
6.3	Linear relationship between water and hydrocarbon bead interaction parameters a_{ij} and the temperature. χ_{ij}^{∞} were calculated before scaling, Equation 6.2. $\chi_{ij}^{\infty}(N_m)$ calculated after scaling, Equation 6.4. a_{ij} calculated using $\chi_{ij}^{\infty}(N_m)$ values in Equation 6.1.	105
6.4	The a_{ij} conservative repulsion parameters for the DPD force field between asphaltene and toluene beads. The parameters were calculated using equations 6.2, 6.4, and 6.1. Infinity dilution activity coefficients were taken from JCOSMO (GERBER and SOARES, 2013; SOARES, 2011) at 298.15 K. Results in DPD units.	108
6.5	Diffusion coefficient D for asphaltene solutions in toluene for different mass fractions $X = 0.02, 0.05, 0.10,$ and 0.15 . D values are higher for low concentrations as a consequence of higher mobility. Low concentration D values are within the experimental range $2.2\text{-}6.3 \cdot 10^{-10}$ m^2/s (ANDREWS <i>et al.</i> , 2006; ÖSTLUND <i>et al.</i> , 2003).	110
6.6	The a_{ij} conservative repulsion parameters for the DPD force field between asphaltene, water, and cyclohexane beads. The parameters were calculate using equations 6.2, 6.4, and 6.1. Infinity dilution activity coefficients were taken from JCOSMO GERBER and SOARES (2013); SOARES (2011) at 298.15 K. Results in DPD units.	111

List of Symbols

D	Diffusion Coefficient, p. 71
$D(t)$	Diffusion Coefficient as a Function of Time, p. 71
D_0	Diffusion Coefficient of a Isolated Particle, p. 72
$G''(\omega)$	Viscous or Loss Modulus, p. 81
$G'(\omega)$	Elastic or Storage Modulus, p. 81
$G(t)$	Relaxation Modulus, p. 81
G_0	Elastic Modulus, p. 81
N	Number of Aggregates, p. 66
$N(r)$	Number of Particles found in each Spherical Shell of Average Radius r , p. 60
N_w	Number of Water Molecules in a DPD Particle, p. 55
Q	Canonical Partition Function, p. 24
R	Gas Constant, p. 56
S	Average Aggregate Size, p. 66
U	Interparticle Interaction Potential, p. 19
V_c	Volume of a Spherical Shell, p. 61
ΔG_{ag}	Aggregation Free Energy, p. 11
Δ	Partition Function of Isothermal-Isobaric Ensemble, p. 25
Ω	Degeneracy, p. 24
α	α Relaxation Time, p. 81

β	β Relaxation Time, p. 81
\mathbf{F}_{ij}^C	Conservative Force between DPD Particles i and j, p. 26
\mathbf{F}_{ij}^D	Dissipative Force between DPD Particles i and j, p. 26
\mathbf{F}_{ij}^R	Random Force between DPD Particles i and j, p. 26
\mathbf{F}_i	Force Vector over Particle i, p. 19
\mathbf{a}_i	Acceleration Vector of Particle i, p. 19
\mathbf{r}_i	Position Vector of particle i, p. 19
\mathbf{v}_i	Velocity Vector of Particle i, p. 19
χ	Flory-Huggins Interaction Parameter, p. 55
δr	Separation Distance, p. 60
δt	Time Step, p. 27
$\delta(t)$	Dirac Delta, p. 27
δ_i^{Hansen}	Hansen Solubility Parameter of Particle i, p. 56
δ_{ij}	Kronecker Delta, p. 27
$\dot{\gamma}$	Shear Rate, p. 76
ϵ	Potential Well Depth for a Lennard-Jones Fluid, p. 12
η	Viscosity, p. 72
$\gamma(t)$	Strain, p. 83
γ_0	Maximum Strain Amplitude, p. 81
γ_{DPD}	DPD Dissipative Force Parameter, p. 27
κ	Dimensionless Isothermal Compressibility, p. 26
μ	Chemical Potential, p. 24
ω	Oscillation Frequency, p. 81
$\omega^C(r_{ij})$	Conservative Weight Function, p. 26
$\omega^D(r_{ij})$	Dissipative Weight Function, p. 27

$\omega^R(r_{ij})$	Random Weight Function, p. 27
$\phi(r_{ij})$	Interaction Energy between Particles, p. 20
$\rho(r)$	Radial Numerical Density, p. 61
ρ	Numerical Density of the Simulation Box, p. 55
$\sigma(t)$	Stress, p. 80
σ	Diameter of a Lennard-Jones Particle, p. 12
σ_{DPD}	DPD Random Force Parameter, p. 27
τ_{xy}	Shear Stress, p. 76
ζ_{ij}	Gaussian Random Number, p. 27
a_{ij}	Maximum Repulsion Parameter between DPD Particles i and j, p. 26
$g(r)$	Radial Distribution Function, p. 60
k_B	Boltzmann Constant, p. 27
m	Mass of a DPD Particle, p. 55
m_i	Mass of Particle i, p. 19
m_{H_2O}	Mass of a Water Molecule, p. 55
r_c	Cutoff Radius, p. 20
v_{ij}	Average Molar Volume between the Particles i and j, p. 56
N	Number of Particles, p. 23
P	Pressure, p. 24
S	Entropy, p. 24
T	Temperature, p. 24
V	Volume, p. 24
A	Helmholtz Free Energy, p. 24
E	Internal Energy, p. 25
G	Gibbs Free Energy, p. 25
H	Enthalpy, p. 25

List of Abbreviations

$E_{cohesive}$	Cohesion Energy, p. 9
ADBS	Dodecyl Benzene Sulfonic Acid, p. 15
GPU	<i>graphics processing units</i> , p. 13
GROMOS	Groningen Molecular Simulation, p. 13
LVR	Linear Viscoelastic Region, p. 80
MD	Molecular Dynamics, p. 19
NPT	<i>Isothermal–Isobaric Ensemble</i> , p. 25
NVE	<i>Microcanonical Ensemble</i> , p. 24
NVT	<i>Canonical Ensemble</i> , p. 24
PMF	Mean Force Potential, p. 11
RDF	<i>radial distribution function</i> , p. 60
RMQ	Quantitative Molecular Representation, p. 10
SAFT	<i>Statistical Associating Fluid Theory</i> , p. 6
SARA	Saturated, Aromatic, Resins and Asphaltenes, p. 14
SRD	<i>Stochastic Rotation Dynamics</i> , p. 14
LAMMPS	<i>Large-scale Atomic/Molecular Massively Parallel Simulator.</i> , p. 22
MSD	<i>Mean Square Displacement</i> , p. 71

Chapter 1

Introduction

1.1 Motivation

During oil extraction and processing there is a high concern about the heavier fractions of oil called paraffins and asphaltenes. The study of the phase behavior of these molecular aggregates is fundamental for the oil industry, notably in flow assurance (ROGEL *et al.*, 2016). In Brazil, the investments to develop new technologies to mitigate precipitation of solids and thus to guarantee oil production and processing increased considerably in the past years (LEITE *et al.*, 2006). Asphaltenes and paraffins are known to cause problems related to deposition in pipelines (CARAUTA *et al.*, 2005; ROGEL *et al.*, 2001). Asphaltene suspensions are systems in which more than one phase coexist, those systems are called complex fluids.

Due to the difficulty of exactly identifying the asphaltene molecule structure in solution, they are commonly classified by means of their solubility. Asphaltene is the oil fraction that is soluble in aromatic solvents and insoluble in aliphatic solvents. Because of their molecular weight and structure, they are susceptible to aggregation, flocculation, and deposition processes (HEADEN *et al.*, 2017). Those molecular aggregates are also known to be related to the rheology, dispersivity, and stabilization of water-in-oil emulsions. Experimental techniques have not been able to decipher the aggregation mechanisms or the phase behavior of asphaltenes yet, due to the great complexity and large number of possible components in solution. One of the most cited aggregation model is the Yen-Mullins model (MULLINS, 2010). According to this model, the asphaltene molecules are represented by polyaromatic nuclei (surrounded by aliphatic chains) that aggregate forming nanoaggregates which in turn also aggregate forming clusters, see Figure 1.1. According to this model, six asphaltene molecules form the nanoaggregates while approximately eight nanoaggre-

gates form one cluster (MULLINS, 2010). Experimental results of electrical conductivity (ZENG *et al.*, 2009) and magnetic nuclear resonance (FREED *et al.*, 2009) indicate that the number of nanoaggregates in one cluster would be 4-8, neutron scattering (HOEPFNER and FOGLER, 2013) data indicate that it would be 3-5.

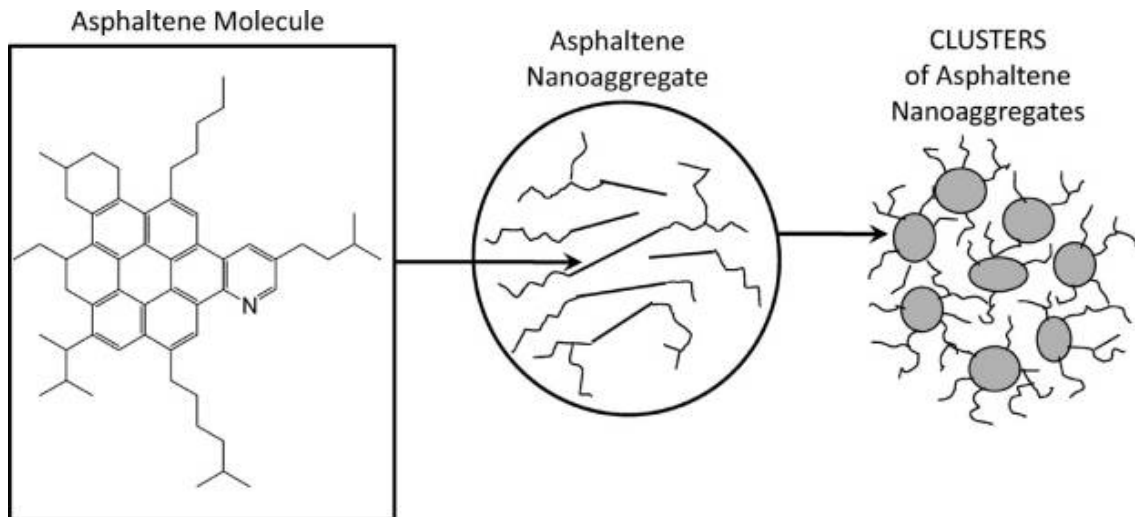


Figure 1.1: Aggregation hierarchy according to the Yen-Mullins model. Asphaltene molecules aggregate first into nanostructures. These nanoaggregates form clusters. (MULLINS, 2010)

Generally, asphaltenes consist of aromatic rings (rings containing heteroatoms are also found) condensed and attached to aliphatic branches. The central aromatic rings are responsible for intermolecular interactions. As those molecules are polarizable, dipole-induced dipole interactions emerge. In addition to this type of interaction, dipole-dipole interactions also arise due to the heteroatoms present in asphaltenes. These interactions are believed to be responsible for aggregation between molecules. Moreover, steric hindrance from the alkane branches counteracts the attraction of the molecule centers and prevents them from approaching. The balance between the attraction and repulsion forces gives the solubility characteristics of asphaltenes.

The attraction forces give rise to the approaching tendency that those molecules present in solution which generate the nanoaggregates and the clusters consequently. As the aggregation process proceeds, these clusters tend to precipitate. In the early stage of the precipitation process, this new phase forms a gelled structure that ages over time becoming a solid that clogs pipes and processing units. Although the thermodynamic studies on asphaltenes and paraffin precipitation are numerous, there are still few studies involving the kinetic part, mainly regarding to the aging mechanism of paraffin and asphaltene aggregates.

Asphaltene deposition is a very important industrial and scientific problem.

Ensuring safe and economically viable oil production requires, as a design basis, a good predictive model and a good understanding of the initial stages of the solid formation, precipitation, and agglomeration in order to meet economic and process safety requirements. Despite the industrial importance, because it causes huge losses, the understanding of the formation of these aggregates is precarious. Experimental and theoretical studies do not converge completely on the asphaltene nature as well as in determining their macroscopic properties. In this context, molecular simulation techniques have emerged in order to expand/improve the knowledge about the mechanisms of aggregation/deposition of asphaltenes. It is known that this phase transition occurs on large time scales (HEADEN *et al.*, 2017), therefore a mesoscale molecular dynamics strategy is required.

In this context, the aim of this work is to apply a mesoscale simulation method to study the characteristics of asphaltene molecules both in bulk phase and in the water/oil interface. Here, the DPD (*Dissipative Particle Dynamics*) mesoscale approach has been used, it will be better discussed in the Method section. A method of counting/detecting clusters of particles should be developed to identify molecule agglomerates. In bulk phase, it is necessary to investigate the structural, dynamical, and rheological behavior of those systems. It is also important to verify whether the asphaltene molecule model proposed here is able to capture the surfactant properties at the water/oil interface.

1.2 General and Specific Objectives

The general objective of this work is to comprehend the bulk and interfacial characteristics of asphaltene aggregation via molecular simulation. Among the specific objectives, we can mention:

1. Implementation of a new algorithm to better count and detect clusters of particles;
2. Radial Distribution Function of asphaltene molecules in bulk phase to analyze the structure of the asphaltene aggregates and calculate the distance between their molecular centers;
3. Contact Angle between asphaltene molecules in bulk phase to verify the preferential orientation of asphaltene molecules in the aggregates, and the analysis of Aggregate Average Size of asphaltene molecules in bulk phase to study the interaction between particles as a function of asphaltene concentration and solvent quality;

4. Number of Clusters of asphaltene molecules in bulk phase to study the asphaltene affinity with the solvents, and Mean Squared Displacement of asphaltene molecules in bulk phase to analyze the asphaltene mobility in the solutions;

5. Viscosity of asphaltene suspensions to analyze the suspension resistance to flow as a function of concentration and solvent quality, and Loss and Storage moduli of asphaltene molecules in bulk phase to study the viscoelastic behavior of asphaltene suspensions at the initial stages of aggregation;

6. Interfacial Tension between water/hydrocarbons using DPD/COSMO SAC to verify if the proposed model is able to capture the experimental data;

7. Radial Distribution function of asphaltene suspensions using DPD/COSMO SAC to verify if the proposed model is able to capture the experimental distance between asphaltene molecular centers, and Diffusion Coefficient of asphaltene molecules using DPD/COSMO SAC to verify if the proposed model to capture the experimental diffusion coefficient of diluted asphaltenes in toluene;

8. Interfacial Tension of the water/oil interface containing asphaltenes, using DPD/COSMO SAC to study the asphaltene surfactant properties;

9. Linear Density Profile of asphaltene molecules at the water/oil interface using DPD/COSMO SAC to analyze the asphaltene concentration at the interface, and Contact Angle between asphaltene molecules and water/oil interface using DPD/COSMO SAC to analyze the asphaltene angle distribution at the interface;

1.3 Thesis Structure

This document consists of seven chapters followed by two appendices. Introduction, motivation, and goals are presented in Chapter 1.

Chapter 2 presents a literature review of asphaltene studies. In Chapter 3 we discuss some methods of molecular simulation.

In Chapter 4, we present a new methodology of counting/detecting clusters that has been developed and verified. (DE OLIVEIRA *et al.*, 2020b)

In Chapter 5, the simulations in bulk phase are presented. (DE OLIVEIRA *et al.*, 2020a)

In Chapter 6, the simulations at the water/oil interface are showed. (DE OLIVEIRA *et al.*, submitted)

In Chapter 7, we present the conclusions and the proposals for future work,

respectively.

In appendix A, a 3D Linear Regression procedure is showed.

In appendix B, the developed clustering algorithm is fully described.

Chapter 2

Literature Review

2.1 Asphaltene Aggregation and Modeling Strategies

Asphaltenes are a group of petroleum compounds that represent its heaviest and polar fraction that are greatly susceptible of aggregating, and flocculating (HEADEN *et al.*, 2017).

Asphaltene molecules may be composed of condensed polyaromatic nuclei or polyaromatic nuclei separated by aliphatic chains. In the first, case we say that the molecule has a "continental" or "island" structure, in the second case, it has an "archipelago" structure (KUZNICKI *et al.*, 2008).

There are two main ways in which asphaltenes can form aggregates. Firstly, the molecule planes align parallel to each other, in this case we say that there is a face-to-face stacking. Secondly, the molecule planes form a 90° angle, in this case there is a T-shaped stacking (SONG *et al.*, 2016). Molecular planes are not exactly parallel during face-to-face stacking, usually there is an *offset* between the geometric center of the molecules.

In the following, some strategies that have been/are employed over the years to analyze the aggregation process of asphaltene suspensions are discussed.

2.1.1 Development of Equations of State

Attempting to describe the macroscopic effect of the asphaltene aggregation process, equations originated from macromolecules and polymers such as SAFT (statistical associating fluid theory) and its modifications were used to a complex system

of hydrocarbons containing asphaltenes (PUNNAPALA and VARGAS, 2013). ARTOLA *et al.* (2011) used the SAFT to explain the precipitation boundary of a simple fluid model. They reported that the precursor to asphaltene precipitation is a liquid-liquid phase separation due to demixing in the fluid. WU *et al.* (1998) used the SAFT model in the framework of McMillan-Mayer theory considering hard sphere repulsive forces, association and dispersion-force interactions. Asphaltenes and resins were considered pseudo-pure components, while the other components were treated as the continuous medium. They were able to explain several experimental observations by considering the asphaltene precipitation as a liquid-liquid equilibrium process.

FIGUERA *et al.* (2010) proposed to use Peng-Robinson equation which allowed to estimate critical properties of the precipitated fraction besides the usual characterization of the heavy fraction, C7+. The difficulty of obtaining an equation of state that adequately represents the complex equilibrium of the crude oil mixture lies precisely in managing the heavier fraction and obtaining its critical properties. In the case of asphaltenes, for example, they decompose before reaching the estimated critical temperature for the heavy fraction. As long as there is no way to properly incorporate these macromolecules, the equations of state will tend to underestimate or overestimate the precipitation conditions.

DUDA and LIRA-GALEANA (2006) developed a simplified analytical solution for the Ornstein-Zernick associative integral equation with the Percus-Yevick approximation for determining structural properties and phase separation of asphaltene models. They studied the effects of pressure, temperature and composition. Asphaltenes were treated as rigid spheres with specific points of association at their interface.

VARAMESH and HOSSEINPOUR (2019) used Cubic Plus Association equation of state (CPA EoS) to predict the asphaltene precipitation in the presence/absence of nanoparticles (Fe_3O_4 and NiO). By knowing the average aggregate size of asphaltene molecules, the CPA EoS was used to determine the amount of asphaltene precipitate. An exponential relationship between the asphaltene self-association energy and the molar density of the surface sites was found in the presence of nanoparticles.

ARYA *et al.* (2017) calculated the asphaltene precipitation onset using different CPA EoS. With the addition of precipitant (n-pentane to n-hexadecane), they fitted a single model parameter. They compared the results with experimental data. They also used Perturbed Chain Statistical Associating Fluid Theory (PC-SAFT) EoS in seven crude oils. PC-SAFT was compared to CPA EoS, the latter showing better

results. PC-SAFT produced some unphysical results.

The main problem with using a classical equation of state lies in the fact that it is unable to describe the asphaltene aggregation and the initial stages of the gel-like structure. Another problem with using equations of state (both classical and perturbation theory-based) is that this macroscopic approach does not allow to relate the structure and the properties; it does not explain the various aspects related to asphaltene deposition problems.

2.1.2 Atomistic Molecular Simulation

ROGEL (1995) investigated asphaltene aggregation by Molecular Dynamics from two predefined structures. Through a combination of Molecular Mechanics and Molecular Dynamics they optimized two possible asphaltene structures. Then, they performed Molecular Dynamics of the two structures in toluene and heptane. From the interaction energies obtained by Molecular Dynamics, the Hildebrand solubility parameters were calculated. The solubility parameter of asphaltene aggregates decreased with increasing the number of aggregates. In heptane, the solubility parameters suggest that the degree of aggregation could generate particles large enough to sediment. Table 2.1 shows the solubility parameters for different aggregates.

Table 2.1: Solubility parameters via molecular simulation of asphaltenes (ROGEL, 1995). As the aggregate size increases, the solubility parameter decreases.

Material	Aggregation state	Solubility Parameter (MPa ^{1/2})	Standard Deviation (MPa ^{1/2})
Asphaltene A	Monomer	18.11	0.3
	Dimer	15.13	0.56
	Trimer	13.46	0.77
	Tetramer	13.05	0.67
Asphaltene B	Monomer	14.42	0.37
	Dimer	15.28	0.35
	Trimer	13.93	0.44

ROGEL and CARBOGNANI (2003) studied a great diversity of asphaltenes in an attempt to estimate their densities. They considered asphaltenes with a large number of condensed aromatic rings (up to 22), the density values obtained were lower than those provided by experimental analysis.

MURGICH *et al.* (1996) carried out micelle formation studies on asphaltenes/resins by Molecular Mechanics and found that asphaltene aggregation occurs

mainly by the approximation of polyaromatic nuclei. They used continental asphaltenes with up to 24 aromatic nuclei.

PACHECO-SÁNCHEZ *et al.* (2003) found via Molecular Dynamics that even small asphaltene structures form dimers, trimers and tetramers on short time scales. Several aggregate formats were verified without predominance of any aggregate type. They also analyzed the structure of asphaltenes in the solid phase, the calculated structure factor corresponded to the literature data (PACHECO-SÁNCHEZ *et al.*, 2004a). PACHECO-SÁNCHEZ *et al.* (2004b) studied the effect of pressure on asphaltenes aggregation according to the Groenzin-Mullins model. By means of *NPT* simulation, they observed that the asphaltene aggregate dissociates with increasing pressure. Aggregates showed face-to-face stacking with an *offset* between their molecular centers, they also observed an average separation of 3.8 Å between the molecular planes.

Using the Groenzin-Mullins model, VICENTE *et al.* (2006) calculated the enthalpy and cohesion energy ($E_{cohesive}$) by Molecular Dynamics for the estimation of the Hildebrand solubility parameter. Their results are close to the literature ones. Table 2.2 shows the calculated values of cohesion energy (function of the enthalpy of mixture) as well as the calculated (δ) and experimental (δ_{exp}) solubility parameters.

Table 2.2: Cohesion energies $E_{cohesive}$ for asphaltene aggregates according to the Groenzin model as well as the calculated Hildebrand solubility parameters (δ) (Through Molecular Dynamics) and experimental values (δ_{exp}). Obtained from VICENTE *et al.* (2006).

Molecule	$E_{cohesive}(10^{-8} \text{ J/m}^3)$	δ (MPa ^{1/2})	δ_{exp} (MPa ^{1/2})
Asphaltene	3.3972±0.0229	18.4314±0.0622	20-22
Toluene	3.3882±0.1178	18.4044±0.3232	18.3
Benzene	3.3589±0.1470	18.8078±0.3957	18.7
Pyridine	4.5284±0.1652	21.2766±0.3885	21.7
n-Pentane	2.0661±0.5222	14.3731±0.1828	14.4
n-Hexane	2.2321±0.0813	14.9379±0.2752	14.9
n-Heptane	2.3446±0.0983	15.3088±0.3258	15.3

CARAUTA *et al.* (2005) simulated (100 ps) asphaltene dimers and found that they bind face-to-face at a distance of 3.6 Å and 5 Å in heptane and toluene, respectively. They found that increasing temperature decreases this distance.

ZHANG and GREENFIELD (2007a,b,c) performed molecular simulation of an asphaltene solution model as a ternary mixture of asphaltenes, resins and maltenes. For the asphaltenes they used the Groenzin-Mullins model and the ARTOK *et al.*

(1999) model. By pyrolysis, nuclear magnetic resonance spectroscopy, and gel permeation they studied the morphology of asphaltene molecules. The simulations were used to estimate dynamic properties such as viscosity and diffusion. They were able to find values close to the literature with one order of magnitude of difference.

KUZNICKI *et al.* (2008); UNGERER *et al.* (2014) conducted studies investigating differences between molecules with different geometries. KUZNICKI *et al.* (2008) performed simulations of twelve continental asphaltene and twelve archipelago-shaped asphaltene (small condensed aromatic nuclei connected) in three different solvents: water, toluene and heptane. Their continental structures could also contain COO^- groups, in this case they are called anionic continentals. The aggregates formed in the three different solvents had similar structures, however with different aggregation intensities, the less polar the solvent the higher the aggregation level.

UNGERER *et al.* (2014) simulated asphaltene with continental or archipelago structures consistent with oil from the arabic region. A continental structure with only eight aromatic rings and another with fifteen aromatic rings have been used. An archipelago structure with three polyaromatic nuclei was also studied. It was observed that there was an aggregation limit for the archipelago model and an "irreversible" aggregation for the continental model of fifteen aromatic rings in both toluene and heptane.

Faced with the difficulty of knowing the exact asphaltene molecule structure, some methods have emerged trying to circumvent this problem. One of the most used is called Quantitative Molecular Representation (RMQ) (SHEREMATA *et al.*, 2004). This method uses small possible asphaltene structures that are linked together through a connection algorithm, thus forming large asphaltene molecules. A minimization algorithm is used, it chooses from those large structures the ones that most closely resemble experimental structures. The disadvantage of this method comes from the need of small pieces of asphaltene that are not exactly real. The fact that it requires experimental data makes the method questionable, as it is hard to determine asphaltene structures experimentally.

HEADEN *et al.* (2009) generated three mixed structures (they merged archipelago and continental structures) by means of RMQ based on experimental nuclear magnetic resonance data from Atabasca bitumen. The molecular weight of 750 Da was considered as the weight reference. From each structure model, six distinct asphaltene molecules were generated which were then simulated in heptane and toluene. Reversible aggregation was observed with reforming aggregates every

20 ns (approximately).

SEDGHI *et al.* (2013) have taken as benchmark the work of HEADEN *et al.* (2009) to study the effects of structural changes. They maintained the same asphaltene concentration as in the original work and observed the formation of nanoaggregates that later formed clusters. They used the *Umbrella Sampling* method (Alternative to the mean force potential method (PMF)) to calculate the dimer formation free energy for each type of asphaltene structure. They concluded that the size of the aromatic ring is the main factor in the aggregation free energy.

As the asphaltenes are the main stabilizers of the water in oil emulsions in the petroleum industry, LV *et al.* (2017) performed molecular dynamics of asphaltenes at the water-oil interface to study their interfacial properties. The stability of asphaltenes at the interface depends on the hydrogen bonds around their polar groups. The bonds serve as anchors that hold the asphaltene molecules at the interface. The properties of asphaltenes at the interface have also been studied using *Umbrella Sampling*. The aggregated state has been found to be more stable for asphaltenes at the interface and the aggregates breakdown increases the free energy of the system.

The asphaltene-asphaltene interaction energy is the sum of Van der Waals, dipole-dipole, induced dipole-dipole, electrostatic and hydrogen bond interactions between two asphaltene molecules. For many models, this energy ranges from -89 kJ/mol (ROGEL, 2000) to -372 kJ/mol (MURGICH *et al.*, 1996). That energy does not include free energy contributions due to solvent-asphaltene interactions or entropic contributions. Aggregation Free Energy ΔG_{ag} includes direct asphaltene-asphaltene contributions and indirect solvent-asphaltene contributions. (HEADEN *et al.*, 2009) calculated the mean force potential between asphaltene molecules through a series of simulations using a *SHAKE* algorithm to keep the asphaltene molecules at a fixed distance. The mean force potential (or the free energy of aggregation) is calculated from the force required to maintain the asphaltene molecules at a fixed distance. SEDGHI *et al.* (2013) used *Umbrella Sampling* method to calculate the dependence of ΔG_{ag} on the separation distance between two asphaltene molecules. They used a spring potential to keep asphaltene molecules within a separation range. The results of both approaches were similar: The heptane solutions showed higher free energy of aggregation, which is in agreement with experimental data. They also performed simulations containing 36 explicit asphaltene molecules (7% by weight) in heptane for 80 ns. At this time scale, complete aggregation occurs. About 20 ns, the first clusters appear containing nanoaggregates of five to ten molecules. HEADEN *et al.* (2017) performed simulations up to 500 ns in toluene and heptane. In toluene, there were no important structural changes between 100 ns and 500 ns. However, in heptane, there was a large increase in the

cluster size. In their simulation, they used a, 80 Å cubic box; however light scattering data provides a radius of gyration for asphaltene molecules around 50 Å, which means that a simulation box of at least 200 Å would be required in each direction to neglect size effects. The main conclusion is that larger time and length scales are needed. For this goal, there are coarse-graining techniques. In coarse-graining methods a group of atoms is grouped into a single particle, which allows to simulate larger time scales with some microscopic detail loss of the simulated system.

2.1.3 Molecular Mechanics and *Coarse-Graining*

ORTEGA-RODRÍGUEZ *et al.* (2003) used Molecular Mechanics to generate asphaltenes and resins structures that were simulated in a continuous medium of fixed dielectric constant. They considered both asphaltene and resin molecules to be single particles and an effective spherical potential (ORTEGA-RODRIGUEZ *et al.*, 2001). They observed that the resins peptide during the simulation and stable clusters appear in toluene.

AGUILERA-MERCADO *et al.* (2006) proposed a model in which resins are represented by spheres, and asphaltene molecules by a central sphere of type 1 surrounded by six spheres of type 2. Particle interactions were accounted for by the Lennard-Jones potential, with specific literature parameters for each type of interaction. The medium was modeled as continuous by a "screening factor" defined by the Hamaker and dielectric constants. They studied the effects of temperature, resin and asphaltene concentrations on the aggregation process. They found that different forms of aggregates can emerge, besides the well-known linear aggregate of condensed aromatic nuclei.

Another coarse-graining model was proposed by JOVER *et al.* (2015) in which all C_6 segments were treated as Lennard-Jones particles; the solvent was treated as Lennard-Jones spheres. The ϵ and σ parameters were chosen to reproduce the experimental density of the liquid solution phase. The solvent was considered pure and the relationship between the solvent nature and the aggregate formation process was investigated. In toluene, the asphaltenes have been found to be soluble, while in heptane, they strongly aggregate.

WANG and FERGUSON (2016) proposed another *coarse-graining* model aiming to simulate microsecond time scales. Through the RMQ, technique they found three structures that were simplified. The *coarse-graining* strategy used was the Martini (MARRINK *et al.*, 2004) force field, typical of lipids, carbohydrates, proteins, polymers, organic liquids, fullerenes and carbon nanotubes (MARRINK and

TIELEMAN, 2013). Heptane and toluene were used as solvents which were simulated by the GROMOS 54A7 force field (SCHMID *et al.*, 2011). They simulated temperature range from 250 K to 450 K. During the simulation, they found out that nanoaggregates formed clusters, according to the Yen-Mullins model. Their conclusion is that at moderate concentrations different cluster types emerge. At high concentrations, a percolated structure emerges with rod-shaped clusters.

ÅSMUND ERVIK *et al.* (2017) developed a Python code named raaSAFT that is appropriate to the setup and running of coarse-grained molecular simulations. Because of the use of SAFT-Mie force field, the coarse-grained pair potentials are closely related to the macroscopic thermodynamic properties of the fluid. They were able to simulate the liquid–liquid equilibrium of a hydrocarbon with water using that code. A large polymer-solvent mixture consisting of 300 polystyrene molecules in 42700 molecules of heptane has also been simulated, the results reproduced well the experimental solubility of the polystyrene.

JIMENEZ-SERRATOS *et al.* (2019) used coarse-grained force fields using the statistical associating fluid theory (SAFT-) EoS, giving a good insight on relating the molecular description and thermophysical data. They constructed asphaltene models by combining different chemical moieties in a group-contribution fashion. The coarse-grained results reproduced well the results of a fully atomistic simulation in terms of cluster size, radii of gyration, and relative-shape-anisotropy-factor distributions.

2.1.4 DPD (*Dissipative Particle Dynamics*)

XU *et al.* (2011) performed simulations of the asphaltene aggregation process (considering resins in the solution) using the DPD strategy, which is also a coarse-grained technique allowing to reach the mesoscale. They used GPU (*graphics processing units*) to improve computational efficiency. They treated aromatic rings as rigid bodies and also observed the formation of face-to-face, offset and T-shaped structures. They obtained an average distance between molecules of 3.6 Å, which agrees with several other studies. The size of the selected clusters is independent of the asphaltene concentration since the resin concentration is high enough. The lower the ratio of saturated/aromatic rings, the more stable the solution. WANG *et al.* (2014) studied the asphaltene aggregation process and molecule diffusion in a solution using DPD integrated with the quaternions (KARNEY, 2007) method in GPUS. They could increase the efficiency by some orders of magnitude in terms of computational time. Using this methodology, simulation of large systems of asphaltene molecules diluted in toluene was possible. They calculated diffusion coefficients ac-

ording to the experimental data. They simulated asphaltene in heptane and found that the system behaves as the Yen-Mullins model, in which the monomers join in nanoaggregates that later form clusters.

ALVAREZ *et al.* (2010) performed molecular simulations of polymer/oil/water emulsions using the DPD approach. Particle interactions were treated using the correlation between the Flory-Huggins solubility parameter and the DPD conservative force parameter (GROOT and WARREN, 1997). Solubility parameters were taken from atomic and molecular models of prototype molecules. The composition of the oil used was the same as in the Mexican heavy oil. For short polymers, coalescence between droplets is disadvantaged because polymers form a film around water molecules.

BOEK *et al.* (2010), using a multi-scale approach, studied asphaltene aggregation and deposition under flow conditions. For the solvent, they used *Stochastic Rotation Dynamics* (SRD), which provides the hydrodynamics and Brownian motion of the medium, while asphaltenes were treated as colloidal spheres that interact by a coulombic potential. The parameters of the macroscopic model were taken from atomistic molecular simulations. Molecular structures were generated by RMQ. The potential of mean force between asphaltene molecules at intermediate distances is proportional to $-1/r^2$. This suggests that asphaltene molecules at short distances tend to align. Another observation of this work is that lubrication layers should appear due to small solvent particles that generate a shielding of colloid-colloid interactions.

CHEN *et al.* (2017a) used DPD to investigate the aggregation process and orientation of asphaltene molecules at the water-oil interface of crude oil emulsions in the mesoscale. Initially, they observed that from a disordered configuration, asphaltenes quickly formed nanoaggregates. All nanoaggregates presented face-to-face structure. At the water-oil interface, continental asphaltenes prefer to orient perpendicularly while archipelago-shaped ones orientate parallel to the interface. These nanoaggregates form a protective film at the interface. As the size of the aliphatic chains of asphaltenes increases, the π - π stacking is disadvantageous. LIU *et al.* (2015) carried out a similar study, but after the building of the asphaltene layer on water, they used ethyl cellulose molecules to promote demulsification.

REZAEI *et al.* (2016) used DPD to study the behavior of different polyaromatic surfactant molecules (which resemble asphaltenes) at the water-oil interface. They have the same polyaromatic nucleus but different endings. The compositions used correspond to those of petroleum (by SARA analysis) of the Persian Gulf; the chosen temperatures were 298 K and 363 K. The DPD interaction parameters

were evaluated according to the known correlation with the Flory-Huggins solubility parameter (GROOT and WARREN, 1997). As the temperature increased, they realized that there was a delay in oil-water separation. Surfactants with more aliphatic terminations showed better performance in reducing surface tension at the water-oil interface.

RUIZ-MORALES and MULLINS (2015) studied the preferential orientation of an asphaltene monomer at the water-oil interface using DPD. Toluene was used to model the oil phase. The simulation began in three distinct ways: with perpendicular monomer, parallel, and with an angle of 45° to the interface. In all situations, the polyaromatic nucleus was parallel to the interface while the aliphatic chains were perpendicular.

Using experimental data from ACEVEDO *et al.* (2010), SILVA (2015) created a model for asphaltene solutions. These systems were modeled by DPD, where each DPD particle corresponds to one of the structures in solution. The experimental solubilities were used to calculate Flory-Huggins solubility parameters, which according to the GROOT and WARREN (1997) method were used to calculate DPD repulsion parameters. For different solvents the interfacial tension between asphaltene and solvent was measured during the simulation. High surface tension values were obtained for decane and pentane (phase separation) and low values for toluene and benzene, indicating dissolution in aromatic solvents.

Adsorption studies of asphaltene on polar substrates were performed by SKARTLIEN *et al.* (2016) using continental asphaltene models. The authors tested solutions with weight percent in the range 10-20%. The structure of the adsorbed surface was very sensitive to the presence of polar groups in the alkyl radicals as well as to the central heteroatoms. Asphaltene monomers irreversibly adsorb on the substrate by the polar group in their branch. In heptane, aggregation occurred with a π - π stacking between aromatic nuclei. When the branches showed no polar groups only the heteroatoms in the core had an affinity with the substrate, but the central polyaromatic core showed no orientational preference. An important result is that as asphaltene molecules connect to the substrate, they shield the interactions of free asphaltene with the substrate, making adsorption of the remaining molecules more difficult, this leads to the generation of a monolayer around the substrate. The general conclusion is that the number and position of the polar groups of the asphaltene branches determine the degree of adsorption/aggregation for continental asphaltene.

The kinetic effects of Dodecyl Benzene Sulfonic Acid (ADBS) on the aggregation of asphaltene molecules were studied by SKARTLIEN *et al.* (2017) using

DPD. In the absence of inhibitors, the aggregation is initiated by kinetic/diffusive capture between polar branches rather than by interactions between aromatic nuclei. The main reason for this should be the fact that branches have greater mobility than heavy aromatic nuclei. ADBS molecules contain polar groups that bind to the asphaltenes' polar branches, making them heavier and then suppressing the onset of aggregation. Another amphiphilic inhibitor without an aromatic ring was tested and resulted in a higher aggregation rate. Asphaltenes adsorption on a polar surface was disfavored by the presence of substrate-bounded ADBS, occupying a large portion of its area, forming a monolayer.

SONG *et al.* (2016), using DPD, studied the effects of shear on the aggregation of asphaltene molecules in heptane. Continental and archipelago-shaped molecules were generated. Archipelago-like molecular structures formed more compact structures due to inter and intramolecular interactions. Without a flow field, it was observed that the nanoaggregates arrange in either T-shaped or face-to-face clusters. With the advent of shear, these clusters were broken. The radii of gyration of continental asphaltenes ranged from 8.43 Å to 8.75 Å under different shear rates. The radius of gyration of archipelago-shaped structures has greatly increased when the shear rate is close to 0.1 ps⁻¹, with an average value of 22.4 Å when the shear is greater than 0.2 ps⁻¹. This indicates that archipelago-shaped asphaltenes are elongated as shear occurs. Viscosity decreases with increasing shear rate as larger clusters are destroyed.

In order to know the influence of lighter hydrocarbon fractions on the rheology of asphaltenes solutions, WANG *et al.* (2015) performed DPD simulations. The addition of lighter fractions decreased the viscosity of the medium. The pseudo-plastic behavior of the solutions decreases as the lighter fraction increases. It was noticed that the flow influenced both the aggregation and the spatial orientation of the asphaltenes. The relationship between viscosity and asphaltene mass fraction in emulsion systems was also studied. In all emulsions studied, increasing the asphaltene content increased the viscosity of the solutions. The surfactant nature of asphaltenes has also been studied, showing that they are excellent surfactants of oil-water emulsions.

To explore the behavior of asphaltene aggregates in heavy oils at the mesoscale, ZHANG *et al.* (2010) conduct a study using the DPD approach. Rigid bodies are used to display the aromatic rings of resins and asphaltenes. The model molecules and interaction parameters were taken from previous work (ZHANG *et al.*, 2010). Face-to-face aggregates were observed, with a distance between layers and ordering that correspond to other simulations and results from x-ray data and transmission electron microscopy. A relationship between stability and component ratio fractions

was established.

ZHANG *et al.* (2011) created three rigid body simulation algorithms based on the DPD method. Thus they were able to derive equations for the rotation of rigid bodies in non-conservative media. The aromatic rings of asphaltenes and resins were treated as rigid bodies. To integrate the equations of motion, they used quaternion methods that proved to be very effective. They studied asphaltene aggregation in diluted toluene solutions. They verified the formation of reversible nanoaggregates that break up and rebuild. The diffusion coefficients obtained are in agreement with experimental data.

YAMANOI *et al.* (2011) reproduced static and dynamic properties of entangled linear polymer systems; they verified the transition from plateau regime to terminal zone as long as the transition from Rouse dynamics to the entangled regime. JAMALI *et al.* (2013) carried out DPD simulations of colloidal suspensions, performing simple shear they were able to capture the transition from shear-thinning to shear-thickening. JAMALI *et al.* (2015b) revisited the multi-body dissipative particle dynamics (MDPD) theory and established a relationship between the Flory-Huggins parameter, fluid compressibility, and MDPD parameters. The diffusion coefficient and zero shear viscosity were also evaluated. An extensive analysis of viscosity in DPD fluids has been made by BOROMAND *et al.* (2015). Both zero-shear and shear viscosities were calculated using the microscopic pressure tensor. Shear viscosity was also calculated for Poiseuille flow. They reported the difficulty of reproducing correct velocity profiles at high values of DPD parameters, modifications in Lees-Edward boundary conditions were proposed to address this problem. KHANI *et al.* (2015) studied the entropic and enthalpic factors leading to aggregation/dispersion of nanorods in a homopolymer matrix. JAMALI *et al.* (2015a) proposed a new thermostat for non-equilibrium simulation of DPD fluids based on the Gaussian distribution of particles. The thermostat proved to maintain the temperature over a wide range of shear rates and dissipative parameters, which enlarges the DPD usability in non-equilibrium simulations.

2.1.5 General Comments

We noticed that the studies that have already been carried out about the aggregation process of asphaltenes in solution are largely based on determining their structural properties. Many atomic and mesoscale tests were performed to try to obtain information on nanoclusters of asphaltene molecules. Some studies have shown the concern of determining diffusion coefficient and viscosity, but the main goal was to relate parameters that influence the structure of the nanoaggregates. There is

still a lack of information in the literature about the kinetics of aggregation of asphaltene molecules. The viscoelastic behavior of asphaltene suspensions has been studied experimentally at the macroscopic scale; however, nothing has been done at the initial stages of aggregation. The DPD conservative force parameter calculation is still the object of debate in the literature, sometimes it is roughly determined. Methods of determining the DPD conservative force parameter should be improved. Our work aims to study the behavior of asphaltene molecules during the early stages of aggregation, which is not yet available in the literature. This type of aggregation happens over long time scales makes it impossible to be dealt with classical molecular simulation strategies. To work around this problem, we use the DPD force field. To analyze the kinetics of aggregation of asphaltene molecules in solution, we developed an algorithm of detecting/counting clusters of molecules. A thorough analysis of the rheological behavior of asphaltene suspensions has been carried out, varying concentration and solvent quality. The study of the viscoelastic behavior of asphaltene suspensions at the initial aggregation stages is also still missing in the literature, our work fulfills this gap. Although some studies have been performed about the surfactant characteristics of asphaltenes at the water/oil interface, the onset of the critical micelle concentration, i.e., studying the interface saturation, is still unrevealed by the literature. We proposed a more physically consistent methodology of determining the DPD conservative force parameter that has been able to access the interfacial properties of asphaltene molecules, showing promising insights about the interfacial tension evolution as a function of asphaltene concentration.

Chapter 3

Method

3.1 Molecular Dynamics

Molecular dynamics (MD) is a simulation technique in which the evolution of a system of particles is obtained by numerical integration of the classical Newton's equations of motion. This technique was developed during the 50's and 60's by ALDER and WAINWRIGHT (1957); GIBSON *et al.* (1960); RAHMAN (1964). The time evolution of a system consisting of N particles is described by the following equations of motion:

$$\frac{\partial \mathbf{r}_i}{\partial t} = \mathbf{v}_i \quad (3.1)$$

$$\frac{\partial \mathbf{v}_i}{\partial t} = \mathbf{a}_i \quad (3.2)$$

Where \mathbf{r}_i , \mathbf{v}_i , \mathbf{a}_i are the position, velocity and acceleration vectors of the i-th particle. The particle acceleration is given by the Newton's 2nd law of motion:

$$\mathbf{F}_i = m_i \mathbf{a}_i \quad (3.3)$$

Where m_i , \mathbf{F}_i are the mass and the total force applied to particle i. The force (which is conservative) is given by the gradient of interparticle interaction potential U with respect to particle positions:

$$\mathbf{F}_i = -\nabla_{\mathbf{r}_i} U(\mathbf{r}_i, \dots, \mathbf{r}_N) \quad (3.4)$$

The potential U is usually defined as the sum of the interaction energies be-

tween particles $\phi(r_{ij})$ (supposing pairwise additive potential without external field).

$$U(\mathbf{r}_1, \dots, \mathbf{r}_N) = \sum_i \sum_{j>i} \phi(r_{ij}) \quad (3.5)$$

Where $r_{ij} = |\mathbf{r}_i - \mathbf{r}_j|$ is the distance between particles i and j . The condition $j > i$ in the second summation ensures that interparticle's contribution will be accounted once.

The most common example of pair potential is the Lennard-Jones potential (LENNARD-JONES, 1924). It is the sum of two contributions: a long-range attraction (Van der Waals Forces) and a short-range repulsion from overlapping electron orbitals.

$$\phi_{LJ}(r) = 4\epsilon \left[\left(\frac{\sigma}{r}\right)^{12} - \left(\frac{\sigma}{r}\right)^6 \right] \quad (3.6)$$

Where ϵ determines the depth of the potential well and σ determines the distance at which the potential crosses the zero point and remains infinitely positive; σ therefore is related to the particle size. The distance from which the interaction potential is practically zero is called *cutoff radius*, r_c . The Lennard-Jones potential was used in Liquid Argon (RAHMAN, 1964) simulations, it is still widespread in the literature, see Figure 3.1.

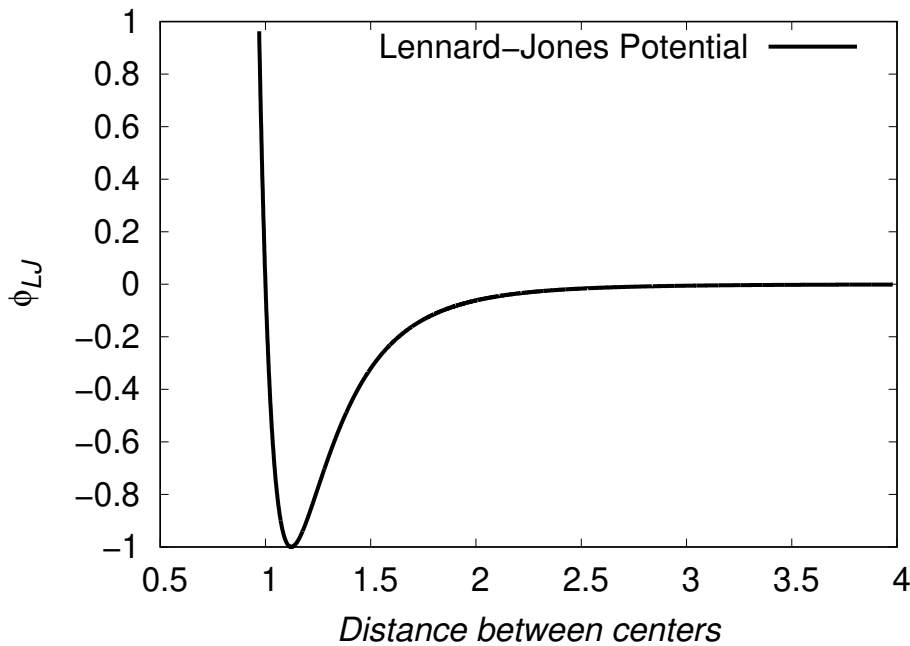


Figure 3.1: Graph of the classical Lennard-Jones potential for $\epsilon = 1$ e $\sigma = 1$.

Another important point to consider when implementing a molecular dynamics

algorithm is how the boundary conditions are handled. Usually *periodic boundary conditions* are used. In this case, we first define a simulation box where all particles are placed, this is the initial configuration. When a particle crosses any edge of the simulation box, an identical one is inserted on an opposite side. This makes the simulation box to be replicated. That would mean that sufficiently close particles (less than r_c) would interact not only with others within the simulation box, but also with their images in neighboring boxes. A simplification of this complicated interaction scheme is given by the *minimum-image convention*: If all sides of the simulation box are greater than $2r_c$, any image of a particle j will be separated from itself by a distance greater than $2r_c$, which means that another particle i within the original box and far less than r_c from the particle j will interact with at most one image of particle j . In other words, if all dimensions of the simulation box are larger than $2r_c$, any particle inside the box will interact only with its closest image (RAPAPORT, 2004).

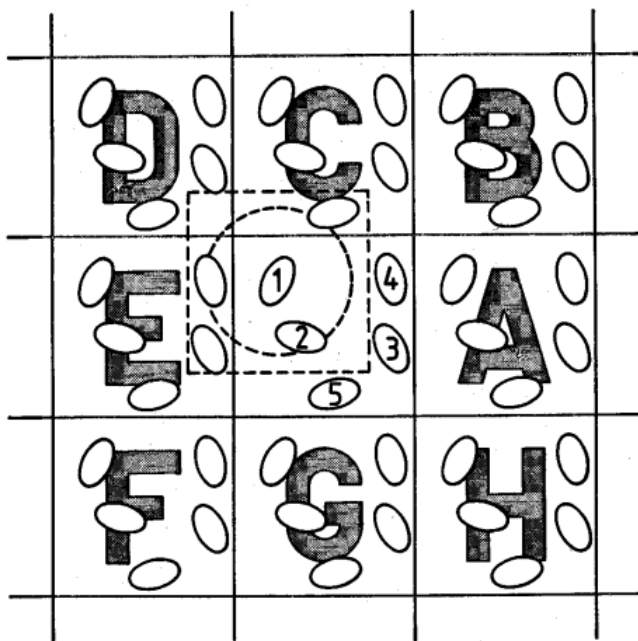


Figure 3.2: *Periodic boundary conditions and the minimum-image convention.* Figure extracted from (ALLEN and TILDESLEY, 1991).

There is a common computational time optimization technique called *neighbor list* that was introduced by (VERLET, 1967). Even though using the cutoff radius significantly improves the calculation time, at each time step it will be necessary to calculate the distances between all particles in the system to know which ones are less than r_c . The *neighbor list* contains all particles next to each other within a sphere of size r_c approximately. This list does not need to be updated every time step, so it saves time on calculating the distances between all particles in each time step. Usually the list is updated within a arbitrary number of time steps, which is

every 10-20 time steps usually.

Through classical molecular dynamics, one can calculate macroscopic thermodynamic properties such as: pressure, energy, heat capacity and so on. The connection between microscopic measurements of simulated particles and macroscopic properties is made by the statistical mechanics. Molecular Dynamics generates a sequence of points in the phase space as a function of time, i.e. any calculated average will be an average over time. While thermodynamic properties are defined in terms of averages of statistical *ensembles* over a large number of system replicas. The link between the temporal and ensemble average is established by the ergodic hypothesis which states that both are equal:

$$\langle A \rangle_{ensemble} = \langle A \rangle_{time} \quad (3.7)$$

Where A is a mechanical property of the system. This is based on the premise that if a system evolves infinitely in time, it will necessarily go through every possible micro state. In practice this means that the more time steps you use the more accurate the averages will be. Since the simulations are finite, it is necessary to ensure a sufficient number of time steps for a reasonable description of phase space.

The biggest limitation of molecular dynamics is the high computational cost of simulating atom positions, those simulations are often called microscopic. Viable time steps in Molecular Dynamics are on the order of a few femtoseconds (TEWARY, 2009). This limitation is the main reason for adopting coarse-graining techniques, such as DPD, that allow you to use longer time steps.

3.2 Integration Schemes

There is a wide number of established methods in the literature for integrating the equations of motion used in molecular dynamics (RAPAPORT, 2004). In this work we used the *Velocity-Verlet*, which is the method implemented in the simulation software employed: *LAMMPS*.

The *Velocity-Verlet* method is a variation of the traditional algorithm developed by Loup Verlet (VERLET, 1967). It is classified as a symplectic method because of its property of conserving the total energy and momentum of the system, it also does not accumulate errors. Its formulation can be obtained by a simple sequence of algebraic manipulations.

Since the particle's classical trajectory is continuous, the position of the particle

i, \mathbf{r}_i , at a time point $t + \delta t$, can be approximated by a Taylor series expansion truncated in the second term order:

$$\mathbf{r}_i(t_0 + \Delta t) = \mathbf{r}_i(t_0) + \Delta t \mathbf{v}_i(t_0) + \frac{1}{2} \Delta t^2 \mathbf{a}_i(t_0) + \mathcal{O}(\Delta t^3) \quad (3.8)$$

Where t_0 represents any reference time, Δt , is the time step and \mathbf{v}_i , \mathbf{a}_i , are the velocity and acceleration vectors of particle i, respectively. This means that the position of a particle i at the moment $t_0 + \Delta t$ can be obtained from \mathbf{r}_i , \mathbf{v}_i and \mathbf{a}_i at the instant t_0 . To obtain velocity at a future time, it is necessary to use a mathematical device based on two Taylor series expansions for velocity, such that the final result (TUCKERMAN, 2010) is:

$$\mathbf{v}_i(t_0 + \Delta t) = \mathbf{v}_i(t_0) + \frac{1}{2} \Delta t [\mathbf{a}_i(t_0) + \mathbf{a}_i(t_0 + \Delta t)] + \mathcal{O}(\Delta t^3) \quad (3.9)$$

The accelerations in both t_0 and $t_0 + \Delta t$ are obtained by Newton's Second Law, considering the interactions between the particle i and neighboring particles by the expression:

$$\mathbf{a}_i = \frac{1}{m_i} \sum_{j \neq i} \mathbf{f}_{ij}(\mathbf{r}_{ij}, t) \quad (3.10)$$

The calculation of acceleration makes it possible to update position and velocity. In molecular dynamics simulations, the calculation of the interaction forces between particles is the most time consuming step which is responsible for large computational times. As the acceleration calculation is directly related to the calculation of the potentials, predictor-corrector methods are avoided, since the acceleration of each particle would have to be calculated more than once for each integration step.

3.3 Microscopic States and *Ensembles*

The microscopic state of a system is defined by a set of position and velocity coordinates of N particles in the system. Thus the set $(r_1, \dots, r_N, v_1, \dots, v_N)$ represents one possible microscopic state of the system. The set of states of a system constitutes a statistical set (*Ensemble*). The following three common ensembles will be presented.

3.3.1 *Microcanonical Ensemble (NVE)*

The statistical ensemble with specified Energy (E), Volume (V), and number of particles N, is called *Microcanonical Ensemble*, it represents an isolated system. From this ensemble, we define a Ω (degeneracy) which represents the total number of possible microscopic states of the system. Gibbs's 'equal a priori' hypothesis states that all the microscopic states of the *Microcanonical Ensemble* are equally likely. Boltzmann's equation shows that the system entropy S is related to this microcanonical partition function:

$$S = k_B \ln \Omega(E, V, N)$$

From the partition function, it is possible to obtain other thermodynamic properties:

$$\frac{1}{T} = k_B \left(\frac{\partial \ln \Omega}{\partial E} \right)_{V, N} \quad (3.11)$$

$$\frac{P}{T} = k_B \left(\frac{\partial \ln \Omega}{\partial V} \right)_{E, N} \quad (3.12)$$

$$\frac{\mu}{T} = -k_B \left(\frac{\partial \ln \Omega}{\partial N} \right)_{E, V} \quad (3.13)$$

Where T , P , μ is the temperature, pressure, and chemical potential, respectively.

3.3.2 *Canonical Ensemble (NVT)*

This ensemble is characterized by a specified number of particles N, volume V , and temperature T. From this ensemble, a canonical partition function Q is defined, which indicates the number of microscopic states of the system. This canonical partition function is given by:

$$Q(T, V, N) = \sum_E \Omega(E, V, N) \exp \left(-\frac{E(V, N)}{k_B T} \right) \quad (3.14)$$

$$A(T, V, N) = -k_B T \ln Q(T, V, N) \quad (3.15)$$

The summation in Equation 3.14 is over all the mechanical energies of the

system. From the partition function, one can obtain the following macroscopic thermodynamic properties of the system:

$$E = k_B T^2 \left(\frac{\partial \ln Q}{\partial T} \right)_{N,V} \quad (3.16)$$

$$P = k_B T \left(\frac{\partial \ln Q}{\partial V} \right)_{N,T} \quad (3.17)$$

$$S = k_B \ln Q + k_B T \left(\frac{\partial \ln Q}{\partial T} \right)_{N,V} \quad (3.18)$$

Where E is the internal energy.

3.3.3 *Isothermal–Isobaric Ensemble (NPT)*

This ensemble is characterized by a specified number of N particles, P pressure, and T temperature. From this ensemble, it is defined a isothermal-isobaric partition function Δ , which indicates the number of microscopic states of the system. The Δ partition function is given by:

$$\Delta(P, T, N) = \sum_V \sum_E \Omega(E, V, N) \exp \left(-\frac{E(V, N)}{k_B T} \right) \exp \left(-\frac{PV}{k_B T} \right) \quad (3.19)$$

$$G(P, T, N) = -k_B T \ln \Delta(P, T, N) \quad (3.20)$$

For this ensemble, the following thermodynamic properties are directly obtained:

$$V = -k_B T \left(\frac{\partial \ln \Delta}{\partial P} \right)_{N,T} \quad (3.21)$$

$$H = k_B T^2 \left(\frac{\partial \ln \Delta}{\partial T} \right)_{N,P} \quad (3.22)$$

$$S = k_B \ln \Delta + k_B T^2 \left(\frac{\partial \ln \Delta}{\partial T} \right)_{N,P} \quad (3.23)$$

Where H is the enthalpy of the system.

3.4 The DPD method

The original DPD method was originally developed by Hoogerbrugge and Koelman (HOGERBRUGGE and KOELMAN, 1992; KOELMAN and HOGERBRUGGE, 1993), as a technique for mesoscopic simulation of complex fluids. Besides interactions based on conservative potentials (as in Molecular Dynamics) it includes dissipative and stochastic interactions. This approach is based on the Langevin equation, a stochastic differential equation that describes Brownian motion in a potential, it represents the omitted degrees of freedom by a viscous and a random term.

The original model is described as:

$$\frac{\partial \mathbf{r}_i}{\partial t} = \mathbf{v}_i \quad (3.24)$$

$$m_i \frac{\partial \mathbf{v}_i}{\partial t} = \mathbf{F}_i \quad (3.25)$$

The total force \mathbf{F}_i acting on each particle consists of three parts:

$$\mathbf{F}_i = \sum_{j \neq i} (\mathbf{F}_{ij}^C + \mathbf{F}_{ij}^R + \mathbf{F}_{ij}^D) \quad (3.26)$$

Where \mathbf{F}_{ij}^C , \mathbf{F}_{ij}^R , and \mathbf{F}_{ij}^D are the conservative, random, and dissipative components of total force, respectively (ESPANOL and WARREN, 1995).

These forces, whose expressions are expressed below, act until r_c .

$$\mathbf{F}_{ij}^C = -a_{ij} \omega^C(r_{ij}) \hat{\mathbf{r}}_{ij} \quad (3.27)$$

$$\mathbf{F}_{ij}^R = \sigma_{DPD} \omega^R(r_{ij}) \hat{\mathbf{r}}_{ij} \zeta_{ij} / \sqrt{\delta t} \quad (3.28)$$

$$\mathbf{F}_{ij}^D = -\gamma_{DPD} \omega^D(r_{ij}) \hat{\mathbf{r}}_{ij} (\mathbf{v}_{ij} \cdot \hat{\mathbf{r}}_{ij}) \quad (3.29)$$

Where a_{ij} is the maximum repulsion between particles i and j , $\mathbf{r}_{ij} = \mathbf{r}_j - \mathbf{r}_i$, $\omega^C(r_{ij}) = 1 - \frac{|\mathbf{r}_{ij}|}{r_c}$.

The maximum repulsion parameter (a_{ii}) between two identical particles is related to the dimensionless compressibility of the system (κ). The dimensionless

compressibility is given by the following expression:

$$\kappa^{-1} = \frac{1}{k_B T} \left(\frac{\partial P}{\partial \rho} \right)_T \quad (3.30)$$

Where P is the pressure and ρ is the numerical density of particles. GROOT and WARREN (1997) found the DPD fluid equation of state:

$$P = \rho k_B T + \lambda a_{ii} \rho^2 \quad (3.31)$$

Where $\lambda = 0.101 \pm 0.001$. With this information we can find the relationship between the a_{ii} parameter and κ :

$$\kappa^{-1} = 1 + \frac{2\lambda a_{ii} \rho}{k_B T} \quad (3.32)$$

If the water compressibility ($\kappa \simeq 16$) is reproduced, we have $a_{ii} = 75 \frac{k_B T}{\rho}$. In the same work (GROOT and WARREN, 1997), they proposed a relationship for the repulsion parameter between two distinct particles based on Flory-Huggins theory:

$$a_{ij} = a_{ii} + \frac{\chi k_B T}{0,306} \quad (3.33)$$

The random and dissipative forces act as a thermostat and their parameters are given by σ_{DPD} and γ_{DPD} . $\omega^R(r_{ij})$ and $\omega^D(r_{ij})$ are the weight functions of the random and dissipative forces, respectively. The other terms are: δt the time step, k_B the boltzmann constant, T the thermostat temperature and ζ_{ij} a Gaussian random number with the following properties:

$$\zeta_{ij}(t) = \zeta_{ji}(t) \quad (3.34)$$

$$\langle \zeta_{ij}(t) \rangle = 0 \quad (3.35)$$

$$\langle \zeta_{ij}(t) \zeta_{i'j'}(t') \rangle = (\delta_{ii'} \delta_{jj'} + \delta_{ij'} \delta_{ji'}) \delta(t - t') \quad (3.36)$$

Where δ_{ij} is the Kronecker delta function and $\delta(t)$ is the Dirac delta function. The symmetry condition between ζ_{ij} and ζ_{ji} guarantees the conservation of angular momentum by the stochastic force. In practice, ζ_{ij} is commonly implemented as an uniform random number instead of gaussian, which is less time consuming to be generated (GROOT and WARREN, 1997).

The conservative force is a linear function of the distance, which goes to finite values at zero interparticle distance and goes to zero at a distance equals to the

cutoff radius. Therefore the potential is *soft*, since that force does not go to infinity at zero interparticle distance.

Despite qualitative observations, there was no theoretical justification to show that DPD captured the correct hydrodynamic behavior of the system. This lasted until Español and Warren (ESPAÑOL and WARREN, 1995) formulated the DPD Fokker-Plank equation to study the equilibrium properties of the stochastic differential equation that governs DPD, and then Español (ESPAÑOL, 1995) to be able to derive macroscopic properties from the microscopic description.

They showed that the dissipative and random forces are not independent, they are related by the Fluctuation-Dissipation Theorem (NYQUIST, 1928). This theorem is based on the idea that the response of a system under thermodynamic equilibrium to a small applied force is the same as its response to a spontaneous fluctuation of the equilibrium state. That is, these two forces balance each other to keep the system temperature constant. The conditions that relate the dissipative and random forces ensuring thermodynamic equilibrium/thermostating the system are:

$$\omega^D(r_{ij}) = [\omega^R(r_{ij})]^2 = \left(1 - \frac{|\mathbf{r}_{ij}|}{r_c}\right)^2 \quad (3.37)$$

$$\gamma_{DPD} = \frac{\sigma_{DPD}^2}{2k_B T} \quad (3.38)$$

γ_{DPD} and σ_{DPD} parameters are adjusted to keep the system temperature constant.

The manner to simulate molecular motion at time and length scales larger than typical classical molecular dynamics scales (10^{-12} s - 10^{-9} s, 10^{-9} m) is given by two strategies: The first is to join several atoms together forming a single particle which is called “coarse-graining“ strategy (see Figure 3.3); The second is to make these particles to interact through a soft potential. Since the thermodynamics needs to be correctly described at long scales, the liquid (and its components) compressibility must be correctly described (WARREN, 1998). To achieve this goal, one is free to choose an effective *soft* interparticle interaction that meets the above criteria. This means that the *hard core* of particles should be removed. Since the *hard core* is responsible for the small time steps used, now greater time steps can be performed.

This thermostat is particularly special as it conserves the angular momentum leading to a correct description of the hydrodynamics of the system. All acting forces (conservative, random and dissipative) over a given particle are the result of their interactions with nearby particles. Since the system obeys Newton’s third

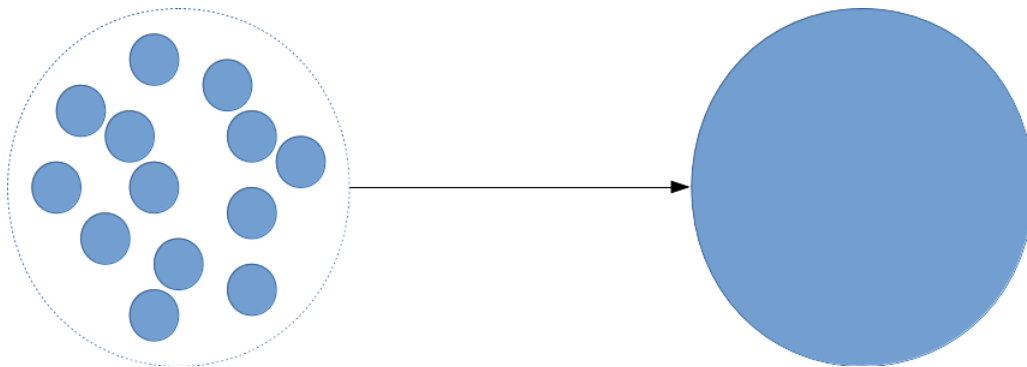


Figure 3.3: Example of coarse-grained representation of a collection of particles.

law, the sum of all forces in the system must be zero (the action on a particle is counterbalanced by the reaction on another). Moreover, if we take each random portion of the liquid volume, the sum of the forces in this random portion of fluid is also zero, therefore the acceleration of this liquid portion is equals to the sum of the forces crossing the liquid volume boundary and this is the condition that generates the Navier-Stokes equations. Therefore, regardless the conservative interaction is chosen, if that interaction is local and satisfies the third law of Newton it will always preserve the hydrodynamics of the system. Reproducing the hydrodynamics of the system is essential for the correct description of the phase transition (VARGA *et al.*, 2015; WARREN, 1998).

In summary, the DPD method fits the main obstacles related to the molecular simulation of asphaltenes suspensions: It allows to simulate longer time steps and captures the hydrodynamic behavior of the suspension. In addition, the fact that the force depends only on the positions \mathbf{r}_{ij} and relative velocities \mathbf{v}_{ij} make the model invariant with respect to the inertial frame of reference which is one of the fundamental laws of physics. In addition to the forces already mentioned, the particles that constitute the same molecule are subject to other types of interaction such as bonding, angle and improper interactions.

3.5 Simulator *LAMMPS*

The large-scale Atomic/Molecular Massively Parallel Simulator (*LAMMPS*) open source software (PLIMPTON, 1995) was used in this work to perform the molecular simulation studies. It is written in C++ language and allows to develop calculations with parallel processing because it employs MPI (Message Passing Interface) system. *LAMMPS* supports many types of interatomic potentials, it can be applied to atoms and clusters of particles, metals, polymers, proteins, DNA, mesoscopic systems, granular systems and various combinations among them. Al-

though *LAMMPS* works efficiently on only one processor, it was specially designed to perform calculations using parallelization. *LAMMPS* was used to perform the simulations, but the properties were calculated in Fortran postprocessing.

Chapter 4

Clustering Algorithm

This Chapter is based on (DE OLIVEIRA *et al.*, 2020b)

Molecular dynamics (MD) is a powerful technique used to simulate a large number of systems, such as microscopic systems, choline chloride/urea deep eutectic solvent in water (FETISOV *et al.*, 2018), protein structure in the explicit solvent (ŚLEDŹ and CAFLISCH, 2018), electrode materials for the development of new batteries (TRUONG *et al.*, 2016) or the energy and the dynamics associated with drug-target recognition and binding (DE VIVO *et al.*, 2016). For the mesoscopic scale, such as the dynamics of 'blob' particles in an incompressible fluid (USABIAGA *et al.*, 2014) or the electrokinetic phenomena governed by Poisson-Nernst-Planck and the Navier-Stokes equations (DENG *et al.*, 2016). In many cases, during the simulation occurs the aggregation of particles which can influence the structural, mechanical, and rheological properties of those systems (HEYES and MELROSE, 1989), as such in HEADEN *et al.* (2017), RADOLA *et al.* (2015), and LIONBERGER and RUSSEL (1994). As clustering of molecules and atoms could explain the behavior and properties of many systems (BÜRGI, 2015; SCHMIDT and KRISCHER, 2015), the need for an algorithm to determine the number of clusters, their mean size, and other aggregated particle characteristics is essential. The Hoshen-Kopelman (HK) algorithm (HOSHEN and KOPELMAN, 1976) is undoubtedly the most known and cited algorithm used to analyze clustering in a lattice model. Its advantage was the need for only one single pass through the lattice, which improved the efficiency. Before the HK algorithm, systems up to tens of thousands of sites could be analyzed (HOSHEN *et al.*, 1997); using it, RAPAPORT (1992) was able to study a lattice containing $4.096310 \cdot 10^{11}$ sites. ZHANG and SEATON (1996), studying fouling in a catalysis reactor, treated the pore probability occupation using the HK algorithm. KINNEY *et al.* (1995), using HK algorithm, carried out cluster analysis in bones and identified the influence of isolated and embedded pores in osteoporosis. The

enhanced Hoshen-Kopelman (EHK) algorithm HOSHEN *et al.* (1997) emerged as an extension of the previous one in which the squared radius of gyration and the internal perimeter of clusters have been calculated. The EHK algorithm has been used in image processing (HOSHEN, 1998, 1999). The parallelization of the HK algorithm has been commented and proposed (BABALIEVSKI, 1998; FRIJTERS *et al.*, 2015).

AL-FUTAISI and PATZEK (2003) proposed an extension of the HK algorithm for non-lattice environments, fixed by METZGER *et al.* (2006). TALEGHANI and DADVAR (2014) used it to study non-isothermal drying in a two-dimensional pore network. GAWLINSKI and STANLEY (1981) investigated the connectivity between discs randomly disposed on the surface; they calculated the critical exponents for ordinary and continuum system percolation. Results showed that both systems are in the same universality class. BUG *et al.* (1985) studied the aspect-ratio dependence of the critical percolation threshold for systems of rods; it seems that the threshold is proportional to the inverse of the expected excluded volume. Many recent developments in this field have been discussed by BALBERG (1987) using the modified HK algorithm.

In the context of molecular dynamics, LAMMPS PLIMPTON (1995) is a popular software that performs both equilibrium and non-equilibrium simulations. The `compute cluster/atom` (com) implemented in LAMMPS can perform cluster analysis such as the one we propose in this work. However, its clustering method is not described in the documentation, so that the only comparison that can be done is a performance comparison demonstrated in development part of this paper. Another tool extensively used for molecular dynamics visualization is Visual Molecular Dynamics VMD (HUMPHREY *et al.*, 1996), which includes some post-processing calculations, among them the cluster analysis. In VMD, cluster analysis is performed employing the Quality Cluster Algorithm (HEYER *et al.*, 1999) (`measure cluster` command (vmd)), which was designed for gene expression data or clusters of `Open Reading Frames` (ORFs). A common specificity of this method is that the cluster size should be previously set, and then the ORFs are considered together, analyzing the jackknife correlation between them. That should be considered a disadvantage compared to the method proposed here, where the cluster size is an output. In VMD, the number of cluster is set as an input, which is generally not desirable for cluster analysis where the number of clusters, sizes, and their derived properties are to be discovered instead.

Herein, we propose an extension of AL-FUTAISI and PATZEK (2003) algorithm, which can perform cluster detection and labeling to be useful in molecular simulation. The algorithm simplifies the original one and has been prepared to

be incorporated into any molecular dynamics code. The proposed labeling routine is faster than the AL-FUTAISI and PATZEK algorithm. This chapter was systematized as follows: In the first part, we present the original algorithm and the proposed modifications. Then, we show two applications: Aggregation of Lennard-Jones particles under Brownian dynamics and asphaltene aggregation in solvent heptane. We present a complete description of the code at the final section.

4.1 Algorithm Implementation

In the AL-FUTAISI and PATZEK algorithm, nodes and links are defined. The nodes are connected (by links) to identify clusters. That algorithm was prepared to be applied in invasion percolation (WILKINSON and WILLEMSSEN, 1983); therefore, some modifications should be made to adapt it to the molecular simulation method. The original code is based on links and nodes occupancy; they exist regardless they are occupied or not. In the molecular dynamics context, the occupancy idea is not useful because particles/molecules (nodes) always exist, and links should be verified. Therefore, all variables related to links and nodes occupancy are no longer necessary, making the proposed algorithm more straightforward. Links between particles are determined before the clustering detection part of the code. The following conditions were reproduced/adapted in our code (in SUBROUTINE `clustering`, see the appendix):

1. If one node (particle/molecule) has NO connected neighbors, it is a single cluster, and a new cluster label will be assigned. The case where nodes are unoccupied does not make sense in this context;
2. If a node has connected neighbors, but they have not been labeled yet, a new cluster label is assigned to this node;
3. If a node has connected neighbors, and they have already been labeled (one at least), this node and its neighbors will receive the minimum cluster label among all neighbors.

The algorithm has been written in FORTRAN. A MATLAB version of the proposed `clustering` routine was prepared to enable a comparison with the AL-FUTAISI and PATZEK algorithm to be made. The results are presented in the next section. The original code was written in MATLAB using predefined functions that do not exist in FORTRAN. Therefore, it was impossible to analyze both codes in FORTRAN, which is more suitable for molecular dynamics. The proposed algorithm has been divided

into two SUBROUTINES: `neighboring` and `clustering`. `Neighboring` is responsible for identifying connections between molecules; it has no corresponding part in the AL-FUTAISI and PATZEK code because links are provided as an input in that algorithm; in the proposed algorithm, they are found instead. `Clustering` finds the number of clusters and the number of molecules associated to them. That subroutine is analogous to the AL-FUTAISI and PATZEK code.

A copy of the algorithm, including all details, is provided in the appendix. The first part of the algorithm considers that particle's positions are stored in the matrices `rx`, `ry`, and `rz`. If two particles belonging to different molecules are distant less than `dist_cluster` those molecules are considered aggregated, and the vector `n_contacts_per_molecule` is updated. Then, the number of contacts with this molecule is verified. There is a limit over the maximum number of contacts per particle, represented by the variable `max_contacts`. Imposing that limit is essential to create `node_next(m,n)`. The matrix `node_next(m,n)` stores the molecule `n` connected to the molecule `m`. The number of links is also updated.

Consider the example in Figure 4.1.

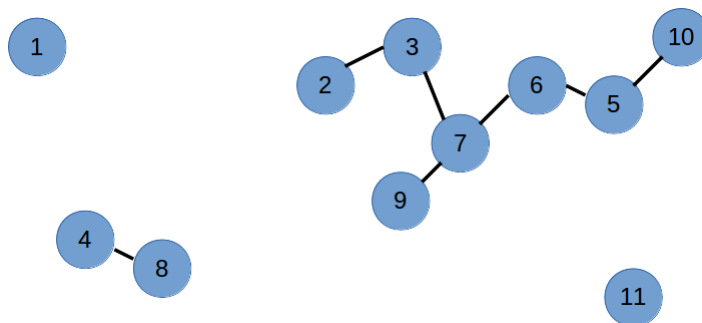


Figure 4.1: Example: system of molecules whose contacts have been verified in SUBROUTINE `neighboring`.

The arguments `node_next`, `n_contacts_per_molecule` and `n_links` are then passed to the subroutine `clustering` that contains the central part of the algorithm responsible for labeling clusters. In the first loop (through all molecules), the three clustering conditions are tested. If a molecule has no neighbors, it is a single cluster. If a molecule has neighbors, but they have not been labeled yet, that molecule will receive a new cluster label, which is the mark of a new cluster. If a molecule has labeled neighbors, that molecule (and its neighbors) will receive the minimum label value among their neighbors. The vector `nodeL` contains the cluster label to which that specific molecule belongs. As initially different molecules belonging to the same cluster can have different labels, an iterative procedure is necessary to fix the cluster labels. After that step, the vector `nodeL` will have the following cluster labels in the example of Figure 4.1.

```
nodeL(1) = 1
nodeL(2) = 2
nodeL(3) = 2
nodeL(4) = 3
nodeL(5) = 4
nodeL(6) = 2
nodeL(7) = 2
nodeL(8) = 3
nodeL(9) = 2
nodeL(10) = 4
nodeL(11) = 5
Number of clusters = 5
```

Figure 4.2: Vector `nodeL` labels after the first clustering step for the stated example. It contains the cluster label for each molecule.

The `DO WHILE` loop will assure that the cluster labels and, consequently, the number of clusters are being counted correctly, it will iterate while the number of iterations `N` is less than the limit `tol` and `condition1` is `TRUE`. Firstly, the previous labeling procedure is repeated; this is the first label correction. Then the second `DO` loop will verify whether all neighbors of a specific molecule have different cluster labels; if it is the case, molecules pertaining to the same cluster still have different labels, and the outermost loop needs to iterate again. If all molecule neighbors pertaining to the same cluster have the same label, all molecules have been labeled correctly, which means that there are no redundancies, and `condition1` is `FALSE`, which finishes the `DO WHILE` loop. Now, for the studied example, `nodeL` will be:

```
nodeL(1) = 1
nodeL(2) = 2
nodeL(3) = 2
nodeL(4) = 3
nodeL(5) = 2
nodeL(6) = 2
nodeL(7) = 2
nodeL(8) = 3
nodeL(9) = 2
nodeL(10) = 2
nodeL(11) = 5
Number of clusters = 5
```

Figure 4.3: Vector `nodeL` labels after the correction label step for the stated example. `nodeL` contains the cluster label for each molecule.

At this point, the vector `nodeL` contains the cluster label corresponding to each molecule. There is no order in the cluster numbering which means that, for instance, it could exist three clusters with labels 1, 3, 5. The next part of the algorithm will find the correct number of clusters based on the vector `nodeL`. Two conditions are proven looping the number of molecules: `condition2` checks if a molecule `j`, ahead in the vector `nodeL` compared to `i`, has the same label of a molecule `i`. `condition3` checks, back in the vector `nodeL` compared to molecule `i`, if a molecule `j` DOES NOT have the same label as molecule `i`. If `condition2` and `condition3` are `TRUE` there are molecules forth (only) with the same label as molecule `i` which means that this is a cluster of many molecules. It is important to note that as `nodeL` is being swept from 1 to `n_molecules`, the case where a molecule `i` has the same label as only previous molecules is automatically satisfied and counted because of the loop direction. If `condition2` is `FALSE` and `condition3` is `TRUE`, that molecule has no other molecules with its same label, neither forth nor back, which means that this molecule is a single cluster. The vector `id` contains the label corresponding to each cluster; therefore, the number of non-zero elements in that vector will be the number of clusters. At the end of that loop, the variable `n_clusters` stores the number of clusters. The output file `clustering.out` contains information about all clusters and molecules belonging to each cluster. The result for our example is:

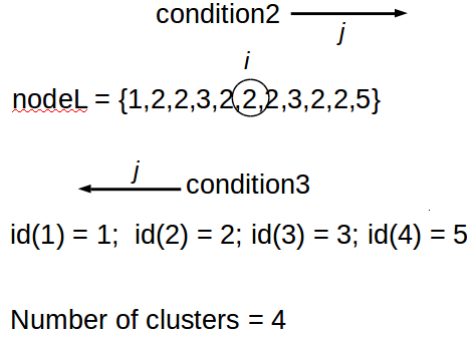


Figure 4.4: Final result for the stated example using the proposed algorithm. The Figure also indicates the scan direction in `nodeL` to verify if `condition2` and `condition3` are being satisfied.

4.2 Application 1 - Aggregation of Lennard-Jones Particles

For that application 1000 particles interacting via Lennard-Jones potential were simulated. Four systems were tested using reduced Lennard-Jones temperature $T^* = 0.5, 0.3$ and volume fractions $\phi = 0.05$ and 0.16 . The volume fraction is calculated by:

$$\phi = \frac{4}{3}\pi a^3 \frac{N}{V} \quad (4.1)$$

Where a is the spherical particle radius, N is the total number of particles, and V the volume system. Brownian dynamics has been used to model solvent interactions implicitly. Figure 4.5 shows initial and final configurations for all systems. Temperature (T), distance (L), and time (t) are dimensionless, referenced as reduced Lennard-Jones quantities T^* , L^* and t^* :

$$T^* = \frac{k_B T}{\epsilon}, \quad L^* = \frac{L}{\sigma}, \quad t^* = t \left(\frac{\epsilon}{m \sigma^2} \right)^{1/2} \quad (4.2)$$

Where k_B is the Boltzmann constant, and m is the mass of the particle. ϵ and σ are Lennard-Jones parameters representing the depth of potential well and particle diameter, respectively. All parameters were set to 1, and the potential was truncated at 2.5σ . The cutoff aggregation used here is 1.4 in reduced units as it is the first minimum of radial distribution function for all cases (this is equivalent to 1.4σ).

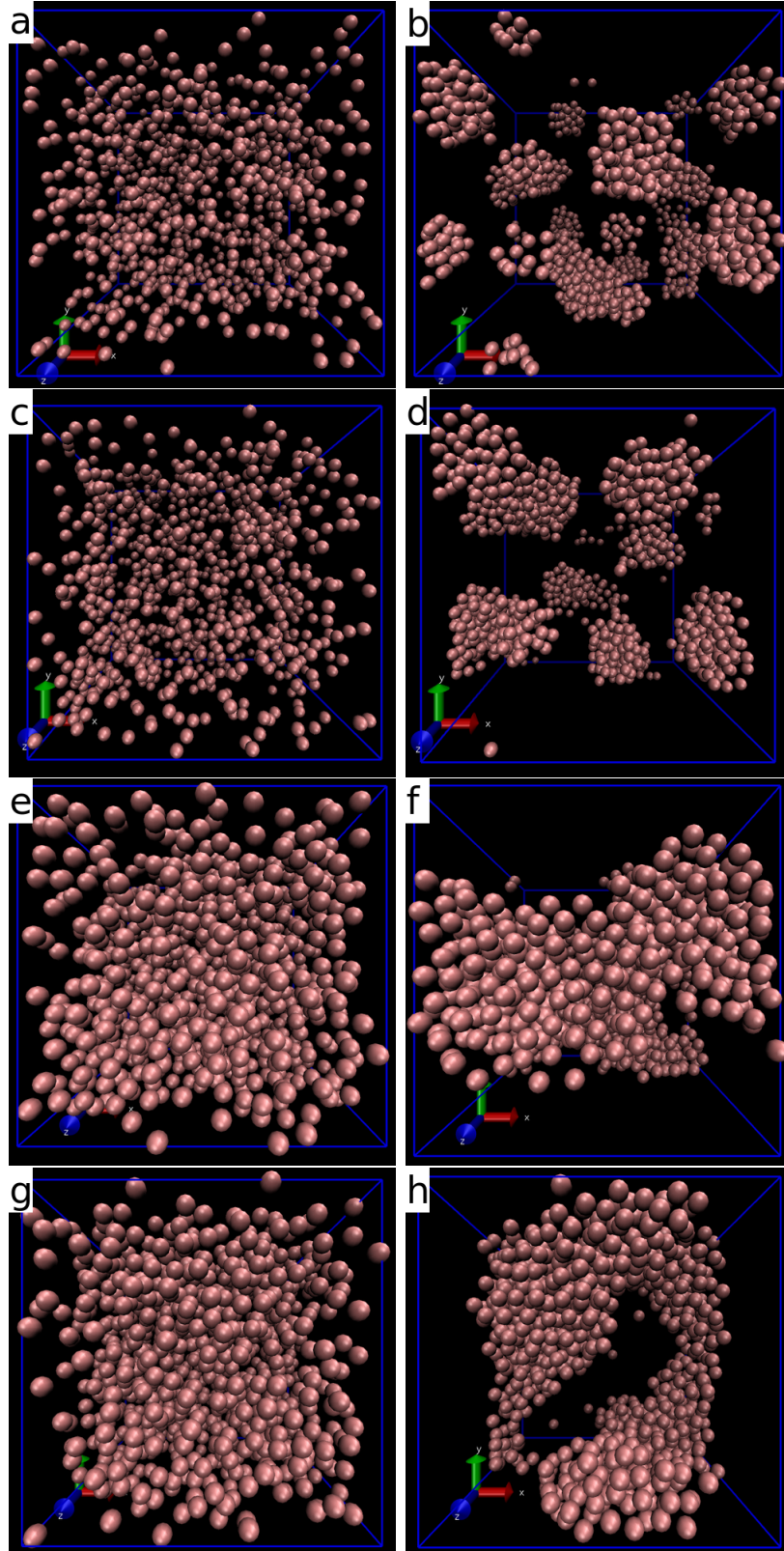


Figure 4.5: Initial and final configurations for Brownian dynamics of Lennard-Jones particles at different temperatures and volume fractions. At the initial configurations particles are randomly dispersed in the medium, they aggregate over time. a) $T^* = 0.3$ and $\phi = 0.05$ at $t^* = 0$. b) $T^* = 0.3$ and $\phi = 0.05$ at $t^* = 74$. c) $T^* = 0.5$ and $\phi = 0.05$ at $t^* = 0$. d) $T^* = 0.5$ and $\phi = 0.05$ at $t^* = 74$. e) $T^* = 0.3$ and $\phi = 0.16$ at $t^* = 0$. f) $T^* = 0.3$ and $\phi = 0.16$ at $t^* = 74$. g) $T^* = 0.5$ and $\phi = 0.16$ at $t^* = 0$. h) $T^* = 0.5$ and $\phi = 0.16$ at $t^* = 74$.

As it can be seen in Figure 4.5, initially, particles are dispersed in the medium. The interplay between interparticle interactions and solvent dissipation leads to an aggregation process, which can be observed at the final time $t^* = 74$. At low mass fractions, Figures 4.5b and 4.5d, the final configurations present isolated clusters. At higher mass fractions, Figures 4.5f and 4.5h, particles span over all space, which appears to be a percolated state. According to ZACCARELLI (2007) the percolation regime is necessary for gel transition, although it is not sufficient. Colloidal gels are an important class of materials that present viscoelastic behavior (ZIA *et al.*, 2014) and have many applications as in drug delivery (GUVENDIREN *et al.*, 2012), ZnO deposition (ZNAIDI *et al.*, 2003), or semiconductors (GAPONIK *et al.*, 2011).

To better understand the aggregation process, the Mean Square Displacement (MSD) and Diffusion Coefficient (Derivative of the MSD in time) have been calculated and shown in the Figures 4.6-4.7.

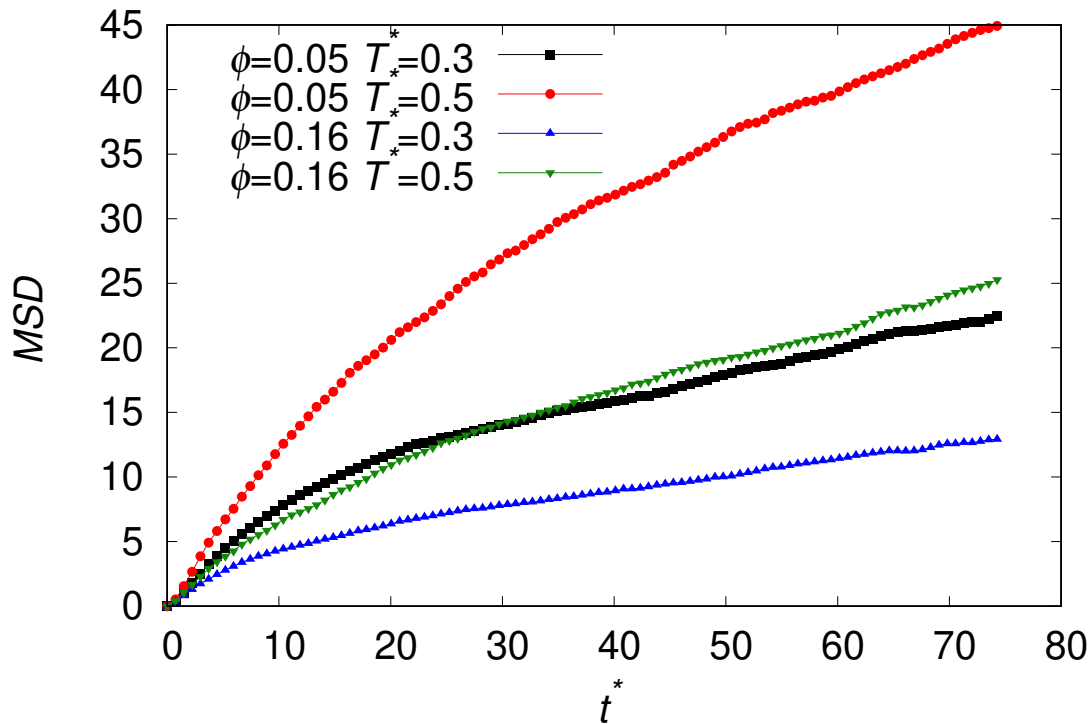


Figure 4.6: Mean Square Displacement (MSD) for Lennard-Jones particles under Brownian dynamics at different temperatures and volume fractions. t^* represents time in Lennard-Jones units.

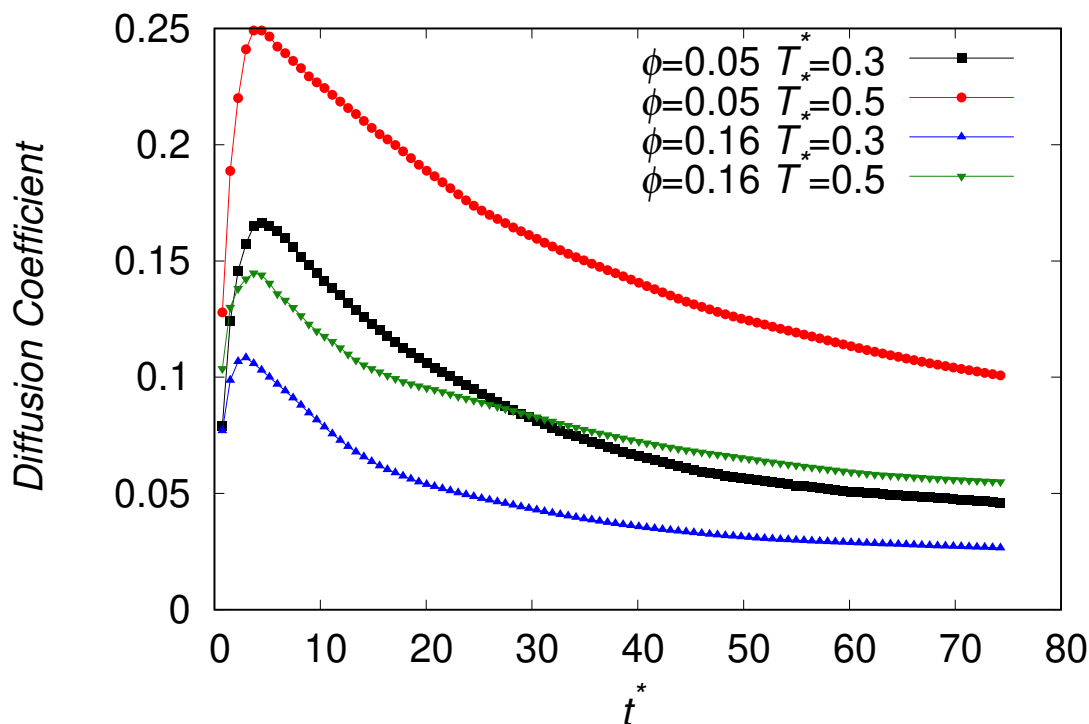


Figure 4.7: Diffusion Coefficient for Lennard-Jones particles under Brownian dynamics at different temperatures and volume fractions. t^* represents time in Lennard-Jones units.

In all cases, at the final stages, the MSD curves grow slower than initially, which is a sign of arrested phases. At higher mass fractions, enthalpic interactions are larger, and the interchange particle between clusters is disfavored, which leads to lower mobility and lower MSD values at long times. The long-time Diffusion Coefficient decreases in time as aggregation proceeds, higher mass fractions, and lower temperatures result in lower Diffusion Coefficient as expected. Particle motion at the final stages occurs mainly through the surface, which takes a long time to contribute to the MSD . Therefore, the dynamics of the system, in all cases, is dictated by particle motion rather than cluster motion (collective motion).

The number of clusters in Figure 4.8 reveals that the aggregation process is favored either by increasing volume fraction or decreasing temperature. At high mass fraction, there is a larger probability of connecting particles. Moreover, when particle velocities decrease at low temperatures, the intermolecular forces become greater, causing particles to move closer to each other. As the attraction between particles increases, their motion decreases, and consequently, fewer collisions are promoted. In Table 4.1 the number of clusters at the final timestep is showed for all cases. This table reinforces that, as shown in Figure 4.5, at low mass fractions, the final configuration is composed of isolated clusters surrounded by the solvent field.

While at high mass fraction ($\phi = 0.16$), particles form four large structures at $T^* = 0.5$ and one big structure at $T^* = 0.3$. Therefore, at $\phi = 0.16$ and $T^* = 0.3$ the system is percolated. At high mass fractions, those structures seem to equilibrate at the initial stages of aggregation ($t^* = 13$); at low mass fractions, this process takes longer because of the small probability of contacts. The time evolution of the number of links is showed for different volume fractions and temperatures in Figure 4.9. That Figure corroborates the number of cluster analysis: as volume fraction increases and temperature decreases, the number of links increases, which should decrease the number of clusters.

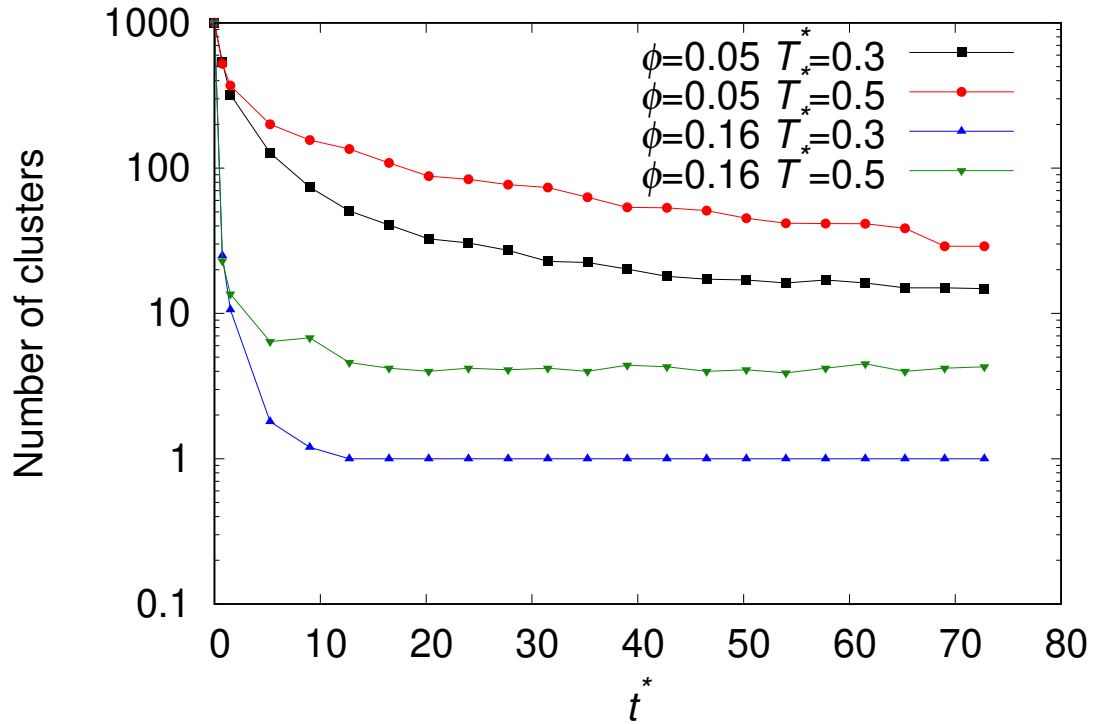


Figure 4.8: Number of cluster evolution for Lennard-Jones particles under Brownian dynamics at different temperatures and volume fractions. t^* represents time in Lennard-Jones units.

Table 4.1: Final number of clusters for aggregation of Lennard-Jones particles at different volume fractions and temperatures.

	$T^* = 0.3$	$T^* = 0.5$
$\phi = 0.05$	15	29
$\phi = 0.16$	1	4

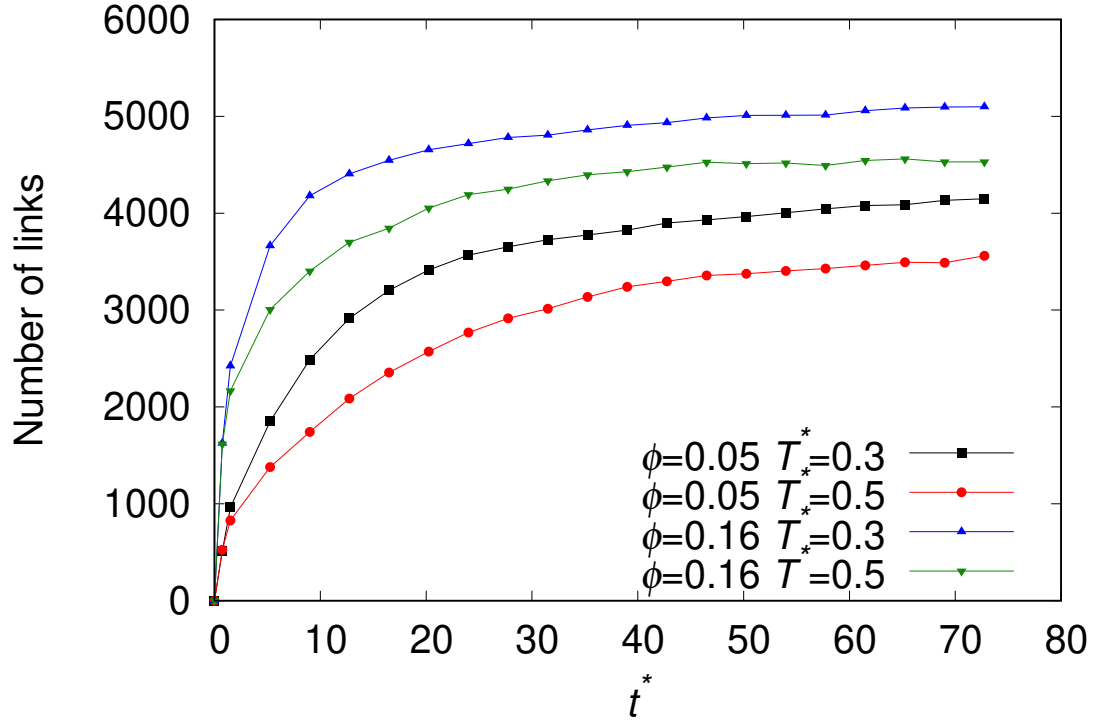


Figure 4.9: Number of links (proportional to the mean size) evolution for Lennard-Jones particles under Brownian Dynamics at different temperatures and volume fractions. t^* represents time in Lennard-Jones units.

A comparison between the Al-Futaisi and Patzek algorithm results and the MATLAB version of the proposed `clustering` routine is shown in Figure 4.10. Both algorithms generate the same results. However, as it can be seen in Figure 4.11 the proposed routine is less time consuming. The average consumed time for each code is similar in all cases because the total number of particles is constant.

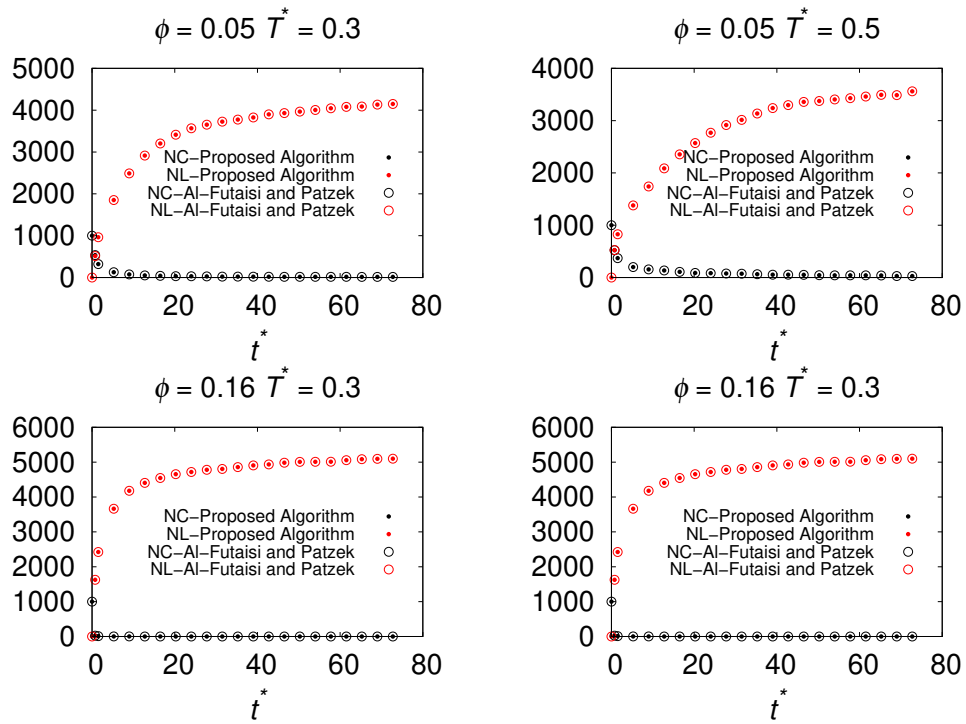


Figure 4.10: Number of clusters and numbers of links obtained by using Al-Futaisi and Patzek algorithm and the MATLAB version of the proposed clustering routine. Both algorithms produce the same results.

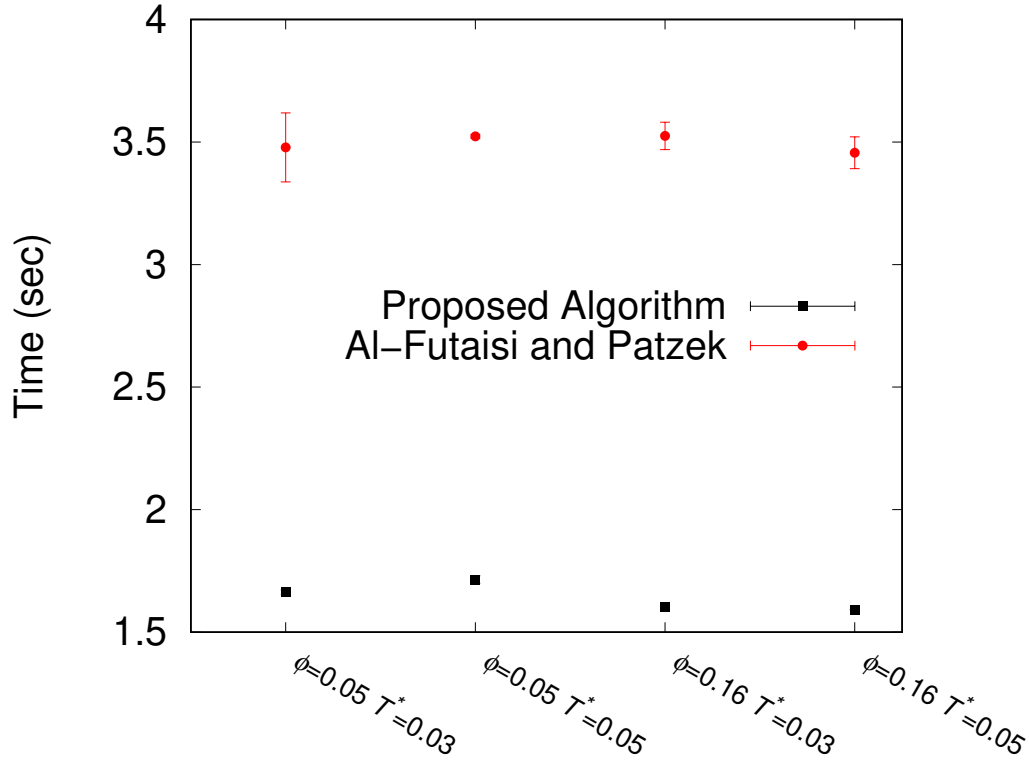


Figure 4.11: Average spent time comparison for both algorithms (using the MATLAB version of the proposed clustering routine) for 100 timesteps. The proposed routine is less time consuming. Triplicate has been performed for average and standard deviation calculations. In some cases standard deviations are too small, seeming not visible.

Our method has also been compared to the cluster analysis promoted by LAMMPS. As it is done on-the-fly in LAMMPS, two runs were carried out for each case to calculate the duration of LAMMPS cluster analysis: A simulation considering clustering analysis and outputting it (1); the same simulation without clustering analysis (2). The time consumed for clustering analysis is found by subtracting the duration of simulations (1) - (2). The results are shown in Table 4.2 for 1000 particles and 1000 timesteps, where the proposed algorithm performed better than LAMMPS cluster analysis algorithm.

Table 4.2: Comparison between LAMMPS cluster analysis and the algorithm proposed in this work. 1000 particles were simulated with 1000 timesteps. (1) LAMMPS time duration for simulation running the cluster analysis. (2) LAMMPS time duration for simulation without cluster analysis. Tests were run in serial to avoid parallelism bias. Triplicate has been performed for average and standard deviation calculations. Time in seconds.

	(1)	(2)	(1)-(2)	Proposed algorithm
$\phi = 0.05 T^* = 0.3$	13.46 ± 0.64	7.93 ± 0.59	5.53 ± 0.14	3.27 ± 0.07
$\phi = 0.05 T^* = 0.5$	13.75 ± 0.42	8.19 ± 0.14	5.57 ± 0.29	3.31 ± 0.12
$\phi = 0.16 T^* = 0.3$	13.24 ± 0.61	7.93 ± 0.39	5.30 ± 0.27	3.28 ± 0.09
$\phi = 0.16 T^* = 0.5$	13.44 ± 0.55	7.98 ± 0.41	5.46 ± 0.22	3.22 ± 0.08

4.3 Application 2 - Asphaltene Aggregation in Heptane

Asphaltenes are the heaviest fraction of crude oil (AVID *et al.*, 2004; DE OLIVEIRA *et al.*, 2020a). They are known to precipitate during oil extraction, which can be a huge problem for the industry (LIN *et al.*, 2016). In this example, a collection of configurations were generated by molecular simulation. Each asphaltene molecule is composed of sixteen particles. When two particles pertaining to different molecules are close enough, one contact is verified. The cutoff aggregation distance used is 7.1 Å (1 Å = 10^{-10} m), which is the first minimum of the radial distribution function, representing the aggregation first shell. Figures 4.12-4.13 show an example of initial and final configurations. The simulation has been performed during 90 ns (1 ns = 10^{-9} s). Figure 4.14 shows the time evolution of the number of clusters and the number of links for each number of molecules comparing the proposed and Al-Futaisi and Patzek algorithms. Initially, each molecule corresponds to one isolated cluster. As simulation proceeds, molecules aggregate, and the number of clusters decreases. By using the same argument, the number of links increases. At the end of the simulation, curves reach a plateau, which means that the equilibrium state has been achieved. Both algorithms produce the same result. The elapsed time performed by Al-Futaisi and Patzek’s code and the proposed `clustering` routine have been plotted in Figure 4.15. It is worth commenting that the proposed algorithm has a dependence on the degree of aggregation (loops from 1 to `n_contacts_per_molecule`), which could impair the performance of the method in the limit of too many particles. The parallelizing procedure in `neighboring` routine allowed to have a higher performance, which can be seen in Table 4.3 for different systems with an increasing number of molecules.

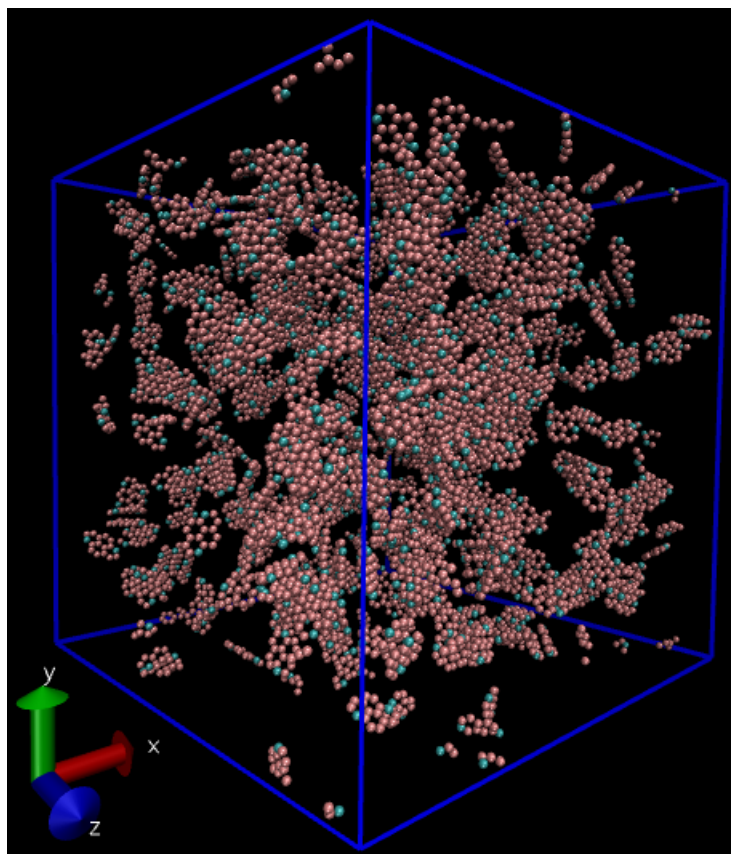


Figure 4.12: Initial configuration. Molecules are randomly dispersed in the medium. Only asphaltene (solute) molecules are shown for better viewing.

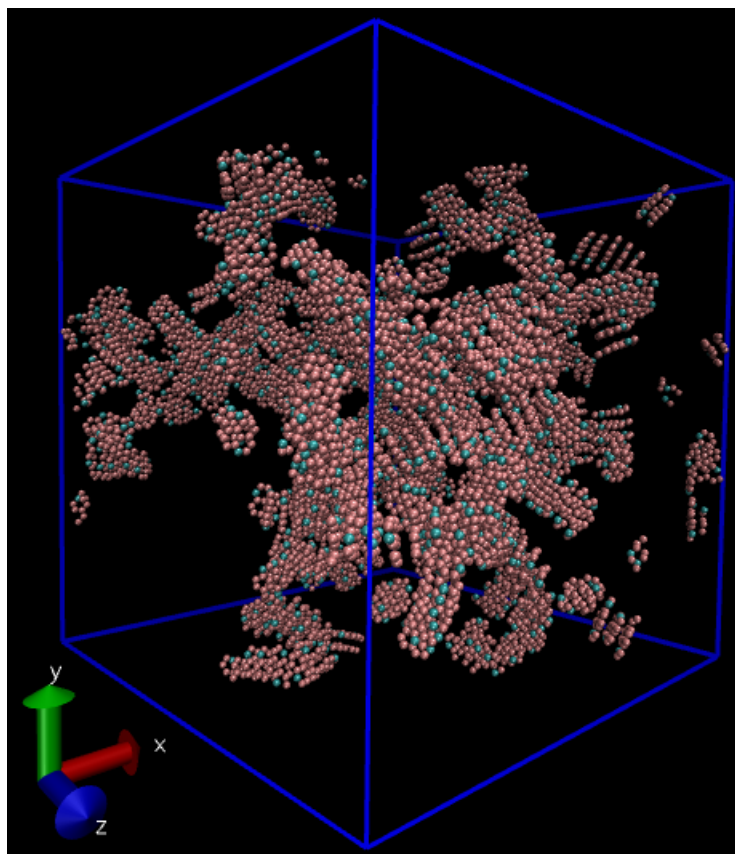


Figure 4.13: Final configuration. Asphaltene molecules are forming a aggregated structure. Only asphaltene (solute) molecules are shown for better viewing.

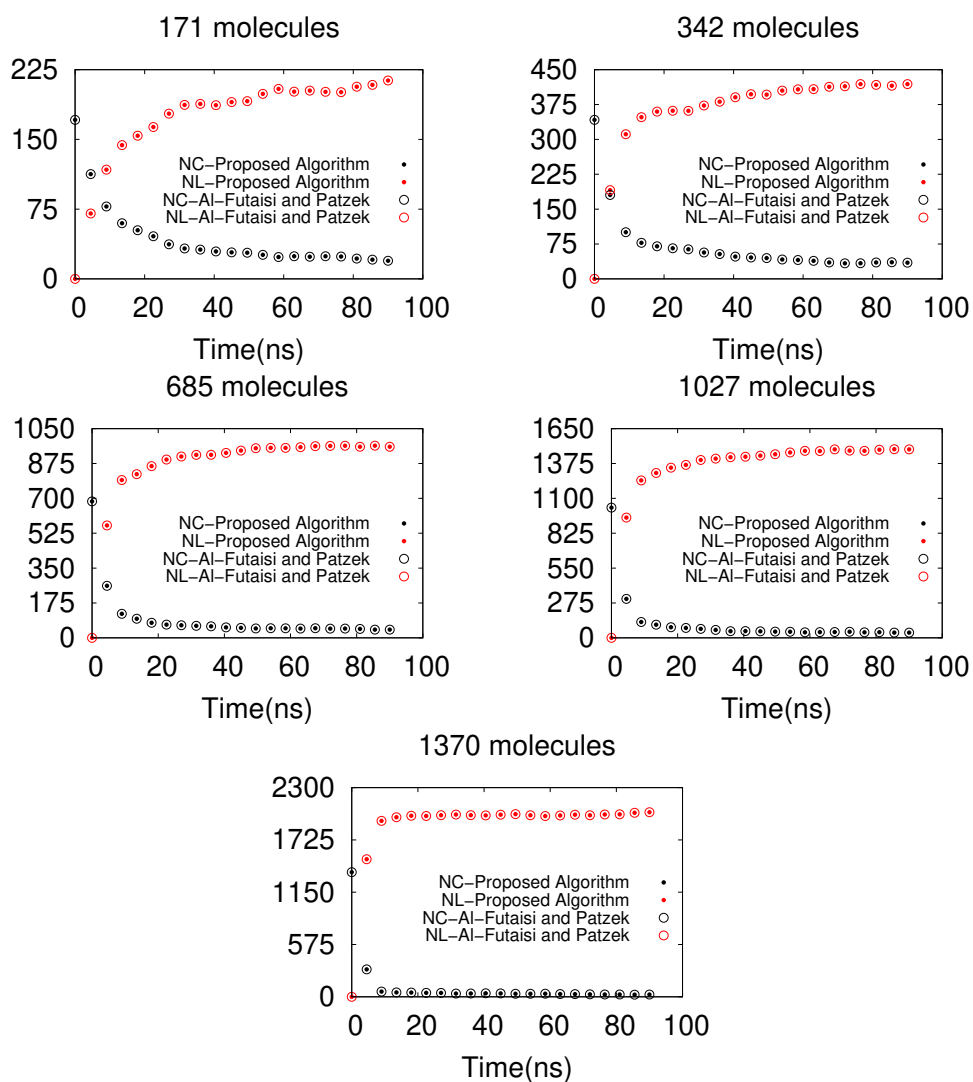


Figure 4.14: Time evolution of the number of clusters (NC) and links (NL) of asphaltene molecules for Al-Futaisi and Patzek algorithm and the proposed clustering routine. The number of clusters is diminishing as initially each molecule represents one isolated cluster which is aggregating in time. Curves tend to constant values as equilibrium is being attained. Both algorithms give the same results.

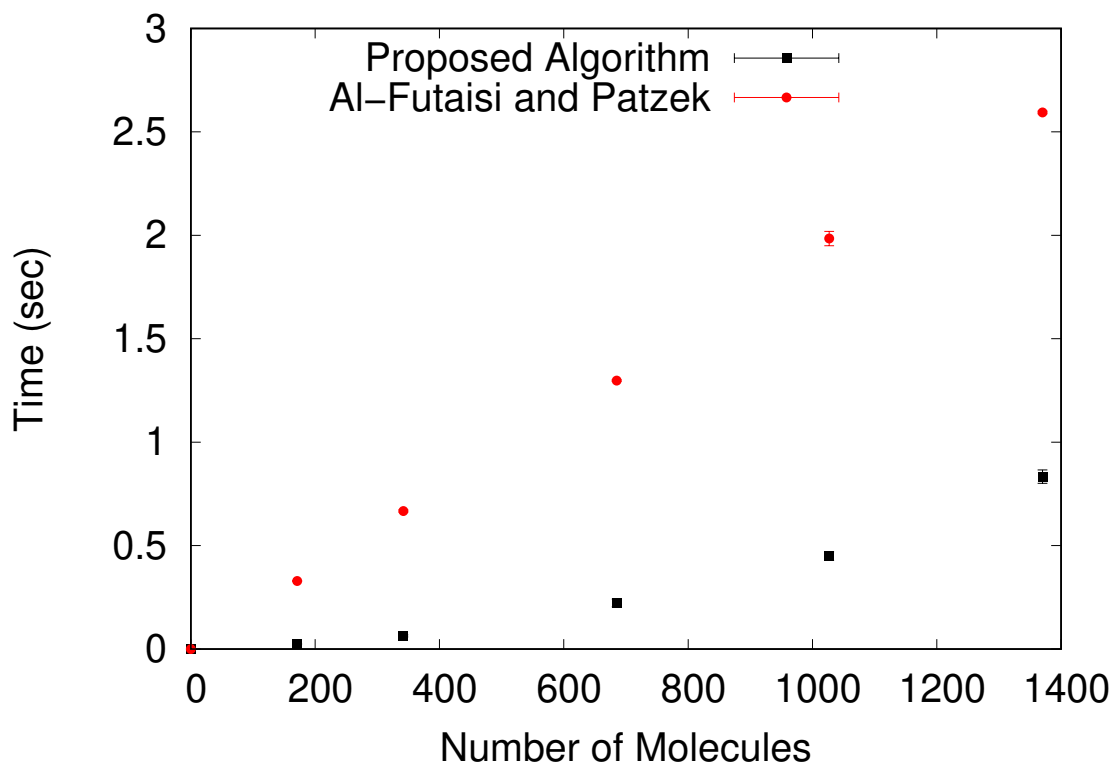


Figure 4.15: Time performance comparison between Al-Futaisi and Patzek algorithm and the proposed clustering routine for 100 timesteps. The proposed routine is faster. Triplicate has been performed for average and standard deviation calculations. In some cases standard deviations are too small, seeming not visible.

Table 4.3: Influence of neighboring routine parallelization on its running time for different number of molecules (100 run timesteps). Time in seconds and % of improvement compared to 1 processor. Triplicate has been performed for average and standard deviation calculations.

Number of molecules	1 processor	4 processors	8 processors
171	6.825 ± 0.033	1.764 ± 0.021 (74.15%)	1.217 ± 0.009 (82.17%)
342	27.500 ± 0.087	7.026 ± 0.055 (74.45%)	4.795 ± 0.031 (82.56%)
685	111.863 ± 0.277	28.147 ± 0.120 (74.84%)	20.189 ± 0.235 (81.95%)
1027	265.401 ± 0.387	66.567 ± 0.075 (74.92%)	48.181 ± 0.166 (81.85%)
1370	472.411 ± 0.068	118.567 ± 0.082 (74.90%)	83.056 ± 0.614 (82.42%)

When different concentrations are compared in terms of numbers of links (Figure 4.16), as the number of molecules increases, the number of connections also augments. High concentration decreases the distance between molecules, which makes the formation of the links more manageable. The larger number of links is not reflected in a lower number of clusters, as shown in Figure 4.17. Initially, different systems contain a different number of clusters (the number of molecules at the

beginning). The extent of aggregation to which each system is subjected is better understood if the number of clusters evolution is normalized by the initial number of clusters, which can be observed in the inset of Figure 4.17. In the inset graph, as the concentration increases, the normalized number of clusters decreases, resulting in a higher number of links.

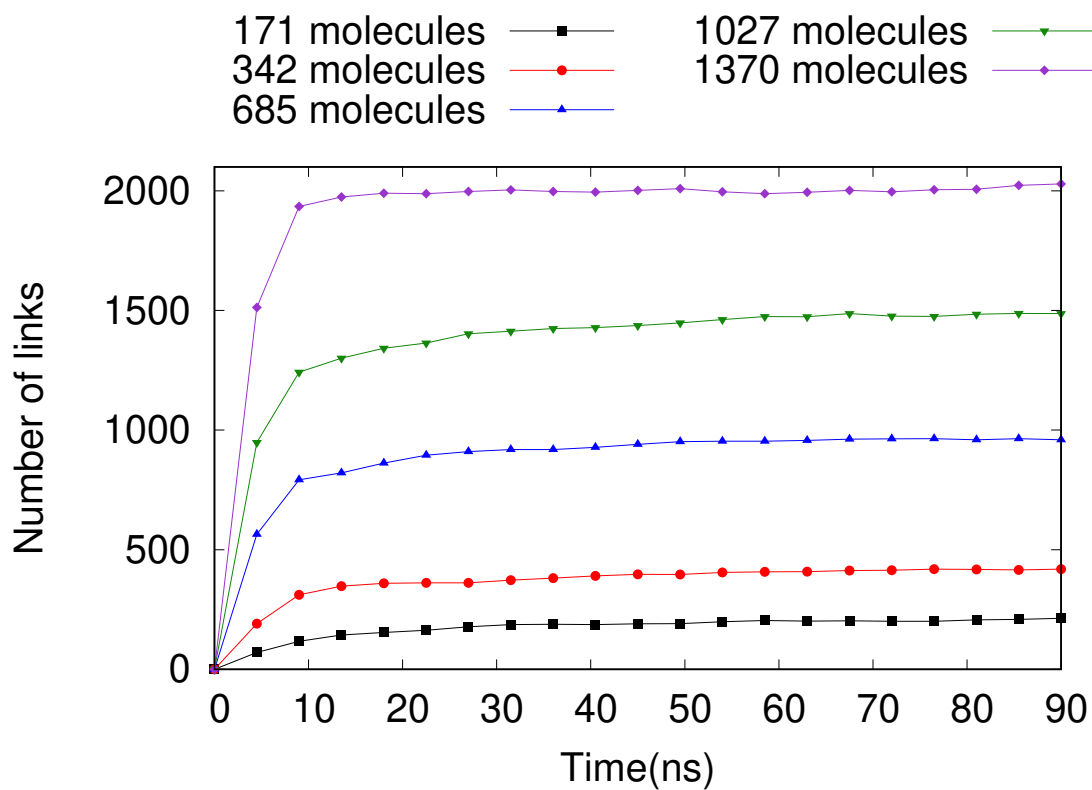


Figure 4.16: Evolution of number of links comparing different asphaltene concentrations.

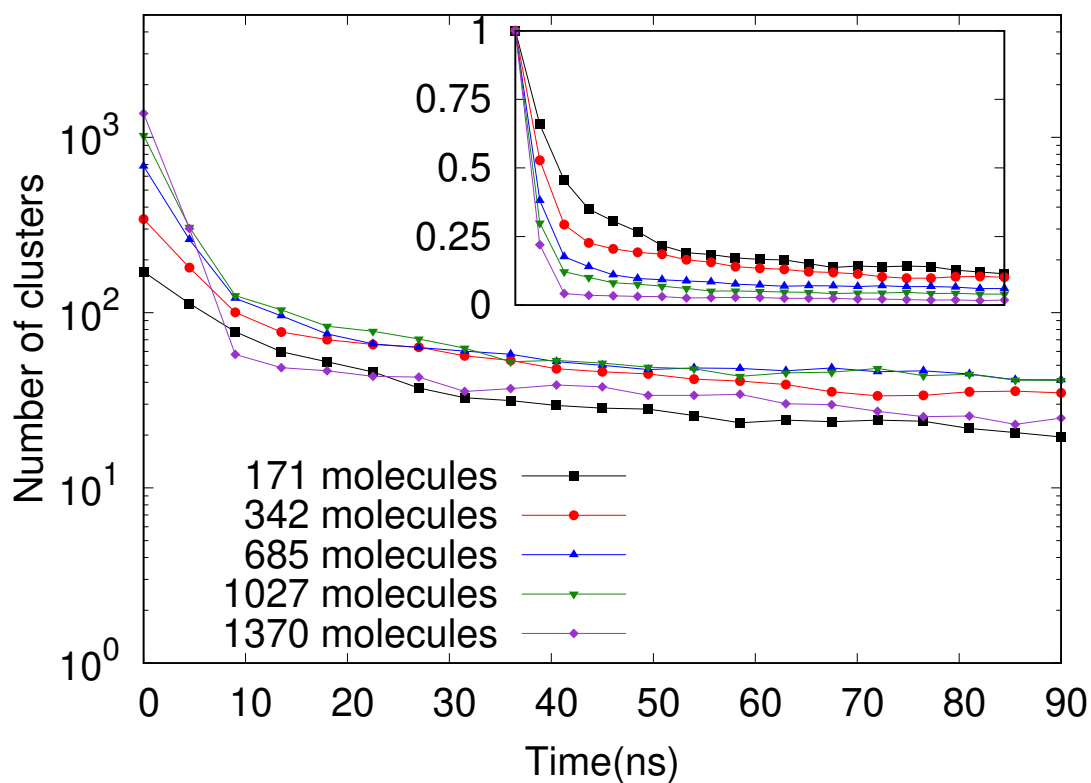


Figure 4.17: Evolution of number of clusters comparing different asphaltene concentrations. The inset represents the curves normalized by the initial number of clusters (number of molecules). As the concentration increases, the plateau to which those curves tend decreases, as a consequence of high number of links (See Figure 4.16.)

Chapter 5

Bulk Simulation of Asphaltene Aggregation

This Chapter is based on (DE OLIVEIRA *et al.*, 2020a)

In this Chapter the effects of different concentrations and solvents in asphaltene solutions properties were studied using a mesoscale simulation approach named dissipative particle dynamics (DPD). Structural analysis revealed the predominance of parallel stacking between molecular planes. The time evolution of number of aggregates showed that the number of aggregates diminishes for both solvents, which makes sense as initially each aggregate represents isolated molecules. Viscosity has been calculated for all cases and the results show that solute-solvent interactions have a great impact on the viscosity of the material which becomes less important as the entropy becomes dominant when mass fraction increases. The viscoelastic behavior of asphaltene suspensions has been analysed for the first using a molecular dynamics approach. All systems presented greater viscous (liquidlike) behavior under high frequencies which is consistent with soft particles.

5.1 Coarse-Graining and Simulation Details

Determining a coarse-graining model for real molecules is not simple, ESPAÑOL and WARREN (2017) published a review paper commenting on strategies and problems related to coarse-graining in the DPD method. The main problem to generate coarse-grained structures for asphaltenes lies on the impossibility of fixing the number of compounds and their structure in the crude oil. In terms of DPD coarse-graining, the work published by ZHANG *et al.* (2010) was the basis for many others (CHEN *et al.*, 2017a; SONG *et al.*, 2016; WANG *et al.*, 2014; XU *et al.*,

2011) all of them were capable to reproduce aggregation and structural/dynamical features of asphaltene suspensions. In this work the Song's molecules were used (SONG *et al.*, 2016). Despite all uncertainty related to what asphaltene molecules look like, it is accepted that they are constituted of aromatic rings, alkyl side chains and heteroatoms. The molecule showed in Figure 5.1 has an island structure which means that it is formed by many central rings surrounded by side chains. This structure is referenced as "like hand" structure, with the palm represented by the central core and fingers representing side chains. Three types of particles were used: B bead (blue) represents a moiety of aromatic rings which represents the benzene, H bead (green) represents a butane molecule which forms the alkyl side chains and T bead (red) that represents a thiourea molecule which has been chosen as the heteroatom group. In this section, each bead corresponds to the volume of three water molecules.

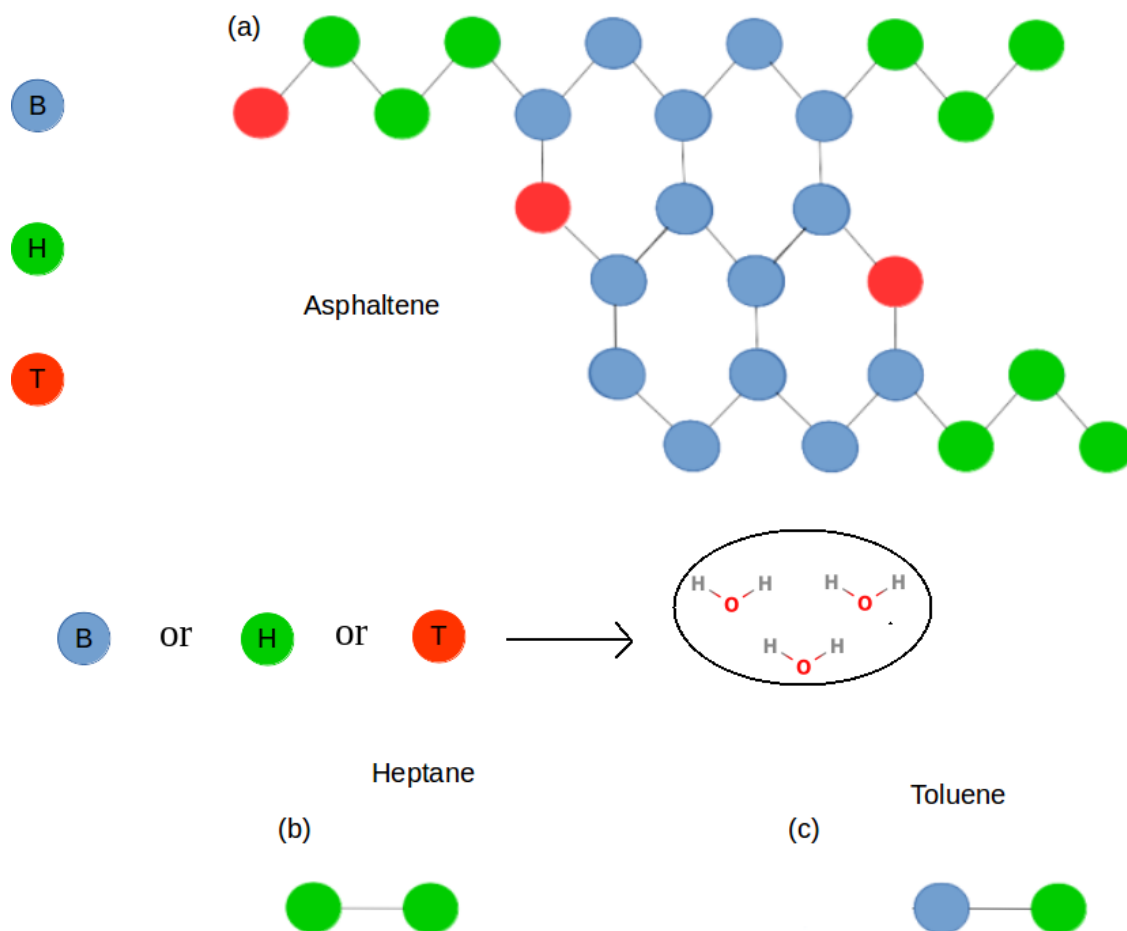


Figure 5.1: Molecules representation: B bead (blue) represents a moiety of aromatic rings which is the benzene in this approach, H bead (green) represents a butane molecule which forms the alkyl side chains, T bead (red) represents a thiourea molecule which is the heteroatom group. (a) Asphaltene molecule structure. (b) Heptane molecule structure formed by two butane molecules. (c) Toluene molecule structure formed by butane and benzene. each bead corresponds to the volume of three water molecules.

Figure 5.2 shows the structural formula of this hypothetical asphaltene molecule.

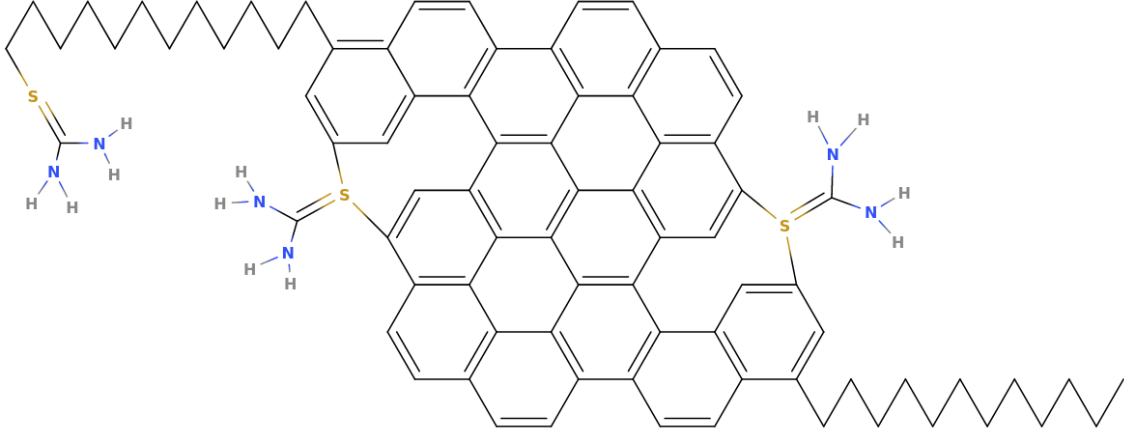


Figure 5.2: Structural formula of the hypothetical asphaltene molecule model used in this work. The heteroatoms were described in detail.

Following the methodology of GROOT and WARREN each particle (B, H or T) corresponds to N_w water particles. A cube of size r_c^3 and density ρ (DPD particles for r_c^3) has ρN_w water molecules. The volume of one water molecule, for liquid water at room temperature, is estimated at 30 \AA^3 (GROOT, 2004). Applying the same proportion to the case with ρN_w water molecules, we get the following expression:

$$r_c = 3.107(\rho N_w)^{1/3} \text{ \AA} \quad (5.1)$$

This expression gives the length scale of the system. The time scale, τ , will be:

$$\tau = r_c \sqrt{\frac{m}{k_B T}} \quad (5.2)$$

Where m is the mass of a DPD particle, that is, $m = N_w m_{H_2O}$, and m_{H_2O} is the mass of a water molecule, 54 u.m.a. . As the number of interactions increases with the number of particles, the DPD method is more efficient when $\rho = 3$ (GROOT and WARREN, 1997). $N_w = 3$ was chosen as the number of water molecules in one DPD particle, see Figure 5.1. The energy scale is given by $k_B T$. Therefore, for this coarse-graining $r_c = 6.46 \text{ \AA}$, $m = 54 \text{ amu}$ and $\tau = 3.02 \text{ ps}$.

The DPD conservative force parameter (a_{ij}) is determined by its relationship with the Flory-Huggins χ parameter (GROOT and WARREN, 1997):

$$a_{ij} = a_{ii} + \left(\frac{0.3 \text{ kcal}}{\text{mol \AA}} \right) \chi_{ij} \quad (5.3)$$

Table 5.1: Hansen solubility parameters (δ^{Hansen}) and molar volume (v) of particles B, H e T at 298 K.

Particle	δ (J/cm^3) ^{1/2}	v (cm^3/mol)
Benzene (B)	18.51	89.4
Butane (H)	14.10	101.4
Thiourea (T)	33.01	72.8

Table 5.2: Interaction parameters a_{ij} between particles B,H e T in DPD units.

	B	H	T
B	62.0	80.4	100.5
H	80.4	81.0	119.1
T	100.5	119.1	47.0

To obtain the water compressibility with three water molecules per DPD particle, a_{ii} must be $\frac{7.15 \text{ kcal}}{\text{mol}\text{\AA}}$. The values of the χ parameter are found by the following expression:

$$\chi_{ij} = \frac{v_{ij}}{RT} (\delta_i^{Hansen} - \delta_j^{Hansen})^2 \quad (5.4)$$

Where R is the gas constant. v_{ij} is the average molar volume between particles i and j . In equation 5.4, δ_i^{Hansen} and δ_j^{Hansen} are the Hansen solubility parameters of particles i and j , respectively. The Hansen solubility parameter have already been used in several studies (ORTEGA-RODRIGUEZ *et al.*, 2001; SHI *et al.*, 2015) and probed to produce good results for the calculation of asphaltene properties at the water-oil interface.

The Table 5.1, shows the interaction parameters for the simulated molecules. The data was taken from HANSEN (2007).

The conservative force parameters were obtained from SONG *et al.* (2016), they are shown in Table 5.2:

The dissipative and random force parameters used were $\gamma_{DPD} = 4.5$ and $\sigma_{DPD} = 3$ in DPD units as previous stated by GROOT and WARREN (1997). The bond potential is harmonic, given by:

$$E_{bond} = K_{bond}(r - r_0)^2 \quad (5.5)$$

Where $K_{bond} = 150.0 \text{ kcal/mol/\AA}^2$ and $r_0 = 3 \text{ \AA}$ between aromatic beads and $K_{bond} = 1.5 \text{ kcal/mol/\AA}^2$, $r_0 = 4.25 \text{ \AA}$ between aliphatic beads and aliphatic-

aromatic interactions. The angle potential used is:

$$E_{angle} = K_{angle}(1 - \cos(\theta - \theta_0)) \quad (5.6)$$

Where $K_{angle} = 300.0$ kcal/mol and $\theta_0 = 120^\circ$ is the equilibrium angle. The improper potential used is:

$$E_{improper} = K_{improper}(1 + d \cos(n\phi)) \quad (5.7)$$

Where $K_{improper} = 12.5$, $d = -1$ and $n = 2$. The intramolecular parameters were chosen in order to keep the molecule rigidity without promoting undesirable heating.

Equilibration simulations were firstly carried out and then, aggregation and shearing were performed. Figure 5.3 shows the temporal/sequential scheme.

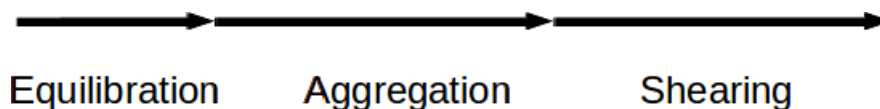


Figure 5.3: Sequential scheme of equilibration, aggregation and shearing simulations.

The simulation geometry is a cubic box with edge equals to 200 Å, the mass fractions used were $X = 0.05, 0.1, 0.2, 0.3$ and 0.4 . Toluene and heptane were used as solvents. The equilibrium temperature was set to 298 K for all simulations. Periodic boundary conditions were applied in each direction. Right after the equilibration timesteps, the time was set to 0, this is when aggregation starts. Nonequilibrium simulations (Shear) started after aggregation. Timestep of 15 fs was used and $6 \cdot 10^6$ timesteps were performed in both aggregation and shear simulations. LAMMPS has been used as simulation tool because of parallelization procedure.

5.2 Microstructure

Before analyzing the aggregate structures, the equilibrium conditions were verified. The equilibration runs were performed within $6 \cdot 10^5$ timesteps, 10% of total simulation time. The temperature equilibrated quite well for all cases. The equilibrium pressure dropped as the mass fraction was increased either in heptane or toluene which is explained by the fact that asphaltenes molecules diffuse slower than

the solvent ones, decreasing the kinetic contribution of the virial term in pressure calculation (TSAI, 1979). Figure 5.4 shows that the temperature initially increases reaching the equilibrium temperature after $4 \cdot 10^4$ timesteps. The pressure equilibration profiles, Figure 5.5, shows a rapid decrease in heptane, but in toluene the initial pressure oscillates between negative and positive values, which can be explained by solute - solvent interactions. In the toluene case, there is a higher density of relatively attractive interactions which causes a contraction effect and a dramatical increase in pressure and temperature. The oscillations represent the thermostat attempts to stabilize the systems towards equilibration.

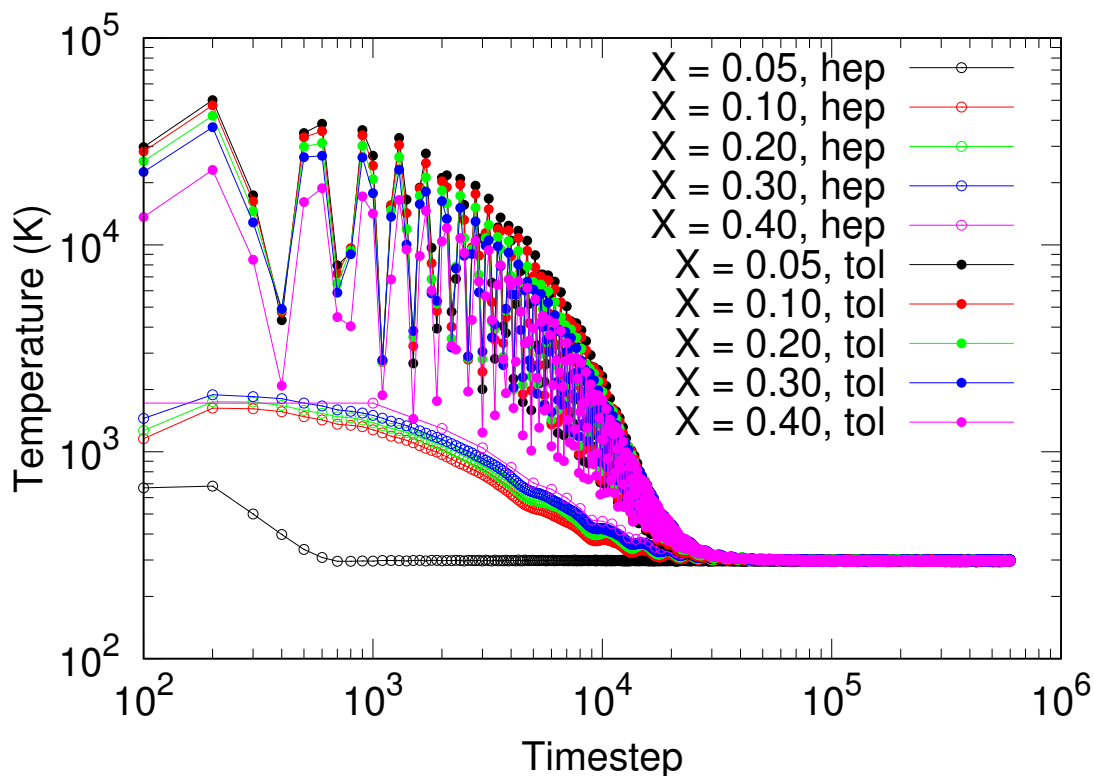


Figure 5.4: Temperature equilibration profile for asphaltene simulation in heptane and toluene. Different colors represent different mass fractions.

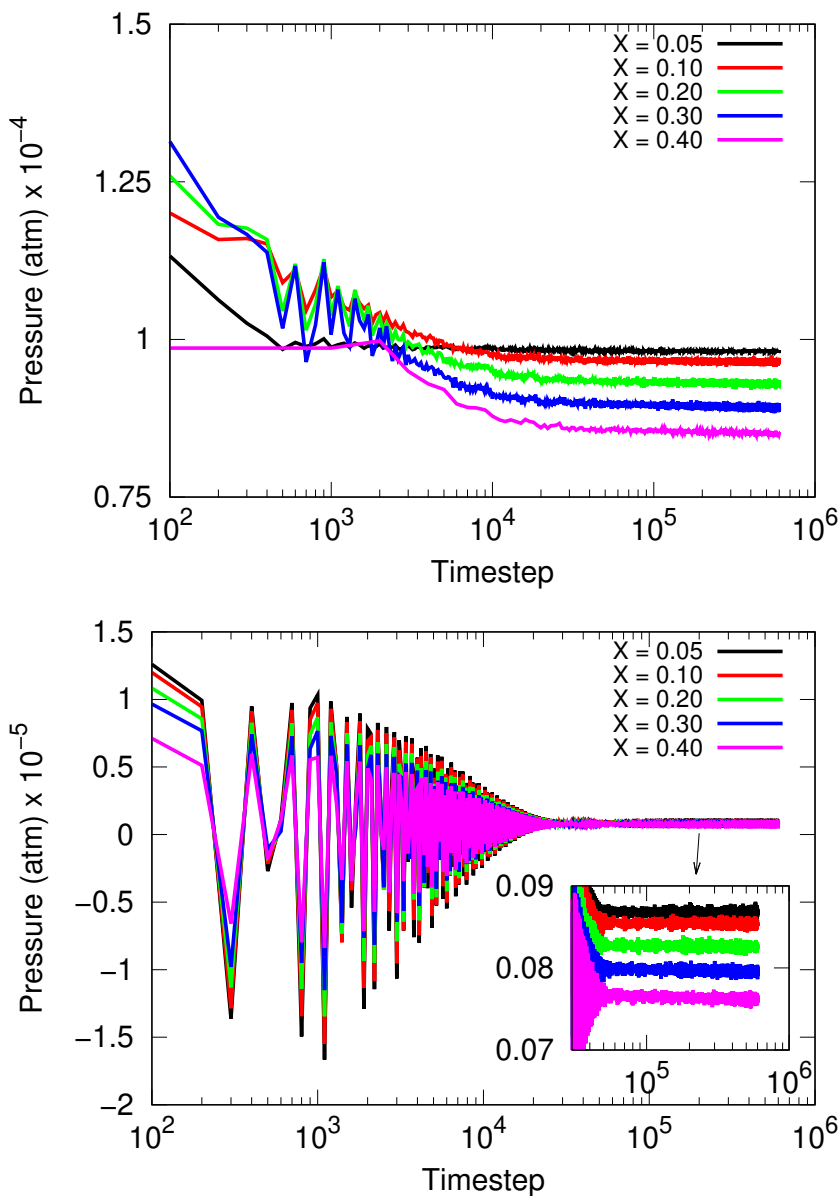


Figure 5.5: Pressure equilibration profile for asphaltene simulation in heptane (top) and toluene (bottom). Different colors represent different mass fractions.

Figure 5.6 shows the three ways that molecules approach each other and aggregate. Firstly they can aggregate face-face, caused by the balance between π - σ attractions and π - π repulsion (HUNTER and SANDERS, 1990), secondly they can assume offset structure. Thirdly molecules can get T-shaped geometry. The same structures were obtained by ZHANG *et al.* (2010) and XU *et al.* (2011).

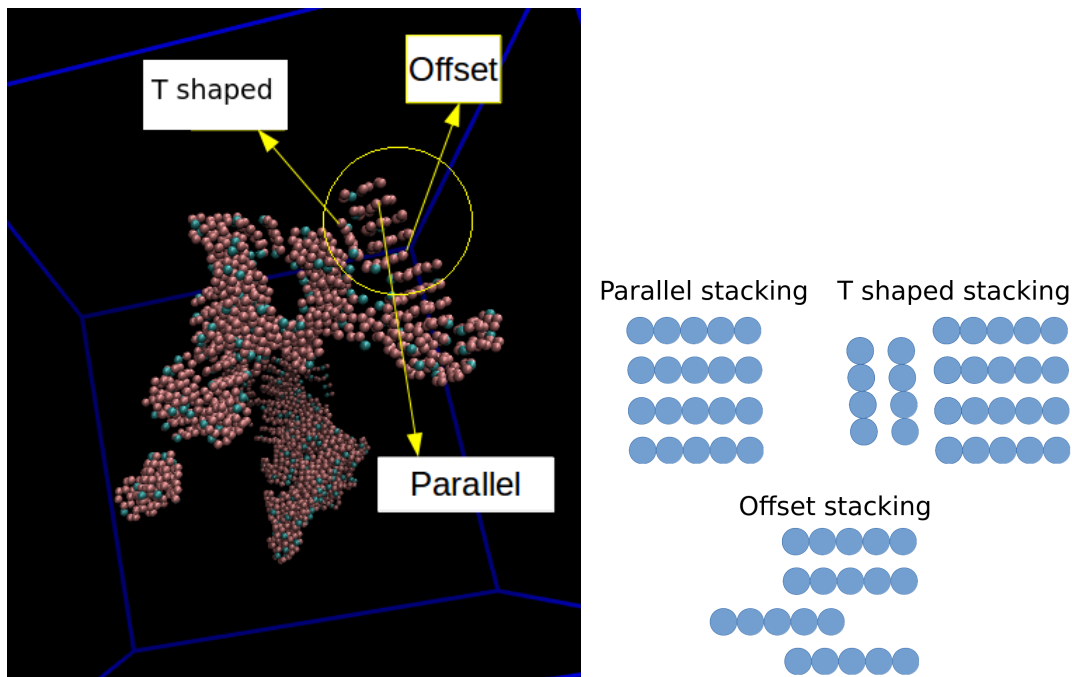


Figure 5.6: (Left) Parallel, T-shaped and offset conformations have been found, as obtained by previous works (XU *et al.*, 2011; ZHANG *et al.*, 2010). Only asphaltene particles are shown to better visualization. (Right) Schematically representation of stacking types.

5.2.1 Radial Distribution Function - $g(r)$

It is possible to know some aspects of the average microscopic structure of the materials by using pair correlation functions. These functions allow to establish connections between fluid structure and macroscopic thermodynamic properties (MCQUARRIE, 2004). One of the simplest correlation functions is the radial distribution function (RDF - *Radial distribution function*), which describes the average distribution of atoms around a specific one. The RDF indicates the probability of finding a pair of atoms, separated by a distance r , with respect to the probability of a random distribution. This function is commonly represented by $g(r)$.

In fluid systems, atoms and molecules move randomly and continuously. RDF is useful for describing the average fluid structure. For the calculation of $g(r)$ a specific particle is selected, a series of concentric spherical shells is established around it, separated by a small fixed distance δr . Static images of the system are obtained and the number of particles $N(r)$ found in each spherical shell of average radius r is counted in uncorrelated time intervals. At the end, the average number of $N(r)$ particles in each shell is calculated. $N(r)$ is divided by the volume of the spherical

shell V_c to obtain the radial numerical density $\rho(r)$.

$$V_c = \frac{4\pi}{3}(R^3 - r^3) \quad (5.8)$$

$$\rho(r) = \frac{N(r)}{V_c} \quad (5.9)$$

For a homogeneous and one-component system, RDF is obtained by normalizing $\rho(r)$ by the average numerical density of atoms (*bulk number density*), ρ , of the system (HIRSCHFELDER *et al.*, 1964). The result is time averaged.

$$g(r) = \frac{\rho(r)}{\rho} \quad (5.10)$$

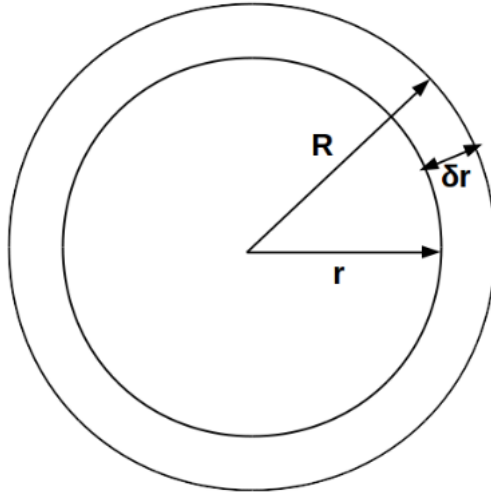


Figure 5.7: Scheme for counting particles and calculating $g(r)$.

For the case where $g(r) = 1$, there is a complete randomness in the particle distribution. The function $g(r)$ indicates how the particle positions are correlated, that is, how the position of one particle influences the position of the others. Naturally, as r increases, the particle positions become uncorrelated, that is $\lim_{r \rightarrow \infty} g(r) = 1$.

One of the characteristics of the radial distribution functions is that they can be used to calculate macroscopic thermodynamic properties, since the hypothesis of pairwise-additivity of the potentials is considered. Configurational thermodynamic properties are correlated with the the radial distribution function, such as energy (E) and system pressure (P):

$$E = \frac{3}{2}Nk_B T + \frac{1}{2}N\rho \int_0^\infty U(r)g(r)4\pi r^2 dr \quad (5.11)$$

$$P = \frac{Nk_B T}{V} - \frac{N\rho}{6Vk_B T} \int_0^\infty r \frac{dU(r)}{dr} g(r) 4\pi r^2 dr \quad (5.12)$$

Figure 5.8 shows the typical RDF of a Lennard-Jones fluid (Argon) at different temperatures.

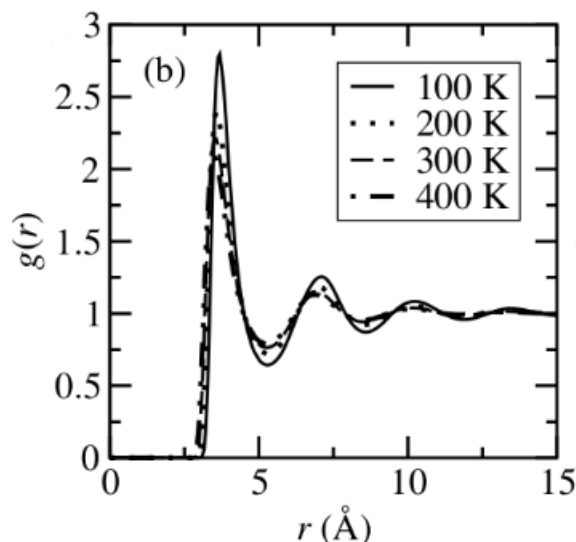


Figure 5.8: Radial Distribution Function extracted from TUCKERMAN (2010) for a Lennard-Jones fluid with $\sigma = 3.405 \text{ \AA}$ and $\epsilon/k_B = 119.8 \text{ K}$ (Argon).

The center-to-center radial distribution function $g(r)$ has been calculated to study the asphaltene aggregation structure. The distance between center of mass molecules was considered in this calculation. Comparing different mass fractions, Figures 5.9, it is observed that lower mass fractions produce higher first peaks in the radial distribution function which is explained by greater volume exclusion effects at large concentrations which harms ordering. Similar results were obtained by CHEN *et al.* (2017a). When different solvents are compared for the same mass fraction, the $g(r)$ curves are basically the same, that is, the microstructure is the same regardless the solvent is used. This is opposite of what would be expected. Toluene is a better solvent than heptane for asphaltene molecules thus less ordering would be expected to be observed for it. The results show that the radial distribution function give information about nanoaggregation, but it is not the best way to understand solubility which is more related to larger aggregation. As the interactions between aromatic cores are the main force leading to nanoaggregation, the number of asphaltene molecules is a much stronger factor in determining the final structure than the solute-solvent interactions. The experimental distance between asphaltene molecule planes is about 3-4 Å (ALVAREZ-RAMIREZ *et al.*, 2006; MULLINS, 2010; PACHECO-SÁNCHEZ *et al.*, 2003). The first peak of $g(r)$ occurs at $\sim 5.8 \text{ \AA}$ in the

present simulations, which agrees with Song’s results. This distance is higher than the experimental because molecular planes are often displaced from their centers (offset) (SEDGHI *et al.*, 2013). At lower mass fractions $g(r)$ is not going to 1 which means that in those cases there is a higher order correlation.

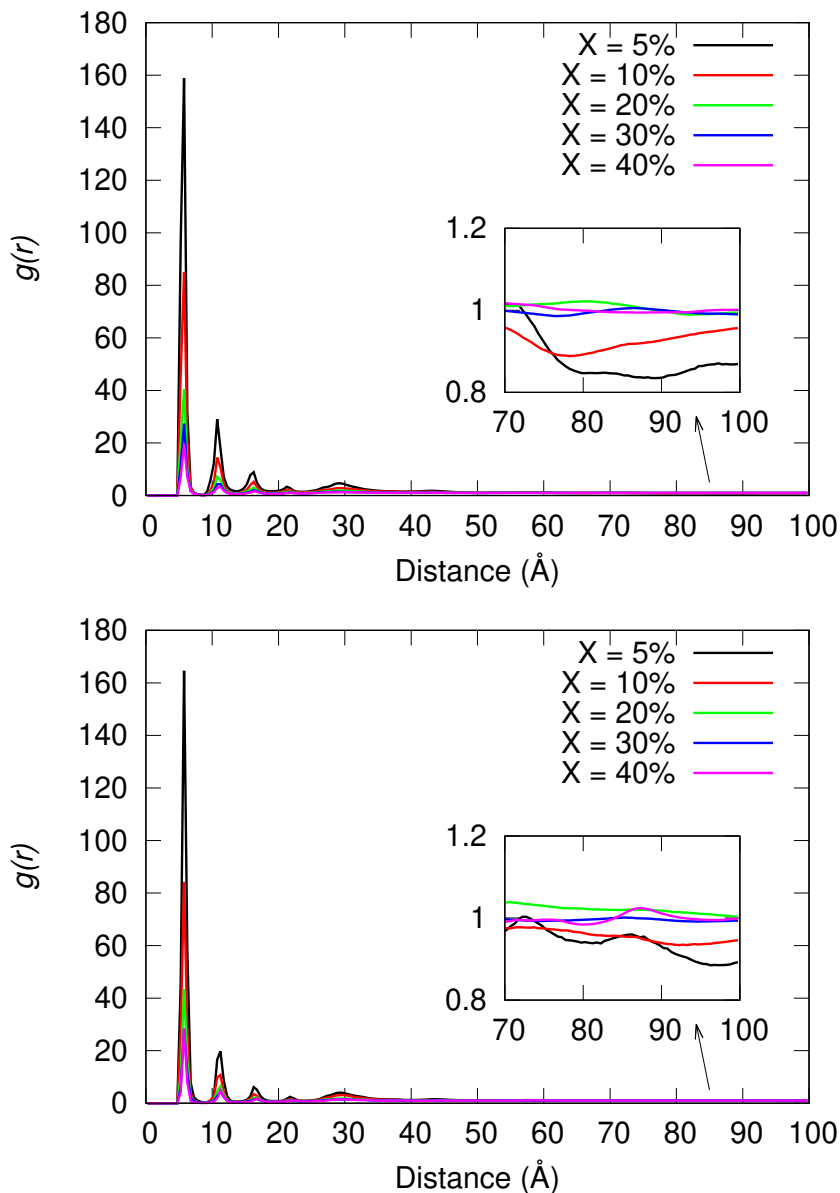


Figure 5.9: Radial distribution function $g(r)$ for center of mass distances between asphaltene molecules in heptane (top) and toluene (bottom) at 90 ns. The insets show $g(r)$ at long distances. Different colors represent different mass fractions.

5.2.2 Angle Between Molecules

The angle between asphaltenes (See Figure 5.10) was calculated in order to better understand the structure of the formed nanoaggregates. in addition to par-

allel structure, the asphaltenes can also stack *offset* or T-shaped. ZHANG and GREENFIELD (2007a) stated that two asphaltene molecules are ordered when the angle between their planes is 0° (parallel) and disordered when the angle between their planes is 90° .

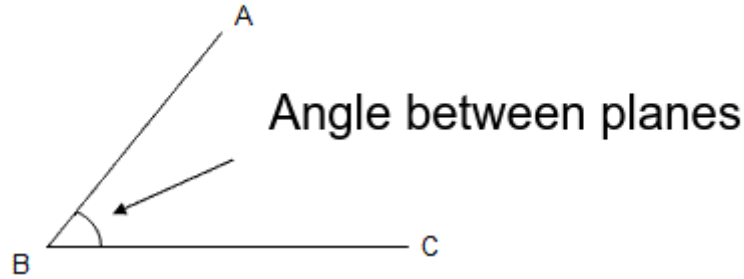


Figure 5.10: Angle between asphaltene planes. Each asphaltene is represented by the straight lines AB and BC.

The angle between asphaltenes was calculated for each case at the end of the simulations, with that information angle probability histograms are presented. Optimization algorithm was used to find the plan equation that best fit the particles belonging to the same molecule. The acute angle θ between the planes $a_1x + b_1y + c_1z + 1 = 0$ and $a_2x + b_2y + c_2z + 1 = 0$ is calculated using:

$$\cos(\theta) = \frac{a_1a_2 + b_1b_2 + c_1c_2}{\sqrt{(a_1^2 + b_1^2 + c_1^2)(a_2^2 + b_2^2 + c_2^2)}} \quad (5.13)$$

Through Figures 5.11-5.12 it can be seen that almost 30%-60% of contact angles are in between 0° - 7.2° which reveals the predominance of parallel structure contacts. One contact is verified when two particles belonging to different molecules are separated by a distance smaller than $1.1 r_c$. The $1.1 r_c$ distance has been chosen because it is the distance of the first minimum on $g(r)$ which means that it is the distance of the first shell aggregation.

Angle Probability

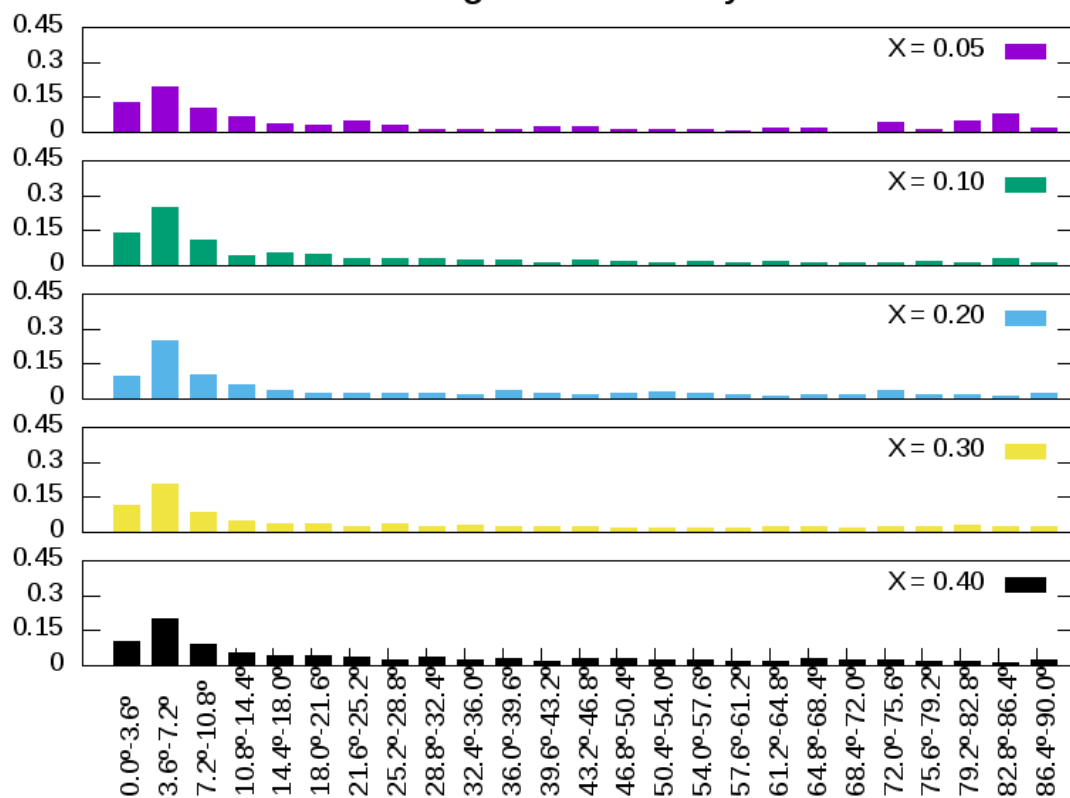


Figure 5.11: Angle distributions histograms for asphaltene solution in heptane for different mass fractions at 90 ns. It is shown that the most part of molecules are stacked parallel to each other.

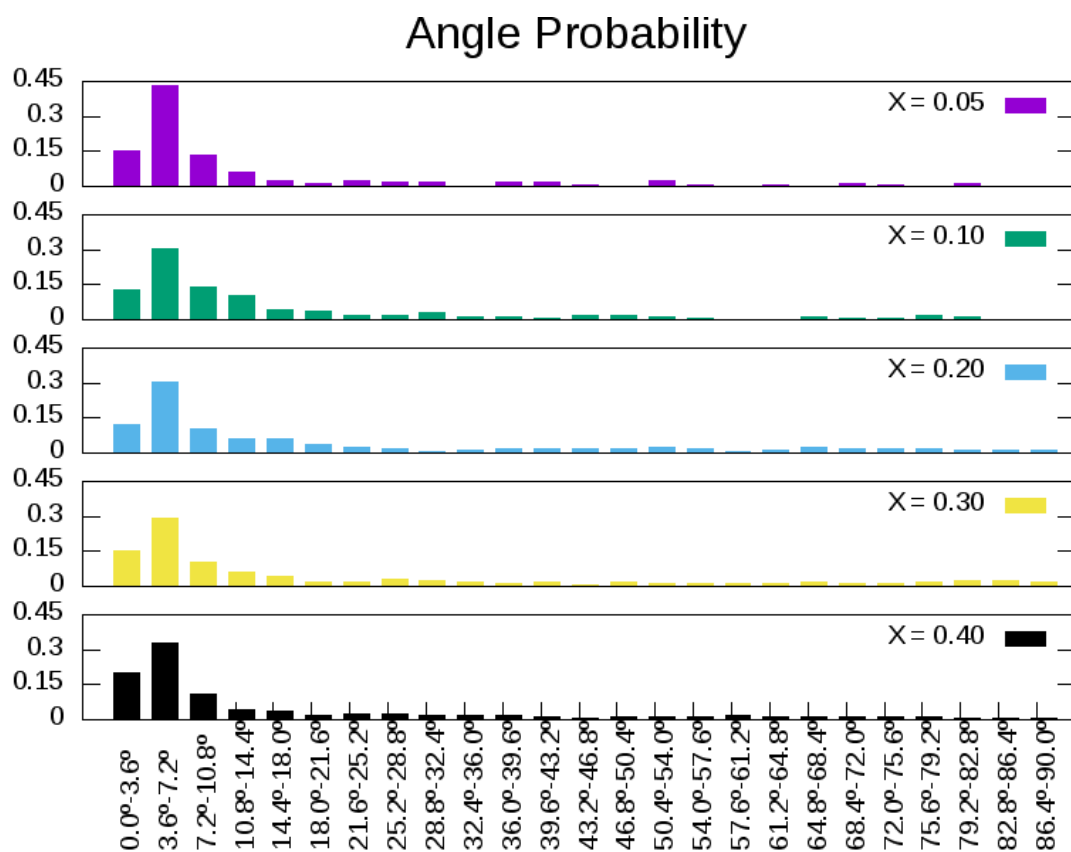


Figure 5.12: Angle distributions histograms for asphaltene solution in toluene for different mass fractions at 90 ns. It is shown that the most part of molecules are stacked parallel to each other.

The applied 3D regression methodology for determining the plan that best passes through all particles of the molecule is explained in the appendices.

5.3 Kinetics of Aggregation

In order to have a better understanding about aggregate structure, the time evolution of the number of aggregates (N) and average aggregate size (S) were calculated. The contact criterion used here is the same as the angle distribution calculations. Initially, each molecule represents an isolated aggregate. In Figure 5.13 the number of aggregates decreases with time for all mass fractions and in both solvents, which was expected as long as molecules aggregate over time. The number of clusters scales with the inverse of time. The graphs show the curves normalized by the initial number of aggregates, the 5%-30% curves collapses to one single curve which means that the kinetics of formed aggregates is similar. At higher mass fractions there are large fluctuations at the final stages of aggregation which is due to volume exclusion effects. To understand the effects of solubility, the average

aggregate size has been calculated by the parameter S :

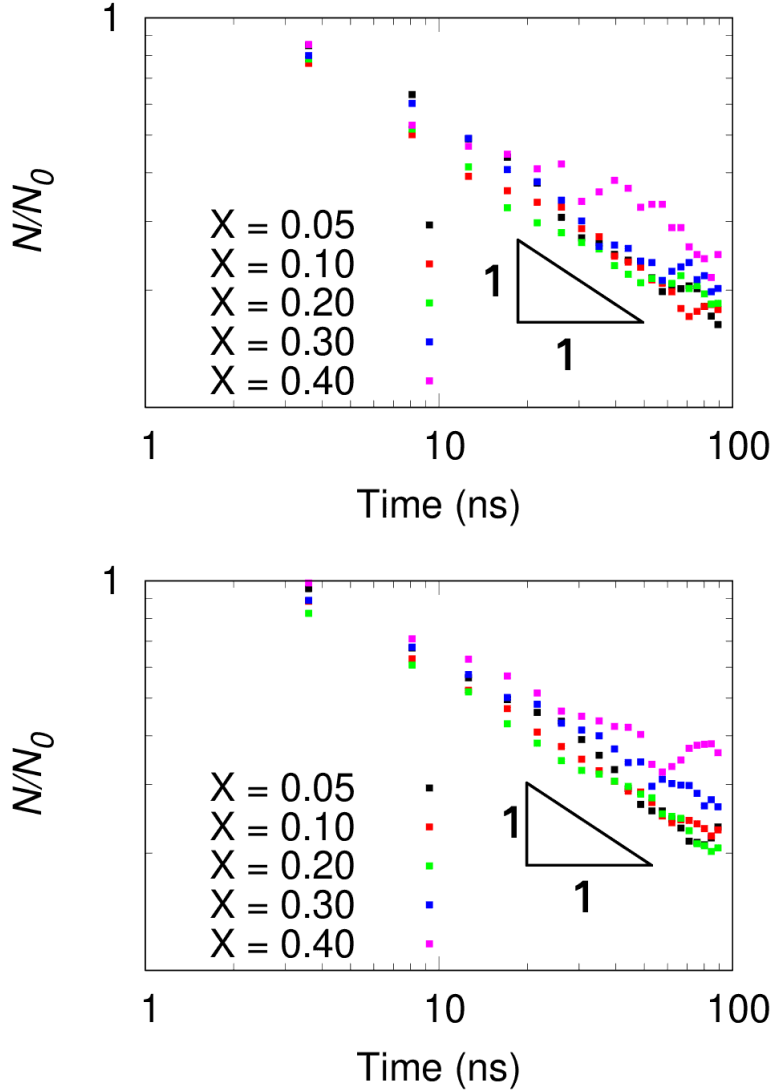


Figure 5.13: Number of aggregates evolution as a function of time for suspensions in heptane (top) and toluene (bottom). The number of aggregates N is normalized by the initial number of aggregates N_0 . The cutoff distance separation is $1.1 r_c$, in other words if two particles belonging to different molecules are separated by a distance smaller than $1.1 r_c$ these molecules are aggregated.

$$S = \frac{\sum_s s^2 n_s}{\sum_s s n_s} \quad (5.14)$$

Where n_s is the number of aggregates containing s molecules. The 40% curve in heptane is almost constant compared to the other mass fractions because of the high density which makes aggregating harder, this means that aggregates of similar size are being created. Lower mass fractions have two distinct regimes: The first one occurs until ~ 40 ns, where molecules are forming the initial aggregates, the second one is remarked by connections between the initial aggregates which

forms large structures. The final stage has a lower growing rate due to the larger size of aggregates compared to isolated molecules. It is interesting to note that 30% and 40% curves in toluene show larger fluctuations. Those fluctuations emerge from a competition between enthalpic and entropic interactions which is higher in the toluene case, as asphaltenes have better affinity with it. When enthalpic interactions predominates molecules separate. Higher mass fractions produce larger asphaltene aggregates which are less stable. Those results are shown in Figure 5.14. As shown in Figure 5.15, the average aggregate size is always larger in heptane for various mass fractions. This is due to the better solubility of asphaltene molecules in toluene which is in good agreement with experimental results (MCLEAN and KILPATRICK, 1997).

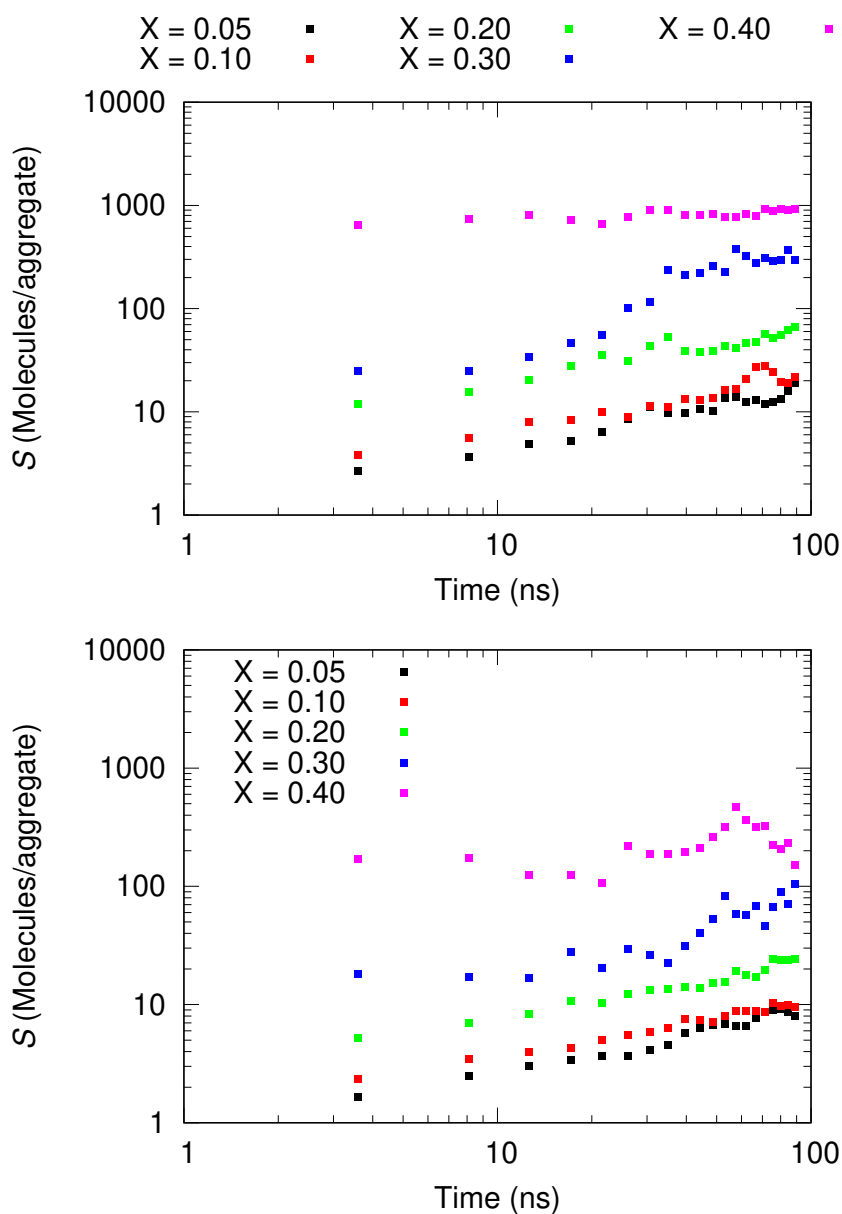


Figure 5.14: Average aggregate size S in function of time for asphaltene in heptane (top) and toluene (bottom). S is calculated using Equation 5.14 which takes into account the number of aggregates n_s of s molecules.

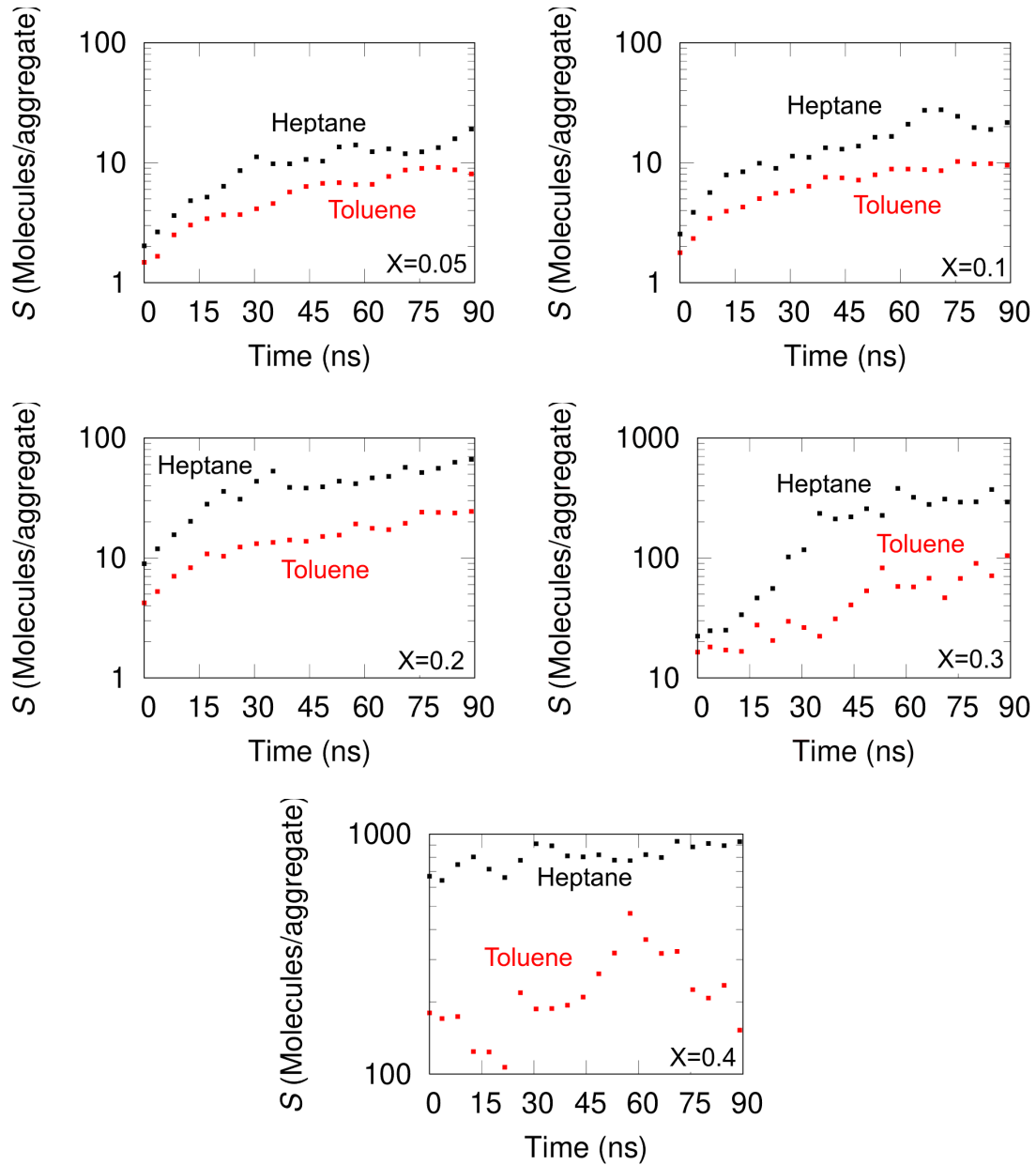


Figure 5.15: Average aggregate size S comparison between solvents for different mass fractions in function of time. Solutions in heptane have larger aggregates, therefore asphaltenes are more diluted in toluene.

(ZIRRAHI *et al.*, 2019) have recently proposed a new methodology for calculating aggregation of particles. Using scaling relations, they developed an algorithm which can decrease aggregating computational time. They have been able to capture asphaltene onset precipitation and particle size distribution. According to their results the number of clusters evolution scales linearly with the inverse of time which is also observed in our results. They reported an increasing aggregate diameter size in time. Considering that aggregate diameter and S are related, our results agree with their simulations. Even though we have not been able to proceed the study on

asphaltene onset precipitation due to the long time required, our simulations bring a practical insight about future asphaltene precipitation.

The developed cluster algorithm used in the above calculations has been explained in the previous section.

5.4 Dynamics of Aggregation

The Mean Square Displacement - MSD , it is calculated by:

$$MSD(t) = \frac{1}{N_{total}} \sum_{n=1}^{N_{total}} (r_n(t) - r_n(0))^2 \quad (5.15)$$

Where r_n is the position of a specified centroid n , and N_{total} is the total number of asphaltene molecules. The $(r_n(t) - r_n(0))^2$ is the squared displacement of a molecule center n at time t , then the MSD is a measure of the molecular mobility.

The MSD provides information about the dynamic behavior of the system, besides the diffusion coefficient. Figure 5.16 describes three typical behaviors. Figure 5.16(a) shows the diffusion of a simple system, in a homogeneous medium, typical Fickian diffusion. Figure 5.16(b) indicates that the system is confined, there is a natural deviation from Fickian behavior. Figure 5.16(c) indicates the expected behavior for the diffusion in concentrated polymeric structures (e.g. membranes), where barriers and closed cavities exist, creating correlations at certain distances and two different diffusion regimes.

The derivative of the MSD in time gives the diffusion coefficient D . For the three-dimensional case, the diffusion coefficient is:

$$D(t) = \frac{1}{6} \frac{d(MSD(t))}{dt} \quad (5.16)$$

Diffusion is said to be restricted when the particles diffuse in a structured environment such as in pores or within a cell. When diffusive particles have an asymmetric shape, diffusion is said to be anisotropic and the diffusion coefficient is no longer a scalar but a vector.

The diffusion coefficient of spherical particles moving freely in an isotropic fluid

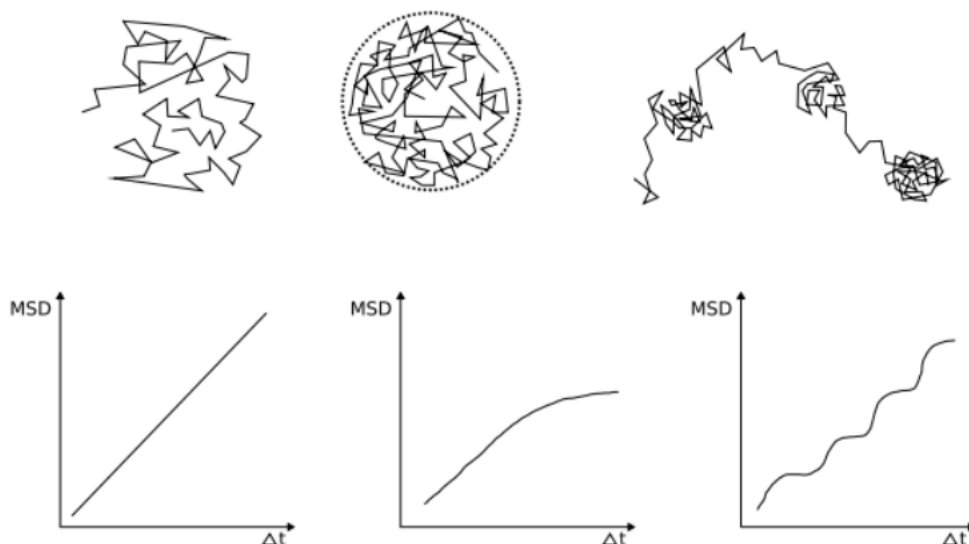


Figure 5.16: Random movements and their MSD . From the left to the right: Isotropic random movement, confined and partially confined. Image obtained from SCHWEIZER (2007).

is given by (ZIA *et al.*, 2014):

$$D_0 = \frac{k_B T}{3\pi\eta d} \quad (5.17)$$

Where η is the system viscosity and d is the particle diameter.

From Figure 5.17 it can be seen that for all cases the MSD starts from a rapid increase which is related to the free movement of molecules. After that, the movement of molecules is hindered which is characteristic of arrested phases. These results confirm that at the aggregating initial stages those systems undergo sol-gel transition (BOURIAT *et al.*, 2004; JESTIN *et al.*, 2007). This transition occurs at around 20-40 ns, which is the the same time observed for first step of aggregation in the kinetics of aggregation section. It is noticed that the higher the mass fraction is, less movement is experienced by molecules. To calculate diffusion coefficient, short and very long timescales are neglected. The experimental infinite dilution diffusion coefficient of asphaltenes in toluene is $2.2-6.3 \cdot 10^{-10} \text{ m}^2/\text{s}$ (ANDREWS *et al.*, 2006; ÖSTLUND *et al.*, 2003). The diffusion coefficient obtained in this work for 5% asphaltenes in toluene is $\sim 2.96 \cdot 10^{-10} \text{ m}^2/\text{s}$ which is within the experimental data range.

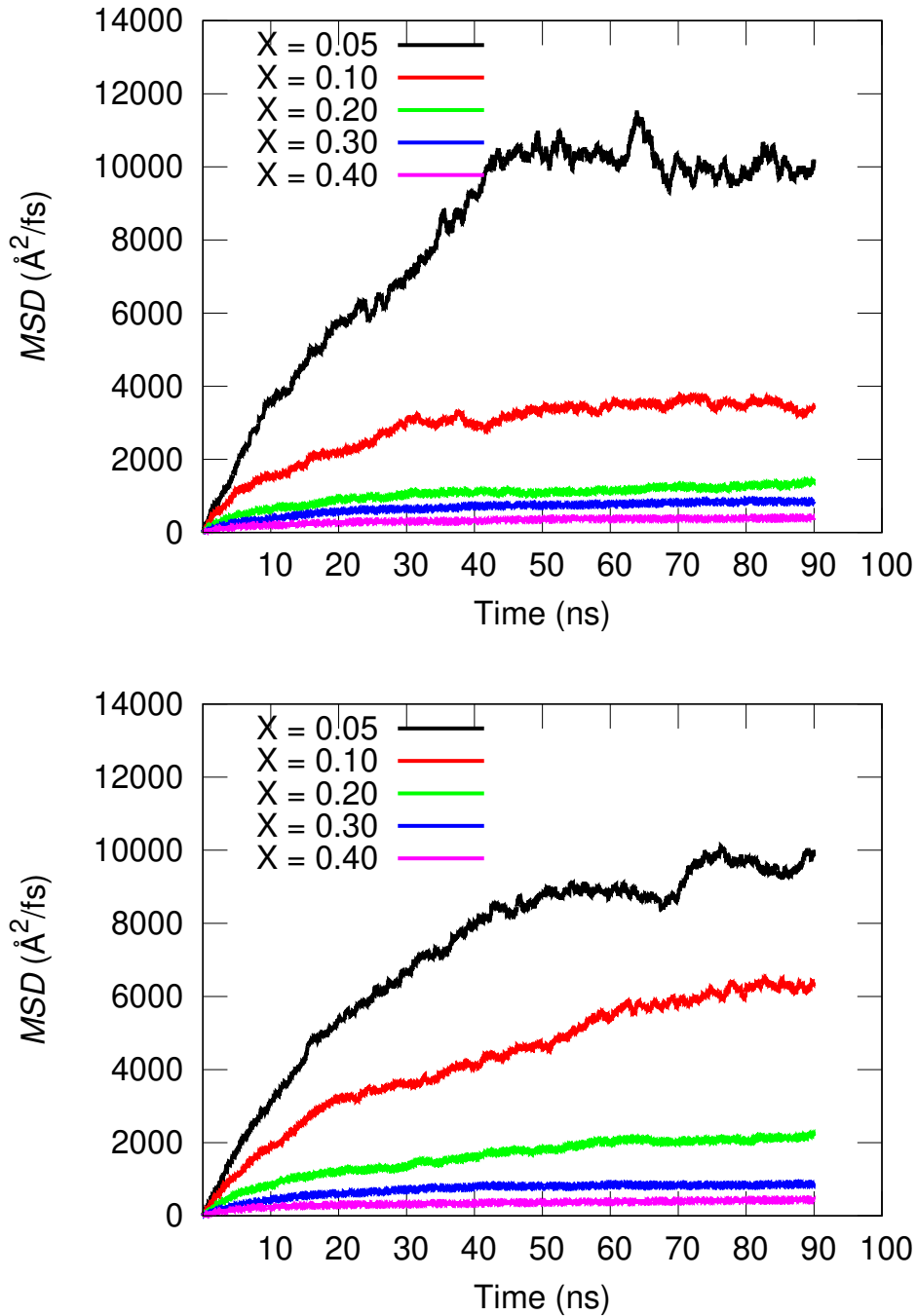


Figure 5.17: *MSD* curves for asphaltene in (top) heptane and (bottom) toluene for different mass fractions. The molecule centroids were used in the *MSD* calculation (Equation 5.15). The *MSD* measures the molecule mobility, as it can be seen their movement is being arrested in time.

In the recent work of AHMADI *et al.* (2018) they performed Brownian dynamics of asphaltene suspensions in heptane and heptol (mixture of heptane and toluene). Nanoaggregates were observed which could form fractal structures at low volume fractions and percolated structures at higher volume fractions. The percolated state is a prerequisite for gelation transition (ZACCARELLI, 2007). The

self-diffusion coefficient significantly decreases as volume fraction increases in both solvents. In the present simulation the same trends are observed, although in their results hydrodynamics is not being conserved.

5.5 Rheological Properties

5.5.1 Thermostat

Rheological properties of the system are investigated by applying either simple shear or oscillatory shear flow. One of the shortcomings of DPD is known to be its inability in stabilizing the temperature under shear flow specially at high shear rates (KHANI *et al.*, 2013; MOSHFEGH *et al.*, 2015). MOSHFEGH and JABBARZADEH (2015a,b) showed that the DPD thermostat is highly influenced by parameterization and integration methods. They found that promoting smooth momentum transfer (Modified Lees-Edwards periodic boundary condition (CHATTERJEE, 2007)) from the bulk to the boundaries, the artifacts (jumps) in velocity profile and temperature are avoided. Low values of the exponent of the weight function of the DPD method and high values of the dissipation γ parameter produce the same artifacts which are also corrected by the Modified Lees-Edwards periodic boundary condition. In the present simulations, a NVT/SLLOD thermostat was used in order to conserve the temperature under shear while subjecting the system to similar conditions. In this case NVT/SLLOD means that the particle equations of motion will be integrated in NVT ensemble solving the SLLOD equations of motion (EVANS and MORRIS, 1984). The SLLOD equations of motion are equivalent to Newton's equations of motion for shear flow, in LAMMPS they are coupled to Nose/Hoover thermostat (MARTYNA *et al.*, 1992). *MSD* results shown in Figure 5.18 confirm the ability of the thermostat in producing the same dynamics as the DPD thermostat. As the hydrodynamics is closely related to the solvent behavior, if the solvents behave the same way in both thermostats the hydrodynamics interactions (friction) will affect the solutions similarly. By Figure 5.18, it is seen that in the timescale of this study there is no differences on these approaches, therefore the Nose/Hoover thermostat was chosen for the rheological part which allowed to have stable temperatures along with the simulations.

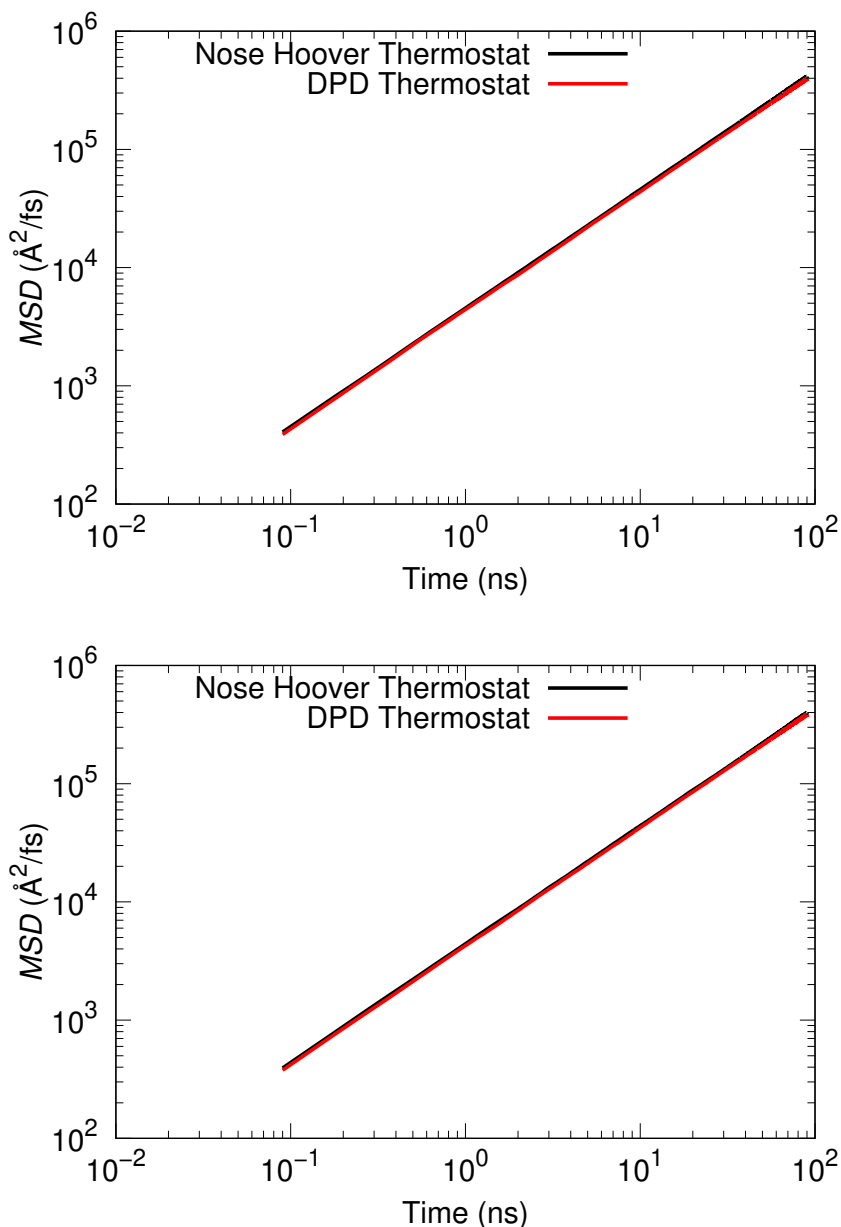


Figure 5.18: *MSD* curves for pure solvent (top) heptane and (bottom) toluene using DPD and Nose Hoover Thermostat.

5.5.2 Viscosity

Deformation was imposed on the simulation box using the *fix deform* of *LAMMPS* for the viscosity calculation. The top of the box is continuously deformed using a constant shear rate that must be specified (in units of $1/time$). The process is similar to the application of Lees-Edwards boundary conditions (LEES and EDWARDS, 1972) (Figure 5.19), that is, a linear velocity profile (shear rate) is imposed on the particles which generates a momentum flux (shear stress). The Equation 5.18 defines the viscosity function η .

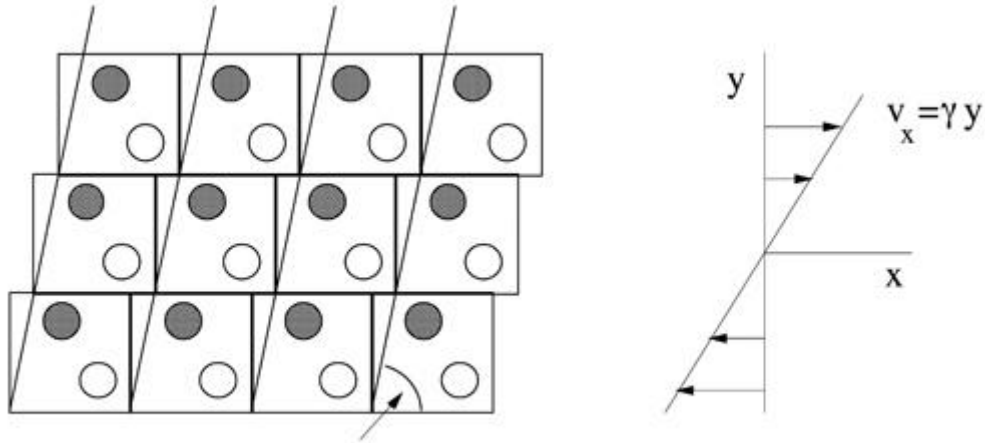


Figure 5.19: Application of a linear velocity profile on the simulation box.

$$\tau_{xy} = \eta \dot{\gamma} \quad (5.18)$$

Although this strategy is widely used, there are some problems using it. Firstly, the inclusion of an extra velocity in the integration of the equations of motion makes the system no longer Hamiltonian. The linear profile that is imposed on the system is not necessarily the one that occurs at the molecular level, so the comparison with experimental data can be compromised. For simple fluids, this approach does not cause problems, but for complex fluids it can generate erroneous values (HESS, 2002).

Highly viscous fluids transportation is a large problem in petroleum industry (MARTÍNEZ-PALOU *et al.*, 2011). The study of viscosity behavior under different shear rates and different mass fractions is crucial and could be beneficial to oil exploitation. The timestep and the total simulation time of this part were the same used in the structural/dynamical part. Figure 5.20 shows viscosity against shear rate for different mass fractions in toluene and heptane. Simple shear has been applied right after aggregation process. As shown in Figure 5.21, shearing breaks down the structure previous acquired. The viscosity decreases with shear rate for all cases which is explained by: as the structure breaks down, the asphaltenes flow parallel to each other, forming fluid layers, each fluid layer is "sliding" over the other ones, which facilitates the flow and reduces viscosity. It can be said that the shear stress induces a transition in the fluid structure, decreasing the size of the aggregates and forming parallel structures. In other words, increasing shear rate improves fluid flowing. Therefore, the suspensions present shear-thinning behavior over all probed shear rates, similar results have been obtained by WINKLER *et al.* (2014) and

JAMALI *et al.* (2015c) studying the rheology of soft colloidal systems. At lower mass fractions clearly the viscosities in toluene are higher than in heptane, which is explained by the fact that toluene experimentally has higher viscosity than heptane (REID *et al.*, 1987). At higher mass fractions those differences are not too evident because solvent influence loses importance. It is also important to notice that at lower mass fractions the systems tend to present higher newtonian behavior as they approach the simple fluid behavior (solvent behavior). Comparing simulations with the same solvent and different mass fractions, as the concentration increases, the viscosity increases, which is a consequence of the nanoaggregate size increase that augments the resistance to the momentum transfer.

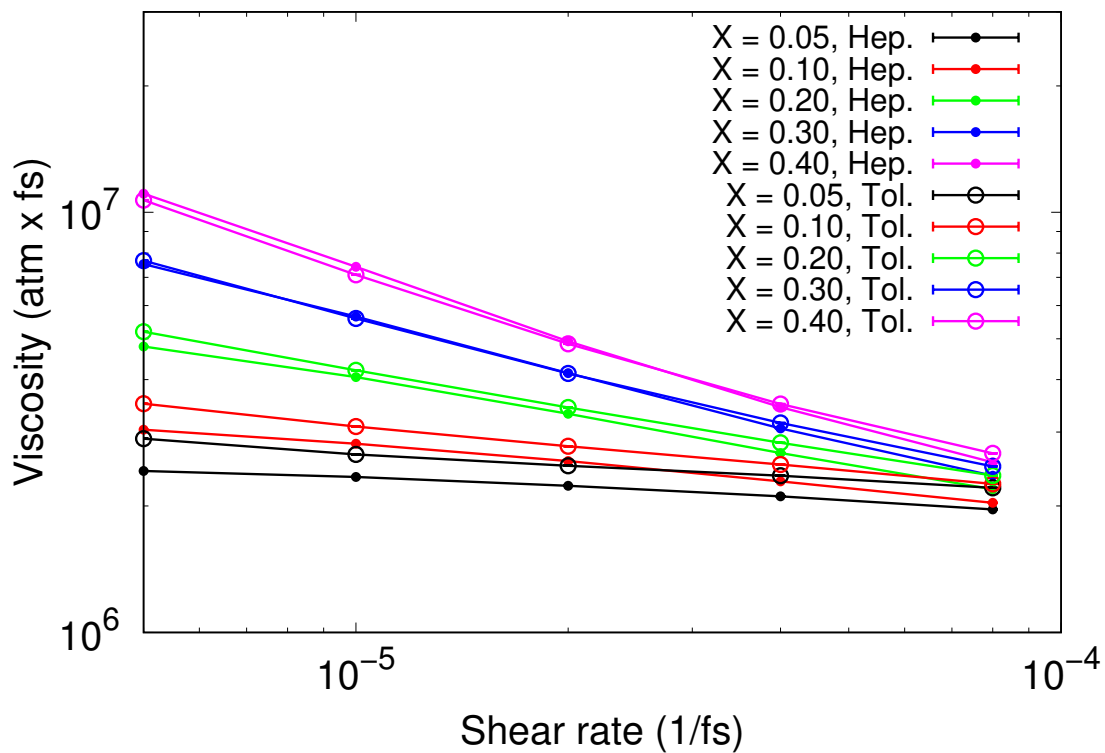
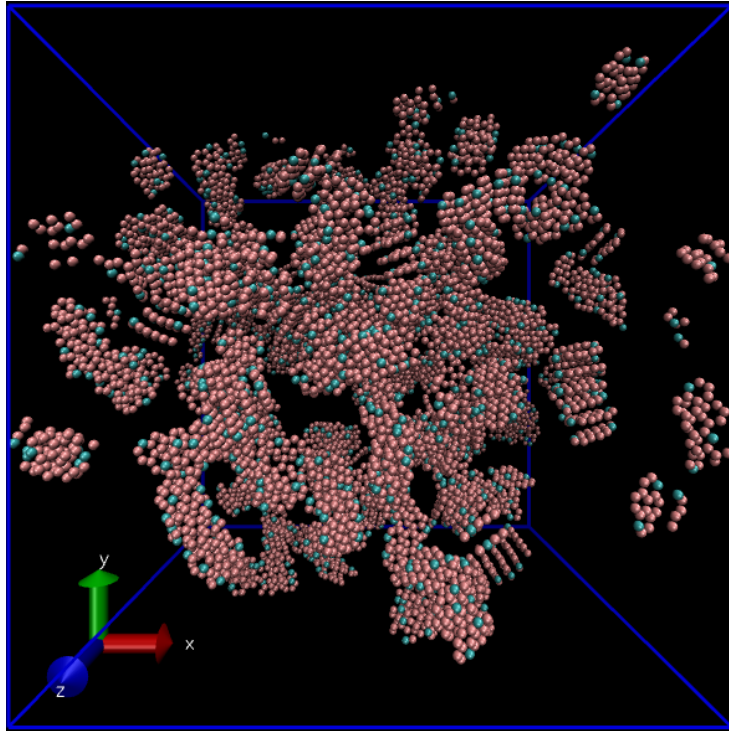
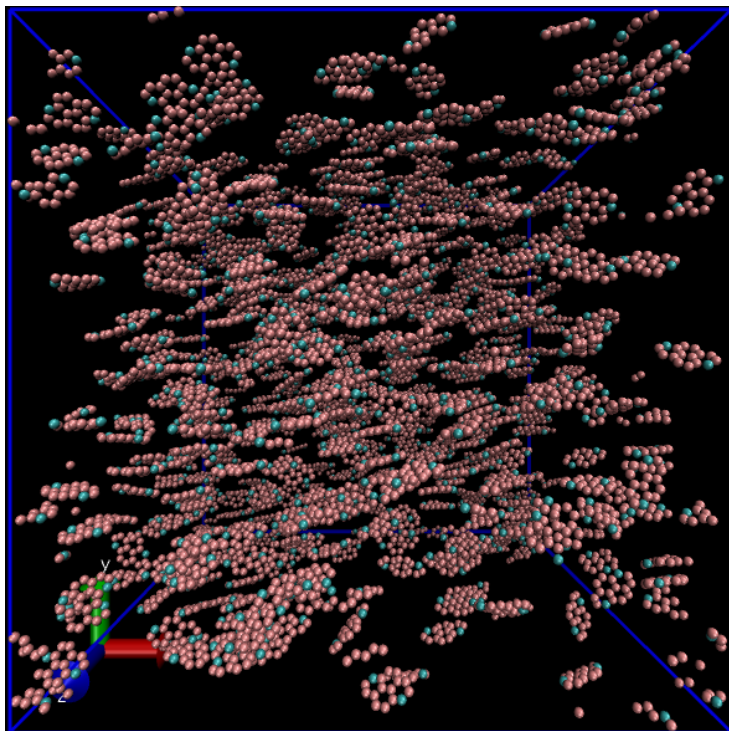


Figure 5.20: Viscosity as a function shear rate for different solvents and mass fractions. Viscosity is calculated dividing the stress by a constant shear rate applied at the box edge in one direction. Shear-thinning behavior has been verified over all shear rates. Lower mass fractions present higher Newtonian behavior.



(a) time = 90 ns



(b) time = 180 ns

Figure 5.21: Snapshot of asphaltene structure with and without shear rate for mass fraction of 0.20 in toluene. (a) Structure acquired after 90 ns of aggregation. (b) Structural breaking with shear simulation, shear started right after aggregation and lasted 90 ns more.

Aggregate analysis has also been made during shear to investigate how aggregate breaking is occurring (See Figures 5.22-5.23). At around 20 ns (of shearing) the number of aggregates becomes constant. At low mass fractions and low shear rates the systems seem to maintain their structures despite of the imposed shear, which means that the energy used to promote flowing is not high enough to separate molecules. When sheared structures at the highest shear rate are fully developed, the number of aggregates is almost independent of the solvent for the same mass fraction, probably because shearing overtakes particle interactions. Intermediary mass fractions produce higher number of aggregates. It seems that there is a limit below which higher mass fraction generate more clusters. Above this limit aligned molecules move so close to each other that they are considered as clustered by the algorithm.

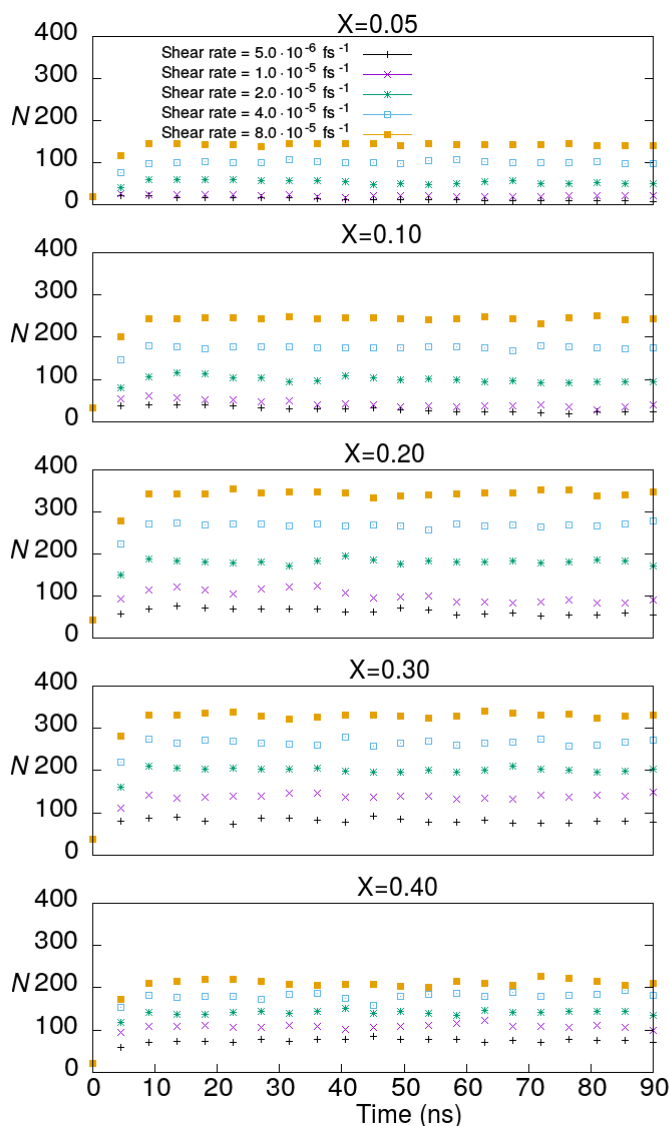


Figure 5.22: Number of aggregates N against time during simple shear for asphaltenes in heptane at different mass fractions. The number of aggregates is growing which means molecules are being separated.

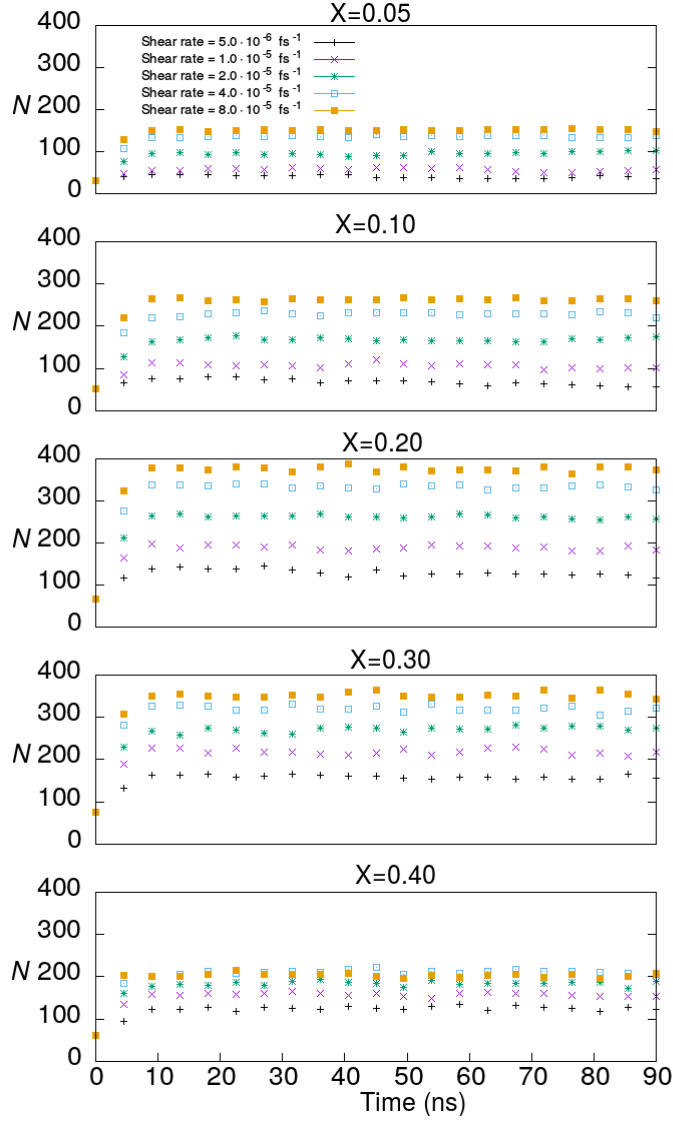


Figure 5.23: Number of aggregates N against time during simple shear for asphaltene in toluene at different mass fractions. The number of aggregates is growing which means molecules are being separated.

5.5.3 Oscillatory Shear and Linear Viscoelastic Regime (LVR)

Viscoelastic materials present both viscous and elastic characteristics under shear, each one has its own relaxation times. When the stress is small enough, the relationship between stress and strain is linear and the material is said to be in the Linear Viscoelastic Regime (LVR). In this linear regime, the relationship between stress $\sigma(t)$ and strain rate $\dot{\gamma}(t)$ is given by the general linear viscoelastic model (BIRD *et al.*, 1977):

$$\sigma(t) = \int_{-\infty}^t G(t-s)\dot{\gamma}(s)ds \quad (5.19)$$

Table 5.3: Relaxation modulus $G(t)$ for simple linear viscoelastic models. δ is the Dirac delta function.

Model	$G(t \geq 0)$
Newtonian fluid	η
Hookean solid	G_0
Maxwell model	$G_0 \exp(-\frac{G_0 t}{\eta})$
Kelvin-Voigt model	$2\eta\delta(t) + G_0$

Where $G(t)$ is relaxation modulus and $\dot{\gamma}(t) = \frac{d\gamma(t)}{dt}$ is the strain rate. Note that the stress responds to the deformation history, therefore, $G(t) = 0$ for $t < 0$. The material for which $G(t)$ decays to zero in a long time is called viscoelastic fluid. A material for which $G(t)$ has an asymptotic value other than zero, that is, $G(\infty) = \lim_{t \rightarrow \infty} G(t) = G_0 \neq 0$, is called a viscoelastic solid.

There are many models for viscoelastic behavior (BIRD *et al.*, 1977), at both ends are the Newtonian fluid and Hookean solid. Newtonian fluid is purely viscous, with a viscosity η , the Hookean solid is purely elastic, with an elastic modulus G_0 . Table 5.3 shows $G(t)$ for some simple models. Although these models are instructive for understanding the basic concepts of linear viscoelasticity, realistic materials have more complex behavior. In particular, colloidal gels often exhibit two relaxation processes, similarly to glassy materials (LARSON, 1999). While particles in a glassy material are confined locally due to *caging*, in a gel they are confined due to interparticle interactions. On short time scales, particles are free to diffuse within their confined environment. This phenomenon marks the β relaxation time. The time required for the particles to diffuse out of their confined environment is called α relaxation time. As the attractive forces increase, the particles become more confined and the relaxation times increase. Both of these relaxation processes decay more slowly than a simple exponential decay, which indicates the presence of several relaxation modes (D'ARJUZON *et al.*, 2003).

Gels are considered viscoelastic fluids throughout the time scale of interest in this work. In theory, the finite attraction force leads to finite relaxation times and $G(t)$ to goes to zero over long times, which would classify them as viscoelastic fluids. However, as the interaction forces increase, these relaxation times may be greater than the time scales possible to be performed by computer simulation. There are several tests that can be performed to determine $G(t)$ (BIRD *et al.*, 1977). The oscillatory is one of the most widely experimentally used, therefore we will use it.

Oscillatory shear is done by applying a frequency ω and maximum strain amplitude γ_0 . The response to the oscillatory stress is characterized by the elastic (or storage) modulus $G'(\omega)$ and the viscous (or loss) modulus $G''(\omega)$ which depend on

the oscillation frequency. These moduli are related to $G(t)$ by means of Fourier transforms, as it will be shown below. In addition to being able to measure properties for different frequencies, those measurements can be directly compared to experimental data since the oscillatory technique is widely used. The disadvantage of this method is the need of long simulation times to allow to get suitable averages. The strain rate is given by:

$$\dot{\gamma}(t) = \omega\gamma_0 \cos(\omega t) \quad (5.20)$$

For a viscoelastic fluid, the stress response is given by:

$$\sigma(t) = \omega\gamma_0 \int_0^\infty G(s) \cos(\omega t - \omega s) ds \quad (5.21)$$

Replacing the trigonometric identity we have:

$$\sigma(t) = \omega\gamma_0 \sin(\omega t) \int_0^\infty G(s) \sin(\omega s) ds + \omega\gamma_0 \cos(\omega t) \int_0^\infty G(s) \cos(\omega s) ds \quad (5.22)$$

Where $G'(\omega)$ and $G''(\omega)$ are defined as:

$$G'(\omega) = \omega \int_0^\infty G(s) \sin(\omega s) ds \quad (5.23)$$

$$G''(\omega) = \omega \int_0^\infty G(s) \cos(\omega s) ds \quad (5.24)$$

Thus:

$$\sigma(t) = \gamma_0 \sin(\omega t) G'(\omega) + \gamma_0 \cos(\omega t) G''(\omega) \quad (5.25)$$

According to Equation 5.25, the viscous modulus is linked to the strain rate and the elastic modulus is linked to the strain. The viscous modulus represents the energy dissipation, it is commonly called the loss modulus. The other one represents the energy storage in the stress form, it is called the storage modulus. The oscillatory test consists of applying a frequency (ω) and a maximum strain amplitude (γ_0) to the simulation box. A stress response is produced to the imposed oscillatory strain. As in the linear viscoelastic region the stress is proportional to the strain, it will also be oscillatory. However, strain and stress will have different amplitudes and will be offset by an angle δ . Figure 5.24 shows the strain and the stress response as a function of time.

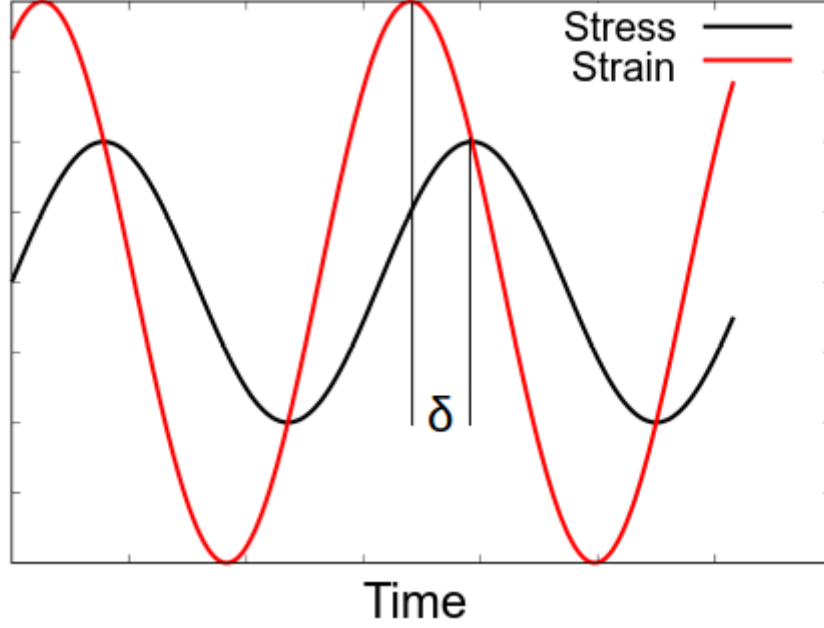


Figure 5.24: Stress and strain curves for oscillatory test. The phase angle δ is related to the observation time, given by $\delta = \omega(t_2 - t_1)$.

The stress response is:

$$\sigma(t) = \sigma_0 \sin(\omega t + \delta) = \sigma_0 \cos(\delta) \sin(\omega t) + \sigma_0 \sin(\delta) \cos(\omega t) \quad (5.26)$$

Comparing Equation 5.26 with Equation 5.25 one finds the G' and G'' expressions as a function of the angle phase δ :

$$G'(\omega) = \frac{\sigma_0}{\gamma_0} \cos(\delta) \quad (5.27)$$

$$G''(\omega) = \frac{\sigma_0}{\gamma_0} \sin(\delta) \quad (5.28)$$

Equations 5.26 and 5.25 separate the stress signal into two parts: one is in phase with strain ($\gamma(t) = \gamma_0 \sin(\omega t)$), that is $\delta = 0^\circ$, and another one which totally out of phase, that is $\delta = 90^\circ$. therefore, $G'(\omega)$ and $G''(\omega)$ ponder how important each of those contributions is.

Molecular Dynamics investigations are mostly focused on structural behavior and aggregation process. Due to limited computational resources, only small systems could be performed up to date. Larger time and length scales are required to have deeper insights about clustering formation, dynamics, and rheological properties (HEADEN *et al.*, 2017). The asphaltene solubility in the oil phase is strongly

related to the degree of aggregation. There is experimental evidence that the film of asphaltene formed at the oil/water interface presents a highly viscoelastic behavior, which is a consequence of the cross-links between those aggregates (ACEVEDO *et al.*, 1993; ESE *et al.*, 1998). That is associated with a gelation transition whose reproduction is crucial to have an accurate model to simulate asphaltenes. FAN *et al.* (2010b) studied the effects of concentration, aging, and the solvent aromaticity on the viscoelastic properties of asphaltene films at the toluene-heptane/brine interface by means of interfacial shear rheology using a biconical geometry rheometer. At low concentrations (~ 2 g/L) they were not able to detect any elastic behavior, which means that the system is viscous-dominated. For concentrations ranging between 5-10 g/L, the viscoelastic region was independent of concentration with a threshold of $\sim 1.5\%$. After 20h of aging, toluene-heptane 6:4 proportion and 0.1% of strain, the systems are all elastic behaved, 7 and 10 g/L curves are within the experimental uncertainty of each other which suggests that the interface is saturated. At low concentrations, the size and the number of aggregates were small. At high concentrations, there are more and larger aggregates that enable the interfacial film formation with an increasing number of layers. Solutions at 100% of toluene presented a purely liquid interface with a constant loss modulus. The asphaltene molecules tend to stay in the bulk phase as the solvent aromaticity is increased, which prevents the emergence of an active stabilized surface.

The non-Newtonian characteristic of our suspensions encouraged the analysis of their liquidlike (viscous) and solidlike (elastic) behavior. As the linear viscoelastic behavior is crucial to make a connection between theories and experiments (TSENG *et al.*, 2010), a small amplitude oscillatory shear has been applied to the studied systems. Various materials have been analyzed by this method, such as polymers (FERRY, 1980) or complex fluids (LARSON, 1999). As it is known that strain and stress are phase shifted, the equation $\sigma(t) = \sigma_0 \sin(\omega t + \delta)$ has been used as a model for estimating σ_0 and δ via *swarm* optimization (KENNEDY and EBERHART, 1995) for each case. With the σ_0 and δ values we could calculate G' and G'' . Figure 5.25 shows an example of the fitting procedure. The Strain, Stress and Stress fitted curves are similar for all cases. It is worth commenting that the strain values were multiplied by the edge length of the simulation box, so it has Angstrom units, as a consequence G' , and G'' will have units of stress/length.

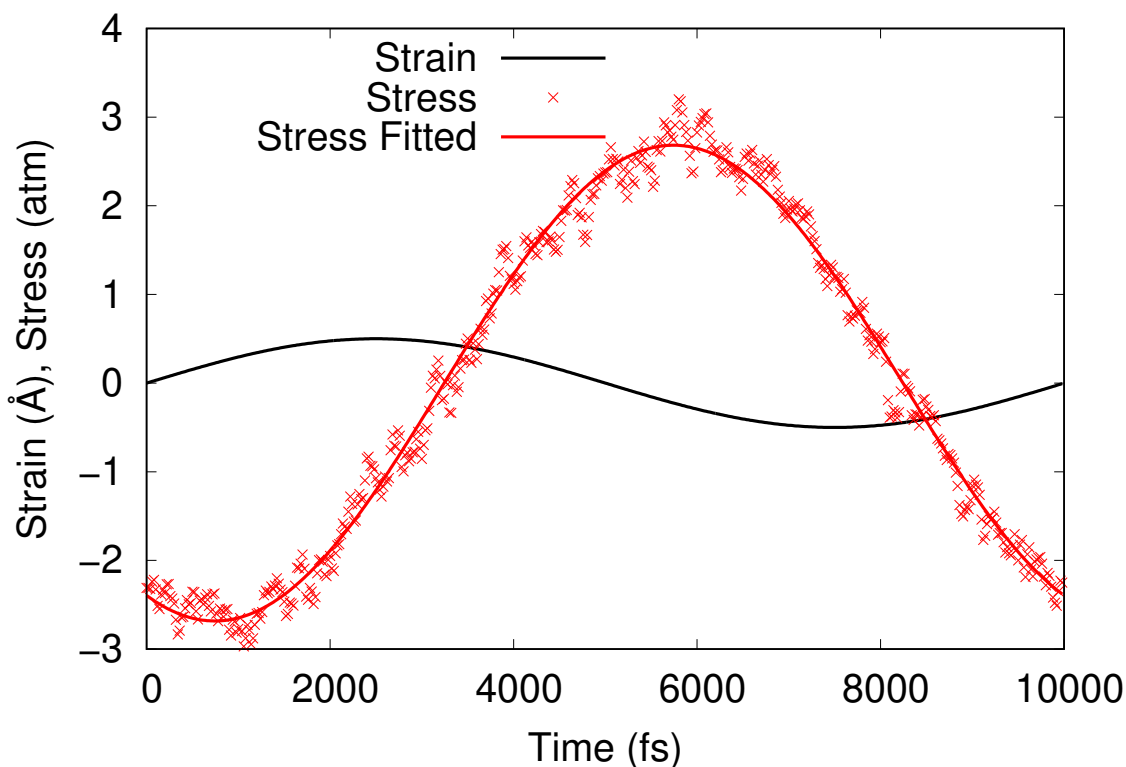


Figure 5.25: Strain, Stress (generated by the simulator) and Stress Fitted (calculated using equation $\sigma(t) = \sigma_0 \sin(\omega t + \delta)$ after estimating σ_0 and δ by *swarm* optimization procedure) curves for small amplitude oscillatory shear applied to asphaltene solution in heptane at 298 K, $X = 0.4$, amplitude deformation = 0.8 \AA , frequency = $6.28 \cdot 10^{11} \text{ rad/s}$. The strain values were multiplied by the edge length of the simulation box, so it has angstrom units.

Simulations at constant frequency were performed in order to verify the strain amplitude limit for the linear viscoelastic region. Both solvents were analyzed at $X = 0.5, 0.4$ in Figure 5.26. G' must be constant in the linear region, decreasing abruptly at higher strain amplitudes. It is unclear where in between 1 \AA and 5 \AA the storage modulus decays for all cases. Therefore, strain amplitude = 0.5 \AA has been chosen as the linear viscoelastic threshold. The linear viscoelastic region in toluene extends over a larger strain amplitude than in heptane. Moreover, G' is in general higher in toluene. Interactions between smaller clusters in toluene should improve the elastic behavior of those suspensions. The higher toluene viscosity is also playing against the system relaxation which manifests mesoscopically as a higher solidlike behavior. The frequency influence has been studied in Figures 5.27-5.31 where constant strain amplitude = 0.5 \AA was applied. In general, the viscous behavior prevailed over all frequencies and mass fractions. The only elastic-dominated system was obtained at the highest mass fraction and at low frequencies. This reveals that those asphaltene molecules have a small ability to store energy rather than dissipate it, which only prevails at high mass fractions. In the low frequency regime the Brownian diffusion is

greater than the oscillatory shear which allows the system to relax quickly dissipating the energy given by the flow, therefore G'' is greater than G' . In the limit of high mass fractions, the dominating entropic interactions (over Brownian motion) which are conservative in nature should improve the energy storage. The viscous dominant behavior remaining at the highest frequencies was expected as DPD particles are soft. The lack of hard core facilitates the alignment of molecules during shear which increases the system ability to dissipate energy and also reflect the shear-thinning behavior of those systems.

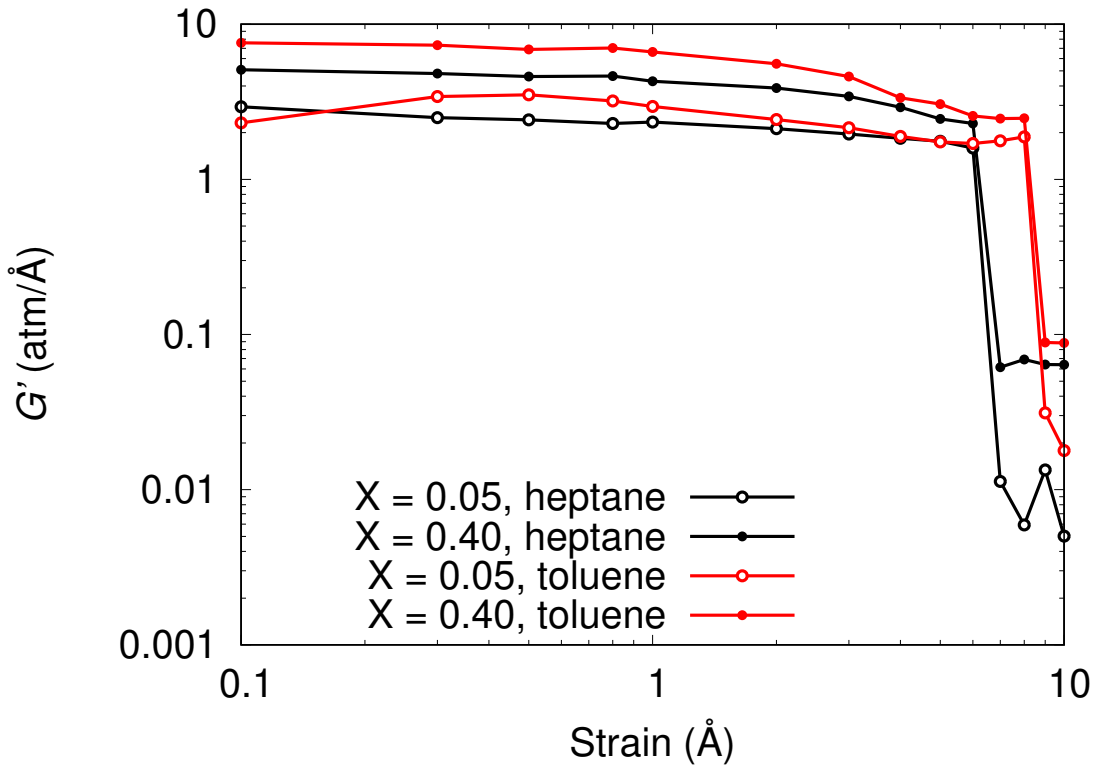


Figure 5.26: Linear viscoelastic region for asphaltene in heptane and toluene at different mass fractions and 298 K. Storage modulus G' against strain amplitude at frequency $= 6.28 \cdot 10^{11}$ rad/s. G' is calculated by $G' = \frac{\sigma_0 \cos(\delta)}{\gamma_0}$ after estimating σ_0 and δ by *swarm* optimization procedure. The strain values were multiplied by the edge length of the simulation box, so it has angstrom units, as a consequence G' , and G'' will have units of stress/length.

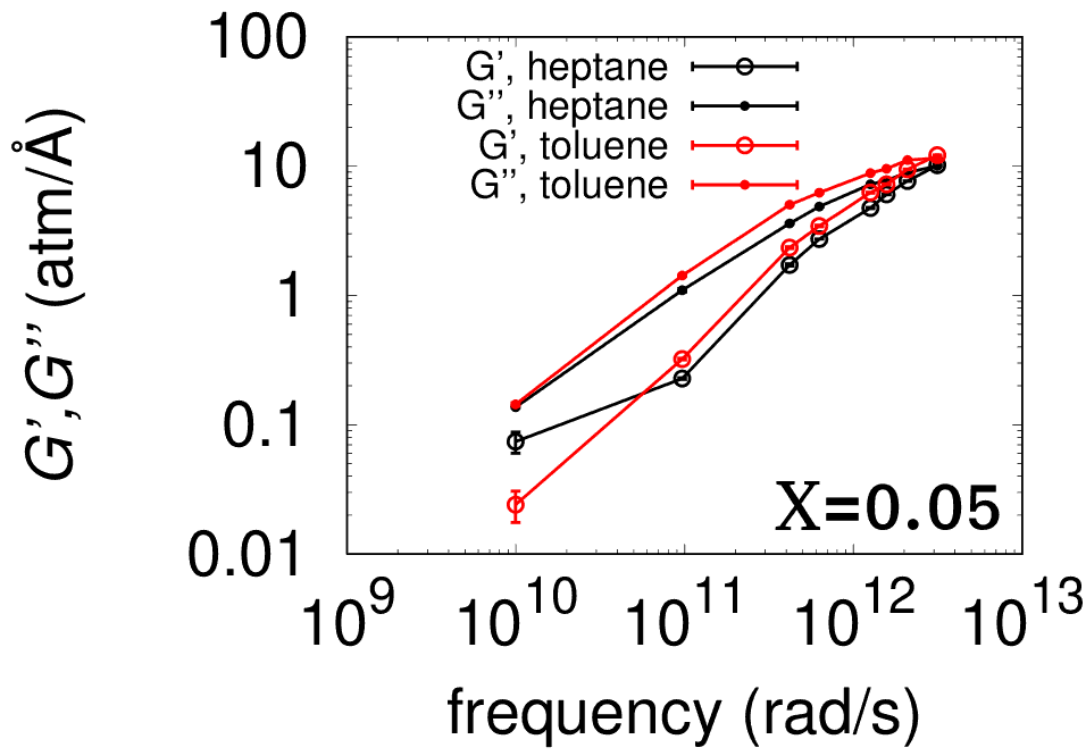


Figure 5.27: Storage (G') and loss moduli (G'') evolution over frequency for asphaltene suspensions at different mass fractions and strain amplitude = 0.5 \AA . The strain values were multiplied by the edge length of the simulation box, so it has angstrom units, as a consequence G' , and G'' will have units of stress/length.

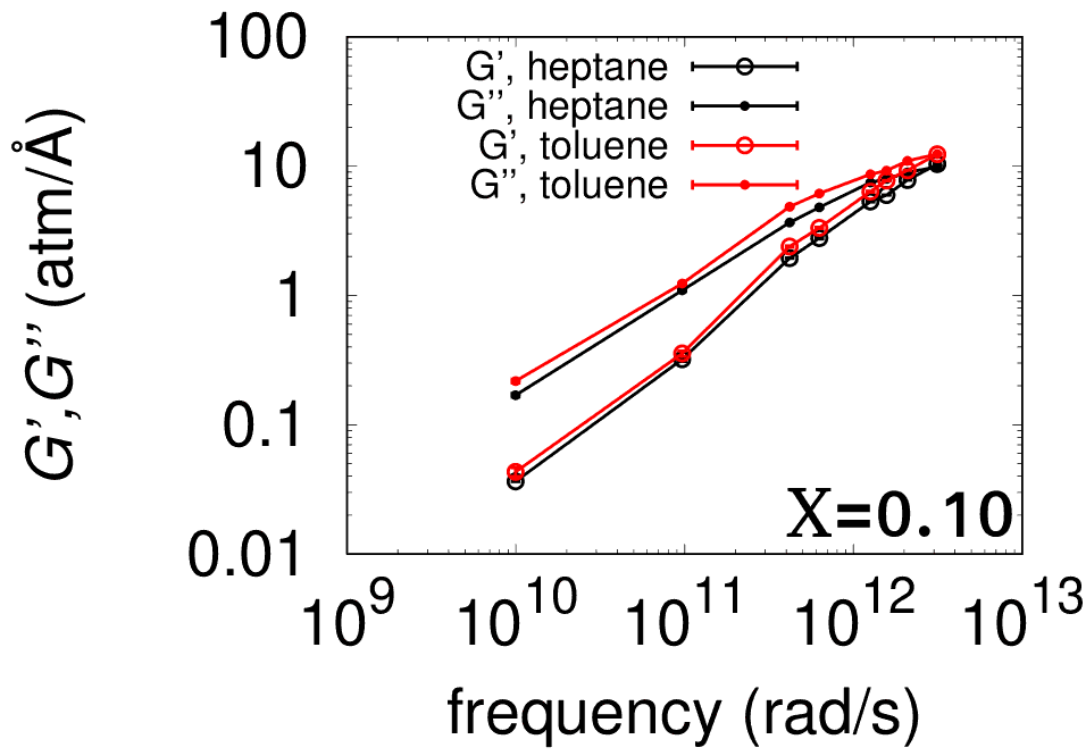


Figure 5.28: Storage (G') and loss moduli (G'') evolution over frequency for asphaltene suspensions at different mass fractions and strain amplitude = 0.5 \AA . The strain values were multiplied by the edge length of the simulation box, so it has angstrom units, as a consequence G' , and G'' will have units of stress/length.

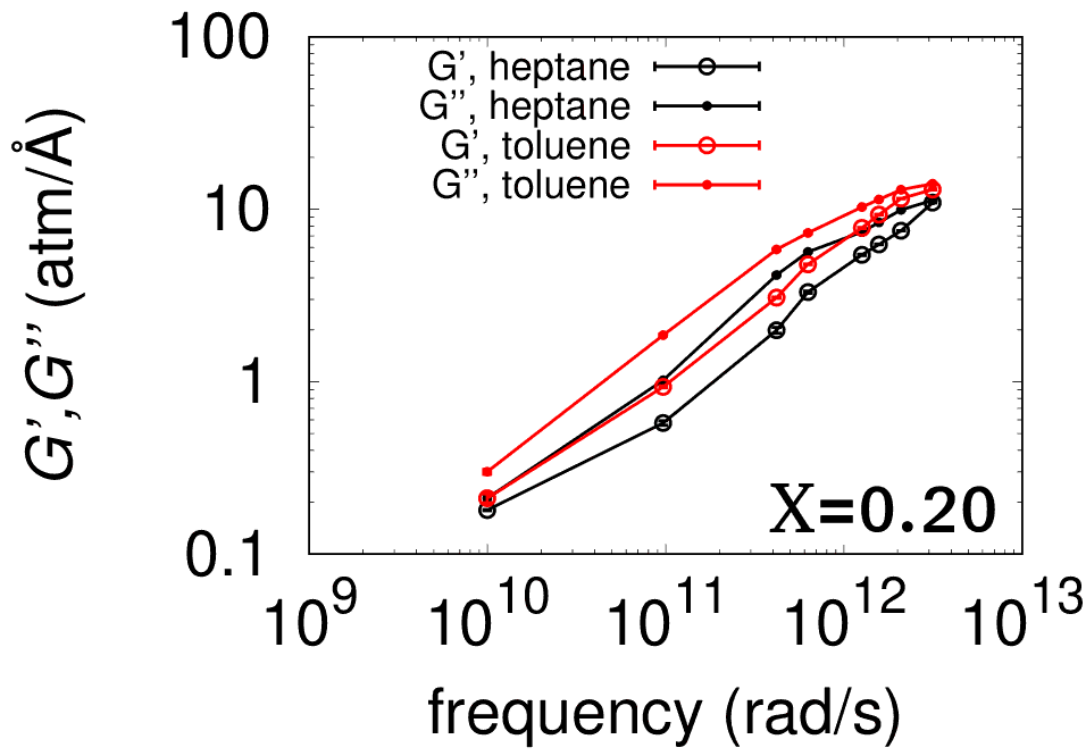


Figure 5.29: Storage (G') and loss moduli (G'') evolution over frequency for asphaltene suspensions at different mass fractions and strain amplitude = 0.5 \AA . The strain values were multiplied by the edge length of the simulation box, so it has angstrom units, as a consequence G' , and G'' will have units of stress/length.

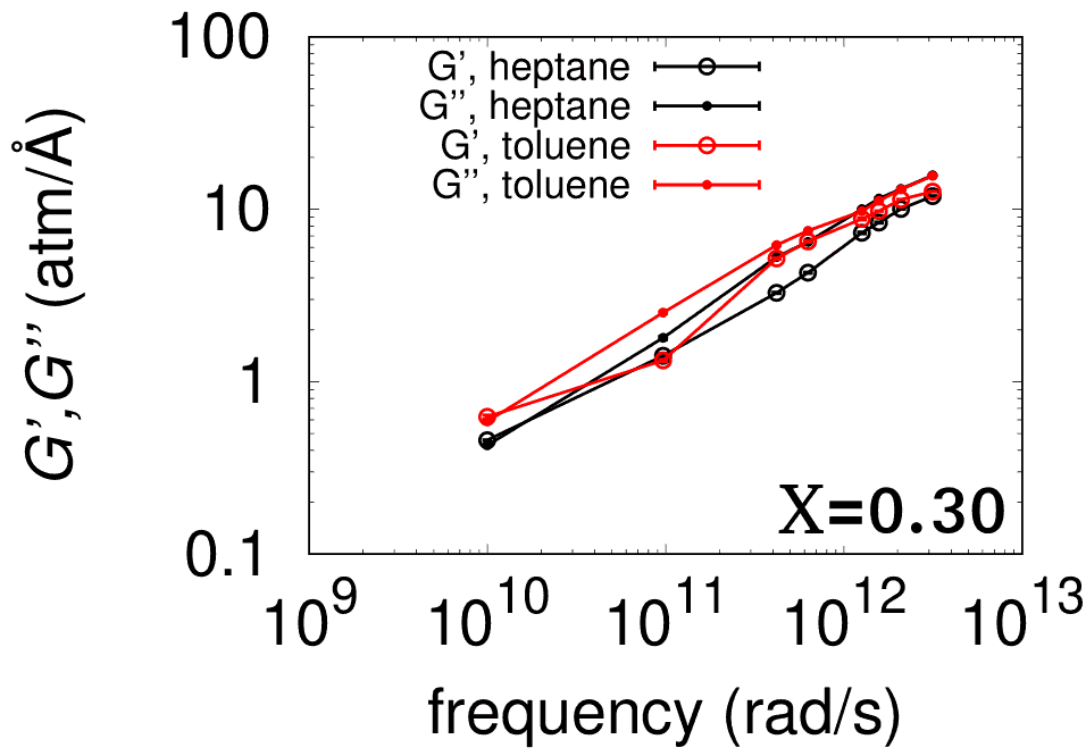


Figure 5.30: Storage (G') and loss moduli (G'') evolution over frequency for asphaltene suspensions at different mass fractions and strain amplitude = 0.5 \AA . The strain values were multiplied by the edge length of the simulation box, so it has angstrom units, as a consequence G' , and G'' will have units of stress/length.

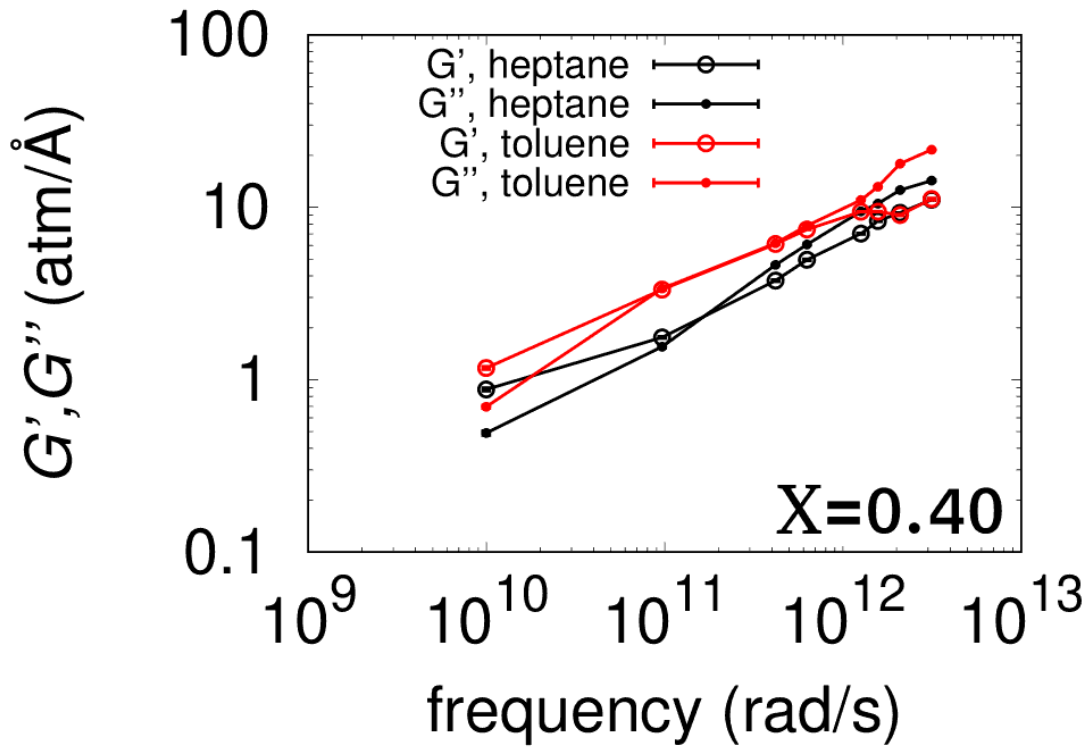


Figure 5.31: Storage (G') and loss moduli (G'') evolution over frequency for asphaltene suspensions at different mass fractions and strain amplitude = 0.5 \AA . The strain values were multiplied by the edge length of the simulation box, so it has angstrom units, as a consequence G' , and G'' will have units of stress/length.

In the experiments by FAN *et al.* (2010a) about the asphaltene film formation at the oil-water interface, they did not observe any elastic behavior for all tested concentrations until $\sim 5\text{h}$ of aging which means that at the initial stages the system behavior is liquidlike. HARBOTTLE *et al.* (2014) performed oscillatory measurements to understand the viscoelastic behavior of asphaltene films and their effects in drop coalescence. They observed that the drop coalescence time is related to the aging time which in turn is related to the storage modulus. At higher time ages, the structured film is more rigid, presenting higher storage modulus, which disfavors drops to coalesce, resulting in higher coalescence times. They stated that the viscous behavior comes from Brownian diffusion of asphaltene molecules from bulk phase to the interface. On the other hand, the elastic behavior would come from the cross-links between nanoaggregates, which increase continuously at longer time while the surface asphaltene accumulation is reaching saturation. For this reason, at long time, G' grows fast while G'' presents slow growing. Therefore, the present simulations behave like the initial stages of asphaltene film formation. The formation of aggregates can explain the solvent aromaticity influence in the interfacial rheology. In poor solvents, the asphaltene molecules tend to settle at the interface,

which enhances its elastic behavior as larger and numerous aggregates deposit and create links. In the case of bulk rheology, as carried out in this thesis, there is no interface, which means that the formation of the cross-links is the only factor leading to cohesive energy formation. As small clusters have a higher contact area, the connections between clusters are benefited in good solvents such as toluene, which results in higher moduli comparing to heptane.

The study of the viscoelastic behavior of asphaltene suspensions in bulk phase promoted here is important as a basis for the recognition of the precipitation conditions that may occur during oil exploitation, which is essential for the flow assurance.

Chapter 6

Asphaltenes at the Water/Oil Interface

This Chapter is based on (DE OLIVEIRA *et al.*, submitted)

Asphaltenes are the heaviest fraction of the crude oil. Its deposition causes large problems during oil exploitation. Sometimes it is difficult to separate the asphaltenes from the oil because of the very stable water in oil emulsions that they form. The Dissipative Particle Dynamics (DPD) molecular simulation method has been used in this section to study the interfacial properties of asphaltene molecules at the water-oil interface. The COSMO-SAC method was used to systematically obtaining the conservative force DPD parameters.

Removing water from the oil can be challenging in many cases because of the very stable water-oil emulsions which naturally emerge from the asphaltene molecules forming a film at the water-oil interface, which acts as an active surface molecule (YARRANTON *et al.*, 2000). Experimentally, BOURIAT *et al.* (2004) observed that the asphaltene film formation at the interface between water and cyclohexane produces a crosslinked structure that ages with time. A clear sol-gel transition zone has been detected. The average adsorbed area was 2 nm^2 which indicates that isolated (or small clusters) molecules connect to the interface rather than large clusters. CHANG *et al.* (2018) measured the mechanical properties of the water-asphaltene-oil interface. They observed that asphaltenes increased the stiffness of the interface, causing a crossover from viscous to elastic dominated behavior. Heterogeneities at the interface have also been found, which led to anisotropic strain decay. SHI *et al.* (2017) used atomic force microscopy (AFM) to measure the interfacial forces between water-oil emulsions droplets in organic solvent with adsorbed asphaltene molecules and found that the steric repulsion between asphaltene aliphatic

chains inhibits coalescence, which caused droplet stabilization. The authors studied the asphaltene concentration influence in the adhesion forces between droplets. By using lateral shear, they were able to break up the asphaltene films, permitting droplets to coalesce. CHANG *et al.* (2019) studied the effects of ethylcellulose in the rheology of asphaltene film formed at the oil-water interface. The asphaltene film presented heterogeneities, which means that there are stiff and less stiff (soft) regions at the interface. It was observed that the presence of ethylcellulose softens the asphaltene film by both competing with asphaltene for the adsorbing area or by penetrating the soft regions. Therefore chemical demulsifiers should readily attack soft regions, which decreases the interfacial stiffness.

Computationally, Molecular dynamics have also been carried out in an attempt to better understand the effects of asphaltene molecules at the water-oil interface. LIU *et al.* (2015) studied the orientation of asphaltene molecules at the water interface by Molecular Dynamics (MD). The asphaltene molecules showed parallel stacking led by π - π interactions between aromatic cores; the same molecules oriented perpendicular to the water interface. They also verified the demulsification by ethylcellulose, i.e., asphaltene molecules detaching from the droplets.

For large systems, mesoscale approaches are a promising tool (GLOTZER and PAUL, 2002; SHINTO, 2012). Those coarse-graining methodologies (GROOT and WARREN, 1997; MARRINK *et al.*, 2007) allow simulating large time and length scales by joining several atoms into a single particle. DPD (**D**issipative **P**article **D**ynamics) is a widespread coarse-graining method that has been used in many applications such as block copolymers (QIAN *et al.*, 2006), vesicle formation (YAMAMOTO *et al.*, 2002), the momentum transfer mechanisms mediated by Janus rods at polymer interfaces (PAIVA *et al.*, 2020), surfactants (ANDREATTA *et al.*, 2005), and carbon nanotubes (CHAKRABORTY *et al.*, 2013). REZAEI *et al.* (2016) used DPD to study the behavior of asphaltene-like molecules with different terminal groups at the oil-water interface. They considered SARA crude oil model from the Persian Gulf as the oil composition and concluded that as the terminal groups became more polar, lower values of the interfacial tension (IFT) were obtained due to more significant interactions between side chains and water, which facilitates the water-oil separation. RUIZ-MORALES and MULLINS RUIZ-MORALES and MULLINS (2015) constructed an asphaltene molecule model based on the DPD approach and tested different force field parameters. They found that the molecular planes stay parallel to the water-oil interface while the alkyl chains are perpendicular. Some asphaltene molecules went to the oil phase due to steric repulsion and jamming. SILVA (2015) using experimental solubility parameters, calculated the Flory-Huggins interaction parameters and then the DPD conservative parameters

based on the GROOT and WARREN (1997) methodology. The IFT evolution of the asphaltene-oil interface as a function of the polarity degree of different solvents was performed. In pentane, the highest IFT (interface emergence) was observed, while in benzene the lowest IFT (dissolution) was obtained, that agrees with experimental results. WANG *et al.* (2015) used GPU-accelerated DPD simulations to study heavy, light, and emulsion crude oil systems. The asphaltenes formed large aggregates in their heavy crude oil, which enhances the suspension viscosity. The addition of light fractions lowered the asphaltene mass fraction and aggregate size, which also increased the Newtonian suspension behavior. Regarding the asphaltene surfactant characteristics, they observed that asphaltene molecules increased the dispersion of the emulsions. CHEN *et al.* (2017a) studied the structure and orientation of asphaltene molecules at the oil-water interface using both continental and archipelago-like structures by means of DPD and found that the change from parallel to perpendicular molecular orientation occurs when archipelago-like molecules replace continental molecules. They also observed that the presence of heteroatoms in the asphaltene molecules is the main drive force leading to the molecule adsorption at the interface, while the aromatic cores are responsible for parallel molecular stacking. DE OLIVEIRA *et al.* (2020a) studied the viscoelastic behavior of asphaltene model molecules using the DPD coarse-graining method in toluene and heptane. They were able to describe the structural and dynamical properties of those molecules according to the solvent used. The authors also tested several mass fractions and concluded that the increase of the mass fraction causes an increase in the viscosity, which is higher in toluene because its viscosity is higher than the heptane viscosity. Oscillatory rheology was promoted by molecular simulations, and the results showed that at the initial aggregation stages, the suspensions have higher liquidlike behavior, which is confirmed by experimental results. DUAN *et al.* (2017) promoted both experimental tests and molecular simulation of asphaltenes and polyacrylamide (PAM) at the water-oil interface. Their results demonstrated that asphaltene nanoaggregates form at the interface, enhancing its rigidity and making the drop-drop coalescence more difficult. The increment of PAM in the system generates a layer-by-layer structure, which also augments the stability of water-in-oil emulsions.

COSMO methodologies have been used for calculating many substance properties. FINGERHUT *et al.* (2017) tested two COSMO-SAC models: COSMO-SAC2010 HSIEH *et al.* (2010) model and COSMO-SAC-dsp HSIEH *et al.* (2014). COSMO-SAC2010 HSIEH *et al.* (2010) model improvement over the original COSMO-SAC LIN and SANDLER (2002), lies in the recognizing different strengths of hydrogen bonding interactions, which depends on the type of hydrogen bonding

donors and acceptors. Whereas COSMO-SAC-dsp has a correction term based on molecular simulation data, taking into account the dispersive intermolecular interactions explicitly. The authors have proven that the latter presents a lower mean absolute deviation of the infinity dilution activity coefficient, being more accurate. MERKER *et al.* (2013) analyzed the gas solubility of oxygen, CO₂ and their mixtures. They compared experimental data, molecular simulation, and COSMO-SAC. COSMO-SAC results were far better than the Peng-Robinson equation of state as in predictive as in adjusted mode. LEE and LIN (2015) developed a new method to screen ionic liquids to be used in the CO₂ capture process. They used COSMO-SAC to calculate de infinity dilution activity coefficient of the gas in the ionic liquid. The substances CO₂, CH₄, N₂ and H₂ were tested in terms of solubility, selectivity, and the temperature dependency of solubility, showing promising results. Their methodology is promising in screening the best ionic liquid candidates for CO₂ capture. CHEN *et al.* (2017b) applied COSMO-SAC to select the best extractant from forty organic solvents, including alkanes, arenes, ethers, esters and ketones, to treat phenolic effluents in the industry. COSMO-SAC has also been used to predict tie-line data, and showed good agreement with the respective experiments. SOARES (2011), and GERBER and SOARES (2013) developed and provided new and free software to determine activity coefficients from COSMO-SAC named JCOSMO. They recalibrated the COSMO-SAC model and compared infinity dilution activity coefficient with UNIFAC (Do) CONSTANTINESCU and GMEHLING (2016); GMEHLING (1994); JAKOB *et al.* (2006). Their COSMO-SAC implementation showed better agreement with experimental data for molecules with several functional groups or when functional groups appear in an unusual way, which reinforces this new methodology as a promising tool. ALASIRI and CHAPMAN (2017) used COSMORS to calculate the DPD interaction parameters studying the alkane-water interface and demonstrated that their methodology is capable of reproducing quite well the IFTs of those systems. Dmol3 commercial software was used to obtain the infinity diluted activity coefficient required. ALASIRI *et al.* (2019) used the same method to study the effect of head groups, salts, and temperature on interfacial properties of water-octane-surfactant systems. They used sodium dodecyl sulfate (SDS), dodecyltrimethylammonium bromide (DTAB), and dodecyldimethylamine oxide (DDAO) as surfactants. Experimental IFTs were obtained from pendant drop method, which agreed semiqualitatively with DPD simulations.

A molecular dynamics study of the asphaltene surfactant properties at the water/oil interface is still in lack in the literature. Here, the COSMO-SAC method was used to evaluate the DPD-binary-interaction parameters between asphaltene, water, and cyclohexane beads. To verify the quality of these parameters and the ability of

the DPD in describing the thermodynamic properties, we calculated the interface tension (IFT) of different hydrocarbons and water and compared those with experimental data. The asphaltene structural properties and diffusion coefficient were also calculated to verify if this new methodology can reproduce experimental data of diluted asphaltene in toluene. The first peak of the radial distribution function ($g(r)$) occurs about 5.08 Å, and the diffusion coefficient of diluted asphaltene in toluene (5% and 10% mass fractions) agrees well with experimental literature data. Simulations of asphaltene at the water-oil (cyclohexane) interface were run, and the obtained IFTs agree well with the experimental available data in terms of CMC (critical micelle concentration). This is the first time that a mesoscale molecular dynamics study has been able to capture the asphaltene surfactant characteristics. This new methodology based on free COSMO-SAC software has proven to be very simple and useful in determining the characteristics of asphaltene molecules acting as surfactant at the water-oil interface.

6.1 Coarse-Graining and Simulation Details

The simulations performed in this work were carried out using the LAMMPS package (PLIMPTON, 1995), which has been chosen because of parallelization. The dissipative and random force parameters used were $\gamma = 4.5$ and $\sigma = 3$ in DPD units as determined by GROOT and WARREN (1997). For the DPD method each bead corresponds to N_m (degree of coarse-graining) water molecules. Following the coarse-graining of ALASIRI *et al.* (2019), $N_m = 4$, which means that each DPD bead corresponds to the volume of 4 water molecules for the coarse-graining used here. The total system numerical density ρ was set to 3 (in DPD units) (GROOT and WARREN, 1997). The way of calculating the time, mass, length and energy scales was described at the previous section.

The asphaltene molecule used here was obtained from (SONG *et al.*, 2016), Figure 6.1. Even though the asphaltene molecular structure is not completely understood (OK *et al.*, 2019), it is known that its hypothetical configuration is constituted of aromatic rings, alkyl side chains and heteroatoms. Figure 6.1 shows the molecular structure that was used here; it has a island structure, which means that it is formed by many central rings surrounded by side chains. This structure is referenced as “like hand” structure, with the palm represented by the central core and fingers representing side chains. Three types of particles were used: B bead (blue) represents a moiety of aromatic rings which represents the benzene, H bead (green) represents a butane molecule which forms the alkyl side chains, and T bead (red) that repre-

sents the thioglycolic acid molecule which has been chosen as the heteroatom group, having greater affinity to water than the other beads. The degree of coarse-graining $N_m = 4$.

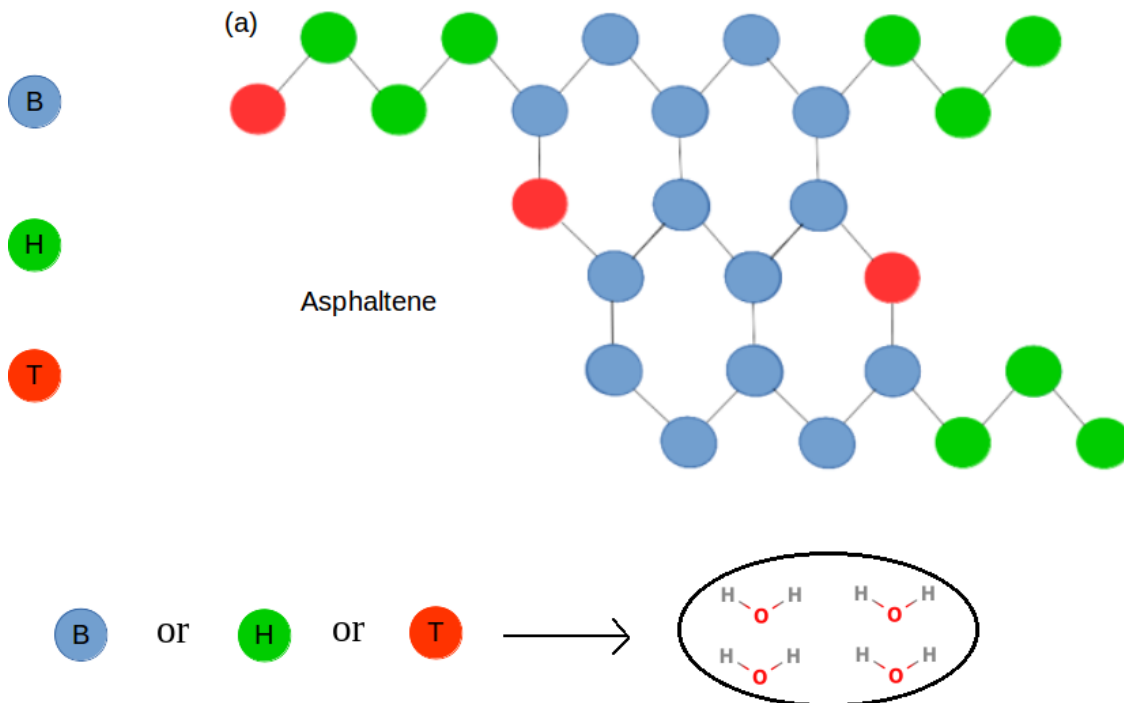


Figure 6.1: Asphaltene molecular structure representation: B bead (blue) represents a moiety of aromatic rings which is the benzene in this approach, H bead (green) represents a butane molecule which forms the alkyl side chains, T bead (red) represents the thioglycolic acid molecule which is the heteroatom group. Each bead corresponds to the volume of 4 water molecules.

Figure 5.2 shows the structural formula of this hypothetical asphaltene molecule.

In the DPD method, all particles should have approximately the same size (MAITI and MCGROTHER, 2004). Water, n-butane, benzene, thioglycolic acid, toluene, n-propane, n-decane, and cyclohexane have been used, the molecular volumes were obtained from MULLINS *et al.* (2006). Table 6.1 shows that all beads have almost the same size considering the coarse-graining of each molecule, as required by DPD method. The bond constant force K_{bond} , Equation 5.5, was set to 1000 for bonds between beads in the polyaromatic asphaltene nuclei, and 100 for the alkyl side chain bonds, while the equilibrium distances r_0 were 0.8 and 0.9, respectively. The angle constant force K_{angle} , Equation 5.6, was 125, and the equilibrium angle $\theta_0 = 120^\circ$. For the improper expression energy, Equation 5.7, the parameters were set as $K_{improper} = 5$, $d = -1$ e $n = 2$ to keep the asphaltene molecule flat. All

in DPD units.

Table 6.1: Bead sizes of molecules studied in this section, data taken from MULLINS *et al.* (2006).

Molecule	Size (\AA^3)
n-Butane	102.43
Benzene	110.22
Cyclohexane	129.72
n-Decane	233.48
n-Propane	80.70
Thioglycolic Acid	102.99
Toluene	132.25
Water	25.74

GROOT and WARREN (1997) running a series of simulations varying the numerical density ρ and values of the like-like bead conservative interaction a_{ii} , have found the following relationship between a_{ii} and ρ , $a_{ii}\rho = 75k_B T$. Thus, the interaction parameter between equal beads is 25, in DPD units, for $\rho = 3$. The same authors, aiming to find a method to determine the unlike-unlike (a_{ij}) bead conservative interaction, used the Flory-Huggins polymer solution theory to establish a linear expression between a_{ij} and the Flory-Huggins interaction parameter χ_{ij} :

$$\chi_{ij} = 0.286(a_{ij} - a_{ii}) \quad \text{for } \rho = 3 \quad (6.1)$$

A methodology for the calculation of the Flory-Huggins parameter is necessary to determine the unlike bead interaction a_{ij} . In this approach, the Flory-Huggins lattice theory is used to match the phase behavior of real fluids and the DPD molecular simulation method. The COSMO-SAC (conductor-like screening segment activity coefficient) theory has been created by LIN and SANDLER (2002) as a strategy to obtain the thermodynamic properties of liquids and liquid mixtures. It is based on COSMO (KLAMT and SCHÜÜRMAN, 1993), which uses quantum calculations to calculate the dielectric screening energy in solvents. Cosmo-based methods move a molecule from vacuum to a perfect conductor and then to a real solvent medium. More details about the COSMO-based procedure can be found elsewhere (KLAMT, 1995; KLAMT and ECKERT, 2000; KLAMT and SCHÜÜRMAN, 1993; KLAMT *et al.*, 1998; LIN and SANDLER, 2002). ALASIRI and CHAPMAN (2017) have found a relationship between the infinity dilution activity coefficient (γ) and the

Flory-Huggins parameter χ for a solute(*i*)/solvent(*j*) system:

$$\chi_{ij}^{\infty} = \ln(\gamma_i)^{\infty} + \ln(\nu_{ij}) - \left(1 - \frac{1}{\nu_{ij}}\right) \quad (6.2)$$

Where γ_i^{∞} is the infinity dilution activity coefficient, and ν_{ij} is the volume ratio between the solute and solvent. The estimation of the activity coefficient is made by COSMO-SAC, using the free software JCOSMO GERBER and SOARES (2013); SOARES (2011), which was developed by GERBER and SOARES (2013); SOARES (2011). It is clear that having the tools for calculating the activity coefficient between two components, using Equation 6.2 and then Equation 6.1, it is possible to calculate the unlike conservative interaction between two different beads.

6.2 Hydrocarbon-Water Systems

Firstly, Dissipative Particle Dynamics was used to simulate the interfacial characteristics of alkane-water systems. A box of $23 r_C \times 23 r_C \times 31.5 r_C$ with 50000 beads has been created, half of the beads being water and half composing the alkanes. Periodic boundary conditions were applied, and in the initial condition, all particles were placed randomly within the simulation box. A total of 600000 timesteps were carried out ($\Delta t = 0.002\tau$), among which the first 20% were equilibration steps, followed by the production steps. The interfacial properties of hexane, octane, and dodecane were tested in water. To keep a consistent coarse-graining degree, the hexane molecule was created with 2 propane beads ($N_m = 3$), while octane and dodecane were composed of 2, and 3 butane beads, respectively, maintaining $N_m = 4$. The alkanes are treated as bonded monomers of propane and butane. The IFTs were calculated by KHEDR and STRIOLO (2018):

$$\text{IFT} = \frac{1}{2} \left(P_{zz} - \frac{P_{xx} + P_{yy}}{2} \right) L_Z \quad (6.3)$$

Where P_{xx} , P_{yy} , and P_{zz} are the diagonal components of the system stress tensor for the equilibrated system. L_Z is the z box edge length. To convert this DPD unit value into real units, we used a factor of $k_B T / r_C^2$. Initially, all particles are randomly dispersed in the simulation box. After the equilibrium has been reached, the system separates into two phases, forming two well-defined interfaces (due to the periodic box). The 1/2 factor multiplying Equation 6.3 is due to those two interfaces that are formed, as shown in Figure 6.2.

The interaction parameters between water and alkane beads were calculated

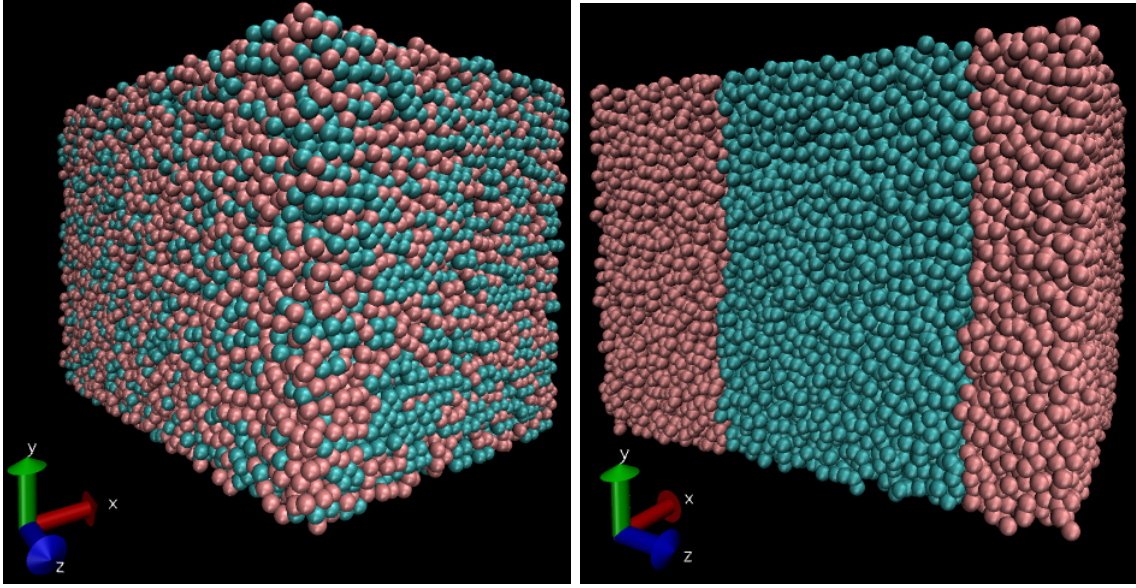


Figure 6.2: Water-octane molecular simulation at the initial step and at the final equilibration step. Water is represented by blue beads, whereas octane by pink beads. Two interfaces naturally form, which leads to a $1/2$ multiplication prefactor in Equation 6.3.

by using Equations 6.2, 6.1. The Flory-Huggins parameters (χ_{ij}^∞) were calculated using the infinity dilution activity coefficients from JCOSMO for different temperatures. According to MAITI and MCGROTHER (2004), the a_{ij} parameters should be scaled, taking into account the bead size. In Equation 6.2, there are discrepancies between the water and alkane molecular volume because one water bead is supposed to include N_m water molecules. Hence, avoiding these unphysical size discrepancies requires multiplying χ_{ij}^∞ by N_m before calculating a_{ij} . That scaling does not affect the a_{ii} value. So that:

$$\chi_{ij}^\infty(N_m) = N_m \chi_{ij}^\infty \quad (6.4)$$

As the Flory-Huggins parameters are temperature dependent, we could find a linear relationship between the a_{ij} parameters and the temperature. For the bead interactions promoted in this section, the results are shown in Table 6.2. As the bead size increases, the a_{ij} also increases, meaning that the repulsion between water and larger alkanes is higher than with small alkanes. The slope of the fits are negative, which means that as the temperature increases, a_{ij} decreases, resulting in better affinity between water/alkanes at higher temperatures. The slope decay is almost the same for the two interaction types. Even though the classical Flory-Huggins parameter in DPD GROOT and WARREN (1997) depends on the interaction energy between species, numerical densities, and temperature, it is also dependent on the

two species sizes in this strategy.

Table 6.2: Linear relationship between water and alkane bead interaction parameters a_{ij} and the temperature. χ_{ij}^{∞} were calculated before scaling, Equation 6.2. $\chi_{ij}^{\infty}(N_m)$ calculated after scaling, Equation 6.4. a_{ij} calculated using $\chi_{ij}^{\infty}(N_m)$ values in Equation 6.1.

Bead	χ_{ij}^{∞}	$\chi_{ij}^{\infty}(N_m)$	a_{ij}	R^2
Butane	$-0.013 \cdot T(^{\circ}\text{C}) + 8.988$	$-0.050 \cdot T(^{\circ}\text{C}) + 35.954$	$-0.176 \cdot T(^{\circ}\text{C}) + 150.712$	0.999
Propane	$-0.010 \cdot T(^{\circ}\text{C}) + 7.582$	$-0.031 \cdot T(^{\circ}\text{C}) + 22.745$	$-0.108 \cdot T(^{\circ}\text{C}) + 104.528$	0.999

Simulations were conducted varying the temperature to compare our results with ZEPPIERI *et al.* (2001)'s experimental data. Figures 6.3-6.5 show the IFT curves against temperature for the alkane/water systems. The sharp red lines are the experimental values, while the black ones are the DPD simulated values. The error bars denote the standard deviations. As the standard deviations almost include all experimental points, it means that the simulated IFTs represent well those points. Therefore, the DPD conservative parameters calculated by COSMO-SAC seem to reproduce well the interfacial properties of alkane/water systems, which is a bright signal of the usability of that method.

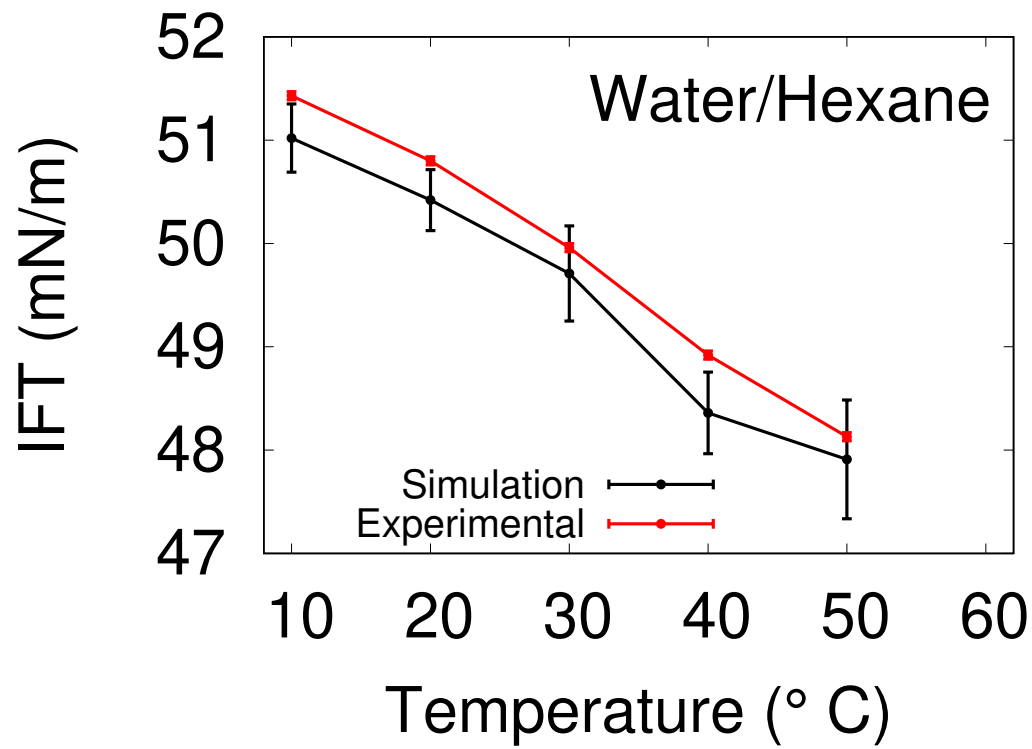


Figure 6.3: Water/hexane IFT calculation for different temperatures using DPD. The black curve is the DPD simulation, and the red curve is the experimental data ZEPPIERI *et al.* (2001). Standard deviations are shown as error bars.

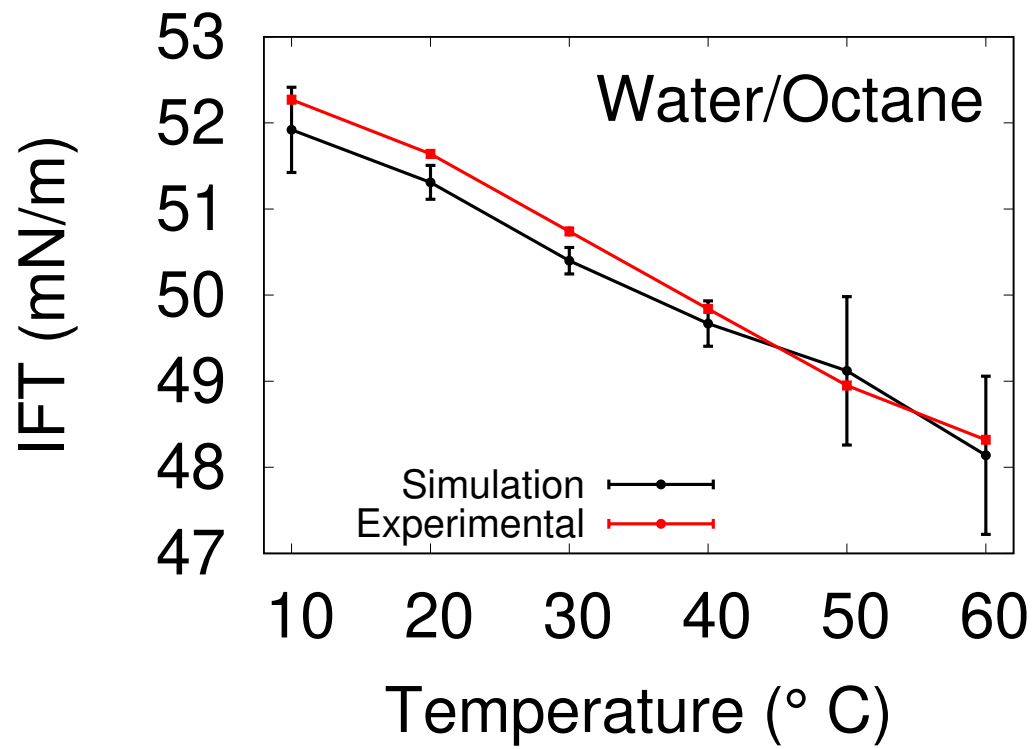


Figure 6.4: Water/octane IFT calculation for different temperatures using DPD. The black curve is the DPD simulation, and the red curve is the experimental data ZEPPIERI *et al.* (2001). Standard deviations are shown as error bars.

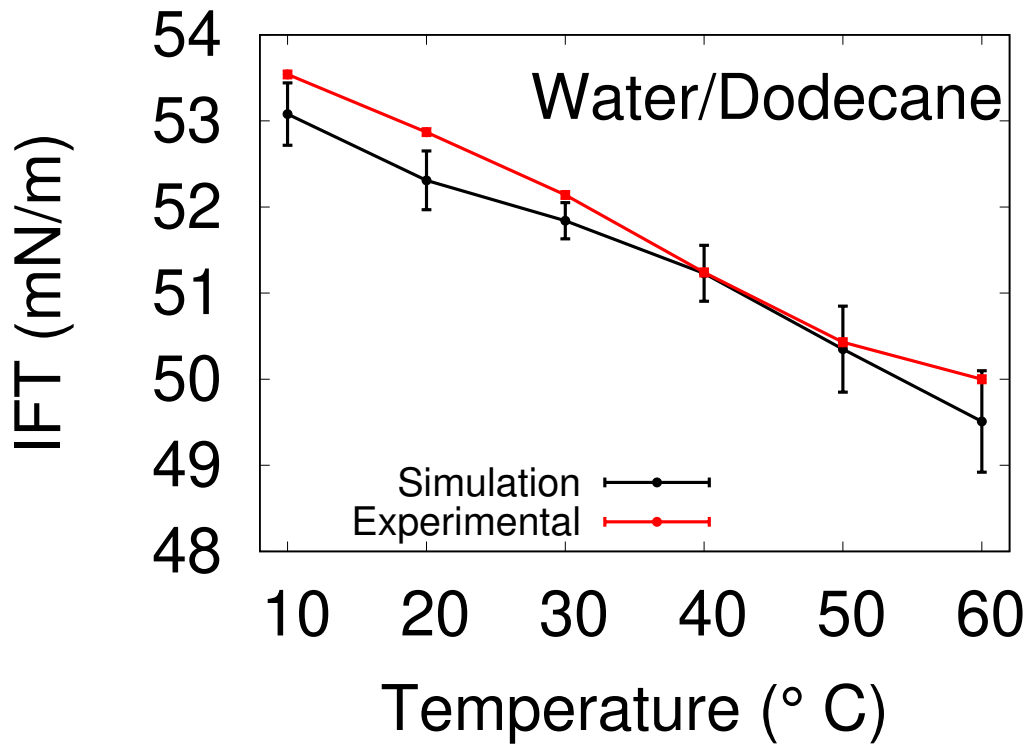


Figure 6.5: Water/dodecane IFT calculation for different temperatures using DPD. The black curve is the DPD simulation, and the red curve is the experimental data ZEPPIERI *et al.* (2001). Standard deviations are shown as error bars.

The same strategy was applied to calculate the interfacial tension of n-decane, cyclohexane, and benzene in water. The simulated conditions were the same, except for the decane for which a coarse-graining degree $N_m = 5$ (two n-pentane monomers forming one decane molecule) was used, whereas for the benzene and cyclohexane $N_m = 4$. The DPD parameters are shown in Table 6.3, while the IFT curves compared to experimental values are presented in Figures 6.6-6.7.

Table 6.3: Linear relationship between water and hydrocarbon bead interaction parameters a_{ij} and the temperature. χ_{ij}^∞ were calculated before scaling, Equation 6.2. $\chi_{ij}^\infty(N_m)$ calculated after scaling, Equation 6.4. a_{ij} calculated using $\chi_{ij}^\infty(N_m)$ values in Equation 6.1.

Bead	χ_{ij}^∞	$\chi_{ij}^\infty(N_m)$	a_{ij}	R^2
Benzene	$-0.006 \cdot T(^{\circ}\text{C}) + 6.726$	$-0.025 \cdot T(^{\circ}\text{C}) + 26.903$	$-0.088 \cdot T(^{\circ}\text{C}) + 119.067$	0.999
Cyclohexane	$-0.015 \cdot T(^{\circ}\text{C}) + 10.396$	$-0.059 \cdot T(^{\circ}\text{C}) + 41.584$	$-0.205 \cdot T(^{\circ}\text{C}) + 170.397$	0.999
n-Pentane	$-0.014 \cdot T(^{\circ}\text{C}) + 10.350$	$-0.074 \cdot T(^{\circ}\text{C}) + 51.750$	$-0.257 \cdot T(^{\circ}\text{C}) + 205.941$	0.999

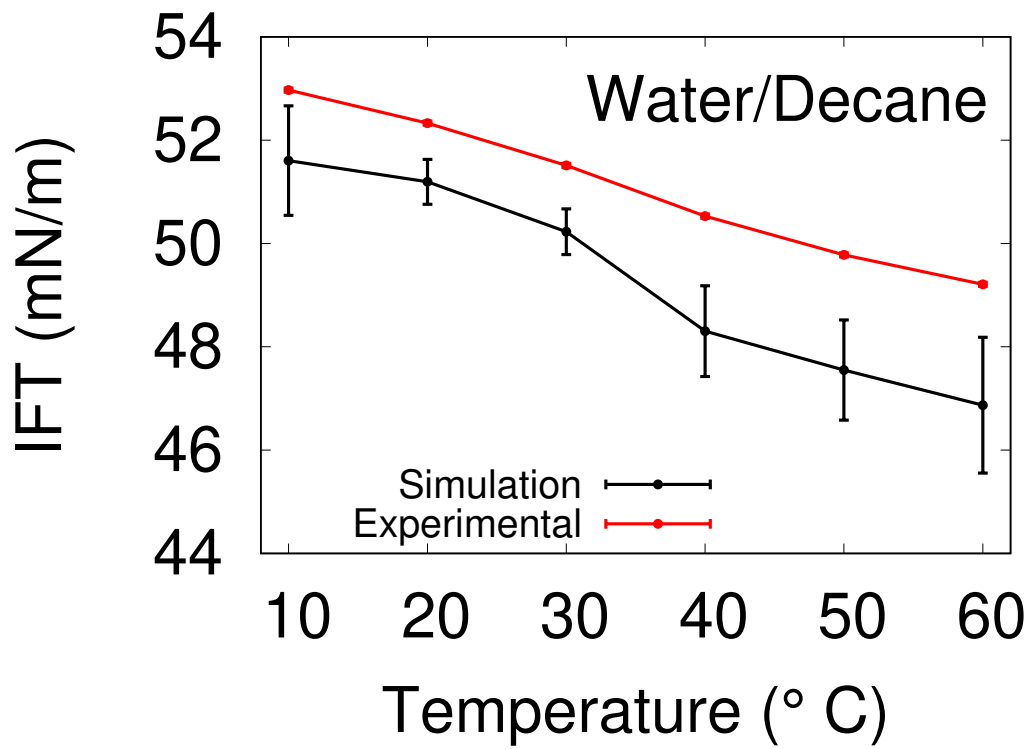


Figure 6.6: Water/decane IFT calculation for different temperatures using DPD. The black curve is the DPD simulation, and the red curve is the experimental data ZEPPIERI *et al.* (2001). Standard deviations are shown as error bars.

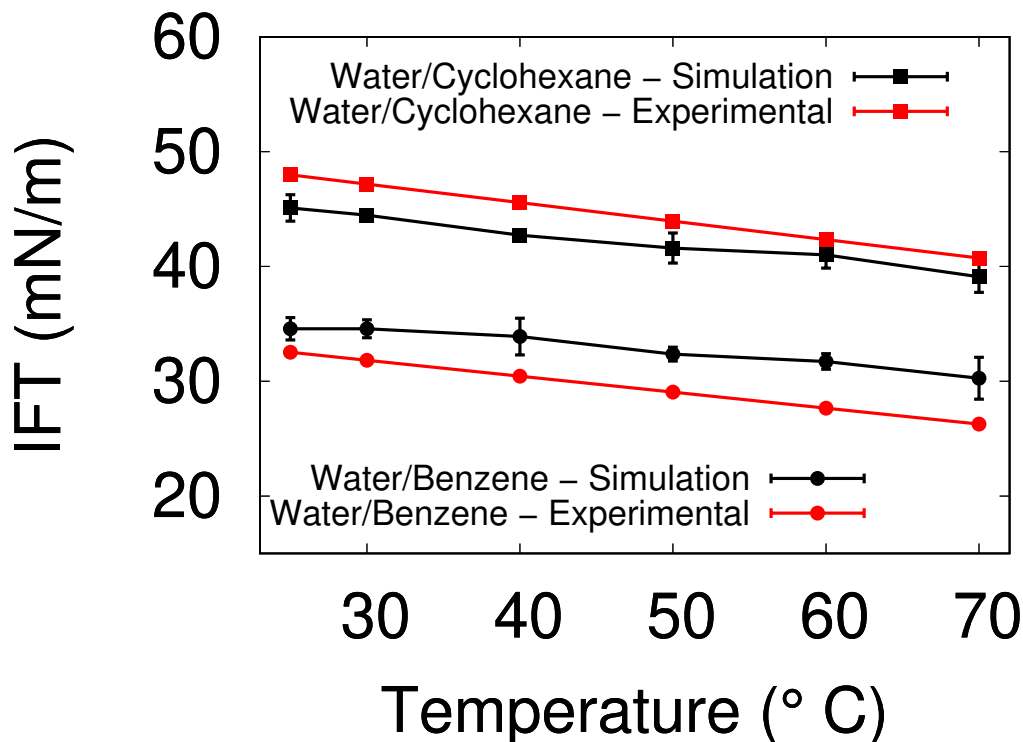


Figure 6.7: Water/benzene and water/cyclohexane IFT calculation for different temperatures using DPD. The black curves are the DPD simulation, and the red curves are the experimental data MAYORAL and GOICOCHEA (2013). Filled points represent water/benzene data; empty points represent water/cyclohexane data. Standard deviations are shown as error bars.

The IFT results for n-decane, benzene, and cyclohexane in water were not as close to experimental data as the previous ones. It seems that the larger the degree of coarse-graining is, or more polar the molecule, the less accurate the model is, which will be the object of further studies.

6.3 Asphaltene Solutions in Toluene

Here, we investigated the ability of the proposed strategy to reproduce the characteristics of asphaltene in toluene solutions. Toluene was chosen as the solvent due to the experimental data related to it regarding asphaltene suspensions. For these simulations, a box of $27.14 r_C \times 27.14 r_C \times 27.14 r_C$ with 60000 beads has been created. The mass fractions $X = 0.02, 0.05, 0.10,$ and 0.15 were tested. Periodic boundary conditions were applied, and initially, all particles were placed randomly within the simulation box. A total of 6000000 timesteps were carried out with $\Delta t = 0.002\tau$, among which the first 50% were equilibration steps, followed by

the production steps. The coarse-graining degree for all beads is again $N_m = 4$, meaning that every bead is composed of 4 water molecules. The asphaltene molecular structure and molecule parameters were described in the Coarse-Graining and Simulation Details section. The interaction parameters between beads were calculated at 298.15 K using the methodology described previously. Those parameters are exhibited in Table 6.4.

Table 6.4: The a_{ij} conservative repulsion parameters for the DPD force field between asphaltene and toluene beads. The parameters were calculated using equations 6.2, 6.4, and 6.1. Infinity dilution activity coefficients were taken from JCOSMO (GERBER and SOARES, 2013; SOARES, 2011) at 298.15 K. Results in DPD units.

	Toluene	Benzene	Butane	Thioglycolic-acid
Toluene	25	25.40	31.20	81.28
Benzene		25	33.93	76.08
Butane			25	126.40
Thioglycolic-acid				25

Firstly, the radial distribution function $g(r)$ of asphaltene molecules was calculated to obtain the interlayer distance between molecular centers d . The center-to-center $g(r)$ was calculated considering the distance between center of mass of asphaltene molecules. The radial distribution function is calculated by dividing the local density by the overall density of the system ρ_a , which in this case is the number of asphaltene molecules divided by the volume. The $g(r)$ first step calculation is performed counting the number of centroids N_r retained in a shell of volume ΔV at a distance r from a specified centroid. The local density is obtained dividing N_r by ΔV , which is ensemble-averaged and then divided by the bulk density ρ_a of the system:

$$g(r) = \langle \frac{N_r}{\Delta V} \rangle > \frac{1}{\rho_a} \quad (6.5)$$

Where $\langle \rangle$ means ensemble average. Figure 6.8 shows the radial distribution function for all asphaltene concentrations against dimensionless distance. The first peak represents the first shell of aggregation, which is related to the interlayer distance d . The interlayer distance obtained in this work is about 5 Å, other authors found similar results by molecular simulation (DE OLIVEIRA *et al.*, 2020a; DUAN *et al.*, 2017). This value is a little higher than the experimental distance 3-4 Å (ALVAREZ-RAMIREZ *et al.*, 2006; MULLINS, 2010; PACHECO-SÁNCHEZ *et al.*, 2003), which is explained by the fact that asphaltenes also aggregate with an offset displacement between their molecular centers (SEDGHI *et al.*, 2013), increasing the distance between them.

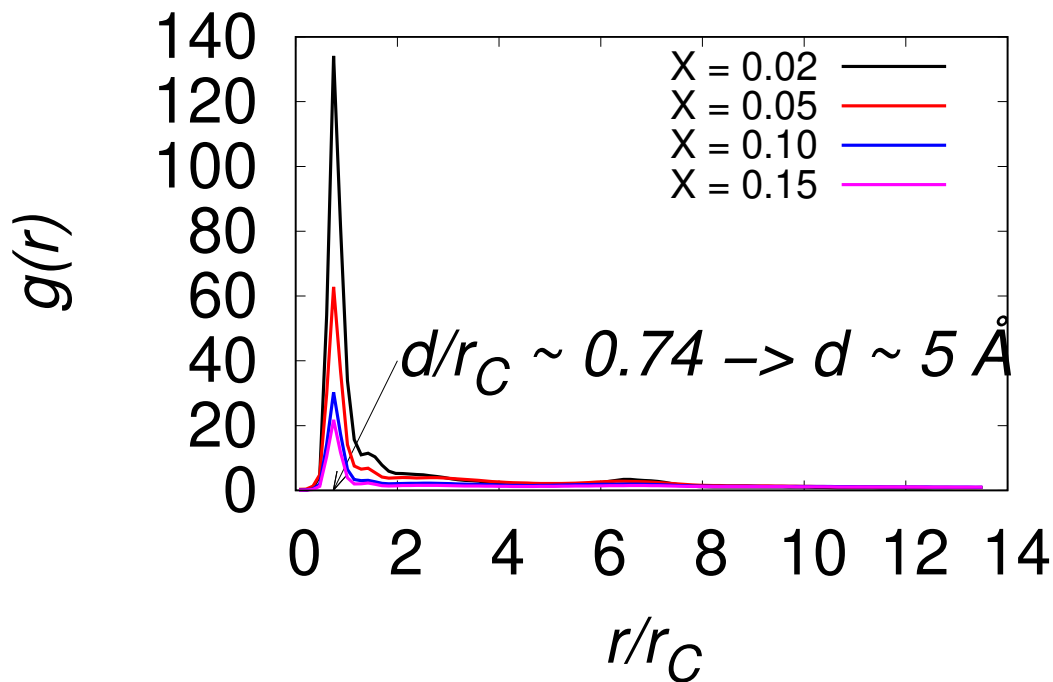


Figure 6.8: Radial Distribution Function $g(r)$ for asphaltene in toluene solutions. The interlayer distance between molecular centers d is represented by the first peak distance, which represents the first shell of aggregation. It is seen that for all concentrations, the interlayer distance d is $\sim 5 \text{ \AA}$, which agrees with several molecular dynamics studies (DE OLIVEIRA *et al.*, 2020a; DUAN *et al.*, 2017).

The Mean Square Displacement (MSD) has also been computed for the center of mass of asphaltene molecules. It is calculated by Equation 5.15. Figure 6.9 shows the MSD curves for the asphaltene solutions in toluene. As the mass fraction increases, the MSD values decrease as a consequence of the lower mobility caused by a higher concentration. The diffusion coefficient D is the derivative of the MSD with respect to time and for the three-dimensional case, it is given by Equation 5.16. As the simulation proceeds, the asphaltene molecules aggregate, which arrests their movement (DE OLIVEIRA *et al.*, 2020a), evidence of a sol-gel transition of asphaltene solutions (BOURIAT *et al.*, 2004; JESTIN *et al.*, 2007) appears. If the system is completely arrested, at long times, very higher concentrations and very low temperatures, the MSD tends to a constant value and the diffusion coefficient is zero. Therefore, to calculate diffusion coefficient, short and very long timescales are neglected; it should be calculated in the MSD linear region, which is plotted in Figure 6.9. Table 6.5 shows the calculated diffusion coefficients for the different concentrations, and it is noticeable that at low concentrations, the diffusion coefficient agrees well with the experimental data for the infinite dilution diffusion coefficient

of asphaltenes in toluene $2.2\text{-}6.3 \cdot 10^{-10} \text{ m}^2/\text{s}$ (ANDREWS *et al.*, 2006; ÖSTLUND *et al.*, 2003).

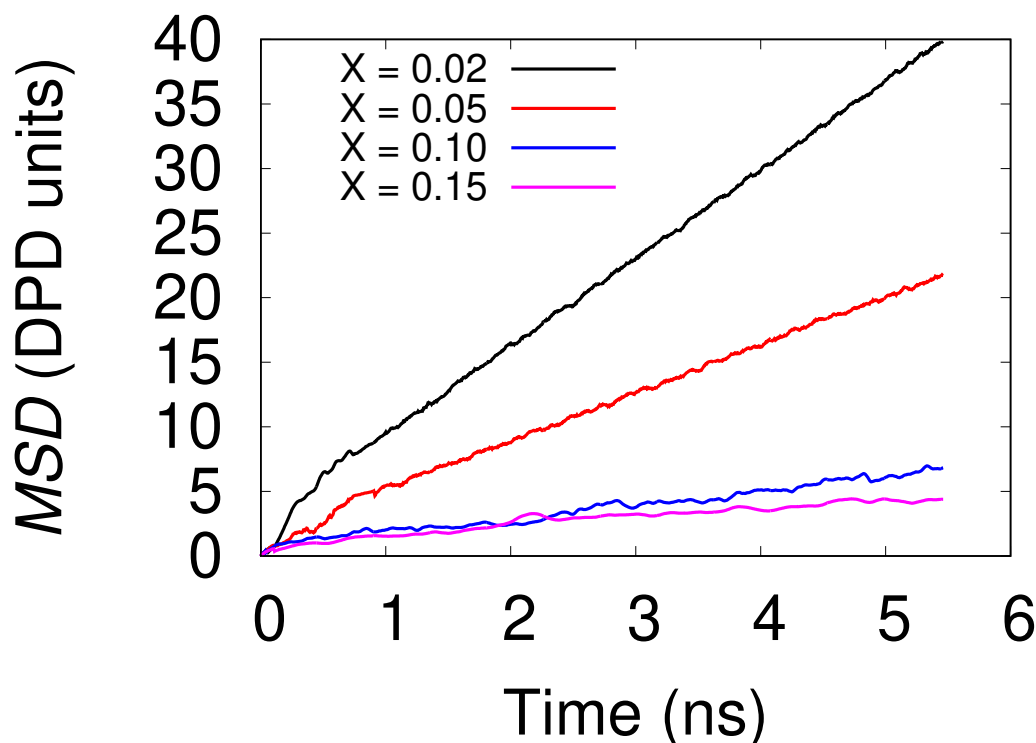


Figure 6.9: *MSD* curves for asphaltene solutions in toluene at different mass fractions $X = 0.02, 0.05, 0.10,$ and 0.15 . At higher concentrations, the *MSD* decreases because of lower particle mobility.

Table 6.5: Diffusion coefficient D for asphaltene solutions in toluene for different mass fractions $X = 0.02, 0.05, 0.10,$ and 0.15 . D values are higher for low concentrations as a consequence of higher mobility. Low concentration D values are within the experimental range $2.2\text{-}6.3 \cdot 10^{-10} \text{ m}^2/\text{s}$ (ANDREWS *et al.*, 2006; ÖSTLUND *et al.*, 2003).

Mass fraction	Diffusion coefficient D (m^2/s)
0.02	$5.2 \cdot 10^{-10} \text{ m}^2/\text{s}$
0.05	$2.9 \cdot 10^{-10} \text{ m}^2/\text{s}$
0.10	$8.2 \cdot 10^{-11} \text{ m}^2/\text{s}$
0.15	$5.3 \cdot 10^{-11} \text{ m}^2/\text{s}$

6.4 Asphaltenes at the Water-Oil Interface

As asphaltene molecules act as surfactants at the water-oil interface, the water-asphaltene-cyclohexane system was selected to study the interfacial properties of as-

phaltenes. For these simulations, concentrations in the range 7.5-150 g/L were carried out. Periodic boundary conditions were applied. A total of 6000000 timesteps were simulated with $\Delta t = 0.002\tau$, among which the first 25% were equilibration steps, followed by the production steps. Again, the coarse-graining degree for all beads is $N_m = 4$, meaning that every bead is composed of 4 water molecules. The asphaltene molecular structure and molecule parameters were described in the Coarse-Graining and Simulation Details section. The interaction parameters between beads were calculated at 298.15 K, those parameters are exhibited in Table 6.6.

Table 6.6: The a_{ij} conservative repulsion parameters for the DPD force field between asphaltene, water, and cyclohexane beads. The parameters were calculate using equations 6.2, 6.4, and 6.1. Infinity dilution activity coefficients were taken from JCOSMO GERBER and SOARES (2013); SOARES (2011) at 298.15 K. Results in DPD units.

	Water	Cyclohexane	Benzene	Butane	Thioglycolic-acid
Water	25	165.36	116.86	146.15	7.19
Cyclohexane		25	35.98	25.57	129.46
Benzene			25	33.93	76.08
Butane				25	126.40
Thioglycolic-acid					25

Experimental data for the interfacial tension of the water-asphaltene-cyclohexane systems at 298 K was published by BOURIAT *et al.* (2004) The simulated interfacial tension of asphaltenes in water/cyclohexane is plotted in Figure 6.10. Our goal is not to try to reproduce the experimental data, since it is not possible to determine the exact asphaltene molecular structure. That being said, from experimental data, it can be seen that the IFT has a decreasing tendency until ~ 17.5 g/L BOURIAT *et al.* (2004), becoming constant afterwards. This constant value can be thought of as the CMC (critical micelle concentration) of the asphaltenes, i.e., this value represents the interface saturation. LOH *et al.* (1999) and ROGEL *et al.* (2000) reported CMC values for asphaltenes ranging from 1-30 g/L depending on the solvent used. The CMC found in this work is about 48 g/L, which is a good indicator of the reliability of the proposed modeling. Figure 6.11 shows the initial micelle formation at 40 g/L.

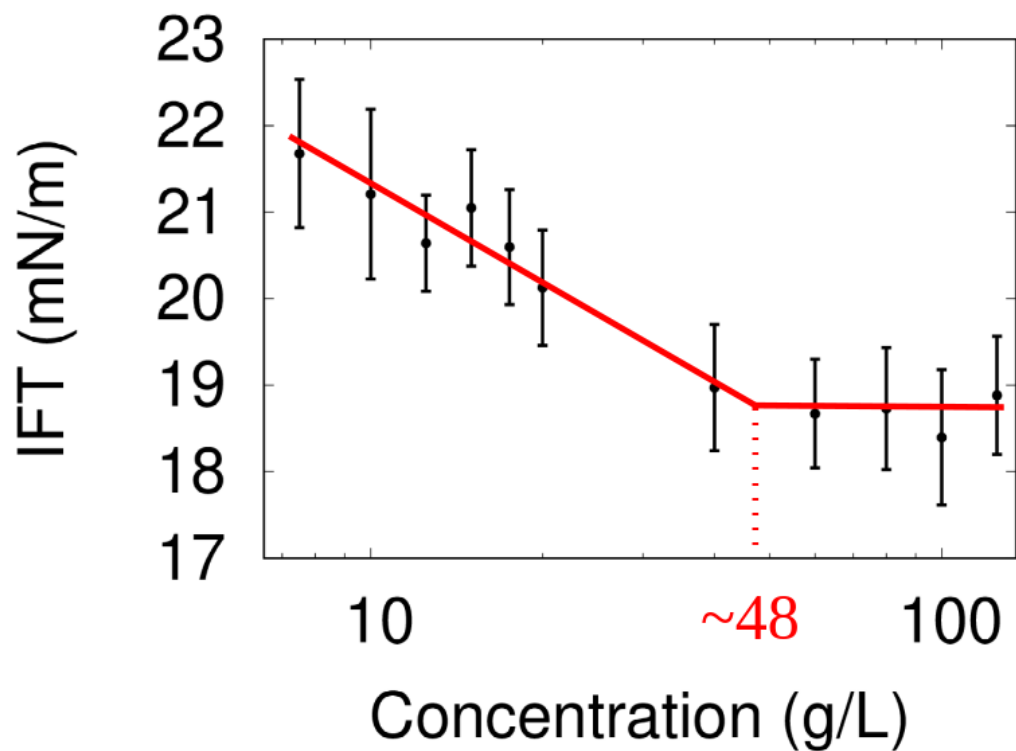


Figure 6.10: Interfacial tension of asphaltenes at the water/cyclohexane interface at 298 K. Results from molecular simulation using DPD/COSMO-SAC. Standard deviations represented by error bars. Red lines to guide the eyes. The CMC is about 48 g/L.

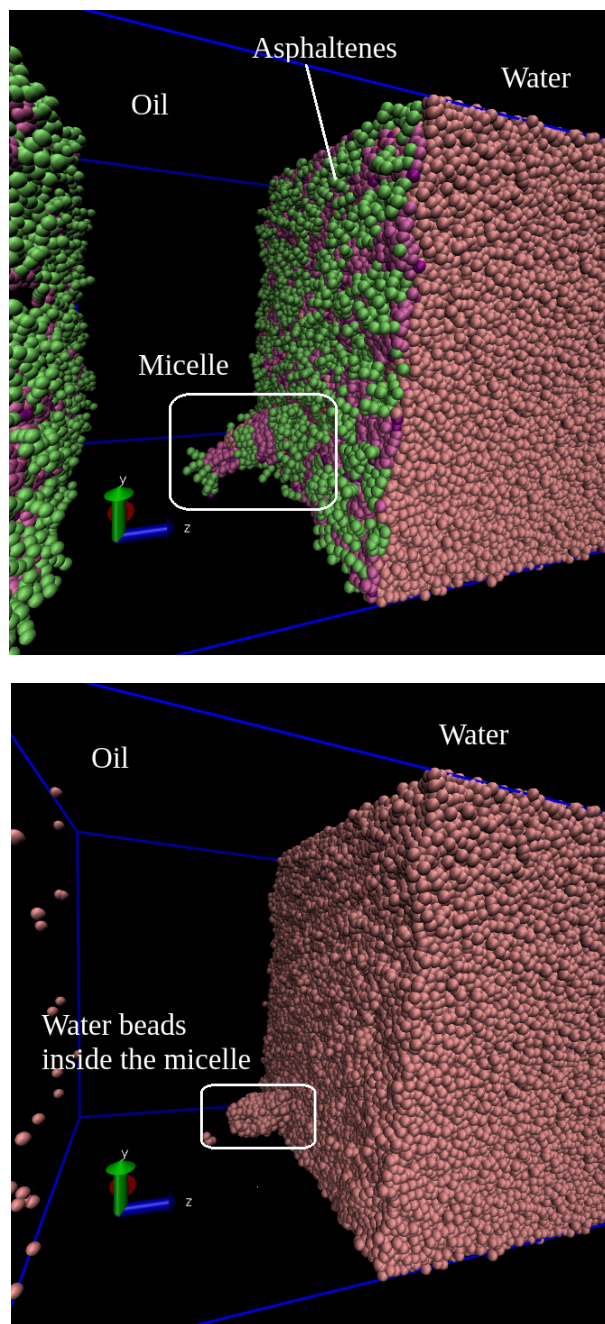


Figure 6.11: Initial micelle formation of asphaltenes in water/cyclohexane interfaces. That figure shows the water in oil micelle formation with asphaltene concentration = 40 g/L. Oil (cyclohexane) beads have been omitted for better visualization.

At concentration 125.0 g/L the interfaces are supersaturated and asphaltene molecules start forming a complex interface which is more evident at 150.0 g/L. At 150.0 g/L the interfaces are no longer planar which makes impossible to calculate the IFT by the methodology used here. The surface geometry becomes spherical-like resembling droplets, which indicates the formation of microemulsions. Figures 6.12-6.13 show the interfaces formed at higher concentrations.

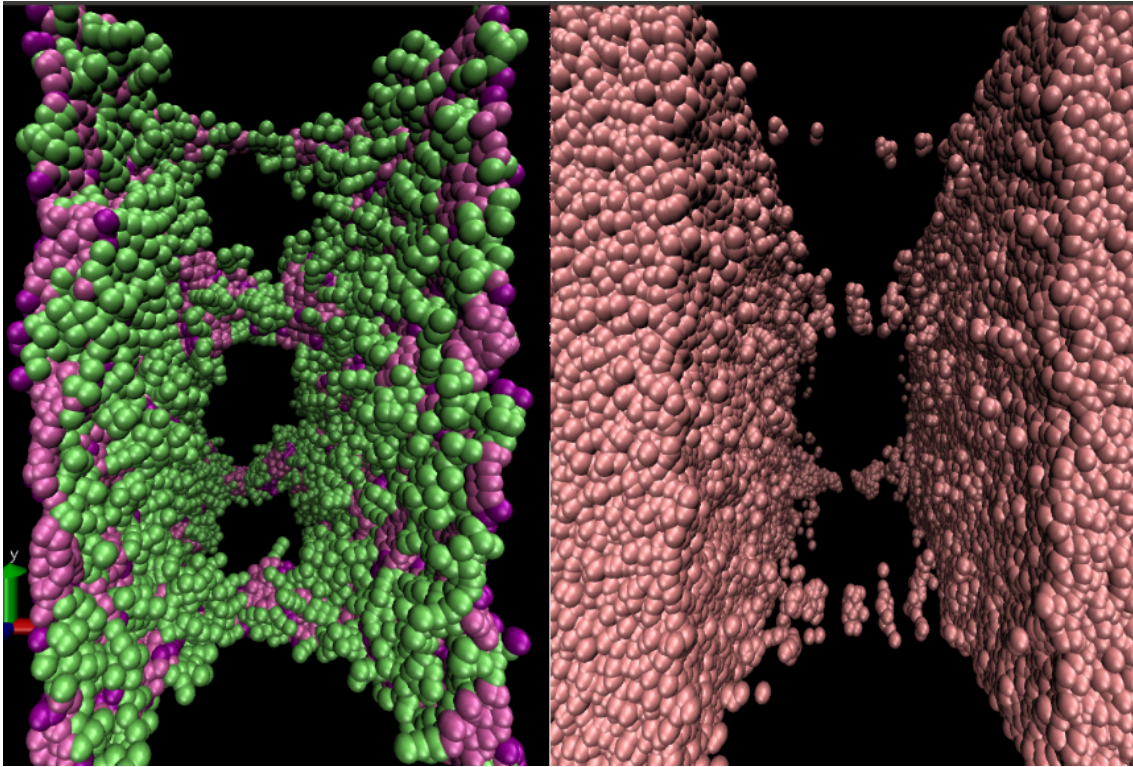


Figure 6.12: Interface formed in the water/cyclohexane system with asphaltene concentration = 125.0 g/L, 298 K. The interface is supersaturated. (left) Asphaltene beads. (right) water beads. Cyclohexane (oil) beads have been omitted for better visualization.

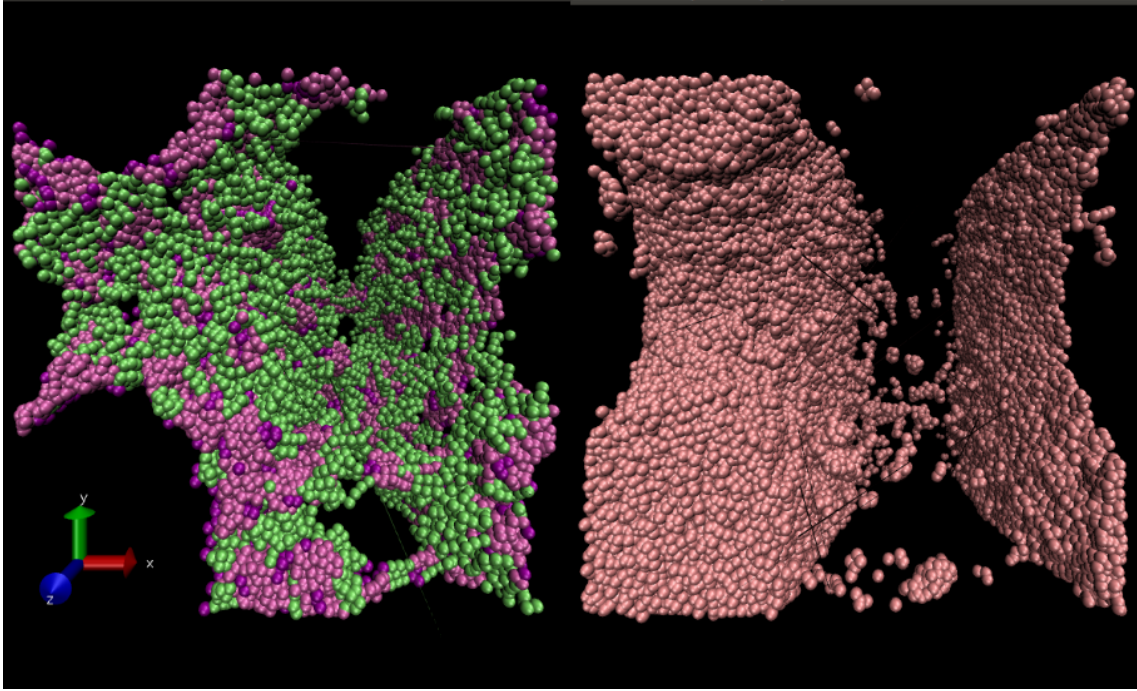


Figure 6.13: Interface formed in the water/cyclohexane system with asphaltene concentration = 150.0 g/L, 298 K. The surface acquires a complex geometry that resembles droplets of a microemulsion. (left) Asphaltene beads. (right) water beads. Cyclohexane (oil) beads have been omitted for better visualization.

The linear density profile (LDP) has also been calculated to study the interface structure. Linear density is calculated by accounting for the number of molecules in each slab b , divided by the slab length Δz . Figure 6.14 has been adapted from GIORGINO (2014) and shows how to divide the cell box into slabs of volume $LxLy\Delta z$.

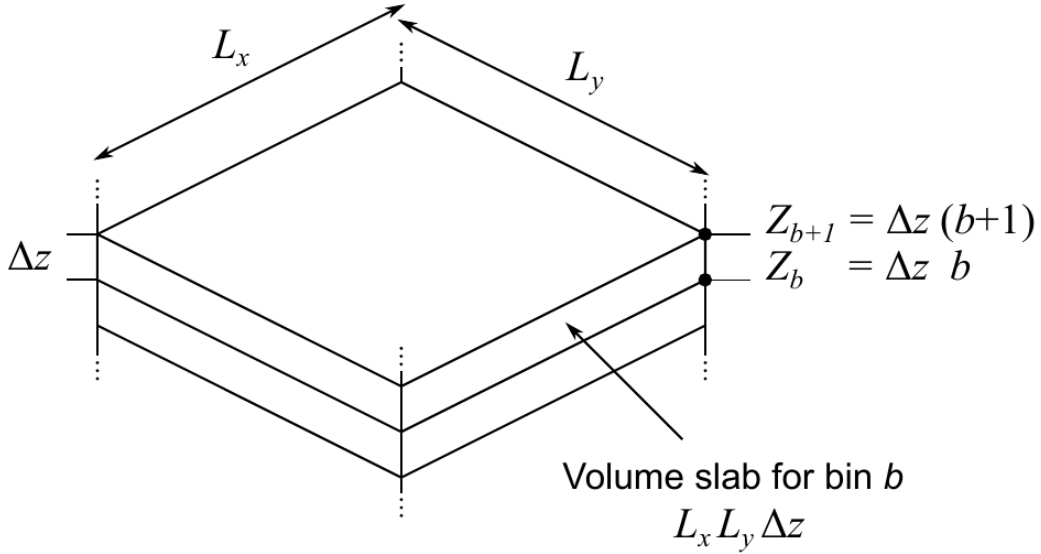


Figure 6.14: Domain division into slabs for linear density calculations. Density is being calculated along with z axis with Δz accuracy. Each slab has a volume $L_x L_y \Delta z$, for linear density $L_x = L_y = 1$. Bin b holds all molecules within $b \leq z/\Delta z \leq b + 1$. Figure obtained from GIORGINO (2014).

Figure 6.15 shows an example of the LDP profile for asphaltene concentration 7.5 g/L. The profile has two peaks representing the two interfaces formed, and both have almost the same peak value which means that the system is well equilibrated with homogeneous interfaces (the same number of molecules at each interface). The LDP values were averaged and the average values and standard deviations (error bars) are plotted in Figure 6.16 against asphaltene concentration. It is seen that the higher the concentration is, the higher the generated peaks are, which is a consequence of the increasing number of asphaltene molecules at each interface. At higher concentrations, the asphaltene molecules supersaturate the interface, which enlarges the LDP profile, increasing the standard deviations.

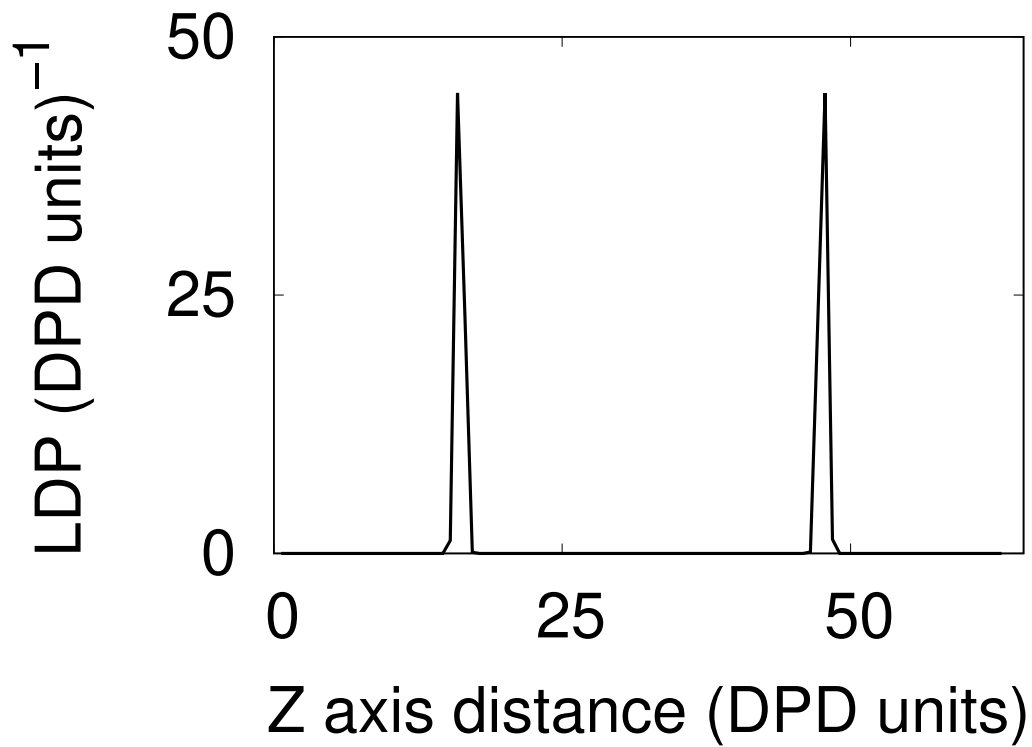


Figure 6.15: Linear Density Profile (LDP) for asphaltene at the water/cyclohexane interface. The asphaltene concentration is 7.5 g/L. The homogeneity of the two peaks means that the system is well equilibrated with the same number of molecules at each interface.

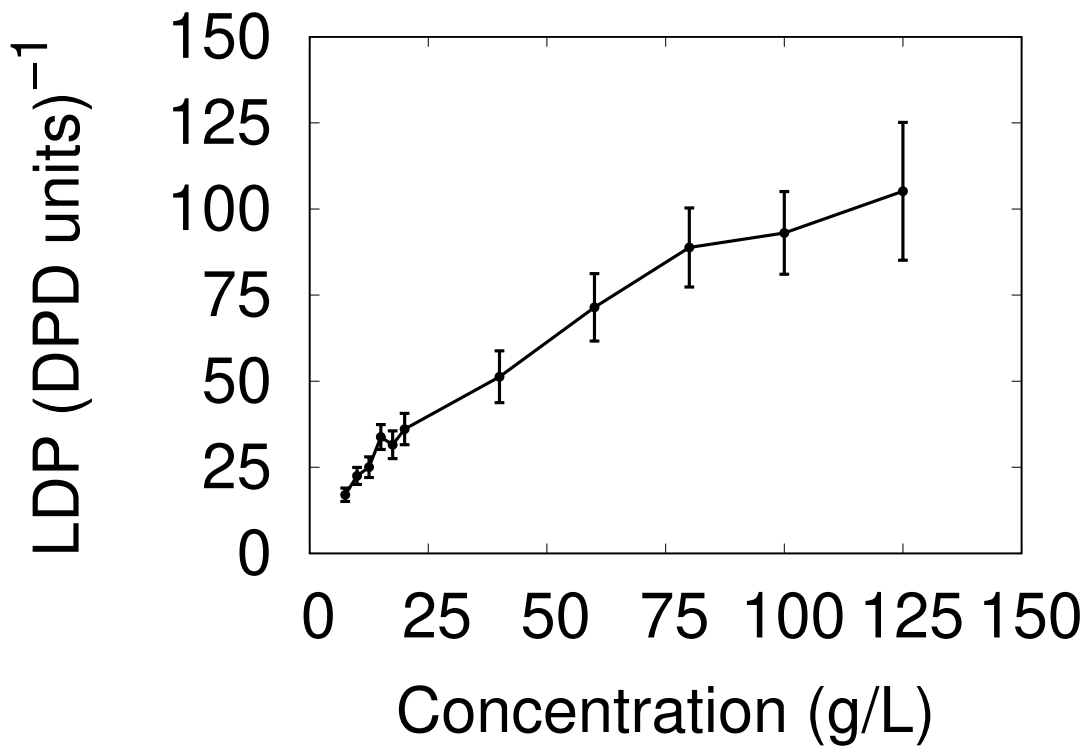


Figure 6.16: Linear Density Profile (LDP) for asphaltenes at the water/cyclohexane interface. Concentrations ranging between 7.5-125 g/L. Higher concentrations produce higher peaks at the interfaces and broader distributions (higher standard deviations), as a consequence of the great number of molecules settling at the interfaces.

The angle θ between the asphaltene molecular planes and the interfaces has also been calculated, see Figure 6.17. The asphaltene molecular plane is defined as the plane α . The molecular plane vector \vec{v} is defined as the position vector between the first and last particle position of the polyaromatic nuclei, as indicated in Figure 6.17. The vector \vec{n} normal to the xy plane (interface occurring in the z direction) is (0,0,1). Therefore, the acute angle θ between the straight line \vec{v} and the plane defined by the normal \vec{n} is calculated by Equation 6.6:

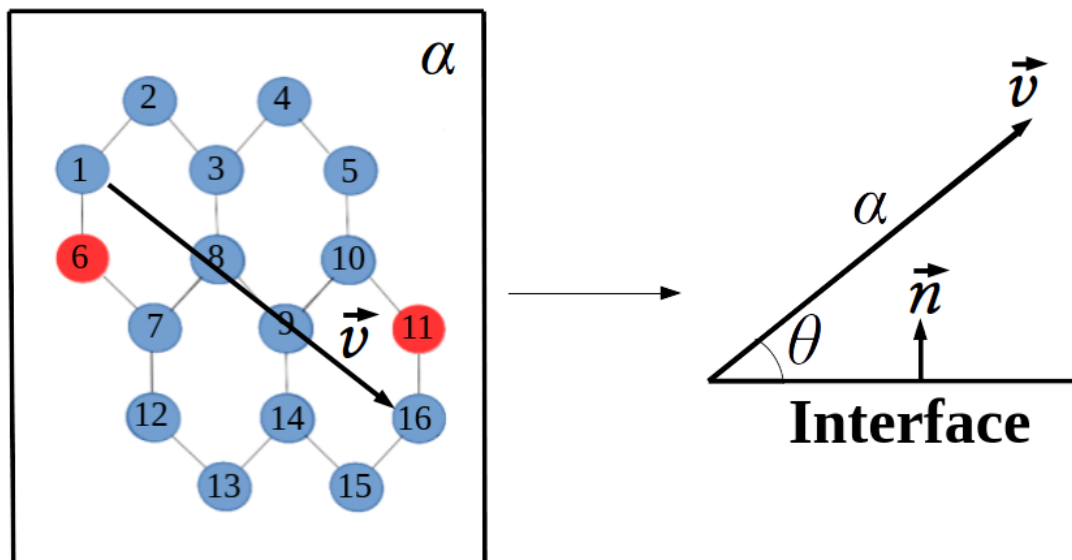


Figure 6.17: Schematic representation of the separation angle θ between asphaltene molecular plane α and the interface. The molecular plane vector is defined by \vec{v} (position vector between the first (1st) and the last particle (16th) of the polyaromatic nuclei), the vector normal to the interface is \vec{n} .

$$\sin \theta = \frac{|\vec{v} \cdot \vec{n}|}{|\vec{v}| |\vec{n}|} \quad (6.6)$$

Aiming at improving the sample of the angle profiles, we calculated the angle θ by ensemble-average (symbol $\langle \rangle$) for the two interfaces. $\langle \theta \rangle$ is calculated by detecting the asphaltene molecules pertaining to both interfaces and then calculating the simple average between all θ angles of each molecule at both interfaces; the result is averaged in time. Figure 6.18 shows the averaged θ angle for all concentrations. It can be seen that at low concentrations ($C < 25$ g/L), the asphaltene molecules settle nearly parallel to the interfaces ($\theta < 10^\circ$), which means that there is enough space for the molecules to arrange at the interface. As the concentration increases ($C \geq 40$ g/L), the asphaltene molecules saturate, and the entropic effects dominate at the interface, which leads to an “expulsion effect”. The asphaltene molecules that migrate from interface to bulk phase (oil) carry water molecules, due to the great affinity between the asphaltene heteroatom and water. This “expulsion effect” displaces the asphaltene molecules from the interface, which increases the angle θ , as an attempt to minimize the free energy at the interfaces.

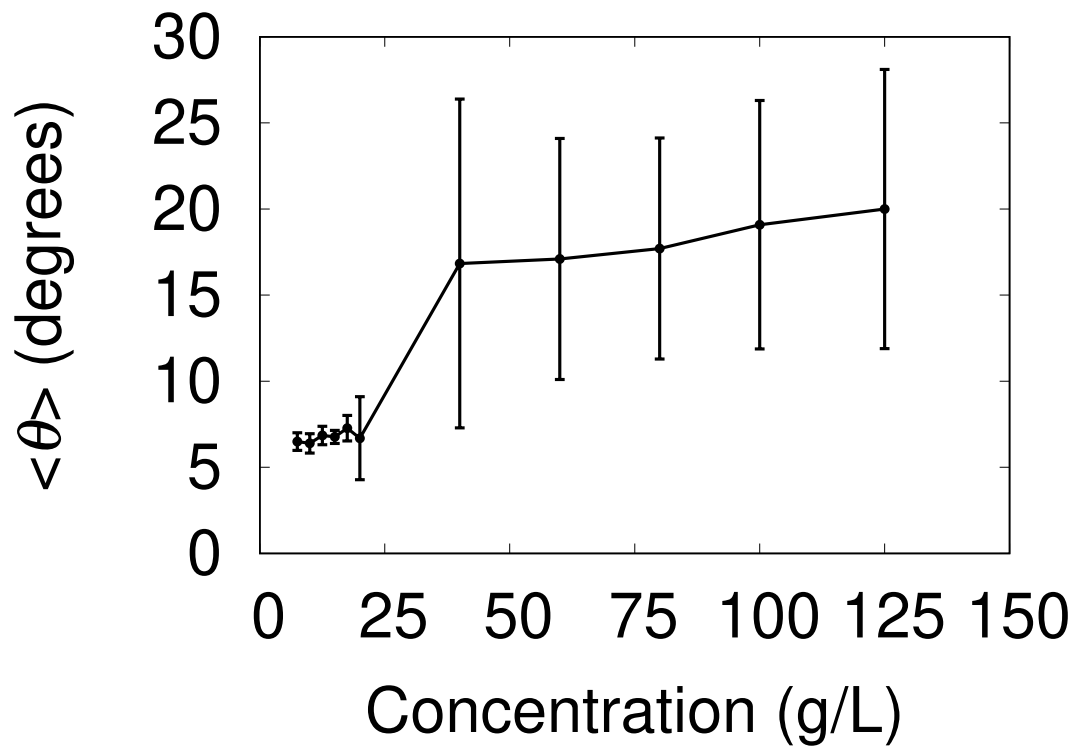


Figure 6.18: $\langle \theta \rangle$ against asphaltene concentration at the water/cyclohexane interface. $\langle \theta \rangle$ is the ensemble-averaged angle between asphaltene molecular planes and the interfaces.

Chapter 7

Conclusions and Future Perspectives

A novel algorithm for cluster labeling in molecular simulation was developed based on the non-lattice version of the Hoshen-Kopelman algorithm. The proposed algorithm has proven to be appropriate, efficient, and faster than the original for studying aggregation in molecular simulation. Good results were obtained. The number of clusters decreases (the number of links increases) in time, as initially, each molecule represents one single cluster. By using our algorithm, it is possible to identify the percolation state of Lennard-Jones particles under Brownian dynamics, which is a prerequisite of gelation transition. We also studied the aggregation of asphaltene model particles. In the timescale simulated, asphaltene molecules tend to form stable aggregates at the final stages. We verified that by increasing eight the saved time was around 80%.

The DPD method was used to investigate the effects of concentration and solvent on asphaltene aggregation and their structural, dynamical, and rheological properties. Asphaltene molecule model and particle parameters were extracted from SONG *et al.* (2016) which has been proven to generate consistent results. A new method of detecting/counting clusters has also been a product of this thesis. The structural behavior was studied by means of radial distribution function $g(r)$ and angle distribution histograms. Radial distribution function showed a first peak around 5.8 Å, which grows as mass fraction diminishes, both results supported by the literature. From angle distribution analysis, it can be seen that parallel stacking predominates over other conformations on the aggregates, which confirms that interactions between polyaromatic nuclei are the main drive force leading to aggregation. Nevertheless T-shaped and offset conformation were also observed as reported by other authors. The number of aggregates evolution shows that the number of aggre-

gates N is decreasing in time, and the average aggregate size S becomes larger which is explained by the fact that molecules are getting closer, forming larger aggregates. Moreover, aggregates in heptane are larger than in toluene, which agrees with experimental results. MSD curves of asphaltene were obtained for both solvents and different mass fractions. At long times, the MSD curves displace from linear behavior, which is related to the gelation transition experienced by those systems and sometimes observed during oil extraction. That behavior is being reported for the first time for mesoscale asphaltene molecular simulations. The diffusion coefficient calculated for asphaltene at $X = 0.05$ is close to the experimental value for diluted suspensions. The simple shear analysis showed that viscosity decreases as shear rate increases due to the alignment between molecules caused by deformation. It is interesting to notice that at higher mass fractions, the viscosity curves for different solvents approach, which means that enthalpic interactions have a minor influence on the viscosity at higher mass fraction. When N is proven concerning shear, there are two main conclusions. At higher mass fraction in both solvents, all tested shear rates led to breaking the structure, which is seen by the increase in N and decrease in S as molecules are being separated. N attained the same value in time for both solvents at the highest shear rate, because shearing becomes more important than particle interactions. At lower mass fraction and low shear rates, the number of aggregates remains approximately constant, which means that the imposed shear is not high enough to destroy the aggregated structure.

Oscillatory shear was used to study the linear viscoelastic regime of asphaltene suspensions through DPD molecular simulations. The literature has never reported it up to date. The range of amplitudes where the storage modulus G' remains constant at low frequency has been determined, and the 0.5 \AA value has been used to proceed with the frequency sweep analysis. At high-frequency regime, all systems showed more pronounced viscous behavior, which is explained by the soft nature of DPD particles. There is a competition between Brownian motion and entropic interactions in the viscoelastic solution behavior at low frequencies. At low mass fractions, Brownian dissipative forces dominates ($G'' > G'$). At high mass fractions, the entropic interactions that should constitute a conservative potential favor energy storage giving rise to higher solidlike behavior ($G' > G''$).

The Dissipative Particle Dynamics, DPD, was used to study the interfacial properties of asphaltenes adsorbed on the water/oil interface. Cyclohexane was used as the oil phase. For unlike beads, the DPD parameters were calculated using COSMO-SAC, which has the advantage of being an open-source, generic way of estimating DPD parameters consistent with real systems. We used interface tension of several hydrocarbon-water systems to validate the methodology, showing very good

agreement over a range of temperatures. To know whether the method can access the structural and the diffusion coefficient of asphaltenes in toluene, we calculated these properties and compared them with experimental data. The Radial Distribution Function and the Mean Squared Displacement obtained here agreed with the experimental data.

The Linear Density Profiles were calculated for different concentrations, showing that the interfaces are homogeneous at low asphaltene concentrations. The angle $\langle \theta \rangle$ between asphaltene molecular planes and the interface has also been analyzed. At low asphaltene concentrations ($C < 25$ g/L), asphaltene tends to settle parallel to the interface as there are few molecules on the interface. At higher concentrations ($C \geq 40$ g/L), the asphaltene molecules are displaced over the interface due to entropic effects, which increases the angle between molecular planes and the interface. Microemulsion tends to be stable at these high asphaltene concentrations, and the interfaces start to be not well defined.

From future perspectives, from the viscoelastic simulations of asphaltene suspensions, experimental data on the rheology of real suspensions could be compared to simulation data obtained by the DPD/COSMO SAC proposed in this thesis.

As discussed in the literature review, during the crude oil extraction, it could precipitate under certain conditions that form solids that clog the pipes. It is necessary to apply stress to restore full operation. The minimum value of applied stress that breaks down the precipitated solids is called yield stress. That parameter is crucial for oil extraction. Its determination can be the subject of further studies, that is, to study which stress value should be applied so that the structure flows.

With a methodology capable of reproducing the rheological behavior of real suspensions, we can come back to the structural study and determine the real force field (and its parameters) that represent the interactions between asphaltenes. And then, we could calculate the second virial coefficient that has to do with the interparticle interactions.

Another interesting study would be to obtain the structure factor of real suspensions by light scattering and to verify if the structural information from molecular simulations are consistent with the experimental light scattering.

The DPD/COSMO SAC methodology developed in this thesis can also be applied to determine inhibitors of asphaltene aggregation. The same methodology can be used to study the properties of water/oil interfaces containing ions, which would be more realistic.

Bibliography

“compute cluster/atom command”. https://lammmps.sandia.gov/doc/compute_cluster_atom.html. Accessed: 2020-10-06.

“measure cluster command”. <http://www-s.ks.uiuc.edu/Research/vmd/vmd-1.9.1/ug/node136.html>. Accessed: 2020-10-06.

ACEVEDO, S., CASTRO, A., VÁSQUEZ, E., et al., 2010, “Investigation of physical chemistry properties of asphaltenes using solubility parameters of asphaltenes and their fractions A1 and A2”, *Energy & Fuels*, v. 24, n. 11, pp. 5921–5933.

ACEVEDO, S., ESCOBAR, G., GUTIÉRREZ, L. B., et al., 1993, “Interfacial rheological studies of extra-heavy crude oils and asphaltenes: Role of the dispersion effect of resins in the adsorption of asphaltenes at the interface of water-in-crude oil emulsions”, *Colloids and Surfaces A: Physicochemical and Engineering Aspects*, v. 71, n. 1, pp. 65 – 71. ISSN: 0927-7757. Availability: <<http://www.sciencedirect.com/science/article/pii/092777579380028D>>.

AGUILERA-MERCADO, B., HERDES, C., MURGICH, J., et al., 2006, “Mesoscopic simulation of aggregation of asphaltene and resin molecules in crude oils”, *Energy & Fuels*, v. 20, n. 1, pp. 327–338.

AHMADI, M., HASSANZADEH, H., ABEDI, J., 2018, “Asphaltene Mesoscale Aggregation Behavior in Organic Solvents—A Brownian Dynamics Study”, *The Journal of Physical Chemistry B*, v. 122, n. 35, pp. 8477–8492.

AL-FUTAISI, A., PATZEK, T. W., 2003, “Extension of Hoshen–Kopelman algorithm to non-lattice environments”, *Physica A: Statistical Mechanics and its Applications*, v. 321, n. 3-4, pp. 665–678.

ALASIRI, H., CHAPMAN, W. G., 2017, “Dissipative particle dynamics (DPD) study of the interfacial tension for alkane/water systems by using

- COSMO-RS to calculate interaction parameters”, *Journal of Molecular Liquids*, v. 246, pp. 131–139.
- ALASIRI, H. S., SULTAN, A. S., CHAPMAN, W. G., 2019, “Effect of surfactant headgroup, salts, and temperature on interfacial properties: Dissipative particle dynamics and experiment for the water/octane/surfactant system”, *Energy & Fuels*, v. 33, n. 7, pp. 6678–6688.
- ALDER, B., WAINWRIGHT, T., 1957, “Phase transition for a hard sphere system”, *The Journal of chemical physics*, v. 27, n. 5, pp. 1208–1209.
- ALLEN, M. P., TILDESLEY, D. J., 1991, *Computer simulation of liquids*. Oxford university press.
- ALVAREZ, F., FLORES, E., CASTRO, L., et al., 2010, “Dissipative particle dynamics (DPD) study of crude oil- water emulsions in the presence of a functionalized co-polymer”, *Energy & Fuels*, v. 25, n. 2, pp. 562–567.
- ALVAREZ-RAMIREZ, F., RAMIREZ-JARAMILLO, E., RUIZ-MORALES, Y., 2006, “Calculation of the interaction potential curve between asphaltene-asphaltene, asphaltene- resin, and resin- resin systems using density functional theory”, *Energy & Fuels*, v. 20, n. 1, pp. 195–204.
- ANDREATTA, G., BOSTROM, N., MULLINS, O. C., 2005, “High-Q Ultrasonic Determination of the Critical Nanoaggregate Concentration of Asphaltenes and the Critical Micelle Concentration of Standard Surfactants”, *Langmuir*, v. 21, n. 7, pp. 2728–2736. Availability: <<https://doi.org/10.1021/la048640t>>. PMID: 15779941.
- ANDREWS, A. B., GUERRA, R. E., MULLINS, O. C., et al., 2006, “Diffusivity of asphaltene molecules by fluorescence correlation spectroscopy”, *The Journal of Physical Chemistry A*, v. 110, n. 26, pp. 8093–8097.
- ARTOK, L., SU, Y., HIROSE, Y., et al., 1999, “Structure and reactivity of petroleum-derived asphaltene”, *Energy & Fuels*, v. 13, n. 2, pp. 287–296.
- ARTOLA, P.-A., PEREIRA, F. E., ADJIMAN, C. S., et al., 2011, “Understanding the fluid phase behaviour of crude oil: Asphaltene precipitation”, *Fluid Phase Equilibria*, v. 306, n. 1, pp. 129–136.
- ARYA, A., LIANG, X., VON SOLMS, N., et al., 2017, “Modeling of Asphaltene Precipitation from Crude Oil with the Cubic Plus Association Equation of State”, *Energy & Fuels*, v. 31, n. 2, pp. 2063–2075.

- AVID, B., SATO, S., TAKANOHASHI, T., et al., 2004, “Characterization of Asphaltenes from Brazilian Vacuum Residue Using Heptane- Toluene Mixtures”, *Energy & Fuels*, v. 18, n. 6, pp. 1792–1797.
- BABALIEVSKI, F., 1998, “Cluster counting: the Hoshen–Kopelman algorithm versus spanning tree approaches”, *International Journal of Modern Physics C*, v. 9, n. 01, pp. 43–60.
- BALBERG, I., 1987, “Recent developments in continuum percolation”, *Philosophical Magazine B*, v. 56, n. 6, pp. 991–1003. Availability: <<https://doi.org/10.1080/13642818708215336>>.
- BIRD, R. B., OTHERS, 1977, *Dynamics of polymeric liquids.-* Wiley.
- BOEK, E. S., HEADEN, T. F., PADDING, J. T., 2010, “Multi-scale simulation of asphaltene aggregation and deposition in capillary flow”, *Faraday discussions*, v. 144, pp. 271–284.
- BOROMAND, A., JAMALI, S., MAIA, J. M., 2015, “Viscosity measurement techniques in dissipative particle dynamics”, *Computer Physics Communications*, v. 196, pp. 149–160.
- BOURIAT, P., EL KERRI, N., GRACIAA, A., et al., 2004, “Properties of a two-dimensional asphaltene network at the water- cyclohexane interface deduced from dynamic tensiometry”, *Langmuir*, v. 20, n. 18, pp. 7459–7464.
- BUG, A. L. R., SAFRAN, S. A., WEBMAN, I., 1985, “Continuum Percolation of Rods”, *Phys. Rev. Lett.*, v. 54 (Apr), pp. 1412–1415. Availability: <<https://link.aps.org/doi/10.1103/PhysRevLett.54.1412>>.
- BÜRGI, T., 2015, “Properties of the gold–sulphur interface: from self-assembled monolayers to clusters”, *Nanoscale*, v. 7, n. 38, pp. 15553–15567.
- CARAUTA, A. N., SEIDL, P. R., CHRISMAN, E. C., et al., 2005, “Modeling solvent effects on asphaltene dimers”, *Energy & fuels*, v. 19, n. 4, pp. 1245–1251.
- CHAKRABORTY, S., CHOUDHURY, C. K., ROY, S., 2013, “Morphology and dynamics of carbon nanotube in polycarbonate carbon nanotube composite from dissipative particle dynamics simulation”, *Macromolecules*, v. 46, n. 9, pp. 3631–3638.
- CHANG, C.-C., NOWBAHAR, A., MANSARD, V., et al., 2018, “Interfacial Rheology and Heterogeneity of Aging Asphaltene Layers at the Water–Oil

Interface”, *Langmuir*, v. 34, n. 19, pp. 5409–5415. Availability: <<https://doi.org/10.1021/acs.langmuir.8b00176>>. PMID: 29685033.

CHANG, C.-C., WILLIAMS, I., NOWBAHAR, A., et al., 2019, “Effect of Ethylcellulose on the Rheology and Mechanical Heterogeneity of Asphaltene Films at the Oil–Water Interface”, *Langmuir*, v. 35, n. 29, pp. 9374–9381. Availability: <<https://doi.org/10.1021/acs.langmuir.9b00834>>. PMID: 31256591.

CHATTERJEE, A., 2007, “Modification to Lees–Edwards periodic boundary condition for dissipative particle dynamics simulation with high dissipation rates”, *Molecular Simulation*, v. 33, n. 15, pp. 1233–1236. Availability: <<https://doi.org/10.1080/08927020701713894>>.

CHEN, J., CHEN, J., ZHONG, C., et al., 2017a, “Mesoscopic probes in asphaltene nanoaggregate structure: from perpendicular to paralleled orientation at the water-in-oil emulsions interface”, *RSC Advances*, v. 7, n. 61, pp. 38193–38203.

CHEN, Y., ZHOU, S., WANG, Y., et al., 2017b, “Screening solvents to extract phenol from aqueous solutions by the COSMO-SAC model and extraction process simulation”, *Fluid Phase Equilibria*, v. 451, pp. 12 – 24. ISSN: 0378-3812. Availability: <<http://www.sciencedirect.com/science/article/pii/S0378381217302996>>.

CONSTANTINESCU, D., GMEHLING, J., 2016, “Further Development of Modified UNIFAC (Dortmund): Revision and Extension 6”, *Journal of Chemical & Engineering Data*, v. 61, n. 8, pp. 2738–2748. Availability: <<https://doi.org/10.1021/acs.jced.6b00136>>.

DE OLIVEIRA, F. C., KHANI, S., MAIA, J. M., et al., 2020a, “Concentration and Solvent Effects on Structural, Dynamical, and Rheological Properties of Asphaltene Suspensions”, *Energy & Fuels*, v. 34, n. 1, pp. 1071–1081. Availability: <<https://doi.org/10.1021/acs.energyfuels.9b03315>>.

DE OLIVEIRA, F. C., KHANI, S., MAIA, J. M., et al., 2020b, “Modified clustering algorithm for molecular simulation”, *Molecular Simulation*, v. 46, n. 18, pp. 1453–1466. Availability: <<https://doi.org/10.1080/08927022.2020.1839661>>.

- DE OLIVEIRA, F. C., MAIA, J. M., TAVARES, F. W., submitted, “Asphaltenes at the water-oil interface using DPD/COSMO-SAC”, *Colloids and Surfaces A: Physicochemical and Engineering Aspects*.
- DE VIVO, M., MASETTI, M., BOTTEGONI, G., et al., 2016, “Role of molecular dynamics and related methods in drug discovery”, *Journal of medicinal chemistry*, v. 59, n. 9, pp. 4035–4061.
- DENG, M., LI, Z., BORODIN, O., et al., 2016, “cDPD: A new dissipative particle dynamics method for modeling electrokinetic phenomena at the mesoscale”, *The Journal of chemical physics*, v. 145, n. 14, pp. 144109.
- DUAN, M., SONG, X., ZHAO, S., et al., 2017, “Layer-by-Layer Assembled Film of Asphaltenes/Polyacrylamide and Its Stability of Water-in-Oil Emulsions: A Combined Experimental and Simulation Study”, *The Journal of Physical Chemistry C*, v. 121, n. 8, pp. 4332–4342.
- DUDA, Y., LIRA-GALEANA, C., 2006, “Thermodynamics of asphaltene structure and aggregation”, *Fluid phase equilibria*, v. 241, n. 1, pp. 257–267.
- D’ARJUZON, R. J., FRITH, W., MELROSE, J. R., 2003, “Brownian dynamics simulations of aging colloidal gels”, *Physical Review E*, v. 67, n. 6, pp. 061404.
- ESE, M.-H., YANG, X., SJÖBLOM, J., 1998, “Film forming properties of asphaltenes and resins. A comparative Langmuir–Blodgett study of crude oils from North Sea, European continent and Venezuela”, *Colloid and Polymer Science*, v. 276, n. 9 (Oct), pp. 800–809. ISSN: 1435-1536. Availability: <<https://doi.org/10.1007/s003960050313>>.
- ESPANOL, P., 1995, “Hydrodynamics from dissipative particle dynamics”, *Physical Review E*, v. 52, n. 2, pp. 1734.
- ESPANOL, P., WARREN, P., 1995, “Statistical mechanics of dissipative particle dynamics”, *EPL (Europhysics Letters)*, v. 30, n. 4, pp. 191.
- ESPAÑOL, P., WARREN, P. B., 2017, “Perspective: Dissipative particle dynamics”, *The Journal of chemical physics*, v. 146, n. 15, pp. 150901.
- EVANS, D. J., MORRISS, G., 1984, “Nonlinear-response theory for steady planar Couette flow”, *Physical Review A*, v. 30, n. 3, pp. 1528.
- FAN, Y., SIMON, S., SJÖBLOM, J., 2010a, “Interfacial shear rheology of asphaltenes at oil–water interface and its relation to emulsion stability:

- Influence of concentration, solvent aromaticity and nonionic surfactant”, *Colloids and Surfaces A: Physicochemical and Engineering Aspects*, v. 366, n. 1-3, pp. 120–128.
- FAN, Y., SIMON, S., SJÖBLOM, J., 2010b, “Interfacial shear rheology of asphaltenes at oil–water interface and its relation to emulsion stability: Influence of concentration, solvent aromaticity and nonionic surfactant”, *Colloids and Surfaces A: Physicochemical and Engineering Aspects*, v. 366, n. 1, pp. 120 – 128. ISSN: 0927-7757. Availability: <<http://www.sciencedirect.com/science/article/pii/S0927775710003316>>.
- FERRY, J. D., 1980, *Viscoelastic properties of polymers*. John Wiley & Sons.
- FETISOV, E. O., HARWOOD, D. B., KUO, I.-F. W., et al., 2018, “First-principles molecular dynamics study of a deep eutectic solvent: choline chloride/urea and its mixture with water”, *The Journal of Physical Chemistry B*, v. 122, n. 3, pp. 1245–1254.
- FIGUERA, L., MARIN, M., LOPEZ, G., et al., 2010, “Characterization and Modelling of Asphaltene Precipitation and Deposition in a Compositional Reservoir”. In: *SPE Annual Technical Conference and Exhibition*. Society of Petroleum Engineers.
- FINGERHUT, R., CHEN, W.-L., SCHEDEMANN, A., et al., 2017, “Comprehensive Assessment of COSMO-SAC Models for Predictions of Fluid-Phase Equilibria”, *Industrial & Engineering Chemistry Research*, v. 56, n. 35, pp. 9868–9884. Availability: <<https://doi.org/10.1021/acs.iecr.7b01360>>.
- FREED, D., LISITZA, N., SEN, P., et al., 2009, “A study of asphaltene nanoaggregation by NMR”, *Energy Fuels*, v. 23, n. 3, pp. 1189–1193.
- FRIJTERS, S., KRÜGER, T., HARTING, J., 2015, “Parallelised Hoshen–Kopelman algorithm for lattice-Boltzmann simulations”, *Computer Physics Communications*, v. 189, pp. 92–98.
- GAPONIK, N., HERRMANN, A.-K., EYCHMULLER, A., 2011, “Colloidal nanocrystal-based gels and aerogels: material aspects and application perspectives”, *The Journal of Physical Chemistry Letters*, v. 3, n. 1, pp. 8–17.
- GAWLINSKI, E. T., STANLEY, H. E., 1981, “Continuum percolation in two dimensions: Monte Carlo tests of scaling and universality for non-interacting discs”, *Journal of Physics A: Mathematical and General*, v. 14, n. 8, pp. L291.

- GERBER, R. P., SOARES, R. D. P., 2013, “Assessing the reliability of predictive activity coefficient models for molecules consisting of several functional groups”, *Brazilian Journal of Chemical Engineering*, v. 30, n. 1, pp. 1–11.
- GIBSON, J., GOLAND, A. N., MILGRAM, M., et al., 1960, “Dynamics of radiation damage”, *Physical Review*, v. 120, n. 4, pp. 1229.
- GIORGINO, T., 2014, “Computing 1-D atomic densities in macromolecular simulations: The density profile tool for VMD”, *Computer Physics Communications*, v. 185, n. 1, pp. 317–322.
- GLOTZER, S. C., PAUL, W., 2002, “Molecular and Mesoscale Simulation Methods for Polymer Materials”, *Annual Review of Materials Research*, v. 32, n. 1, pp. 401–436. Availability: <<https://doi.org/10.1146/annurev.matsci.32.010802.112213>>.
- GMEHLING, J., 1994, “Phasengleichgewichtsmodelle zur Synthese und Auslegung von Trennprozessen”, *Chemie Ingenieur Technik*, v. 66, n. 6, pp. 792–808. Availability: <<https://onlinelibrary.wiley.com/doi/abs/10.1002/cite.330660604>>.
- GROOT, R. D., 2004, “Applications of dissipative particle dynamics”. In: *Novel Methods in Soft Matter Simulations*, Springer, pp. 5–38.
- GROOT, R. D., WARREN, P. B., 1997, “Dissipative particle dynamics: Bridging the gap between atomistic and mesoscopic simulation”, *The Journal of chemical physics*, v. 107, n. 11, pp. 4423–4435.
- GUVENDIREN, M., LU, H. D., BURDICK, J. A., 2012, “Shear-thinning hydrogels for biomedical applications”, *Soft matter*, v. 8, n. 2, pp. 260–272.
- HANSEN, C. M., 2007, *Hansen solubility parameters: a user's handbook*. CRC press.
- HARBOTTLE, D., CHEN, Q., MOORTHY, K., et al., 2014, “Problematic stabilizing films in petroleum emulsions: Shear rheological response of viscoelastic asphaltene films and the effect on drop coalescence”, *Langmuir*, v. 30, n. 23, pp. 6730–6738.
- HEADEN, T., BOEK, E., JACKSON, G., et al., 2017, “Simulation of asphaltene aggregation through molecular dynamics: Insights and limitations”, *Energy & Fuels*, v. 31, n. 2, pp. 1108–1125.

- HEADEN, T. F., BOEK, E. S., SKIPPER, N. T., 2009, “Evidence for asphaltene nanoaggregation in toluene and heptane from molecular dynamics simulations”, *Energy & Fuels*, v. 23, n. 3, pp. 1220–1229.
- HESS, B., 2002, “Determining the shear viscosity of model liquids from molecular dynamics simulations”, *The Journal of chemical physics*, v. 116, n. 1, pp. 209–217.
- HEYER, L. J., KRUGLYAK, S., YOOSEPH, S., 1999, “Exploring expression data: identification and analysis of coexpressed genes”, *Genome research*, v. 9, n. 11, pp. 1106–1115.
- HEYES, D. M., MELROSE, J. R., 1989, “Microscopic Simulation of Rheology: Molecular Dynamics Computations and Percolation theory”, *Molecular Simulation*, v. 2, n. 4-6, pp. 281–300. Availability: <<https://doi.org/10.1080/08927028908034606>>.
- HIRSCHFELDER, J., BIRD, R. B., CURTISS, C. F., 1964, “Molecular theory of gases and liquids”, .
- HOEPFNER, M. P., FOGLER, H. S., 2013, “Multiscale scattering investigations of asphaltene cluster breakup, nanoaggregate dissociation, and molecular ordering”, *Langmuir*, v. 29, n. 49, pp. 15423–15432.
- HOOGERBRUGGE, P., KOELMAN, J., 1992, “Simulating microscopic hydrodynamic phenomena with dissipative particle dynamics”, *EPL (Europhysics Letters)*, v. 19, n. 3, pp. 155.
- HOSHEN, J., BERRY, M., MINSER, K., 1997, “Percolation and cluster structure parameters: The enhanced Hoshen-Kopelman algorithm”, *Physical Review E*, v. 56, n. 2, pp. 1455.
- HOSHEN, J., 1998, “On the application of the enhanced Hoshen-Kopelman algorithm for image analysis”, *Pattern recognition letters*, v. 19, n. 7, pp. 575–584.
- HOSHEN, J., 1999, “The application of the enhanced Hoshen-Kopelman algorithm for processing unbounded images”, *IEEE transactions on image processing*, v. 8, n. 3, pp. 421–425.
- HOSHEN, J., KOPELMAN, R., 1976, “Percolation and cluster distribution. I. Cluster multiple labeling technique and critical concentration algorithm”, *Physical Review B*, v. 14, n. 8, pp. 3438.

- HSIEH, C.-M., SANDLER, S. I., LIN, S.-T., 2010, “Improvements of COSMO-SAC for vapor–liquid and liquid–liquid equilibrium predictions”, *Fluid Phase Equilibria*, v. 297, n. 1, pp. 90 – 97. ISSN: 0378-3812. Availability: <<http://www.sciencedirect.com/science/article/pii/S0378381210003201>>.
- HSIEH, C.-M., LIN, S.-T., VRABEC, J., 2014, “Considering the dispersive interactions in the COSMO-SAC model for more accurate predictions of fluid phase behavior”, *Fluid Phase Equilibria*, v. 367, pp. 109 – 116. ISSN: 0378-3812. Availability: <<http://www.sciencedirect.com/science/article/pii/S0378381214000570>>.
- HUMPHREY, W., DALKE, A., SCHULTEN, K., et al., 1996, “VMD: visual molecular dynamics”, *Journal of molecular graphics*, v. 14, n. 1, pp. 33–38.
- HUNTER, C. A., SANDERS, J. K., 1990, “The nature of. pi.-. pi. interactions”, *Journal of the American Chemical Society*, v. 112, n. 14, pp. 5525–5534.
- JAKOB, A., GRENSEMANN, H., LOHMANN, J., et al., 2006, “Further Development of Modified UNIFAC (Dortmund): Revision and Extension 5”, *Industrial & Engineering Chemistry Research*, v. 45, n. 23, pp. 7924–7933. Availability: <<https://doi.org/10.1021/ie060355c>>.
- JAMALI, S., YAMANOI, M., MAIA, J., 2013, “Bridging the gap between microstructure and macroscopic behavior of monodisperse and bimodal colloidal suspensions”, *Soft Matter*, v. 9, n. 5, pp. 1506–1515.
- JAMALI, S., BOROMAND, A., KHANI, S., et al., 2015a, “Gaussian-inspired auxiliary non-equilibrium thermostat (GIANT) for dissipative particle dynamics simulations”, *Computer Physics Communications*, v. 197, pp. 27–34.
- JAMALI, S., BOROMAND, A., KHANI, S., et al., 2015b, “Generalized mapping of multi-body dissipative particle dynamics onto fluid compressibility and the Flory-Huggins theory”, *The Journal of chemical physics*, v. 142, n. 16, pp. 164902.
- JAMALI, S., BOROMAND, A., WAGNER, N., et al., 2015c, “Microstructure and rheology of soft to rigid shear-thickening colloidal suspensions”, *Journal of Rheology*, v. 59, n. 6, pp. 1377–1395.
- JESTIN, J., SIMON, S., ZUPANCIC, L., et al., 2007, “A small angle neutron scattering study of the adsorbed asphaltene layer in water-in-hydrocarbon emulsions: Structural description related to stability”, *Langmuir*, v. 23, n. 21, pp. 10471–10478.

- JIMENEZ-SERRATOS, G., TOTTON, T. S., JACKSON, G., et al., 2019, “Aggregation behavior of model asphaltenes revealed from large-scale coarse-grained molecular simulations”, *The Journal of Physical Chemistry B*, v. 123, n. 10, pp. 2380–2396.
- JOVER, J. F., MULLER, E. A., HASLAM, A. J., et al., 2015, “Aspects of asphaltene aggregation obtained from coarse-grained molecular modeling”, *Energy & Fuels*, v. 29, n. 2, pp. 556–566.
- KARNEY, C. F., 2007, “Quaternions in molecular modeling”, *Journal of Molecular Graphics and Modelling*, v. 25, n. 5, pp. 595–604.
- KENNEDY, J., EBERHART, R., 1995, “Particle swarm optimization”. In: *Proceedings of ICNN’95-international conference on neural networks*, v. 4, pp. 1942–1948. IEEE.
- KHANI, S., YAMANOI, M., MAIA, J., 2013, “The Lowe-Andersen thermostat as an alternative to the dissipative particle dynamics in the mesoscopic simulation of entangled polymers”, *The Journal of chemical physics*, v. 138, n. 17, pp. 174903.
- KHANI, S., JAMALI, S., BOROMAND, A., et al., 2015, “Polymer-mediated nanorod self-assembly predicted by dissipative particle dynamics simulations”, *Soft matter*, v. 11, n. 34, pp. 6881–6892.
- KHEDR, A., STRIOLO, A., 2018, “DPD Parameters Estimation for Simultaneously Simulating Water–Oil Interfaces and Aqueous Nonionic Surfactants”, *Journal of Chemical Theory and Computation*, v. 14, n. 12, pp. 6460–6471. Availability: <<https://doi.org/10.1021/acs.jctc.8b00476>>. PMID: 30376315.
- KINNEY, J., LANE, N. E., HAUPT, D., 1995, “In vivo, three-dimensional microscopy of trabecular bone”, *Journal of Bone and Mineral Research*, v. 10, n. 2, pp. 264–270.
- KLAMT, A., 1995, “Conductor-like screening model for real solvents: a new approach to the quantitative calculation of solvation phenomena”, *The Journal of Physical Chemistry*, v. 99, n. 7, pp. 2224–2235.
- KLAMT, A., ECKERT, F., 2000, “COSMO-RS: a novel and efficient method for the a priori prediction of thermophysical data of liquids”, *Fluid Phase Equilibria*, v. 172, n. 1, pp. 43–72.

- KLAMT, A., SCHÜÜRMAN, G., 1993, “COSMO: a new approach to dielectric screening in solvents with explicit expressions for the screening energy and its gradient”, *Journal of the Chemical Society, Perkin Transactions 2*, , n. 5, pp. 799–805.
- KLAMT, A., JONAS, V., BÜRGER, T., et al., 1998, “Refinement and parametrization of COSMO-RS”, *The Journal of Physical Chemistry A*, v. 102, n. 26, pp. 5074–5085.
- KOELMAN, J., HOOGERBRUGGE, P., 1993, “Dynamic simulations of hard-sphere suspensions under steady shear”, *EPL (Europhysics Letters)*, v. 21, n. 3, pp. 363.
- KUZNICKI, T., MASLIYAH, J. H., BHATTACHARJEE, S., 2008, “Molecular dynamics study of model molecules resembling asphaltene-like structures in aqueous organic solvent systems”, *Energy & Fuels*, v. 22, n. 4, pp. 2379–2389.
- LARSON, R. G., 1999, *The structure and rheology of complex fluids*, v. 150. Oxford university press New York.
- LEE, B.-S., LIN, S.-T., 2015, “Screening of ionic liquids for CO₂ capture using the COSMO-SAC model”, *Chemical Engineering Science*, v. 121, pp. 157 – 168. ISSN: 0009-2509. Availability: <<http://www.sciencedirect.com/science/article/pii/S0009250914004357>>. 2013 Danckwerts Special Issue on Molecular Modelling in Chemical Engineering.
- LEES, A., EDWARDS, S., 1972, “The computer study of transport processes under extreme conditions”, *Journal of Physics C: Solid State Physics*, v. 5, n. 15, pp. 1921.
- LEITE, L. F., DUQUE DUTRA, L. E., SOUZA ANTUNES, A. M. D., 2006, “Desenvolvimento tecnológico na indústria do petróleo: o ambiente organizacional e seus aspectos habilitadores e inibidores da inovação”, *Revista de Administração-RAUSP*, v. 41, n. 3.
- LENNARD-JONES, J. E., 1924, “On the determination of molecular fields. II. From the equation of state of gas”. In: *Proc. Roy. Soc. A*, v. 106, pp. 463–477.
- LIN, S.-T., SANDLER, S. I., 2002, “A priori phase equilibrium prediction from a segment contribution solvation model”, *Industrial & engineering chemistry research*, v. 41, n. 5, pp. 899–913.

- LIN, Y.-J., HE, P., TAVAKKOLI, M., et al., 2016, “Examining asphaltene solubility on deposition in model porous media”, *Langmuir*, v. 32, n. 34, pp. 8729–8734.
- LIONBERGER, R. A., RUSSEL, W. B., 1994, “High frequency modulus of hard sphere colloids”, *Journal of Rheology*, v. 38, n. 6, pp. 1885–1908. Availability: <<https://doi.org/10.1122/1.550530>>.
- LIU, J., ZHAO, Y., REN, S., 2015, “Molecular dynamics simulation of self-aggregation of asphaltenes at an oil/water interface: formation and destruction of the asphaltene protective film”, *Energy & Fuels*, v. 29, n. 2, pp. 1233–1242.
- LOH, W., MOHAMED, R. S., RAMOS, A. C., 1999, “Aggregation of asphaltenes obtained from a Brazilian crude oil in aromatic solvents”, *Petroleum science and technology*, v. 17, n. 1-2, pp. 147–163.
- LV, G., GAO, F., LIU, G., et al., 2017, “The properties of asphaltene at the oil-water interface: A molecular dynamics simulation”, *Colloids and Surfaces A: Physicochemical and Engineering Aspects*, v. 515, pp. 34–40.
- MAITI, A., MCGROTHER, S., 2004, “Bead-bead interaction parameters in dissipative particle dynamics: Relation to bead-size, solubility parameter, and surface tension”, *The Journal of chemical physics*, v. 120, n. 3, pp. 1594–1601.
- MARRINK, S. J., TIELEMAN, D. P., 2013, “Perspective on the Martini model”, *Chemical Society Reviews*, v. 42, n. 16, pp. 6801–6822.
- MARRINK, S. J., DE VRIES, A. H., MARK, A. E., 2004, “Coarse grained model for semiquantitative lipid simulations”, *The Journal of Physical Chemistry B*, v. 108, n. 2, pp. 750–760.
- MARRINK, S. J., RISSELADA, H. J., YEFIMOV, S., et al., 2007, “The MARTINI force field: coarse grained model for biomolecular simulations”, *The journal of physical chemistry B*, v. 111, n. 27, pp. 7812–7824.
- MARTÍNEZ-PALOU, R., DE LOURDES MOSQUEIRA, M., ZAPATA-RENDÓN, B., et al., 2011, “Transportation of heavy and extra-heavy crude oil by pipeline: A review”, *Journal of petroleum science and engineering*, v. 75, n. 3-4, pp. 274–282.

- MARTYNA, G. J., KLEIN, M. L., TUCKERMAN, M., 1992, “Nosé–Hoover chains: The canonical ensemble via continuous dynamics”, *The Journal of chemical physics*, v. 97, n. 4, pp. 2635–2643.
- MAYORAL, E., GOICOCHEA, A. G., 2013, “Modeling the temperature dependent interfacial tension between organic solvents and water using dissipative particle dynamics”, *The Journal of chemical physics*, v. 138, n. 9, pp. 094703.
- MCLEAN, J. D., KILPATRICK, P. K., 1997, “Effects of Asphaltene Aggregation in Model Heptane–Toluene Mixtures on Stability of Water-in-Oil Emulsions”, *Journal of Colloid and Interface Science*, v. 196, n. 1, pp. 23 – 34. ISSN: 0021-9797. Availability: <<http://www.sciencedirect.com/science/article/pii/S0021979797951778>>.
- MCQUARRIE, D., 2004, “Statistical mechanics. 2000”, *Sausalito, Calif.: University Science Books*, v. 12, pp. 641.
- MERKER, T., HSIEH, C.-M., LIN, S.-T., et al., 2013, “Fluid-phase coexistence for the oxidation of CO₂ expanded cyclohexane: Experiment, molecular simulation, and COSMO-SAC”, *AIChE Journal*, v. 59, n. 6, pp. 2236–2250. Availability: <<https://aiche.onlinelibrary.wiley.com/doi/abs/10.1002/aic.13986>>.
- METZGER, T., IRAWAN, A., TSOTSAS, E., 2006, “Remarks on the paper “Extension of Hoshen–Kopelman algorithm to non-lattice environments” by A. Al-Futaisi and TW Patzek, *Physica A* 321 (2003) 665–678”, *Physica A: Statistical Mechanics and its Applications*, v. 363, n. 2, pp. 558–560.
- MOSHFEGH, A., AHMADI, G., JABBARZADEH, A., 2015, “Thermostatic and rheological responses of DPD fluid to extreme shear under modified Lees–Edwards boundary condition.” *The European physical journal. E, Soft matter*, v. 38, n. 12, pp. 134–134.
- MOSHFEGH, A., JABBARZADEH, A., 2015a, “Modified Lees–Edwards boundary condition for dissipative particle dynamics: hydrodynamics and temperature at high shear rates”, *Molecular Simulation*, v. 41, n. 15, pp. 1264–1277. Availability: <<https://doi.org/10.1080/08927022.2014.976762>>.
- MOSHFEGH, A., JABBARZADEH, A., 2015b, “Dissipative Particle Dynamics: Effects of Parameterization and Thermostating Schemes on Rheology”,

- Soft Materials*, v. 13, n. 2, pp. 106–117. Availability: <<https://doi.org/10.1080/1539445X.2015.1022898>>.
- MULLINS, E., OLDLAND, R., LIU, Y. A., et al., 2006, “Sigma-Profile Database for Using COSMO-Based Thermodynamic Methods”, *Industrial & Engineering Chemistry Research*, v. 45, n. 12, pp. 4389–4415. Availability: <<https://doi.org/10.1021/ie060370h>>.
- MULLINS, O. C., 2010, “The modified Yen model”, *Energy & Fuels*, v. 24, n. 4, pp. 2179–2207.
- MURGICH, J., RODRÍGUEZ, J., ARAY, Y., 1996, “Molecular recognition and molecular mechanics of micelles of some model asphaltenes and resins”, *Energy & Fuels*, v. 10, n. 1, pp. 68–76.
- NYQUIST, H., 1928, “Thermal agitation of electric charge in conductors”, *Physical review*, v. 32, n. 1, pp. 110.
- OK, S., MAHMOODINIA, M., RAJASEKARAN, N., et al., 2019, “Molecular Structure and Solubility Determination of Asphaltenes”, *Energy & Fuels*, v. 33, n. 9, pp. 8259–8270. Availability: <<https://doi.org/10.1021/acs.energyfuels.9b01737>>.
- ORTEGA-RODRIGUEZ, A., LIRA-GALEANA, C., RUIZ-MORALES, Y., et al., 2001, “INTERACTION ENERGY IN MAYA-OIL ASPHALTENES: A MOLECULAR MECHANICS STUDY”, *Petroleum Science and Technology*, v. 19, n. 1-2, pp. 245–256. Availability: <<http://dx.doi.org/10.1081/LFT-100001238>>.
- ORTEGA-RODRÍGUEZ, A., CRUZ, S. A., GIL-VILLEGAS, A., et al., 2003, “Molecular View of the Asphaltene Aggregation Behavior in AsphalteneResin Mixtures”, *Energy & Fuels*, v. 17, n. 4, pp. 1100–1108. Availability: <<http://dx.doi.org/10.1021/ef030005s>>.
- ÖSTLUND, J.-A., NYDÉN, M., AUFLEM, I. H., et al., 2003, “Interactions between asphaltenes and naphthenic acids”, *Energy & Fuels*, v. 17, n. 1, pp. 113–119.
- PACHECO-SÁNCHEZ, J., ZARAGOZA, I., MARTÍNEZ-MAGADÁN, J., 2003, “Asphaltene aggregation under vacuum at different temperatures by molecular dynamics”, *Energy & fuels*, v. 17, n. 5, pp. 1346–1355.

- PACHECO-SÁNCHEZ, J., ALVAREZ-RAMIREZ, F., MARTÍNEZ-MAGADÁN, J., 2004a, “Morphology of aggregated asphaltene structural models”, *Energy & Fuels*, v. 18, n. 6, pp. 1676–1686.
- PACHECO-SÁNCHEZ, J., ZARAGOZA, I., MARTÍNEZ-MAGADÁN, J., 2004b, “Preliminary study of the effect of pressure on asphaltene disassociation by molecular dynamics”, *Petroleum science and technology*, v. 22, n. 7-8, pp. 927–942.
- PAIVA, F. L., SECCHI, A. R., CALADO, V., et al., 2020, “Slip and momentum transfer mechanisms mediated by Janus rods at polymer interfaces”, *Soft Matter*, v. 16, n. 28, pp. 6662–6672.
- PLIMPTON, S., 1995, “Fast parallel algorithms for short-range molecular dynamics”, *Journal of computational physics*, v. 117, n. 1, pp. 1–19.
- PUNNAPALA, S., VARGAS, F. M., 2013, “Revisiting the PC-SAFT characterization procedure for an improved asphaltene precipitation prediction”, *Fuel*, v. 108, pp. 417–429.
- QIAN, H., CHEN, L., LU, Z., et al., 2006, “The influence of molecule flexibility and shape on the morphology of miktoarm block copolymers in two dimensions”, *EPL (Europhysics Letters)*, v. 74, n. 3, pp. 466.
- RADOLA, B., PICAUD, S., VARDANEGA, D., et al., 2015, “Molecular dynamics simulations of the interaction between water molecules and aggregates of acetic or propionic acid molecules”, *The Journal of Physical Chemistry B*, v. 119, n. 51, pp. 15662–15674.
- RAHMAN, A., 1964, “Correlations in the motion of atoms in liquid argon”, *Physical Review*, v. 136, n. 2A, pp. A405.
- RAPAPORT, D. C., 2004, *The art of molecular dynamics simulation*. Cambridge university press.
- RAPAPORT, D. C., 1992, “Cluster size distribution at criticality”, *Journal of statistical physics*, v. 66, n. 1-2, pp. 679–682.
- REID, R. C., PRAUSNITZ, J. M., POLING, B. E., 1987, *The properties of gases and liquids*. McGraw Hill Book Co., New York, NY.
- REZAEI, H., AMJAD-IRANAGH, S., MODARRESS, H., 2016, “Self-Accumulation of Uncharged Polyaromatic Surfactants at Crude Oil–Water Interface: A Mesoscopic DPD Study”, *Energy & Fuels*, v. 30, n. 8, pp. 6626–6639.

- ROGEL, E., 1995, “Studies on asphaltene aggregation via computational chemistry”, *Colloids and Surfaces A: Physicochemical and Engineering Aspects*, v. 104, n. 1, pp. 85–93.
- ROGEL, E., CARBOGNANI, L., 2003, “Density estimation of asphaltenes using molecular dynamics simulations”, *Energy & fuels*, v. 17, n. 2, pp. 378–386.
- ROGEL, E., LEON, O., TORRES, G., et al., 2000, “Aggregation of asphaltenes in organic solvents using surface tension measurements”, *Fuel*, v. 79, n. 11, pp. 1389–1394.
- ROGEL, E., LEON, O., ESPIDEL, Y., et al., 2001, “Asphaltene stability in crude oils”, *SPE Production & Facilities*, v. 16, n. 02, pp. 84–88.
- ROGEL, E., 2000, “Simulation of Interactions in Asphaltene Aggregates”, *Energy & Fuels*, v. 14, n. 3, pp. 566–574. Availability: <<http://dx.doi.org/10.1021/ef990166p>>.
- ROGEL, E., OVALLES, C., BAKE, K. D., et al., 2016, “Asphaltene Densities and Solubility Parameter Distributions: Impact on Asphaltene Gradients”, *Energy & Fuels*, v. 30, n. 11, pp. 9132–9140.
- RUIZ-MORALES, Y., MULLINS, O. C., 2015, “Coarse-grained molecular simulations to investigate asphaltenes at the oil–water interface”, *Energy & Fuels*, v. 29, n. 3, pp. 1597–1609.
- SCHMID, N., EICHENBERGER, A. P., CHOUTKO, A., et al., 2011, “Definition and testing of the GROMOS force-field versions 54A7 and 54B7”, *European biophysics journal*, v. 40, n. 7, pp. 843.
- SCHMIDT, L., KRISCHER, K., 2015, “Clustering as a prerequisite for chimera states in globally coupled systems”, *Physical review letters*, v. 114, n. 3, pp. 034101.
- SCHWEIZER, J. C., 2007, “Practical course: single-particle-tracking”, *Biophysics-Schwille Lab*.
- SEDGHI, M., GOUAL, L., WELCH, W., et al., 2013, “Effect of asphaltene structure on association and aggregation using molecular dynamics”, *The Journal of Physical Chemistry B*, v. 117, n. 18, pp. 5765–5776.
- SHEREMATA, J. M., GRAY, M. R., DETTMAN, H. D., et al., 2004, “Quantitative molecular representation and sequential optimization of Athabasca asphaltenes”, *Energy & Fuels*, v. 18, n. 5, pp. 1377–1384.

- SHI, C., ZHANG, L., XIE, L., et al., 2017, “Surface Interaction of Water-in-Oil Emulsion Droplets with Interfacially Active Asphaltenes”, *Langmuir*, v. 33, n. 5, pp. 1265–1274. Availability: <<https://doi.org/10.1021/acs.langmuir.6b04265>>. PMID: 28081605.
- SHI, K., LIAN, C., BAI, Z., et al., 2015, “Dissipative particle dynamics study of the water/benzene/caprolactam system in the absence or presence of non-ionic surfactants”, *Chemical Engineering Science*, v. 122, pp. 185–196.
- SHINTO, H., 2012, “Computer simulation of wetting, capillary forces, and particle-stabilized emulsions: From molecular-scale to mesoscale modeling”, *Advanced Powder Technology*, v. 23, n. 5, pp. 538 – 547. ISSN: 0921-8831. Availability: <<http://www.sciencedirect.com/science/article/pii/S0921883112000763>>.
- SILVA, C. D. V., 2015, “A Mesoscopic Model for an Asphaltene and Complex Mixtures of Asphaltenes”, *Petroleum Science and Technology*, v. 33, n. 7, pp. 839–845.
- SKARTLIEN, R., SIMON, S., SJÖBLOM, J., 2016, “DPD Molecular Simulations of Asphaltene Adsorption on Hydrophilic Substrates: Effects of Polar Groups and Solubility”, *Journal of Dispersion Science and Technology*, v. 37, n. 6, pp. 866–883.
- SKARTLIEN, R., SIMON, S., SJÖBLOM, J., 2017, “A DPD study of asphaltene aggregation: The role of inhibitor and asphaltene structure in diffusion-limited aggregation”, *Journal of Dispersion Science and Technology*, v. 38, n. 3, pp. 440–450.
- ŚLEDŹ, P., CAFLISCH, A., 2018, “Protein structure-based drug design: from docking to molecular dynamics”, *Current opinion in structural biology*, v. 48, pp. 93–102.
- SOARES, R. D. P., 2011, “The Combinatorial Term for COSMO-Based Activity Coefficient Models”, *Industrial & Engineering Chemistry Research*, v. 50, n. 5, pp. 3060–3063. Availability: <<https://doi.org/10.1021/ie102087p>>.
- SONG, X., SHI, P., ZHAO, S., et al., 2016, “Dissipative Particle Dynamics Study on the Aggregation Behavior of Asphaltenes under Shear Fields”, *Industrial & Engineering Chemistry Research*, v. 55, n. 33, pp. 9077–9086.

- TALEGHANI, S. T., DADVAR, M., 2014, “Two dimensional pore network modelling and simulation of non-isothermal drying by the inclusion of viscous effects”, *International Journal of Multiphase Flow*, v. 62, pp. 37 – 44. ISSN: 0301-9322. Availability: <<http://www.sciencedirect.com/science/article/pii/S0301932214000287>>.
- TEWARY, V. K., 2009, “Extending the time scale in molecular dynamics simulations: Propagation of ripples in graphene”, *Physical Review B*, v. 80, n. 16, pp. 161409.
- TRUONG, Q. D., KEMPAIAH DEVARAJU, M., NGUYEN, D. N., et al., 2016, “Disulfide-bridged (Mo₃S₁₁) cluster polymer: Molecular dynamics and application as electrode material for a rechargeable magnesium battery”, *Nano letters*, v. 16, n. 9, pp. 5829–5835.
- TSAI, D., 1979, “The virial theorem and stress calculation in molecular dynamics”, *The Journal of Chemical Physics*, v. 70, n. 3, pp. 1375–1382.
- TSENG, H.-C., WU, J.-S., CHANG, R.-Y., 2010, “Linear viscoelasticity and thermorheological simplicity of n-hexadecane fluids under oscillatory shear via non-equilibrium molecular dynamics simulations”, *Physical Chemistry Chemical Physics*, v. 12, n. 16, pp. 4051–4065.
- TUCKERMAN, M., 2010, *Statistical mechanics: theory and molecular simulation*. Oxford University Press.
- UNGERER, P., RIGBY, D., LEBLANC, B., et al., 2014, “Sensitivity of the aggregation behaviour of asphaltenes to molecular weight and structure using molecular dynamics”, *Molecular Simulation*, v. 40, n. 1-3, pp. 115–122.
- USABIAGA, F. B., DELGADO-BUSCALIONI, R., GRIFFITH, B. E., et al., 2014, “Inertial coupling method for particles in an incompressible fluctuating fluid”, *Computer Methods in Applied Mechanics and Engineering*, v. 269, pp. 139 – 172. ISSN: 0045-7825. Availability: <<http://www.sciencedirect.com/science/article/pii/S0045782513002818>>.
- VARAMESH, A., HOSSEINPOUR, N., 2019, “Prediction of asphaltene precipitation in reservoir model oils in the presence of Fe₃O₄ and NiO nanoparticles by cubic plus association equation of state”, *Industrial & Engineering Chemistry Research*, v. 58, n. 10, pp. 4293–4302.
- VARGA, Z., WANG, G., SWAN, J., 2015, “The hydrodynamics of colloidal gelation”, *Soft Matter*, v. 11, n. 46, pp. 9009–9019.

- VERLET, L., 1967, "Computer" experiments" on classical fluids. I. Thermodynamical properties of Lennard-Jones molecules", *Physical review*, v. 159, n. 1, pp. 98.
- VICENTE, L., SOTO, C., PACHECO-SÁNCHEZ, H., et al., 2006, "Application of molecular simulation to calculate miscibility of a model asphaltene molecule", *Fluid Phase Equilibria*, v. 239, n. 1, pp. 100–106.
- WANG, J., FERGUSON, A. L., 2016, "Mesoscale Simulation of Asphaltene Aggregation", *The Journal of Physical Chemistry B*, v. 120, n. 32, pp. 8016–8035. Availability: <<http://dx.doi.org/10.1021/acs.jpcc.6b05925>>. PMID: 27455391.
- WANG, S., XU, J., WEN, H., 2014, "The aggregation and diffusion of asphaltenes studied by GPU-accelerated dissipative particle dynamics", *Computer Physics Communications*, v. 185, n. 12, pp. 3069–3078.
- WANG, S., XU, J., WEN, H., 2015, "Dissipative particle dynamics simulation on the rheological properties of heavy crude oil", *Molecular Physics*, v. 113, n. 21, pp. 3325–3335.
- WARREN, P. B., 1998, "Dissipative particle dynamics", *Current opinion in colloid & interface science*, v. 3, n. 6, pp. 620–624.
- WILKINSON, D., WILLEMSSEN, J. F., 1983, "Invasion percolation: a new form of percolation theory", *Journal of Physics A: Mathematical and General*, v. 16, n. 14, pp. 3365.
- WINKLER, R. G., FEDOSOV, D. A., GOMPPER, G., 2014, "Dynamical and rheological properties of soft colloid suspensions", *Current opinion in colloid & interface science*, v. 19, n. 6, pp. 594–610.
- WU, J., PRAUSNITZ, J. M., FIROOZABADI, A., 1998, "Molecular-thermodynamic framework for asphaltene-oil equilibria", *AIChE journal*, v. 44, n. 5, pp. 1188–1199.
- XU, J.-B., ZHANG, S.-F., WU, H., et al., 2011, "Mesoscopic Simulation of Aggregate Structure and Stability of Heavy Crude Oil by GPU Accelerated DPD", *Chemical Engineering Transactions*, v. 24, pp. 1531–1536.
- YAMAMOTO, S., MARUYAMA, Y., HYODO, S.-A., 2002, "Dissipative particle dynamics study of spontaneous vesicle formation of amphiphilic molecules", *The Journal of chemical physics*, v. 116, n. 13, pp. 5842–5849.

- YAMANOI, M., POZO, O., MAIA, J. M., 2011, “Linear and non-linear dynamics of entangled linear polymer melts by modified tunable coarse-grained level Dissipative Particle Dynamics”, *The Journal of chemical physics*, v. 135, n. 4, pp. 044904.
- YARRANTON, H. W., HUSSEIN, H., MASLIYAH, J. H., 2000, “Water-in-hydrocarbon emulsions stabilized by asphaltenes at low concentrations”, *Journal of colloid and interface science*, v. 228, n. 1, pp. 52–63.
- ZACCARELLI, E., 2007, “Colloidal gels: equilibrium and non-equilibrium routes”, *Journal of Physics: Condensed Matter*, v. 19, n. 32, pp. 323101.
- ZENG, H., SONG, Y.-Q., JOHNSON, D. L., et al., 2009, “Critical nanoaggregate concentration of asphaltenes by direct-current (DC) electrical conductivity”, *Energy & Fuels*, v. 23, n. 3, pp. 1201–1208.
- ZEPPIERI, S., RODRÍGUEZ, J., LÓPEZ DE RAMOS, A., 2001, “Interfacial tension of alkane+ water systems”, *Journal of Chemical & Engineering Data*, v. 46, n. 5, pp. 1086–1088.
- ZHANG, L., SEATON, N., 1996, “Simulation of catalyst fouling at the particle and reactor levels”, *Chemical engineering science*, v. 51, n. 12, pp. 3257–3272.
- ZHANG, L., GREENFIELD, M. L., 2007a, “Analyzing properties of model asphalts using molecular simulation”, *Energy & fuels*, v. 21, n. 3, pp. 1712–1716.
- ZHANG, L., GREENFIELD, M. L., 2007b, “Molecular orientation in model asphalts using molecular simulation”, *Energy & fuels*, v. 21, n. 2, pp. 1102–1111.
- ZHANG, L., GREENFIELD, M. L., 2007c, “Relaxation time, diffusion, and viscosity analysis of model asphalt systems using molecular simulation”, *The Journal of chemical physics*, v. 127, n. 19, pp. 194502.
- ZHANG, S.-F., SUN, L.-L., XU, J.-B., et al., 2010, “Aggregate structure in heavy crude oil: using a dissipative particle dynamics based mesoscale platform”, *Energy & Fuels*, v. 24, n. 8, pp. 4312–4326.
- ZHANG, S.-F., SUN, L.-L., XU, J.-B., et al., 2010, “Dissipative particle dynamics simulations on the structure of heavy oil aggregates”, *Acta Physico-Chimica Sinica*, v. 26, n. 1, pp. 57–65.

- ZHANG, S.-F., XU, J.-B., WEN, H., et al., 2011, “Integration of rotational algorithms into dissipative particle dynamics: modeling polyaromatic hydrocarbons on the meso-scale”, *Molecular Physics*, v. 109, n. 15, pp. 1873–1888.
- ZIA, R. N., LANDRUM, B. J., RUSSEL, W. B., 2014, “A micro-mechanical study of coarsening and rheology of colloidal gels: Cage building, cage hopping, and Smoluchowski’s ratchet”, *Journal of Rheology*, v. 58, n. 5, pp. 1121–1157.
- ZIRRAHI, M., AZINFAR, B., HASSANZADEH, H., et al., 2019, “Particles aggregation and fragmentation—A Monte Carlo study”, *Chemical Physics*, v. 517, pp. 6–12.
- ZNAIDI, L., ILLIA, G. S., BENYAHIA, S., et al., 2003, “Oriented ZnO thin films synthesis by sol-gel process for laser application”, *Thin Solid Films*, v. 428, n. 1, pp. 257 – 262. ISSN: 0040-6090. Availability: <<http://www.sciencedirect.com/science/article/pii/S0040609002012191>>. Proceedings of Symposium J on Growth and Evolution of Ultrathin Films: Surface and Interface Geometric and Electronic Structure, of the E-MRS Spring Conference.
- ÅSMUND ERVIK, SERRATOS, G. J., MÜLLER, E. A., 2017, “raaSAFT: A framework enabling coarse-grained molecular dynamics simulations based on the SAFT- Mie force field”, *Computer Physics Communications*, v. 212, pp. 161–179. ISSN: 0010-4655. Availability: <<https://www.sciencedirect.com/science/article/pii/S001046551630251X>>.

Appendices

Appendix A

3D Linear Regression

Given the n point coordinates:

$P_1(X_1, Y_1, Z_1), P_2(X_2, Y_2, Z_2), \dots, P_k(X_k, Y_k, Z_k), \dots, P_n(X_n, Y_n, Z_n)$ which we know that they are close to an unknown plan Γ , our problem is to determine the parameters that characterize this plan such that the sum of the square distances between the points and the plan is minimal.

the plan equation Γ will be: $Ax + By + Cz + 1 = 0$

Let δ_k be the distance between the point $P_k(X_k, Y_k, Z_k)$ and an unknown point $P(x, y, z)$ belonging to the plan Γ :

$$\delta_k^2 = (x - X_k)^2 + (y - Y_k)^2 + (z - Z_k)^2 \quad (\text{A.1})$$

$$\delta_k^2 = (x - X_k)^2 + (y - Y_k)^2 + \left(\frac{-(Ax + By + 1)}{C} - Z_k \right)^2 \quad (\text{A.2})$$

The minimum distance will be reached since P is in H_k (Orthogonal projection of P_k over Γ):

$$\frac{\partial \delta_k^2}{\partial x} = 2(x - X_k) - 2 \frac{A}{C} \left(\frac{-(Ax + By + 1)}{C} - Z_k \right) = 0 \quad (\text{A.3})$$

$$\frac{\partial \delta_k^2}{\partial y} = 2(y - Y_k) - 2 \frac{B}{C} \left(\frac{-(Ax + By + 1)}{C} - Z_k \right) = 0 \quad (\text{A.4})$$

Solving this system of two linear equations gives us the solutions x and y that will be used to calculate $z = \frac{-(Ax + By + 1)}{C}$

$$x = \frac{(B^2 + C^2)X_k - ABY_k - ACZ_k - A}{A^2 + B^2 + C^2} \quad (\text{A.5})$$

$$y = \frac{-ABX_k + (A^2 + C^2)Y_k - BCZ_k - B}{A^2 + B^2 + C^2} \quad (\text{A.6})$$

$$z = \frac{-ACX_k + (A^2 + B^2)Z_k - BCY_k - C}{A^2 + B^2 + C^2} \quad (\text{A.7})$$

Returning to the equation $\delta_k^2 = (x - X_k)^2 + (y - Y_k)^2 + (z - Z_k)^2$ and replacing the x, y, z values we get:

$$\delta_k^2 = \frac{(AX_k + BY_k + CZ_k + 1)^2}{A^2 + B^2 + C^2} \quad (\text{A.8})$$

From where we get the sum of square distances for all points:

$$\sum \delta_k^2 = \frac{1}{A^2 + B^2 + C^2} \sum (AX_k + BY_k + CZ_k + 1)^2 \quad (\text{A.9})$$

Where \sum represents the sum over all points. The minimum value of the sum will be found by making the partial derivatives of $\sum \delta_k^2$ with respect to A, B, C equals to zero.

Promoting the change of variables:

$$a = \frac{A}{C}; \quad b = \frac{B}{C}; \quad \lambda = \frac{-1}{C}; \quad w = \frac{\lambda}{a^2 + b^2 + c^2} \quad (\text{A.10})$$

The sum of the square distances becomes:

$$\sum \delta_k^2 = \frac{1}{a^2 + b^2 + 1} \sum (aX_k + bY_k + Z_k - \lambda)^2 \quad (\text{A.11})$$

The minimum of the sum is obtained by making the partial derivatives with respect to a, b and λ equals to zero. With respect to λ it will be:

$$\frac{\partial}{\partial \lambda} \sum \delta_k^2 = \frac{2}{a^2 + b^2 + 1} \sum (aX_k + bY_k + Z_k - \lambda) = 0 \quad (\text{A.12})$$

From where we get the value $\lambda = \frac{1}{n} (a \sum X_k + b \sum Y_k + \sum Z_k)$

Therefore:

$$\sum \delta_k^2 = \frac{\sum (aX_k + bY_k + Z_k - \frac{1}{n} (a \sum X_k + b \sum Y_k + \sum Z_k))^2}{a^2 + b^2 + 1} \quad (\text{A.13})$$

$$= \frac{\sum \left(a \left(X_k - \frac{1}{n} \sum X_k \right) + b \left(Y_k - \frac{1}{n} \sum Y_k \right) + \left(Z_k - \frac{1}{n} \sum Z_k \right) \right)^2}{a^2 + b^2 + 1} \quad (\text{A.14})$$

In order to simplify we make:

$$x_k = X_k - \frac{1}{n} \sum X_k ; y_k = Y_k - \frac{1}{n} \sum Y_k ; z_k = Z_k - \frac{1}{n} \sum Z_k \quad (\text{A.15})$$

$$\text{Therefore: } \sum \delta_k^2 = \frac{1}{a^2+b^2+1} \sum (ax_k + by_k + z_k)^2$$

A system of two equations and two unknowns (a and b) is obtained by the partial derivatives with respect to a and b :

$$\frac{2}{a^2 + b^2 + 1} \sum (ax_k + by_k + z_k)x_k - \frac{2a}{(a^2 + b^2 + 1)^2} \sum (ax_k + by_k + z_k)^2 = 0 \quad (\text{A.16})$$

$$\frac{2}{a^2 + b^2 + 1} \sum (ax_k + by_k + z_k)y_k - \frac{2b}{(a^2 + b^2 + 1)^2} \sum (ax_k + by_k + z_k)^2 = 0 \quad (\text{A.17})$$

Which are simplified to:

$$\sum (ax_k + by_k + z_k)x_k - \frac{a}{a^2 + b^2 + 1} \sum (ax_k + by_k + z_k)^2 = 0 \quad (\text{A.18})$$

$$\sum (ax_k + by_k + z_k)y_k - \frac{b}{a^2 + b^2 + 1} \sum (ax_k + by_k + z_k)^2 = 0 \quad (\text{A.19})$$

Multiplying the antepenultimate equation by b and the penultimate equation by a we get:

$$\sum (ax_k + by_k + z_k)bx_k - \sum (ax_k + by_k + z_k)ay_k = 0 \quad (\text{A.20})$$

For the next developments we define the following coefficients:

$$S_{xx} = \sum x_k^2 ; S_{yy} = \sum y_k^2 ; S_{zz} = \sum z_k^2 \quad (\text{A.21})$$

$$S_{xy} = \sum x_k y_k ; S_{xz} = \sum x_k z_k ; S_{yz} = \sum y_k z_k \quad (\text{A.22})$$

So the system of equations becomes:

$$(aS_{xx} + bS_{xy} + S_{xz}) - \frac{a(a^2 S_{xx} + b^2 S_{yy} + S_{zz} + 2abS_{xy} + 2aS_{xz} + 2bS_{yz})}{a^2 + b^2 + 1} = 0$$

(A.23)

$$(aS_{xy} + bS_{yy} + S_{yz}) - \frac{b(a^2S_{xx} + b^2S_{yy} + S_{zz} + 2abS_{xy} + 2aS_{xz} + 2bS_{yz})}{a^2 + b^2 + 1} = 0 \quad (\text{A.24})$$

And the equation $\sum(ax_k + by_k + z_k)bx_k - \sum(ax_k + by_k + z_k)ay_k = 0$ becomes:

$$b^2S_{xy} + bS_{xz} + ab(S_{xx} - S_{yy}) - a^2S_{xy} - aS_{yz} = 0 \quad (\text{A.25})$$

$$b^2 = \frac{1}{S_{xy}} (a^2S_{xy} + aS_{yz} - (a(S_{xx} - S_{yy}) + S_{xz})b) \quad (\text{A.26})$$

Putting the previous value of b^2 into the system of equations we arrive at two equations of b as a function of a . Making them equal to each other, we produce a third degree equation with respect to a :

$$c_3a^3 + c_2a^2 + c_1a + c_0 = 0 \quad (\text{A.27})$$

Where:

$$c_0 = S_{yz}(S_{xy}^2 - S_{xz}^2) + S_{xy}S_{xz}(S_{zz} - S_{yy}) \quad (\text{A.28})$$

$$c_1 = S_{xy}^3 + S_{xy}(S_{xz}^2 - 2S_{yz}^2 - S_{zz}^2) + S_{xy}(S_{xx}S_{zz} + S_{yy}S_{zz} - S_{xx}S_{yy}) \quad (\text{A.29})$$

$$+ S_{xz}S_{yz}(S_{yy} + S_{zz} - 2S_{xx}) \quad (\text{A.30})$$

$$c_2 = S_{yz}^3 + S_{yz}(S_{xz}^2 - 2S_{xy}^2 - S_{xx}^2) + S_{yz}(S_{xx}S_{zz} + S_{xx}S_{yy} - S_{yy}S_{zz}) \quad (\text{A.31})$$

$$+ S_{xy}S_{xz}(S_{xx} + S_{yy} - 2S_{zz}) \quad (\text{A.32})$$

$$c_3 = S_{xy}(S_{yz}^2 - S_{xz}^2) + S_{xz}S_{yz}(S_{xx} - S_{yy}) \quad (\text{A.33})$$

This equations has three roots for a , for each of them a corresponding b is calculated:

$$b = \frac{S_{xy}S_{yz}a^2 + (S_{yz}^2 - S_{xy}^2)a - S_{xy}S_{yz}}{(S_{yz}(S_{xx} - S_{yy}) - S_{xy}S_{xz})a + S_{xy}(S_{yy} - S_{zz}) + S_{xz}S_{yz}} \quad (\text{A.34})$$

Among the three roots, the one that generates the smallest value of $\sum \delta_k^2 = \frac{1}{a^2+b^2+1} \sum(ax_k + by_k + z_k)^2$ will be taken.

Knowing a and b we calculate:

$$\lambda = \frac{1}{n}(a \sum X_k + b \sum Y_k + \sum Z_k) \quad (\text{A.35})$$

$$C = \frac{-1}{\lambda} \quad (\text{A.36})$$

$$A = \frac{-a}{\lambda} \quad (\text{A.37})$$

$$B = \frac{-b}{\lambda} \quad (\text{A.38})$$

finally we get the plan equation $\Gamma : Ax + By + Cz + 1 = 0$.

Appendix B

Clustering Algorithm in Fortran 90

A copy of the clustering algorithm is being provided in this section. Matrices `rx`, `ry` and `rz` should be fulfilled with particle positions for clustering verification. The threshold `dist_cluster` ought be previously set. The output file `clustering.out` describes the molecules pertaining to each aggregate, the total number of clusters, the total number of links and the number of iterations to achieve convergence.

```
MODULE cluster_analysis

! Modified Clustering Algorithm for Molecular Simulation
! By: Fellipe Carvalho de Oliveira – COPPE/PEQ/UFRJ

!$ use omp_lib
CONTAINS

SUBROUTINE neighboring(rx, ry, rz, dist_cluster, n_molecules, max_contacts, L, &
                     n_parti_per_molecule)

! Input arguments:
!
!   rx(i,j), ry(i,j), rz(i,j) : x, y, and z positions of particle j pertaining to
!                               molecule i.
!   dist_cluster : limit distance between two particles from different molecules to
!                   consider that those molecules are aggregated.
!   n_molecules : number of molecules
!   max_contacts : maximum number of contacts per molecule
!   L : edge length of the simulation cubic box

IMPLICIT NONE
```

```

REAL(8), INTENT(INOUT) :: dist_cluster, L
REAL(8), DIMENSION(:,:), INTENT(INOUT) :: rx, ry, rz
INTEGER, INTENT(INOUT) :: n_molecules, max_contacts, n_parti_per_molecule
INTEGER :: i, j, m, n
INTEGER, DIMENSION(:), ALLOCATABLE :: n_contacts_per_molecule
INTEGER, DIMENSION(:,:), ALLOCATABLE :: node_next
INTEGER :: n_links = 0
REAL(8) :: dist, dx, dy, dz

! node(i,j) : Matrix containing neighbors of molecule i
ALLOCATE(node_next(n_molecules, max_contacts))

! n_contacts_per_molecule : Vector containing number of contacts of molecule i
ALLOCATE(n_contacts_per_molecule(n_molecules))

node_next = 0
n_contacts_per_molecule = 0

!$OMP PARALLEL DO &
!$OMP DEFAULT(SHARED) PRIVATE(m,n,i,j,dx,dy,dz,dist) &
!$OMP SCHEDULE(DYNAMIC)

!Loop to find molecule neighbors
DO m = 1, n_molecules
  DO n = m+1, n_molecules
    !Looking for some contact between two particles belonging to different molecules
    loop: DO i = 1, n_parti_per_molecule
      DO j = 1, n_parti_per_molecule
        dx = rx(m,i) - rx(n,j)
        dx = dx - L*nint(dx/L)
        dy = ry(m,i) - ry(n,j)
        dy = dy - L*nint(dy/L)
        dz = rz(m,i) - rz(n,j)
        dz = dz - L*nint(dz/L)
        dist = dx*dx+dy*dy+dz*dz

        !Verifying if the distance between two particles is smaller than
        !the cutoff dist_cluster
        IF ((dist < dist_cluster * dist_cluster) .AND. (m /= n)) THEN
          n_contacts_per_molecule(m) = n_contacts_per_molecule(m) + 1
          n_contacts_per_molecule(n) = n_contacts_per_molecule(n) + 1

          IF (n_contacts_per_molecule(m) > max_contacts) STOP "There are more
          than max_contacts particles around one molecule"

          node_next(m, n_contacts_per_molecule(m)) = n
          node_next(n, n_contacts_per_molecule(n)) = m
        ENDIF
      END DO
    END DO
  END DO
END DO

```

```

        n_links = n_links + 1
        EXIT loop
    END IF
END DO
END DO loop
END DO
END DO
!$OMP END PARALLEL DO

!Calling function that find clusters
CALL clustering(node_next, n_contacts_per_molecule, n_links, n_molecules, max_conta

DEALLOCATE(node_next, n_contacts_per_molecule)
END SUBROUTINE neighboring

SUBROUTINE clustering(node_next, n_contacts_per_molecule, n_links, n_molecules, &
                    max_contacts)

! Variables:
!   nodeL(i) : Cluster id that molecule i belongs to
!   clusters(i,j) : Matrix that contains molecules pertaining to cluster i
!   id(i) : Cluster id of cluster i
!   n_mol_per_cluster(i) : Number of molecules of cluster i
!   n_clusters : Total number of clusters
!   N : Number of iterations to fix the cluster labeling
!   tol : Maximum number of iterations to fix the cluster labeling

IMPLICIT NONE
INTEGER, DIMENSION(:), ALLOCATABLE, INTENT(INOUT) :: n_contacts_per_molecule
INTEGER, DIMENSION(:, :), ALLOCATABLE, INTENT(INOUT) :: node_next
INTEGER, INTENT(INOUT) :: n_links, n_molecules, max_contacts
INTEGER :: i, j, status_open
INTEGER, DIMENSION(:), ALLOCATABLE :: nodeL, labels
INTEGER, DIMENSION(:, :), ALLOCATABLE :: clusters
INTEGER, DIMENSION(:), ALLOCATABLE :: id, n_mol_per_cluster
INTEGER :: n_clusters
INTEGER :: N, tol = 1000
LOGICAL :: condition1, condition2, condition3

ALLOCATE(nodeL(n_molecules), labels(max_contacts))
ALLOCATE(clusters(n_molecules, n_molecules), id(n_molecules), &
n_mol_per_cluster(n_molecules))

nodeL = 0
n_clusters = 0
clusters = 0
id = 0
n_mol_per_cluster = 0

```

```

! Creating output file
OPEN(unit=1,file="clustering.out",status="replace",iostat = status_open )
IF (status_open > 0) STOP "error opening clustering.out"

! Determining the initial cluster label to molecules
DO i = 1, n_molecules
  !If this molecule doesn't have any neighbor, it should be a single cluster
  IF (n_contacts_per_molecule(i) == 0 ) THEN
    n_clusters = n_clusters + 1
    nodeL(i) = n_clusters
  ELSE
    labels = 0
    DO j = 1, n_contacts_per_molecule(i)
      labels(j) = nodeL(node_next(i,j))
    END DO

    !Testing if all molecules neighbors haven't been labeled
    IF (MAXVAL(labels) == 0) THEN
      n_clusters = n_clusters + 1
      nodeL(i) = n_clusters
      !If molecule neighbors do have labels, assign the minimum cluster label among
      !them to this molecule and to its neighbors
    ELSE
      nodeL(i) = MINVAL(labels , MASK = labels > 0)
      DO j = 1, n_contacts_per_molecule(i)
        nodeL(node_next(i,j)) = nodeL(i)
      END DO
    END IF
  END IF
END DO

N = 1
condition1 = .TRUE.

! Fixing cluster label of molecules
DO WHILE ( (N < tol) .AND. (condition1 .EQV. .TRUE.) )

  condition1 = .FALSE.

  DO i = 1,n_molecules
    IF (n_contacts_per_molecule(i) /= 0) THEN
      labels = 0
      DO j = 1, n_contacts_per_molecule(i)
        labels(j) = nodeL(node_next(i,j))
      END DO
    END IF
  END DO

```

```

        nodeL(i) = MINVAL(labels , MASK = labels > 0)
        DO j = 1, n_contacts_per_molecule(i)
            nodeL(node_next(i,j)) = nodeL(i)
        END DO
    END IF
END DO

! Checking if all connected particles have the same cluster label
loop2: DO i = 1, n_molecules
    labels = 0
    DO j = 1, n_contacts_per_molecule(i)
        labels(j) = nodeL(node_next(i,j))
    END DO
    DO j = 1, n_contacts_per_molecule(i)
        IF (nodeL(i) /= labels(j)) THEN
            N = N + 1
            condition1 = .TRUE.
            EXIT loop2
        END IF
    END DO
END DO loop2

END DO    ! End do while

! Reseting n_clusters in order to calculate the correct number of clusters
n_clusters = 0

! Finding number of clusters
DO i = 1, n_molecules
    condition2 = .FALSE.

    ! If i = n_molecules this molecules(node) cannot form aggregate forth and
    ! condition1 = .FALSE. , it will have the opportunity to be a single
    ! cluster (if condition3 = .TRUE.)

    IF (i < n_molecules) THEN
        DO j = i+1, n_molecules
            IF (nodeL(i) == nodeL(j) ) THEN
                condition2 = .TRUE.
            END IF
        END DO
    END IF

    condition3 = .TRUE.
    DO j = i, 1, -1
        IF ((nodeL(i) == nodeL(j) ) .AND. (i /= j) ) THEN

```

```

        condition3 = .FALSE.
    END IF
END DO

! Cluster of many particles
IF ((condition2 .EQV. .TRUE. ) .AND. (condition3 .EQV. .TRUE. )) THEN
    n_clusters = n_clusters + 1
    id(n_clusters) = nodeL(i)
END IF

! Cluster of one particle
IF ((condition2 .EQV. .FALSE. ) .AND. (condition3 .EQV. .TRUE. )) THEN
    n_clusters = n_clusters + 1
    id(n_clusters) = nodeL(i)
END IF

END DO

! Creating matrix of clusters
DO i = 1, n_clusters
    DO j = 1, n_molecules
        IF ( id(i) == nodeL(j)) THEN
            n_mol_per_cluster(i) = n_mol_per_cluster(i) + 1
            clusters(i,j) = j
        END IF
    END DO
END DO

! Writing output file
WRITE(1,*) "Numbers of Links ", n_links
WRITE(1,*) "Number of clusters", n_clusters
WRITE(1,*) "Number of iterations for convergence", N
WRITE(1,*)
DO i = 1, n_clusters
    WRITE(1,*) "Cluster : ", i
    WRITE(1, "(1x,a11,i4,a4)") "Molecules (", n_mol_per_cluster(i), ") : "
    DO j = 1, n_molecules
        IF (clusters(i,j) > 0) THEN
            WRITE(1,*) clusters(i,j)
        END IF
    END DO
END DO

DEALLOCATE(nodeL, labels, clusters, id, n_mol_per_cluster)
CLOSE(1)
END SUBROUTINE clustering

```

END MODULE cluster_analysis